

Report No. UMTA-CA-06-0120-81-1

**S.C.R.T.D. LIBRARY**      **BEHAVIOR OF**  
**THE BAY AREA RAPID TRANSIT TUNNELS**  
**THROUGH THE HAYWARD FAULT**

**IAN R. BROWN**  
**TOR L. BREKKE**  
**GREGORY E. KORBIN**



**JUNE 1981**  
**FINAL REPORT**

**DOCUMENT IS AVAILABLE TO THE PUBLIC  
THROUGH THE NATIONAL TECHNICAL  
INFORMATION SERVICE, SPRINGFIELD,  
VIRGINIA 22161**

**Prepared for**

**U.S. DEPARTMENT OF TRANSPORTATION**  
**URBAN MASS TRANSPORTATION ADMINISTRATION**  
**Office of Technology Development and Deployment**  
**Office of Rail and Construction Technology**  
**Washington, D.C. 20590**



**Technical Report Documentation Page**

1. Report No. UMTA-CA-06-0120-81-1		2. Government Accession No.		3. Recipient's Catalog No.	
4. Title and Subtitle Behavior of the Bay Area Rapid Transit Tunnels Through the Hayward Fault.				5. Report Date June 1981	
				6. Performing Organization Code	
7. Author(s) Brown, I. R., Brekke, T. L., and Korbin, G. E.				8. Performing Organization Report No.	
9. Performing Organization Name and Address San Francisco Bay Area Rapid Transit District 800 Madison Street Oakland, California 94607				10. Work Unit No. (TRAIS)	
				11. Contract or Grant No. CA-06-0120	
12. Sponsoring Agency Name and Address U.S. Department of Transportation Urban Mass Transportation Administration 400 Seventh Street, S.W. Washington, D. C. 20590				13. Type of Report and Period Covered FINAL REPORT	
				14. Sponsoring Agency Code	
15. Supplementary Notes Subcontractor: University of California 440 Davis Hall Berkeley, California 94720					
16. Abstract  The Bay Area Rapid Transit twin tunnels through the Berkeley Hills cross the active Hayward Fault near the west portal. This study was undertaken to investigate the response of the tunnels to slow right lateral slippage along the fault. Data from exploration and construction, tunnel instrumentation, and surveying were analyzed. Survey data, coupled with observations of track alignment and cracking pattern in the concrete liner have indicated that slippage of 6-8 mm per year is associated with a narrow shear zone mapped during construction. Finite element methods of analysis were used to model the observed tunnel behaviour, and a strain softening model was used to explain seismic phenomena on the Hayward Fault. Recommendations are made for the future monitoring of tunnel response to fault slippage.					
17. Key Words Tunnel, Lining, Active Fault, Instrumentation, Models, Field Investigation.				18. Distribution Statement Available to the Public through the National Technical Information Service, Springfield, Virginia 22161.	
19. Security Classif. (of this report) <b>Unclassified</b>		20. Security Classif. (of this page) <b>Unclassified</b>		21. No. of Pages	22. Price

04979

TF  
232  
.B76

## ACKNOWLEDGMENTS

The Project Director for this study was Mr. W. R. McCutchen, Manager of Design and Construction, San Francisco Bay Area Rapid Transit District (BART). His continued support of this work is greatly appreciated. Other BART personnel who contributed include Messrs. W. G. Snyder, J. A. Robinson, B. D. Hazelwood, and R. T. Maffei. The encouragement of Mr. G. Butler of the Urban Mass Transit Administration, U.S. Department of Transportation, is also acknowledged.

Professor R. L. Taylor helped with the application of finite element analysis. Professors R. E. Goodman and G. H. Curtis reviewed the work. Drs. W. Ellsworth and W. Stuart of the U.S. Geological Survey, Menlo Park, provided data and advice in the area of seismology and fault modelling. Graduate students Mr. G. Lawton and Mr. K. Saari also contributed to the project.

During the period of this study, Ian Brown was sponsored by the New Zealand Government as a National Research Advisory Council Post-Graduate Fellow.

The figures were draughted by R. E. Babiera, BART, and Maureen Haronga, New Zealand Geological Survey.



## TABLE OF CONTENTS

	<u>Page</u>
1. INTRODUCTION	1
2. ACTIVE FAULT PHENOMENA THAT CAUSE TUNNEL DAMAGE	5
2.1 Definition of an Active Fault	5
2.2 Ground Vibration	6
2.3 Fault Displacement	9
2.4 Squeezing Ground	10
2.5 Legislation to Mitigate Active Fault Phenomena	11
3. CASE HISTORIES	13
3.1 Southern Pacific Railroad Tunnel, Santa Clara County, California	13
3.2 Tanna Tunnel, Japan	13
3.3 Southern Pacific Railroad Tunnels, Kern County, California	15
3.4 Balboa Inlet Tunnel, San Fernando, California	18
3.5 Inatori Tunnel, Japan	19
3.6 San Pablo Tunnel, Contra Costa County, California	19
3.7 Claremont Tunnel, Alameda County, California	22
4. DESIGN CONSIDERATIONS FOR TUNNELS THAT CROSS ACTIVE FAULTS	26
4.1 Site Investigations	26
4.1.1 Geometry of fault zone	26
4.1.2 Properties of fault zone materials	26
4.1.3 Earthquake recurrence intervals	27
4.1.4 Rate of fault slippage	27
4.2 The Design Earthquake	29

	<u>Page</u>
4.3 Static Design Criteria	29
4.4 Seismic Design Criteria	30
4.5 Designs Used for Tunnels that Cross Active Faults	31
5. GEOLOGY OF THE BERKELEY HILLS NEAR THE BART TUNNELS	33
5.1 Stratigraphy	33
5.2 Structure	38
5.3 Hayward Fault	40
6. DESIGN AND CONSTRUCTION OF BART TUNNELS	49
6.1 Site Investigations	49
6.2 Exploration Adits	49
6.3 Tunnel Design	53
6.4 Tunnel Construction	57
6.5 Instrumentation During Tunnel Construction	61
7. RESPONSE OF BART TUNNELS TO FAULT SLIPPAGE	63
7.1 Instrumentation Since Tunnel Construction	63
7.2 Concrete Liner Cracking Pattern	63
7.3 Tunnel Displacement Due to Slippage Along the Hayward Fault	71
7.3.1 Construction Surveys	71
7.3.2 "As Built" Survey	72
7.3.3 Horizontal Alignment Surveys Since Tunnel Construction	72
7.4 Squeezing Ground in the Hayward Fault Zone	86
7.5 Ground-Liner Interaction	87
8. MODEL STUDIES OF FAULT-TUNNEL INTERACTION	93



	<u>Page</u>
8.1 Strike Slip Fault Models	93
8.1.1 Quasi-Static Fault Models	93
Anderson's Model	93
Strain-softening Models	94
Dislocation Models	100
Frictional Models	101
8.1.2 The Mechanics of Shearing along an Inter- connected System of Discontinuities	101
8.1.3 A Model for the Hayward Fault	108
8.2 Two Dimensional Plane Strain Model of a Typical Liner Section	116
8.2.1 Bechtel Design Pressures	119
8.2.2 Pressure Distribution Inferred from Pressure Cell Data	124
8.3 Axi-symmetric Model	124
9. CONCLUSIONS	132
10. RECOMMENDATIONS FOR FURTHER MONITORING	136
10.1 Existing Instrumentation	136
10.2 Proposed Future Instrumentation	137
10.2.1 Vertical alignment across fault zone	137
10.2.2 Axial changes in tunnel length	137
10.2.3 Horizontal alignment across fault zone	138
10.2.4 Ground-lining interaction	138
10.3 Recording System	139
REFERENCES	140

	<u>Page</u>
APPENDIX A    Results of Instrumentation from West Portal Exploration Adit	153
APPENDIX B    Ground Conditions Encountered and Support Used in the C2 Tunnel	171
APPENDIX C    Instrumentation Data from Section of C2 Tunnel in Hayward Fault Zone	175
APPENDIX D    Log of Concrete Liner Cracks in Part of C2 Tunnel	202

## LIST OF FIGURES

	<u>Page</u>
1.1	2
1.2	3
2.1	7
3.1	14
3.2	16
3.3	17
3.4	20
3.5	21
3.6	23
3.7	25
4.1	28
4.2	32
5.1	34
5.2	36

	<u>Page</u>
5.3 Structural map of the Berkeley Hills (after Radbruch and Case, 1967)	39
5.4 Major right-lateral strike-slip faults in the San Francisco Bay area	41
5.5 Epicentres of earthquakes near BART tunnels	45
6.1 Plan and section showing ground conditions instrumentation sites in west portal exploration adit	51
6.2 Position of west portal exploration adit in relation to C2 tunnel	52
6.3 BART Berkeley Hills tunnels, concrete liner reinforcement	56
6.4 BART Berkeley Hills tunnels, temporary support	58
6.5 Excavation of C2 tunnel through Hayward Fault (photograph from BART files)	60
7.1 Section of tunnel in Hayward Fault zone; geology and location of instrumentation	64
7.2 Instrumentation arrangement at Station 1202+77, C2 tunnel	65
7.3 Tape extensometer anchor point location	69
7.4 Laser survey traverses, C1 and C2 tunnels	74
7.5 Laser alignment survey, C1 tunnel	76
7.6 Laser alignment survey, C2 tunnel	77
7.7 Displacement of laser alignment survey Station 2 relative to Station 3, C1 tunnel	78
7.8 Displacement of laser alignment survey Station 8 relative to Station 9, C2 tunnel	79
7.9 BART survey No. C005-2	81
7.10 BART survey No. C003-0	82
7.11 C2 tunnel, looking east, showing shift in track at Hayward Fault	84

	<u>Page</u>	
7.12	Track shift in C2 tunnel measured during December 1980 survey	85
7.13	Maximum rock movement indicator extension	87
7.14	Ground displacement away from the tunnel liner	89
7.15	Comparison of geology and liner crack pattern around Station 1200+80, C2 tunnel	90
7.16	Pressure distribution along C2 tunnel	92
8.1	Principal stress orientations for strike slip faulting	95
8.2	Fault model (after Stuart, 1980)	97
8.3	Finite element model of fault in elastic surroundings	99
8.4	Riedel experiment	102
8.5a	Force displacement curve for Riedel experiment	103
8.5b	Proportion of total movement taken up by shears	103
8.6	Mechanistic terminology for simple shear structures	105
8.7	Stresses at peak strength in a shear box	107
8.8	Pressure cell changes with time as predicted by fault model	111
8.9	Earthquakes in Hayward Fault zone near BART tunnels, cumulative magnitude divided by distance	112
8.10	Earthquakes in Hayward Fault zone near BART tunnels, cumulative antilog magnitude divided by distance	113
8.11	Pressure cell 3, residuals from linear curve fittings	115
8.12	Idealized fault map, Berkeley Hills	117
8.13	Model of BART tunnels used for analysis with program LINER	120
8.14	Moment distribution in tunnel liner, Bechtel design loading	121
8.15	Steel stress, Bechtel design loading	121
8.16	Extradors concrete stress, Bechtel design loading	121

	<u>Page</u>	
8.17	Intradados steel stress in element 2 for various values of modulus of subgrade reaction	122
8.18	Extradados concrete stress in element 5 for various values of modulus of subgrade reaction	122
8.19	Extradados concrete stress in element 8 for various values of modulus of subgrade reaction	123
8.20	Pressure distribution on C2 tunnel liner at Station 1206+31	125
8.21	Definition of axi-symmetric solid	127
8.22	Axi-symmetric finite element model of C1 tunnel and surrounding ground	128
8.23	Deformed mesh	130
A.1	Instrumentation arrangement in west portal exploration adit	154
A.2	(i-xxix) Rock movement indicator readings, and horizontal and vertical pressure curves from instrumentation in west portal exploration adit	154
C.1	(i-xx) Rock movement indicator readings from C2 tunnel, 1967 to 1980	176
C.2	(i-vi) Pressure cell readings from C2 tunnel, 1967 to 1980)	196
D.1	(i-vi) Log of concrete liner cracking from Station 1191+00 to 1210+20, C2 tunnel	203

## LIST OF TABLES

	<u>Page</u>
5.1 Notable earthquakes on the Hayward Fault 1836-1965 (after Bolt and Marion, 1966)	44
5.2 Hayward Fault--measured slippage rates	47
6.1 Summary of ground response, west portal adit	54
7.1 C2 tunnel instrumentation	67

## CONVERSION TABLE

## S.I. Units - U.S. Customary

Length	1 mm	=	$3.937 \times 10^{-2}$ inch
	1 m	=	3.281 feet
	1 km	=	0.6214 mile
Volume	1 litre	=	0.2642 gallon
Mass	1 kg	=	$1.101 \times 10^{-3}$ ton
Density	1 kg/cm <sup>3</sup>	=	$6.243 \times 10^{-2}$ lb/ft <sup>3</sup>
Force	1 kN	=	224.82 lbf
Stress	1 MPa	=	145.04 lb/sq inch
	1 kPa	=	0.145 lb/sq inch



## CHAPTER 1

### INTRODUCTION

The Bay Area Rapid Transit (BART) system provides a modern rail transit service between stations in San Francisco, Alameda, and Contra Costa Counties, California.

On the Concord Line, between Rockridge and Orinda Stations, twin tunnels each 4950m long pass through the Berkeley Hills (Figures 1.1, 1.2). Near the west portal, the tunnels cross the Hayward Fault, a highly active strike-slip fault along which major earthquakes have occurred with associated surface rupture. Slow right lateral slippage along the Hayward Fault has been well documented, particularly in locations where crossed by structures and utilities.

The BART tunnels were constructed about 14 years ago, and concerns were recently raised that by now, fault slippage could have affected the tunnel liner. The research programme undertaken for this dissertation to assess the behaviour of the BART tunnels through the Hayward Fault, followed a request to the University of California from BART's Design and Construction Department.

Numerous construction and investigation data were available, and considerable time was spent reviewing these. Tunnel instrumentation was evaluated, and data recorded since construction were analysed. Data from previous surveys, and surveys undertaken for this project, were reduced and interpreted. A detailed log of concrete liner cracking was prepared for the section of tunnel through the Hayward Fault. An analytical study was made of the interaction between the tunnel liner and ground in the Hayward Fault zone.

Based on this work, and on a review of problems encountered with tunnels across active faults elsewhere, it was possible to explain the observed BART tunnel behaviour.

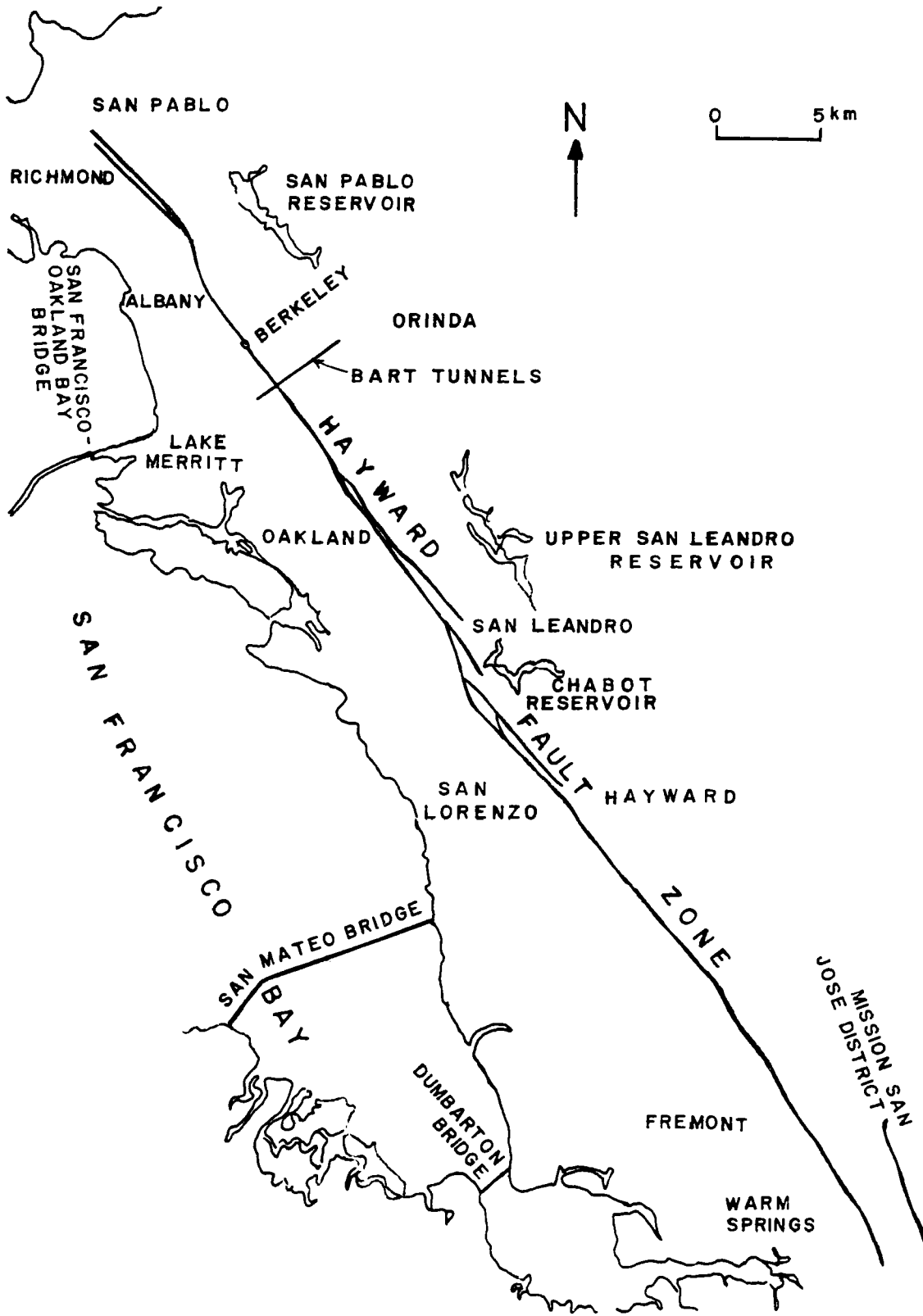


FIGURE 1.1 Location Map, San Francisco Bay Area.

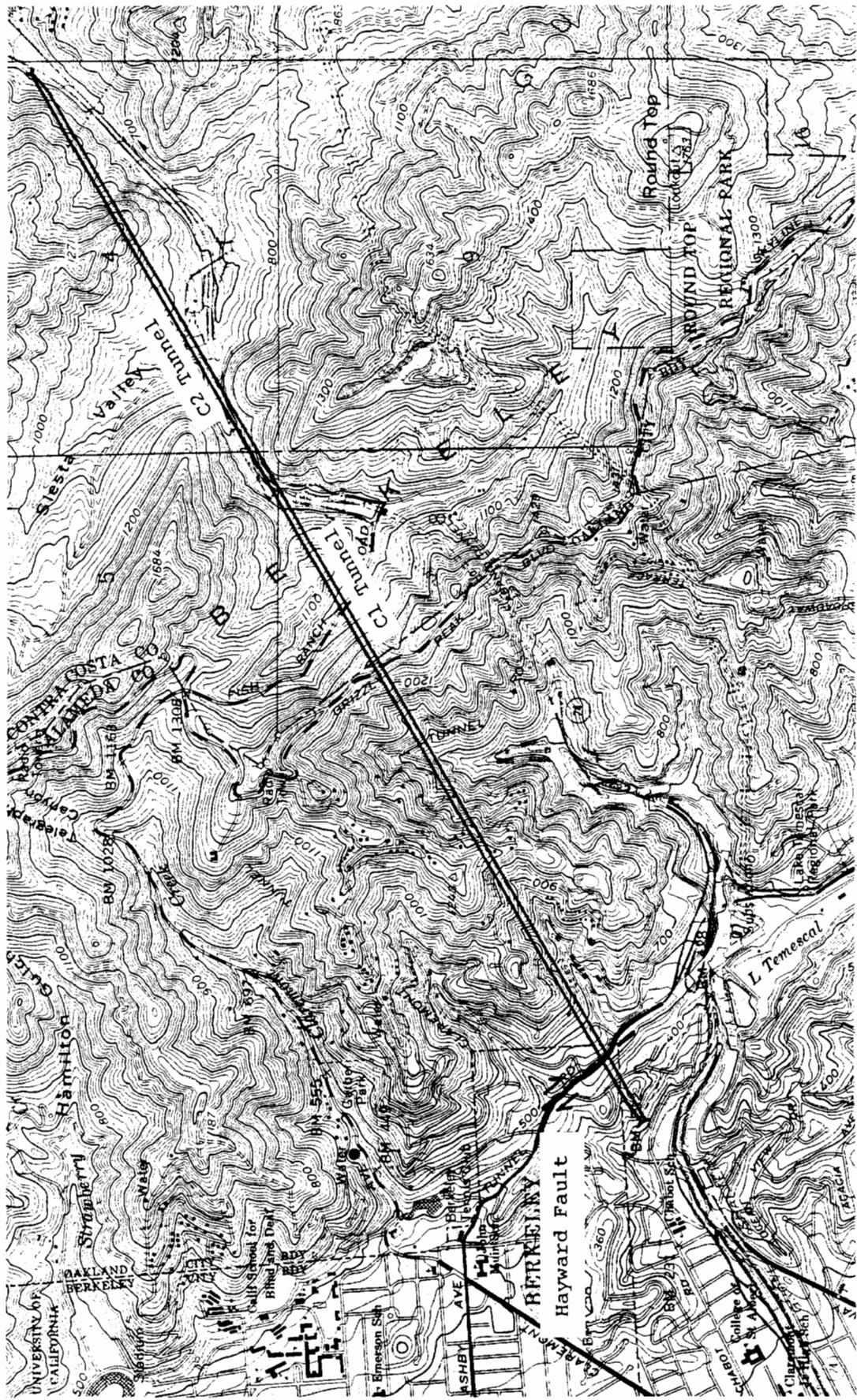


FIGURE 1.2 Location Map, Berkeley Hills.

Recommendations are made for further monitoring in order to safely operate high speed trains in these tunnels.

## CHAPTER 2

### ACTIVE FAULT PHENOMENA THAT CAUSE TUNNEL DAMAGE

#### **2.1. Definition of an Active Fault**

A fault may be defined as a fracture or fracture zone, along which there has been displacement of one side relative to another, and parallel to the fracture. A fault trace is the topographic expression of the intersection of a fault and ground surface. It is therefore used to depict the location of a fault on a map.

An active fault has been defined as one that has had surface displacement within Holocene time (about the last 11,000 years) (Hart, 1978). Other definitions of an active fault have been used. For example, the New Zealand Geological Survey considers an active fault one which has moved in the last 50,000 years, or which shows evidence of repeated movement in the last 500,000 years (Lensen, 1976). A similar definition is used by the U.S. Nuclear Regulatory Commission. The U.S. Water and Power Resources Service, formerly Bureau of Reclamation, designate an active fault as one for which there is evidence of displacement in the past 100,000 years. The U.S. Army Corps of Engineers use a period of 35,000 years.

Active faults may be identified by a number of methods, including direct observation of young fault-related topographic features in the field, or on aerial photographs or other remotely obtained images, surface and subsurface geological mapping, and geophysical investigations. The evidence by which active faults are identified is generally subtle or obscure.

The implication that faults not exhibiting the relevant criteria are inactive is not necessarily valid. A fault may be shown to be inactive on geologic evidence, but such evidence is commonly difficult to obtain. This problem has led to other qualifications as to activity which in California include: potentially active fault - one which shows evidence of surface displacement during Quaternary time (the last 2 to 3 million years); sufficiently active fault - a fault with evidence of Holocene surface displacement along one or more of its segments or branches (Hart, 1978).

## **2.2. Ground Vibration**

When an earthquake occurs along a fault, vibrations at ground surface will be strongest close to the fault plane, attenuating with distance. Although a number of empirical attenuation laws have been developed, it is not clear whether these relations can be applied at depth below the ground surface. The intensity of shaking at a site is related to earthquake magnitude, as well as distance from the earthquake source and local ground conditions, but as the source of ground motion is distributed along a section of a fault, the severity of ground shaking close to a fault may not change greatly as a function of earthquake magnitude.

Seismographs were installed in the Tanna Tunnel following the 1930 Izu earthquake, as well as on the ground surface 160m above it (Nasu, 1931). Both instruments were located in agglomerate and recorded a number of strong aftershocks. It was found that when the fundamental period of the earthquake was less than 1 second, the ratio of amplitude above ground to that below ground was always greater than 2:1. For longer periods, around 4 seconds, the amplitude ratio tended to unity (Figure 2.1).

The effects of ground vibration on tunnel performance have been reviewed by Dowding and Rozen (1978) who surveyed the behaviour of 71 tunnels during earthquakes and compared accelerations at ground surface with tunnel damage. For each site, ground

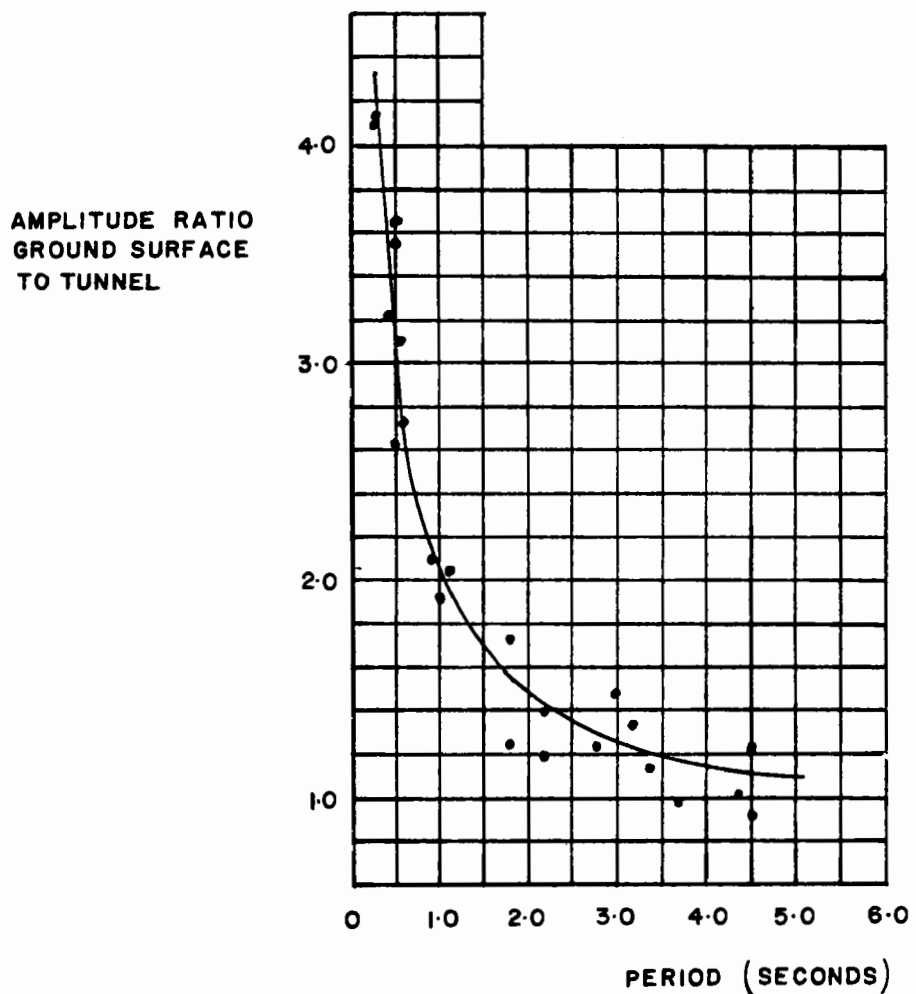


FIGURE 2.1 Amplitude ratio versus period for aftershocks recorded in Tanna Tunnel (after Nasu, 1931).

surface acceleration was calculated based on attenuation relations developed for earthquake magnitude and epicentral distance. No allowance was made for possible attenuation with depth. Correlation of damage to peak ground motion showed that no damage<sup>1</sup> occurred in tunnels where the peak ground acceleration was less than  $0.19g^2$  and peak ground velocity was less than 20cm/sec. Minor damage due to shaking<sup>3</sup> was observed for values of peak acceleration and velocity up to 0.5g and 94cm/sec respectively. Above an acceleration of 0.5g, major rock falls, severe cracking, and collapse occurred.

Owen and Scholl (1980) collected data on 127 underground openings affected by earthquakes, including those described by Dowding and Rozen (1978). They estimated peak ground motion parameters by using attenuation relations that considered location of source, and ground characteristics at the site. Some of Owen and Scholl's ground surface accelerations were higher than those assumed by Dowding and Rozen. It was concluded that little or no damage occurred in rock tunnels for ground surface accelerations below 0.4g. Many instances of damage were close to the ground surface, either near portals or in tunnels with little ground cover. A number of case histories used by Owen and Scholl were from mines, however these data are likely to be misleading when applied to civil engineering structures. Stress changes due to extraction of ore are such that an earthquake can trigger instability, with resulting damage to mine openings. The amount of damage reported may not be directly related to intensity of earthquake shaking.

From observations of tunnels close to nuclear explosions, Owen and Scholl (1980) found that thick tunnel liners suffered more damage than thinner more flexible liners. However such nuclear tests produce vibrations with frequency content, values of peak ground motion parameters, and duration, different from earthquakes. These observations appear to have limited application to ground vibration during earthquakes.

---

<sup>1</sup> defined as no rockfalls in an unlined tunnel

<sup>2</sup> g is the standard acceleration of gravity

<sup>3</sup> defined as reports of rockfalls in an unlined tunnel and minor cracking of lining



### 2.3. Fault Displacement

Historical records of large magnitude earthquakes with shallow focal depths suggest a close relation with surface displacement along a fault. Furthermore, the record of fault activity suggests it is most likely that displacements along a given fault will occur on or near the most recently active fault trace (Taylor and Cluff, 1977). The sense of displacement will most likely follow that of previous events, responding to a tectonic stress field that changes only slowly with time.

Three types of fault displacement are generally recognised: strike-slip, normal, and reverse. Strike-slip fault displacement involves a horizontal lateral motion, usually along a near-vertical fault plane, and normal faults and reverse faults cause dip-slip displacements. These three categories represent the range of fault motions. Commonly the observed fault displacement will involve strike-slip movement with a component of normal or reverse movement, or vertical displacement with a component of strike-slip movement.

The effect of displacement on a tunnel crossing a fault is dependent upon sense of movement of the fault, amount of displacement, and width of the zone over which displacement takes place. Sense of displacement relative to orientation of the tunnel determines whether a section of tunnel in an active fault zone undergoes compression or extension, in addition to shear.

In California, data from small scale geodetic arrays, and continuous monitoring by surface displacement meters across active faults, indicate that slow slippage is a common behaviour of active faults. Fault creep was defined by Burford *et al.* (1978) as "gradual, aseismic slip that is apparently produced by viscous yielding within a relatively weak fault gouge". Because of the material behaviour implied by the use of the term "creep", fault slippage more appropriately describes this phenomenon, and is used throughout this report.

Recognition of fault slippage goes back at least to 1933, when Koch described damage to well casings and to gas, oil, and water lines due to slippage on a low angle thrust fault in

the Buena Vista oil field, Kern County, California. Later observations of slippage along this fault were described by Wilt (1958). Soon after, the effects of slippage were observed along the San Andreas Fault near Holister, California (Steinbrugge and Zacher, 1960), and along the Hayward Fault (Radbruch and Lennert, 1966).

Both discrete slippage events and steady-state slippage have been observed, typically with occasional discrete slip events superimposed on a background of slow, steady slip. Slippage events may have displacements of a few millimeters and durations of several hours. They sometimes begin at different times at adjacent sites (Nason, 1971). King *et al.* (1973) suggested that the low seismic excitation during steady slippage was the result of slow particle motions, rather than low strain energy release.

#### 2.4. Squeezing Ground

Squeezing ground is a time-dependent phenomenon usually associated with tunnel construction through a fault zone. Squeeze occurs when the *in situ* stresses are high relative to the strength of the material. A high stress to strength ratio causes slow, time dependent displacement of ground around the tunnel toward the excavated opening.

From a tunnelling point of view, ground in fault zones normally only causes problems during construction. Materials encountered may range from fractured yet unweathered rock, to a low strength clay gouge requiring special tunnelling techniques.

Peck (1969) demonstrated that squeezing behaviour of clay in a tunnel excavation is related to a stability factor  $N_t$ , where

$$N_t = \frac{P_z - P_a}{S_u}$$

and  $P_z$  = overburden pressure

$P_a$  = tunnel air pressure above atmosphere

$S_u$  = undrained shear strength

Squeezing ground can be expected when  $N_f$  is greater than one. When  $N_f$  is less than 4, the rate of squeeze does not usually cause problems with ground control. At a value of 6 or 7, squeezing ground may cause serious problems with face stability. Squeezing ground causes tunnelling difficulties due to loss of ground, and in shallow tunnels, ground surface settlement may be a problem.

## **2.5. Legislation to Mitigate the Effects of Active Fault Phenomena**

The California State Legislature passed the Alquist-Priolo Special Studies Zones Act in 1972 (Public Resources Code: Division 2, Chapter 7.5). Under this Act, the State Geologist must establish Special Studies Zones to regulate development near the traces of potentially hazardous faults.

To assist cities and counties implement the Alquist-Priolo Special Studies Zones Act, the State Mining and Geology Board established Policies and Criteria. These are discussed by Hart (1980), and they include as Specific Criteria that no structures for human occupancy are permitted on the trace of an active fault. This definition excludes tunnels and other transportation structures. However the Specific Criteria do state that such structures should be sited and designed with due consideration to the hazard of surface faulting.

To January 1, 1977, some 21 potentially active faults had been included in Alquist-Priolo Special Studies Zones. Designated faults near the San Francisco Bay Area included the San Andreas, Hayward, and Calaveras Faults.

The Alquist-Priolo Special Studies Zones Act is concerned with mitigating the localised hazard of surface fault rupture and does not consider the more widespread hazard of strong ground vibration. However ground vibration and soil response may be discussed in the Seismic Safety Element, a mandatory part of the General Plan for a city or county. Although the fault rupture hazard is generally considered to be the most readily mitigated geologic hazard, Hart (1978) found from experience that accurate location and evaluation

of faults was more difficult than initially anticipated. As an example of this, the Greenville Fault in Contra Costa County, California, had been classified as inactive before a magnitude<sup>4</sup> 5.5 earthquake on January 24, 1980, caused surface rupture along the fault.

---

<sup>4</sup> Earthquake magnitudes are in terms of the Richter Scale (Richter 1935).

## CHAPTER 3

### CASE HISTORIES

#### **3.1. Southern Pacific Railroad Tunnel, Santa Clara County, California**

In 1906, an earthquake M 8.25 with its epicentre near San Francisco, California, was associated with relative displacement along about 430km of the San Andreas Fault, and with a maximum horizontal offset of about 5m (Lawson, 1908). A Southern Pacific Railroad tunnel crossed the San Andreas Fault near Wright Station, and during the earthquake there was lateral displacement of 1.4m along a shear zone about 120m from the north-east portal. In this location the tunnel was timber-supported and considerable crushing of timbers and upward heave of rails occurred. Other shear zones with smaller offsets were found at a distance of between 400m and 700m from the portal. These shear zones had a similar orientation to the main fault break. Surveys during tunnel reconstruction indicated that progressively increasing horizontal displacement occurred from a point about 1500m from the main fault break to the shear zone, where 1.4m offset was measured (Figure 3.1). At ground surface immediately above the tunnel, larger displacements were found along the fault trace than were observed underground.

#### **3.2. Tanna Tunnel, Japan**

The Tanna railway tunnel on the main line between Tokyo and Kobe was under construction in 1930 when it was damaged by an earthquake with a magnitude estimated at M 7.1 by Gutenberg and Richter (1954).

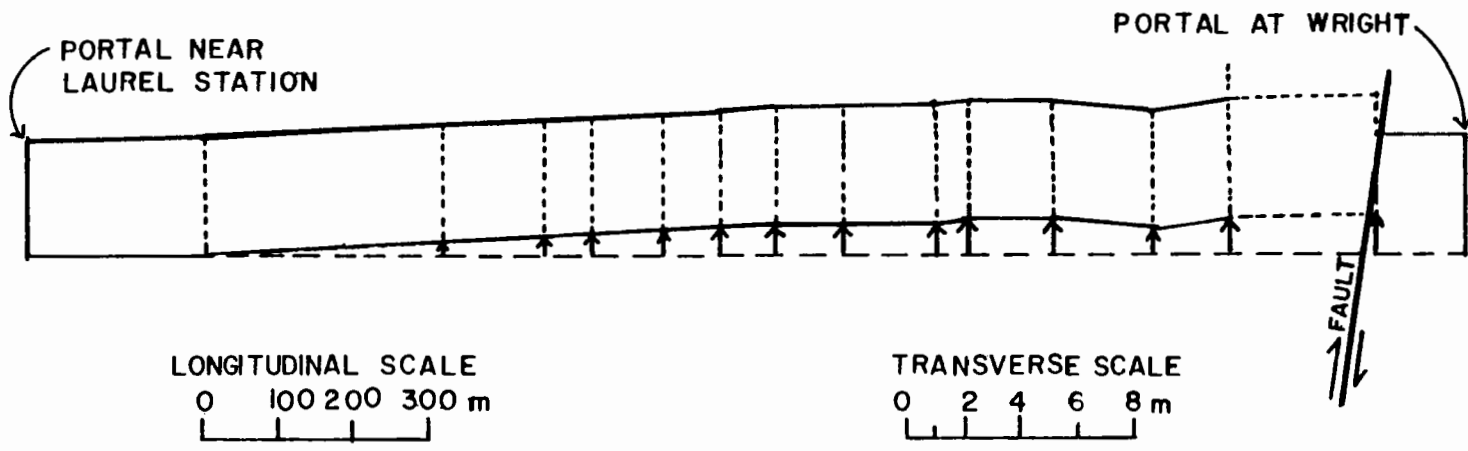


FIGURE 3.1 Deformation of Southern Pacific Railroad tunnel as a result of 1906 earthquake on San Andreas fault (after Lawson, 1908).

Very wet tunnelling conditions required drainage drifts around and ahead of the main tunnel (Figure 3.2). Near the heading of one of the southern drainage drifts, a shear zone displaced left laterally 2.7m and vertically 600mm (Takahasi, 1931). This displacement completely closed the drainage drift. Although the main tunnel heading was estimated to be only about 0.5m east of the active shear zone, the only damage reported was a few cracks in the tunnel walls. At ground surface, about 160m above tunnel invert, fault displacement was less and measured about 1m left lateral and 500mm vertical. Bonilla (1979) discussed reports of a change in strike of the fault between ground surface and in the tunnel. It is possible that the rupture at ground surface was *en echelon* with respect to that in the tunnel.

### **3.3. Southern Pacific Railroad Tunnels, Kern County, California**

In 1952, an earthquake of M 7.7 occurred in Kern County, and was related to strike-slip displacement along the White Wolf Fault. Tunnels Nos 3,4,5 and 6 on the Southern Pacific Railroad between Tehachapi and Bakersfield were seriously damaged (Figure 3.3). The tunnels were located in an area where fault displacements occurred during the earthquake, presumably on an extension of the White Wolf Fault (Kupfer *et al.* 1955).

The tunnels were originally timber-lined. In 1921 they were relined with a reinforced concrete liner placed over the original wood liner. The concrete liner was between 300mm and 600mm thick, with reinforcing concentrated along the intrados. Tunnel walls do not appear to have been connected to the invert and much of the shaking damage was due to different response of walls and invert. The tunnels had limited cover and were close to the side of a valley, which may have led to localised effects during strong ground shaking.

Tunnel No. 3 was most severely damaged near the south portal where the track was shortened and rails buckled. In some areas rails were found under the tunnel wall, indicating that during the earthquake, the wall lifted sufficiently to allow the rail to slide under

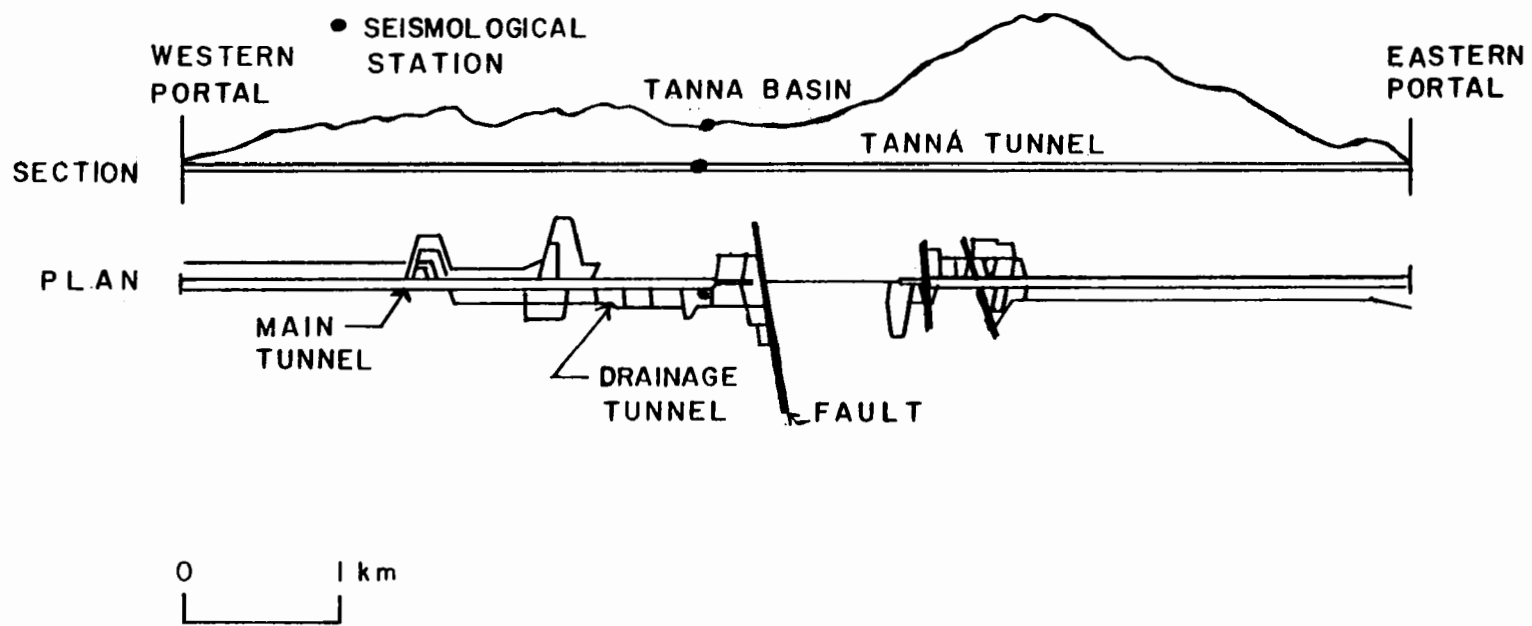


FIGURE 3.2 Tanna Tunnel, showing relation of active fault to tunnel construction (after Nasu, 1931).



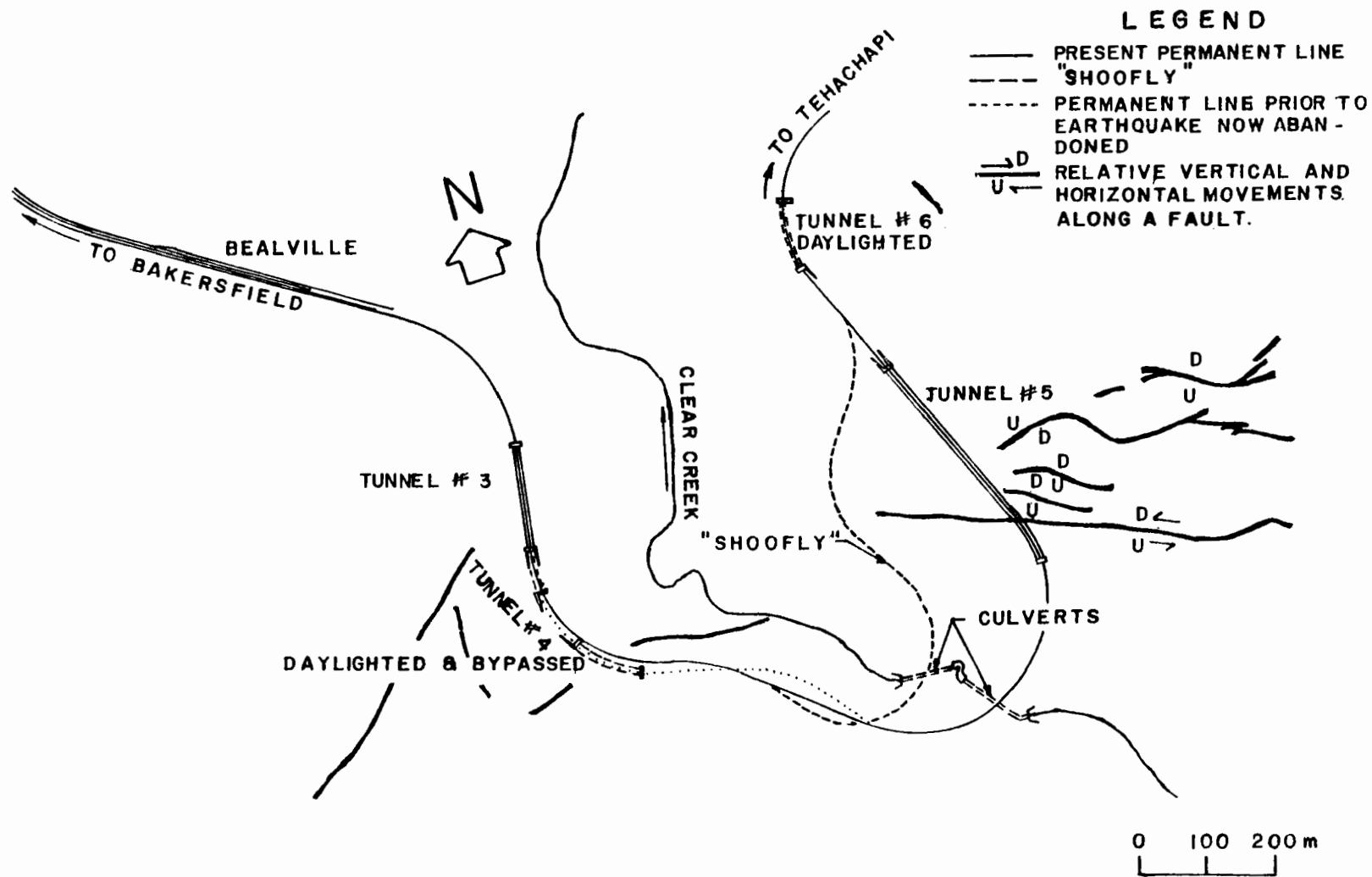


FIGURE 3.3 Southern Pacific Railroad tunnels, Kern County, following 1952 earthquake (after Steinbrugge and Moran, 1954).

(Steinbrugge and Moran, 1954).

Surface cracks were found over the top of Tunnel No 4. This tunnel was extensively damaged and it was by-passed by an open cut for its full length during reconstruction. In the tunnel a 1.22m vertical displacement was found, while directly above the tunnel there was a fissure with practically no vertical offset. The distance between the portals of Tunnels Nos 3 and 4 may have been reduced by up to 1m.

Surface cracks also appeared over Tunnel No. 5 which was extensively damaged. No apparent surface cracks were observed near Tunnel No. 6 which was damaged and subsequently replaced with an open cut.

Other tunnels further away from the fault zone suffered only slight damage due to shaking, generally consisting of opening of construction joints.

#### **3.4. Balboa Inlet Tunnel, San Fernando, California**

The partially completed Balboa Inlet Tunnel of the Metropolitan Water District of Southern California was affected by the San Fernando M 6.6 earthquake of 1971 (Dowd, 1974). The Santa Susana Thrust Fault, along which displacement occurred during the earthquake, crossed the tunnel about 300m from a portal. The reinforced concrete liner was cracked and there was some spalling along a 90m section at the fault crossing. There was also longitudinal cracking in the tunnel liner for some 300m on each side of the fault. The Santa Susana Fault had been inactive since the Middle Pleistocene, and was not considered to be related to faults that were active during the earthquake. Movement along the Santa Susana Fault was considered to be due to the response of an existing fault to stress changes originating in another near-by active fault system (Saul, 1975).

### 3.5. Inatori Tunnel, Japan

On January 14, 1978, an earthquake with a surface wave magnitude of  $M_s$  6.8<sup>1</sup> occurred to the east of the Izu Peninsula (Shimazaki and Somerville, 1978). Surface rupture, *en echelon* in a zone from 30m to 200m wide, was traced for about 3km. There was a maximum of 1.83m right lateral strike-slip with 260mm dip slip component on a steeply dipping fault.

The Inatori railway tunnel crossed the fault at right angles, with a cover of 90m. Over a 20m length, the tunnel had been displaced right-laterally 500 to 700mm (Figure 3.4). This movement caused extension of the tunnel, most of which was believed to have occurred about 120m away from the fault. Horizontal striations were found on the rock behind the concrete liner when the liner was removed for repair. It was inferred by Tsuneishi *et al.* (1978) that the liner was displaced 200mm longitudinally relative to the surrounding rock over a distance of 120m.

### 3.6. San Pablo Tunnel, Contra Costa County, California

The San Pablo tunnel is owned by East Bay Municipal Utility District (EBMUD), and is used to transport water through the Berkeley Hills from the San Pablo reservoir. The tunnel was constructed in 1917-1920, is 4134m long and in cross section is about 2.29m high by 2.44m wide.

A longitudinal section which shows the geology mapped during construction, is given in Figure 3.5. The San Pablo tunnel crosses two major fault zones, the Hayward Fault, and the Wildcat Fault, as well as several unnamed faults. During construction, the Hayward Fault was encountered between 70m and 100m below ground surface. Louderback (1942) described the material in the fault zone :

"...the serpentine is so sheared that it flowed under its own weight into the tunnel like a

<sup>1</sup> surface wave magnitude is more or less equivalent to Richter magnitude.

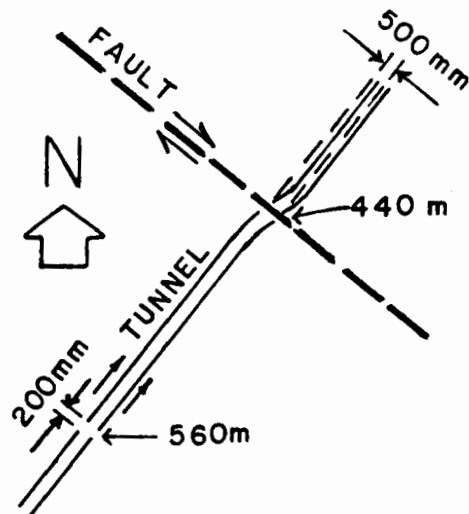
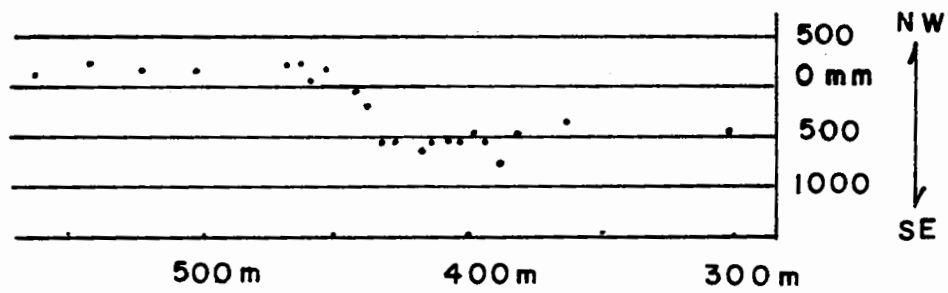


FIGURE 3.4 Deformation of Inatori Tunnel, Japan as a result of the 1978 earthquake (after Tsuneishi *et al.*, 1978).

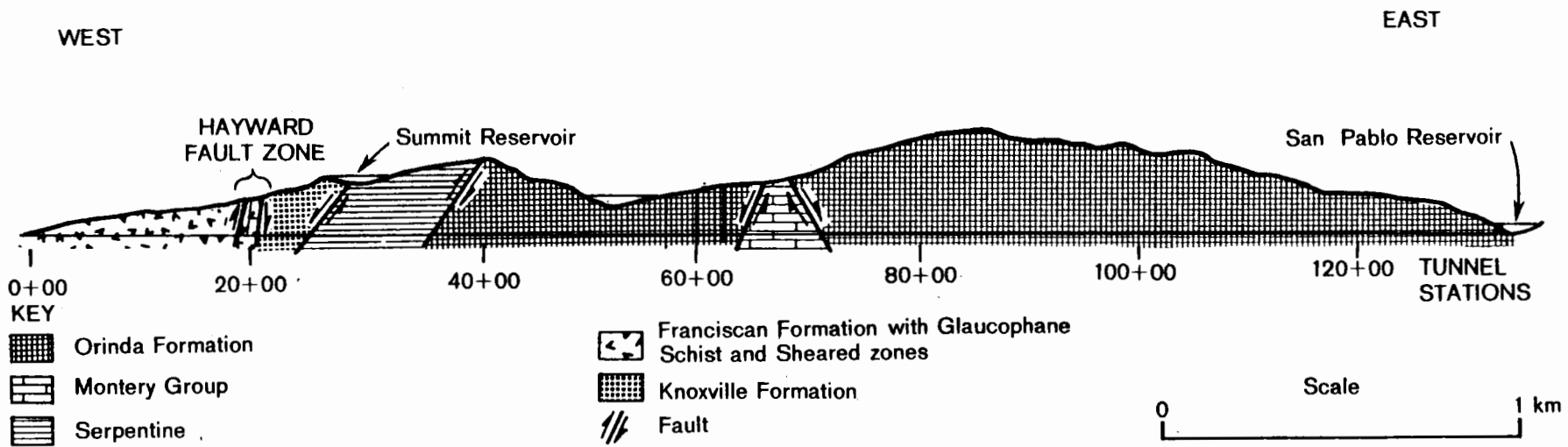


FIGURE 3.5 Section along San Pablo Tunnel through Berkeley Hills (after East Bay Municipal Utility District Drawing 235-P).

viscous liquid and presented a serious problem of control. Parts of the Franciscan Formation there were thoroughly sheared and traversed by innumerable slickensided surfaces, and again with harder residuals, such as masses of crystalline schists, floating in the midst of the sheared weaker material."

In 1933 a major break in the unreinforced concrete liner occurred between Station 20+49 and 22+54. To repair the tunnel, a 1.83m diameter reinforced concrete liner was constructed with circumferential 32mm diameter reinforcing bars at 152mm centres, and longitudinal 19mm diameter reinforcing bars. In 1952-53, further repairs to the tunnel were necessary. The invert was removed and replaced, and a new liner constructed inside the existing liner. In 1969, Burton H. Marliave, consulting geologist to EBMUD, inspected the tunnel and noted a circumferential crack at Station 32+20, and longitudinal cracks at Stations 63+80 and 66+10. At this time, control points were set up for future alignment checks. The tunnel has not been surveyed since (J.C. Dalton, pers. comm.). However, during an inspection in February 1978, apparent horizontal distortion was noted between Stations 86+50 and 87+00.

### **3.7. Claremont Tunnel, Alameda Co., California**

The Claremont water tunnel is part of the EBMUD Mokelumne River Project. It is 5507m long and is located at an elevation of 99m at the west portal (c.f. BART tunnels west portal elevation of 88m about 245m to the south).

Construction of the tunnel has been described by Young (1929). Geology mapped during tunnel construction is shown on a longitudinal section (Figure 3.6). The tunnel has a horseshoe cross section, the arch having a 1.37m radius. Invert and sidewalls have 2.74m radii with their centres on the intrados of the arch. Temporary timber supports were used during construction. Where necessary, a 50mm lagging was used with 200 by 200mm timbers for the walls and arch, or with 300 by 300mm timbers completely around the cross

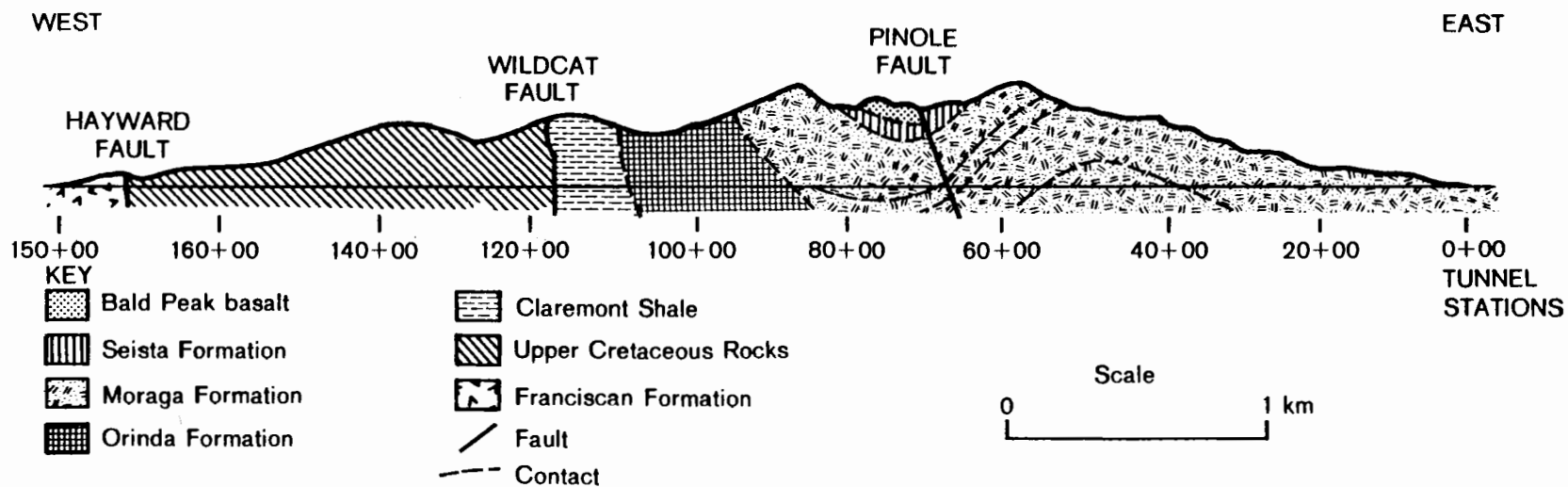


FIGURE 3.6 Section along Claremont Tunnel through Berkeley Hills (after East Bay Municipal Utility District Drawing DH 2120-35).

section where "swelling"<sup>2</sup> ground was encountered. A 300mm thick concrete liner was used in the untimbered section and a minimum concrete thickness of 355mm in the timbered sections.

Apart from the short sections in heavy ground, the tunnel was not reinforced. Reinforcing steel, where used, consisted of 19mm diameter bars at 380mm centres along the inner face, and in walls and invert along the outer face. Longitudinal steel consisted of 12mm diameter bars at 460mm centres. Following completion of the concrete liner, cracking of the unreinforced liner was noted. The cracks were longitudinal, up to 30m long, and occurred mainly in sidewalls between the spring line and a level 1m to 1.2m below. They were located in areas where high ground pressures would be expected, based on the nature of the geological formation.

The tunnel crosses the Hayward Fault near the west portal. During a routine inspection in 1964, the concrete liner in the fault zone was found to be cracked and the invert was buckled (Blanchard and Laverty, 1966). The tunnel alignment was surveyed and 168mm of right lateral offset since construction in 1929 was measured. Changes in elevation since tunnel construction were also measured (Figure 3.7). The tunnel section in the Hayward Fault was relined, as were some other damaged sections in the eastern part of the tunnel.

---

<sup>2</sup> Although the reports from the construction period use the term swelling ground, based on experience in similar geology in the nearby BART tunnels it is considered likely that the ground was squeezing rather than swelling, or a combination of both.



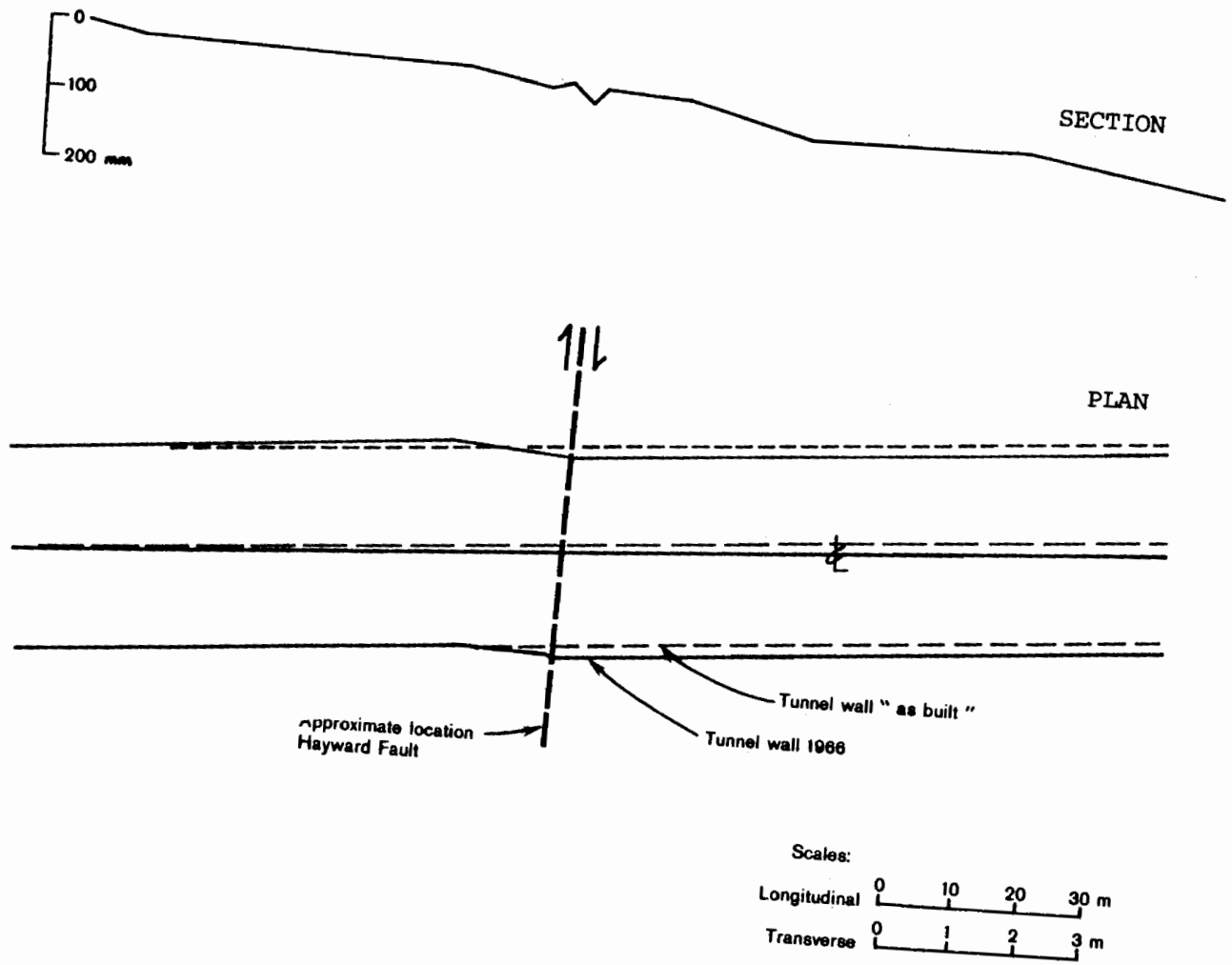


FIGURE 3.7 Claremont Tunnel, liner offsets and changes in level across the Hayward Fault (after East Bay Municipal Utility District Drawing 1551-R).

## CHAPTER 4

### DESIGN CONSIDERATIONS FOR TUNNELS THAT CROSS ACTIVE FAULTS

#### **4.1. Site Investigations**

The nature of an active fault and phenomena that may damage tunnels crossing active faults were discussed in Chapter 2. For tunnel design purposes it is necessary to make a quantitative assessment of these phenomena. The following factors need to be considered: the geometry of the fault zone, the properties of fault zone materials, the average recurrence intervals of damaging ground shaking and fault rupture, and rate of fault slip-page.

##### **4.1.1. Geometry of fault zone**

Geological mapping on a regional scale can establish the location of the fault zone, its tectonic setting, and sense of displacement. Detailed geological mapping is necessary to define fault width, the location of fault traces, and the dimensions of past displacements. Shallow trenching across the fault zone is commonly used to identify the most recently active fault plane or planes of movement, and the width of the disturbed fault zone.

##### **4.1.2. Properties of fault zone materials**

Conventional geotechnical sampling and testing procedures can be used to determine the physical and mechanical properties of fault zone materials. The nature of fault gouge, i.e. highly sheared, heterogeneous mixtures of clays and variably weathered rock fragments, may cause difficulties with sampling and testing. Strength testing should enable an

assessment of whether squeezing ground will be encountered during tunnel excavation.

Howard (1972) used a definition of gouge that "includes all materials within a fault zone or seam regardless of whether the material has been altered to a different mineralogy during or after faulting." His definition was adopted for this study. The gouge material in a given zone may reflect several stages of genesis throughout geological time, and is therefore quite complex in composition and properties.

#### **4.1.3. Earthquake recurrence intervals**

Average earthquake recurrence intervals are based on the records of historic earthquakes. In California this approach is limited by the short period over which records are available, and longer-term periodicity may not be recorded. Detailed studies of Quaternary geology, including the dating of surfaces and geological materials, can extend the history of large magnitude earthquakes and improve the estimate of average recurrence intervals for such events. The use of such studies has been well demonstrated by Sieh (1977) who was able to date large magnitude earthquakes that occurred in pre-historic times along the San Andreas Fault in Southern California.

#### **4.1.4. Rate of fault slippage**

Definitions of active faulting as described in section 2.1, do not include the degree of fault activity. Where adequate data are available, a curve of amount of fault slip against time may be constructed (Figure 4.1). It is important to assess whether fault movements occur as slow slippage, or whether displacements are associated with infrequent earthquakes. If the latter, whether large, very infrequent earthquakes produce the same total displacement as smaller ones that occur more frequently.

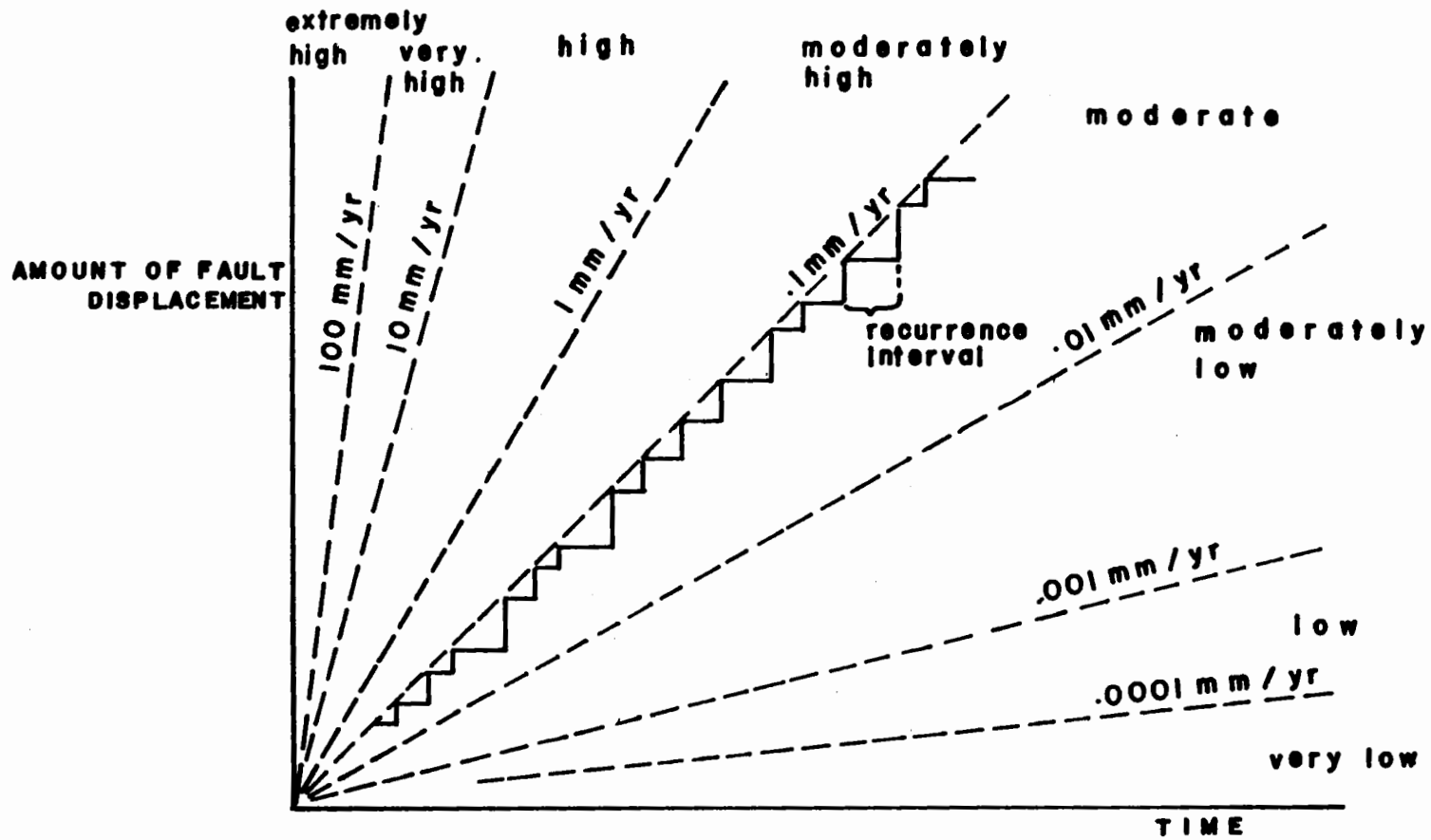


FIGURE 4.1 Fault activity defined by slippage rate (after Cluff, 1978).

#### **4.2. The Design Earthquake**

For engineering design purposes a "design earthquake" or "design event" is commonly used to describe the earthquake magnitude, associated fault displacement, and ground accelerations that should be considered. When the earthquake magnitude is based on an interval of time, it is referred to as the maximum probable earthquake. When it is selected without regard to a time interval, it is called the maximum credible earthquake.

The method used to select the maximum credible earthquake is to estimate the length of rupture that could occur on the fault, and to use a length-magnitude relationship to estimate earthquake magnitude. Relationships of fault displacement and earthquake magnitude can be used to estimate fault displacement. Examples of length-magnitude, and magnitude-fault displacement relationships based on historical earthquake data, were described by Taylor and Cluff (1977).

The maximum probable earthquake is generally based on considerations of regional seismicity. It will have a magnitude at least as great as the maximum historic earthquake. This concept allows selection of an earthquake magnitude which may be significantly lower than the maximum credible earthquake, however there is a risk that the maximum probable earthquake could be exceeded during the design life of the structure.

For a tunnel that crosses an active fault, the most important parameter to assess for design purposes, is amount and sense of fault displacement.

#### **4.3. Static Design Criteria**

The initial stage in design of a tunnel that crosses an active fault, is the design of a liner that will withstand the expected static loads. Various empirical and analytical methods of calculating interaction between ground and tunnel support system are available, and their application to design is well established.

High loading of the tunnel liner may be caused by squeezing ground, although squeezing ground is primarily a problem during tunnel construction. By the time a final liner is installed, the temporary support system may be in equilibrium with the surrounding ground. In that case, loading of the tunnel liner is not expected to increase with time due to squeezing.

When fault dislocation occurs, either due to slippage or rupture during an earthquake, the loading on the tunnel will change. The magnitude and direction of loading will depend upon sense of fault movement relative to tunnel orientation, and the length of tunnel over which distortion takes place. One design criterion in such cases might be that the tunnel should be able to withstand a specified amount of distortion before the liner loses its support capacity, or the tunnel becomes unserviceable.

#### **4.4. Seismic Design Criteria**

When a fault ruptures a tunnel, it is desirable that any structural damage resulting from strong ground shaking is minimal. Seismic loading acts only for a short period, and is in addition to loads that may develop due to fault displacement.

Various theoretical studies have considered the seismic response of tunnels. Generally, only a simplified analysis of the problem has been attempted (Emery and Joshi, 1980 ; Owen *et al.*, 1979 ; Shukla *et al.*, 1980 ; Weidlinger and Nelson, 1980). Exact solutions for vibration of an idealised tunnel were obtained by Lee and Trifunac (1979), however the simplicity of their model limits the application of this work to tunnel design. Owen *et al.* (1980) presented a thorough discussion of the problems of undertaking a dynamic analysis of a tunnel.

Empirical studies of seismic response of tunnels (Duke and Leeds, 1959 ; Dowding and Rozen, 1978) indicated that tunnels generally behave better than surface structures during strong ground shaking. Cases where tunnel damage has occurred during an earthquake are generally confined to unlined, and unreinforced concrete lined tunnels. By

implication, well designed and constructed tunnels have a high resistance to earthquake damage.

#### **4.5. Designs Used for Tunnels That Cross Active Faults**

In the case histories described in Chapter 3, as far as can be determined, none of the tunnels had been designed to take into account possible fault movements. In no case does it appear that the activity of the fault was recognised prior to construction.

From a careful review of the literature, no tunnels can be identified where special designs have been undertaken for sections in an active fault zone. Rosenblueth (1977) suggested a design where a double tunnel is constructed through the fault zone with sufficient clearance that the smaller diameter tunnel may rotate at special joints, but will not shear (Figure 4.2). It is not known whether this concept has been used in practice.

The Californian State Water Project system crosses active faults in the Tehachapi Mountains. Rather than cross these faults in tunnels at great depth with difficult construction problems and a high risk of damage due to subsequent fault slippage, an aqueduct was constructed close to ground surface, even though this decision resulted in high pumping costs. It was considered desirable that structures crossing active faults can be repaired relatively easily when necessary (California Department of Water Resources, 1974).

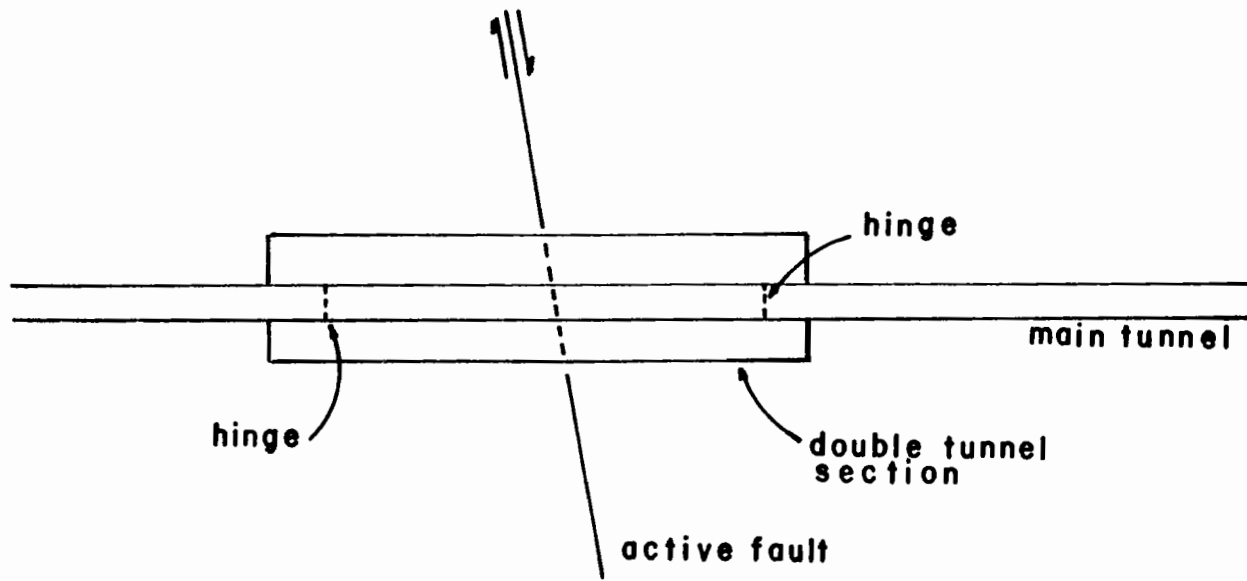


FIGURE 4.2 Special tunnel design for an active fault zone (after Rosenblueth, 1977).



## CHAPTER 5

### GEOLOGY OF THE BERKELEY HILLS NEAR THE BART TUNNELS

The geology of the Berkeley Hills has been described by Case (1963, 1969), Radbruch (1969) and others. Prior to construction of the BART tunnels, a geological study made of the tunnel alignment included surface mapping, cored drill holes, and two exploration adits from both portal sites. During tunnelling, a log was compiled at a scale of 1:240 which showed lithology and structure, as well as details of tunnel excavation and temporary support. A detailed account of the geology of the tunnel alignment was given in a report by Bechtel Incorporated (1968).

A geological map of the area is given in Figure 5.1 (after Radbruch, 1969). This is the most recently published map of the Berkeley Hills, but may be inaccurate in some places. For instance, many of the NE-SW striking faults are significant secondary faults and have greater continuity than shown on Figure 5.1 (R.E. Goodman, pers. comm.). A cross section through the Berkeley Hills along the tunnel alignment was drawn by Bechtel Incorporated (1968) following completion of tunnel excavation (Figure 5.2).

#### 5.1. Stratigraphy

The stratigraphic nomenclature used follows that of Radbruch (1969).

Franciscan Formation (KJfs) (Upper Jurassic?, Cretaceous)

A grey, fine to medium grained sandstone (greywacke) with scattered sheared shale interbeds. The sandstone is generally blocky and moderately strong. The shale is sheared, and often contains clay gouge, and crushed sandstone fragments.

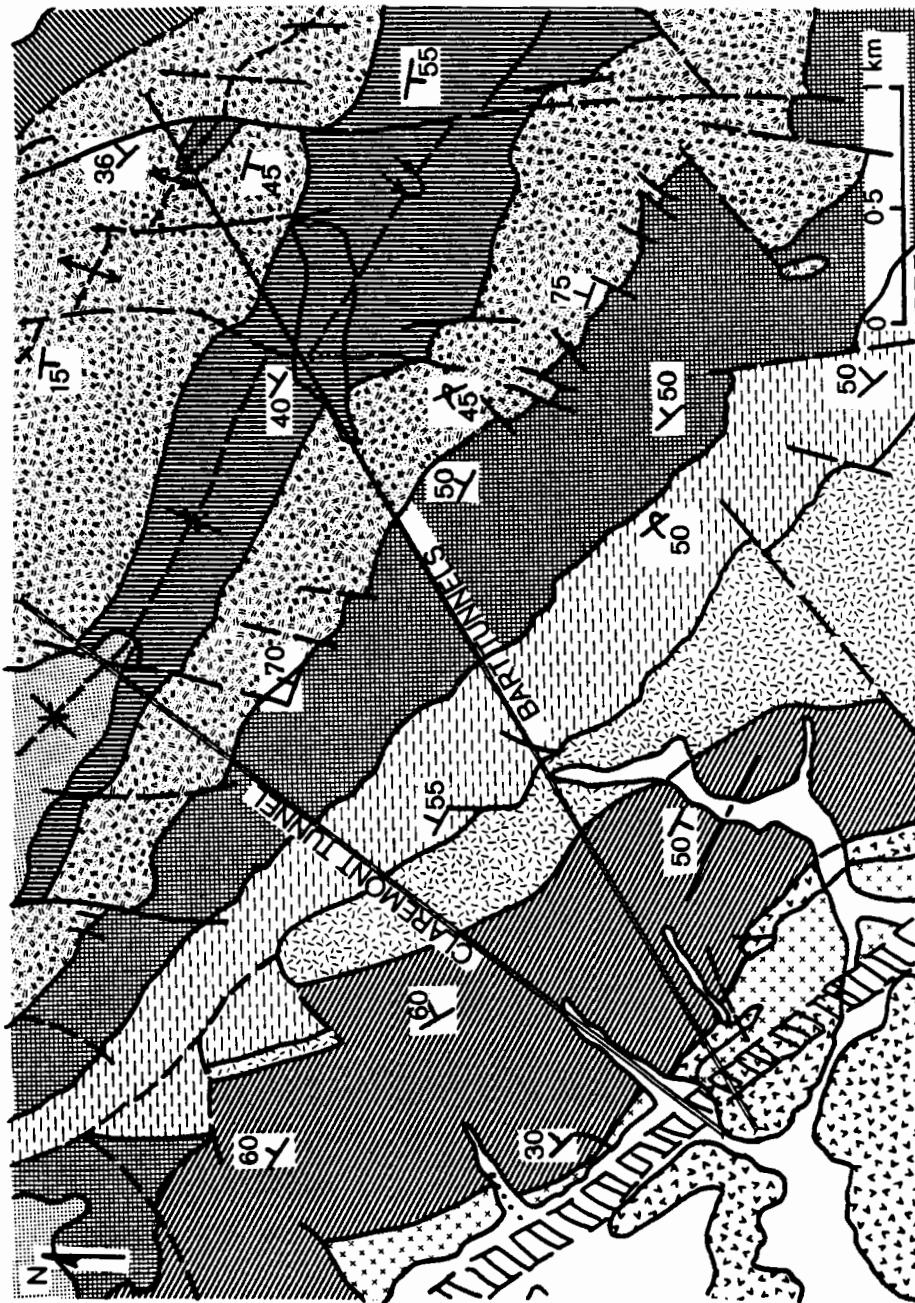











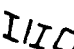

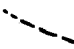


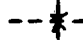
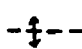


FIGURE 5.1 Geological map of Berkeley Hills near BART tunnels (after Radbruch, 1969).

KEY			
	Q al Alluvium and Fill		
	T L Leona Rhyolite		
	T b p Bald Peak Basalt		
	T s Siesta Formation		
	T c u Contra Costa Group		
	T m Moraga Formation		
	T o r Orinda Formation		
	T C Claremont Shale		
	T u Undifferentiated Tertiary Rocks		
	K u Upper Cretaceous Rocks Undivided		
	K j f s Franciscan Formation		
	Hayward Fault Zone		50 Strike and Dip
	Fault		45 Strike and Dip of Overturned Beds
	Contact		Syncline
			Anticline

Key for Figure 5.1.

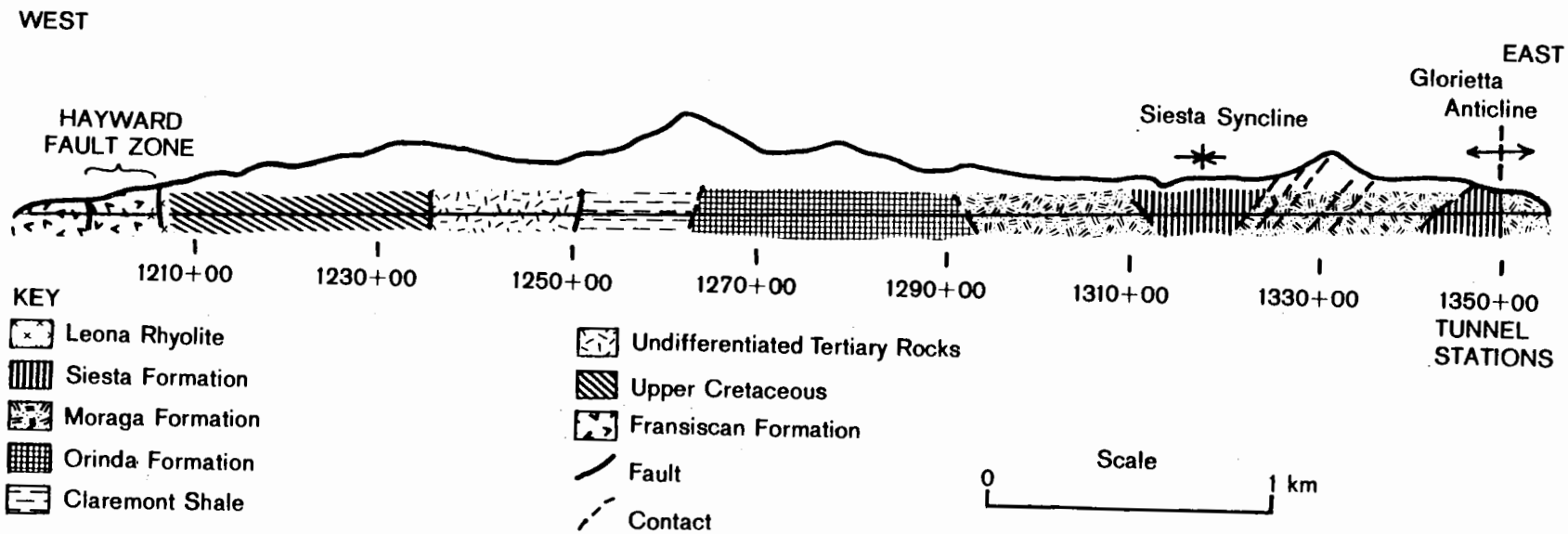


FIGURE 5.2 Section along BART tunnels through Berkeley Hills (after Bechtel Incorporated, 1968).

#### Upper Cretaceous rocks, undivided (Ku) (Upper Cretaceous)

Undivided Cretaceous rocks are mainly interbedded sandstones and shales. The sandstone is grey, fine grained with scattered biotite grains, and is moderately strong. These rocks are generally thin-bedded with occasional massive beds of blocky, jointed sandstone. Shale is black, soft, and generally crushes to sand sizes along closely spaced fractures.

#### Undifferentiated Tertiary Rocks (Tu) (Eocene - Miocene)

The contact between Undifferentiated Cretaceous and Undifferentiated Tertiary rocks in the tunnels is sheared and gradational. The rocks are mainly grey, fine grained, moderately strong sandstones, and soft, slaking shales. This unit includes the Sobrante Sandstone (Tso) of the Monterey Group. There are occasional diabase and sandstone dykes, and thin beds of chert. Beds are generally highly contorted, lenticular and sheared.

#### Claremont Shale (Tc) (Miocene)

Claremont Shale consists of thin-bedded opaline chert and siliceous shale that has been intruded by diabase and sandstone dykes. The chert is brown coloured, brittle and highly fractured. Many chert beds are banded, lenticular, and between one and 50mm thick, with an occasional bed up to 600mm thick. Siliceous shale is brown coloured, varies in strength, and in many places contains thin clay seams. The formation is overturned and dips at a high angle towards the west portal.

#### Orinda Formation (Tor) (Pliocene)

The Orinda Formation consists of siltstone, sandstone and conglomerate with common graded beds. Siltstones are generally massive, moderately strong, but susceptible to slaking. The sandstone is grey coloured, fine-grained, moderately strong and blocky. The conglomerate is generally massive, contains gravels up to 300mm in diameter, and ranges from friable to well cemented.

#### Moraga Formation (Tmb, Tmc) (Pliocene)

The Moraga Formation includes rocks of sedimentary (Tmc) and volcanic (Tmb) origin. Basalt, flow breccia, and tuff were logged as individual units in the tunnel logs, except where they are completely intermixed. The basalt is strong, brittle, and blocky. The flow breccia is red coloured, moderately strong, massive, and contains scattered calcite seams. Tuff is blue and black, fine to medium grained, blocky, and moderately strong. The sedimentary rocks include siltstone, sandstone, and conglomerate. Siltstone has low to moderate strength, is blocky, and slakes. Sandstone and conglomerate are moderately cemented; the sandstone is blocky, the conglomerate is massive. Graded beds are common in the sedimentary rocks, and contacts between volcanic rock types are irregular.

#### Siesta Formation (Ts) (Pliocene)

The Siesta Formation was encountered in the axis of the Siesta Syncline, and comprises interbedded siltstones and sandstones. The siltstone is grey and red, low to moderate strength, contains clay seams and scattered shear zones, and slakes. The sandstone is fine grained, moderately cemented and blocky.

#### Leona Rhyolite (Tl) (Pliocene)

Leona Rhyolite is a silica rich volcanic rock which varies in strength due to the effects of hydrothermal alteration. It is greenish-grey when fresh, contains disseminated pyrite, and may slake. Locally it is brecciated, but its general behaviour is that of a blocky to massive rock.

## 5.2. Structure

The structure of the Berkeley Hills is complex and reflects the style of tectonic deformation that continues to the present. Figure 5.3 shows the major faults and folds in the Berkeley Hills area (after Radbruch and Case, 1967). The most important structural feature is the Hayward Fault zone, along which major right-lateral, as well as some vertical

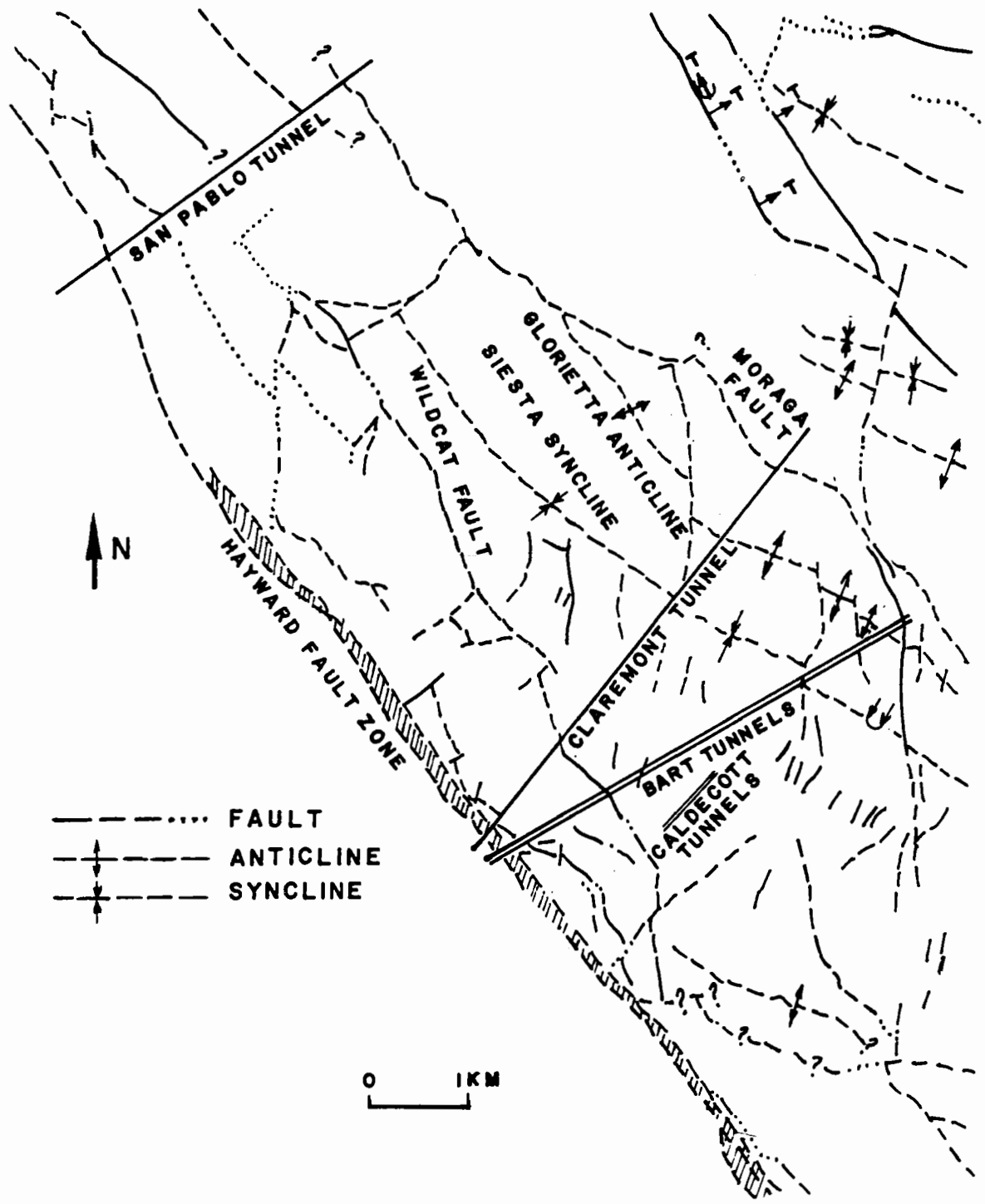


FIGURE 5.3 Structural map of the Berkeley Hills (after Radbruch and Case, 1967).

movement has occurred. Other structural features are considered to have developed with orientations consistent with the tectonic stress field that produces right-lateral slip along the Hayward Fault (Moody and Hill, 1956). These features include the NW-SE trending fold axes (Siesta Syncline, Glorietta Anticline), the NW-SE trending faults (Chabot Fault, Wildcat Fault), and the NE-SW trending faults.

Rocks encountered during construction of the BART tunnels were variably sheared and deformed, indicating a complex history of folding and faulting. Upper Cretaceous rocks were highly contorted and sheared, characterised by slickensided surfaces with minor amounts of clay gouge and crushed rock, principally along shale beds, although some shear zones cut across bedding. Undifferentiated Tertiary rocks were similarly sheared. It was considered by the geologist who logged the tunnels during construction (C.I. Trantham) that the slickensides and minor clay gouge and crush zones between Stations 1236+00 and 1238+70 in the C1 tunnel, and Stations 1236+80 and 1239+30 in the C2 tunnel, might be related to a southward extension of the Wildcat Fault.

Towards the eastern portal, the tunnel crosses the axes of the Siesta Syncline and the Glorietta Anticline, and the Orinda, Moraga, and Siesta Formations are deformed by these structures. In this area, numerous faults were inferred from slickensides, clay gouge, and crushed rocks. These faults were mainly parallel to the bedding planes. The tunnel crossed the axis of the Siesta Syncline where it is intersected by a major fault. At this location, the Siesta Formation was strongly sheared, and squeezing ground was encountered for about 100m.

### **5.3. Hayward Fault**

The tectonic setting of the Hayward Fault is similar and related to that of the San Andreas Fault. The San Andreas, and other north-south trending right-lateral strike-slip faults, delineate the boundary between the North American and Pacific plates (Figure 5.4).



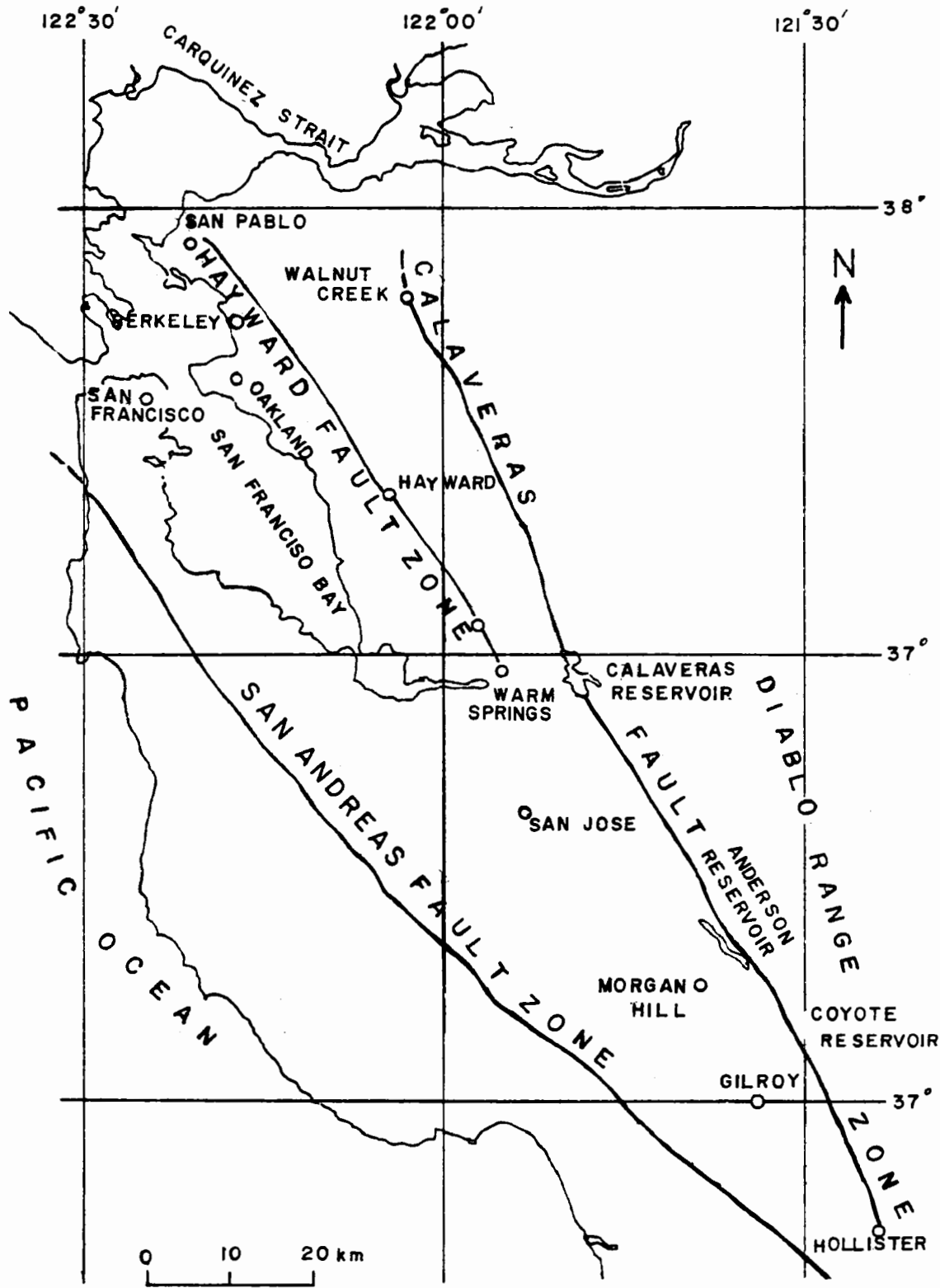


FIGURE 5.4 Major right-lateral strike-slip faults in the San Francisco Bay Area.

The Hayward Fault is at least 80km long and has been mapped from Warm Springs in the south, to San Pablo in the north (Radbruch-Hall, 1974). The surface expression of the Hayward Fault is that of a wide fault zone with characteristic offset streams, spring lines, scarps, and sag ponds, which generally delineate the western front of the hills bordering the east side of San Francisco Bay. The zone in which recent movement has taken place ranges in width from approximately 150m, south of Lake Temescal, to about 2.7km near the Mission San Jose district.

In the Berkeley area, the Hayward Fault zone has been mapped at a scale of 1:24,000 (Radbruch-Hall, 1974). In the vicinity of the BART tunnels, two traces were mapped. These traces are shown to continue to the north, crossing the EBMUD Claremont water tunnel. The eastern trace continues through the University of California Memorial Stadium. Recent investigators (University of California, 1978) have mapped a straight-line fault trace extending from slightly north of the BART tunnels, to the north side of the University of California campus. This fault trace does not coincide with that located in the BART tunnels, and in the EBMUD Claremont tunnel. It was located as a straight line over differing topographies to indicate the vertical nature of the Hayward Fault. While the Hayward Fault on a regional scale is believed to be essentially vertical, near the ground surface where there is reduced confining pressure, fault rupture is able to propagate in directions that reflect the variability of material properties. Thus it is possible that there are deviations from a straight-line trace on a local scale.

The location of active traces of the Hayward Fault were also mapped by Herd (1978). In the Berkeley area, he considered that widespread landslide movement may have given rise to features that have been attributed to fault slippage. At the University of California campus, Herd noted that a prominent south-west facing scarp near Bowles Hall, and damage to Memorial Stadium, could be due to landsliding.

Surface ruptures have occurred along the Hayward Fault during earthquakes; from Mission San Jose to San Pablo in 1836, and from Warm Springs to Berkeley in 1868 (Radbruch, 1967a). Movement has been both vertical and horizontal, with most of the recent movement right lateral. During the 1868 earthquake there was an estimated 1m of horizontal movement, and 500mm of vertical movement (Radbruch, 1967b). Seismicity on the Hayward Fault has been relatively low in the past 45 years, with only four earthquakes of magnitude 4.0 or greater (Table 5.1). The magnitude of the earthquake of October 21 1868, has been estimated at 6.5 (Nason, 1971).

Since January 1969, the United States Geological Survey has maintained a catalogue of earthquakes recorded by a network of 230 seismographs located in central California (McHugh and Lester, 1979). In the period from January 1969 to January 1980, approximately 188 earthquakes were recorded along the Hayward Fault zone within 15km of the BART tunnels, with magnitudes ranging from 0.35 to 3.38. Epicentre locations for all earthquakes recorded in this period are shown in Figure 5.5. Many of the earthquake epicentres lie along a zone coincident with the Hayward Fault. There is a cluster of epicentres to the north-east of the BART tunnels representing the Briones Hills earthquake swarm of January 1977 (Bolt *et al.*, 1977). Focal depths for these earthquakes varied from 0.37km to 14.36km; most focal depths were in the range of 3km to 10km.

Fault slippage measurements at various locations along the Hayward Fault have been undertaken by the U.S. Geological Survey. Creepmeters (wire or rod extensometers) spanning an active trace, have been installed in the Hayward and Fremont areas. A survey array to detect potential movement along multiple fault traces was placed across the width of the fault zone at Pinole Point. The results of this work have been reported by Yamashita *et al.* (1973), and Schultz *et al.* (1976).

The University of California Seismographic Station has continuously monitored the change in aperture of a crack in a culvert located under the University of California

## NOTABLE EARTHQUAKES ON THE HAYWARD FAULT, 1836-1965

Date	Magnitude	Maximum Intensity*
10 June 1836		VIII
21 October 1868		X
17 September 1888		VII
18 November 1888		VII
31 July 1889		VII
02 January 1891		VII
14 January 1900		VI-VII
11 June 1903		VIII
02 August 1903		VIII
01 July 1911		IX
08 October 1915		VIII
16 May 1933	4.5	VIII
08 March 1937	4.5	VII
27 August 1945	4.5	VI
10 June 1949	4.6	VI
17 December 1954	4.5	V
04 September 1955	5.8	VII

\*Rossi-Forel before 1931, Modified Mercalli thereafter.

TABLE 5.1 Notable earthquakes on the Hayward Fault, 1836-1965 (after Bolt and Marion, 1966).

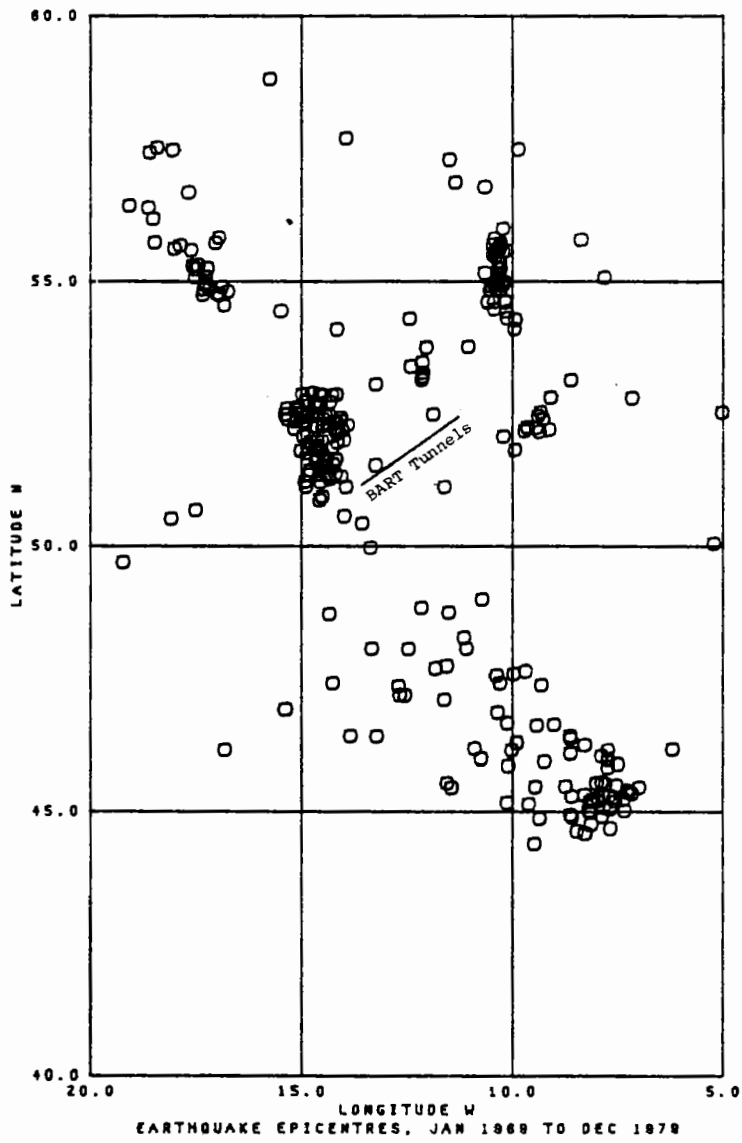


FIGURE 5.5 Epicentres of earthquakes near BART tunnels.

Memorial Stadium and in the Hayward Fault zone (Bolt and Marion, 1966). Between 1965 and 1979, the crack has opened at an average rate of 2.4mm per year (B.A. Bolt, pers. comm.). If the distortion of Memorial Stadium is due to fault slippage, and not intermittent landslide activity, it is likely that only a part of the total fault slippage is recorded because of effects of interaction between soil and culvert structure. National Ocean Survey maintain a survey network at the University of California Memorial Stadium, and it is believed that a slippage rate of 5mm/year observed during the period 1966 to 1969 (Miller 1968, 1970) more closely corresponds to the true slippage rate along that trace of the Hayward Fault. A similar rate at Memorial Stadium has been measured by University of California surveying classes (F.H. Moffitt pers. comm.).

The EBMUD Claremont water tunnel crosses the Hayward Fault close to the BART tunnels (as discussed in section 3.7). Tunnel offsets measured by Blanchard and Laverty (1966) correspond to a rate of fault slippage of 4.8mm per year. Three creepmeters were attached to the tunnel lining in January 1973, but they functioned for a short time only (Schultz *et al.* 1976). A further survey in 1973 indicated that fault slippage was continuing, and that a shortening or compression movement along the tunnel axis across the fault of 39.7mm had occurred between 1968 and 1973 (J. Dalton pers. comm.).

The amount of slippage along the Hayward Fault has been estimated by indirect methods. For example, in built-up areas fault slippage breaks or offsets streets, curbs, sidewalks, culverts (Radbruch and Lennert, 1966), railways (Bonilla, 1966), buildings, pipelines (Cluff and Steinbrugge, 1966), and other structures. Using these data, various estimates are available as to rate of fault slippage. Some of the data refer to displacement of structures that resist fault slippage and can only be considered as a lower bound estimate. Others are based upon measurement of slippage along one fault trace in a wide fault zone, and may also be low estimates. Table 5.2 summarises various fault slippage measurements made along the Hayward Fault. Nason (1971) reviewed available slippage rates and con-

Location	Distance from BART tunnels (km)	Method of measurement	Measurement interval	Right lateral slippage rate (mm/year)	Vertical slippage rate (mm/year)	Reference
San Jose area	65	geodetic network	1951-1963	25		Heade and Small (1966)
		level survey (19.3 km length)	1948-1963		4.33	
Fremont, Prune Ave.	46.8	alignment array, 150 m long (nails in asphalt pavement)	7/28/68 - 1/06/69	9		R. O. Burford, pers. comm.
			7/28/68 - 2/04/70	10		
			7/28/68 - 6/24/70	5		
			7/28/68 - 8/12/71	9		
			7/28/68 - 7/06/72	9		
Fremont, U.S. Gypsum Co.	38.7	2 rod extensometers 12 m long (FMS)	August 1970 - Dec. 1977	3.62		Schultz et al. (1976) R. O. Burford, pers. comm.
Hayward, Palisade St.	25.5	2 rod extensometers 12 m long (RWP 1)	May 1970 - Dec. 1977	3.31		
Hayward, D Street East	24.5	2 rod extensometers 14 m long (RWE)	May 1970 - Dec. 1977	1.10		
Hayward, D Street West	24.5	2 rod extensometers 12 m long (RWW)	May 1970 - Dec. 1977	5.0		
Hayward, Rose St.	23.1	2 rod extensometers 12 m long (RWR)	Nov. 1969 - Dec. 1977	4.75		
BART tunnels	0	alignment survey	Oct. 1976 - June 1979	5.2		
ESMUD Claremont water tunnel	0.2	alignment survey	1935-1968	4.62		J. C. Dalton, pers. comm.
			1968-1973	3.05		
Memorial Stadium, U.C. Berkeley	2.4	Survey network STADIUM	Nov. 1966 - Dec. 1967	4		Miller (1968, 1970)
			Dec. 1967 - Oct. 1969	5		
		LVDT across crack in culvert	Oct. 1965 - Oct. 1979	2.4		Bolt and Marion (1966) B. Bolt, pers. comm.
San Pablo, north of Parchester Village	15.2	alignment array, 189 m long	5/01/68 - 10/27/70	9.58		R. O. Burford, pers. comm.

TABLE 5.2 Hayward Fault--measured slippage rates.

cluded that 5mm to 8mm of right-lateral slip per year was to be expected along the Hayward Fault. For the period 1970 to 1980, Prescott *et al.* (1980) measured a slip rate of 8mm per year. A slip rate of 6mm per year was used by Cluff (1978), who also suggested that maximum slippage during a fault rupture event would be 2m, with a recurrence interval of 300 years.

The detailed structure within the Hayward Fault zone is complex, and is shown at a large scale in Figure 7.1. A significant feature is the various zones of clay-rich gouge. These clay gouges are believed to have formed through the combined process of mechanical crushing of the wall rocks, hydrothermal segregation of phyllosilicates as well as other minerals (Rutter, 1979), weathering, and low grade metamorphism during faulting. Chemical changes are facilitated by mechanical crushing. Nason (1971) analysed samples of clay gouge from the BART Berkeley Hills tunnels and found they contained mostly montmorillonite, serpentine, and chlorite, with minor amounts of amphibole, feldspar, and quartz.



## CHAPTER 6

### DESIGN AND CONSTRUCTION OF BART TUNNELS

#### **6.1. Site Investigations**

The Berkeley Hills tunnels were sited on non-geological criteria, and only the ground conditions around a well defined tunnel alignment were investigated. A total of about 3.1 million dollars was spent on exploration and investigations prior to construction of the tunnels.

Thirty-two NX-sized cored holes were drilled between November 1963 and May 1964, with a total length of about 1524m. These holes were located in portal areas and where depth of cover was shallow. The cores were logged and photographed.

A surface geology map was prepared at a scale of 1:7200, and an interpretative cross section was drawn to show the rock formations that would be encountered during tunneling. The Hayward Fault was located from its topographic expression, and from published geological maps.

The Caldecott tunnel on State Highway 24 crosses the Berkeley Hills to the south-east of the BART tunnels, and at an elevation some 137m higher. During construction of this tunnel in 1963, Bechtel Incorporated geologists logged rock exposed and ground conditions as part of their investigations for the BART tunnels.

#### **6.2. Exploration Adits**

The Board of Consultants for the Berkeley Hills tunnels recommended construction of exploration adits at the east and west portals. These adits were considered necessary to

permit prospective bidders to examine the ground to be encountered, and to develop criteria for tunnel supports. This work was subsequently approved by the Joint Venture Board of Control and the BART District Directors, and a contract for 400,000 dollars was awarded to R.A. Wattson Co. for construction of the adits.

The adits were constructed between May 15 and September 28, 1964. The east adit was 305m long and the west adit was 430m long. The west adit portal was about 27m north of the C2 tunnel centreline, and joined the tunnel alignment at Station 1191+48 (Figure 6.1).

The relationship of the west adit to the full size tunnel is shown in Figure 6.2. It was excavated full face with 1.22m rounds, and was supported with 200mm by 200mm fir timber sets on 1.22m centres. Squeezing ground was encountered in the Hayward Fault zone, and there were water flows of up to 20 litres per second integrated over the length of the adit. Additional support was required in this area; jump sets were installed between the original sets, and diamond-shaped bracing was placed within some of the jump sets.

At locations considered representative of rock encountered, tape extensometer pins and rock movement indicators (RMIs) 0.91m and 3.05m long were located in the walls and crown to measure rock displacements. Load cells were installed between rock and tunnel supports to measure rock loadings at test sites 1 through 6, and within the tunnel supports at test sites 5A. Plate bearing tests were carried out in the eastern portal adit only. The results of the rock testing programme were discussed in a report by Bechtel Incorporated (1966a).

Measurements obtained from the RMIs and tape extensometers showed that in the Franciscan Formation, the rock disturbed by excavation was in general located within 3.05m of the opening, and that 50% to 75% of the movement occurred within the first 1m. Rock movement seemed to stabilise between 5 and 20 days after excavation. In the Hayward Fault zone about one quarter of the total rock movement occurred within the first 1m of

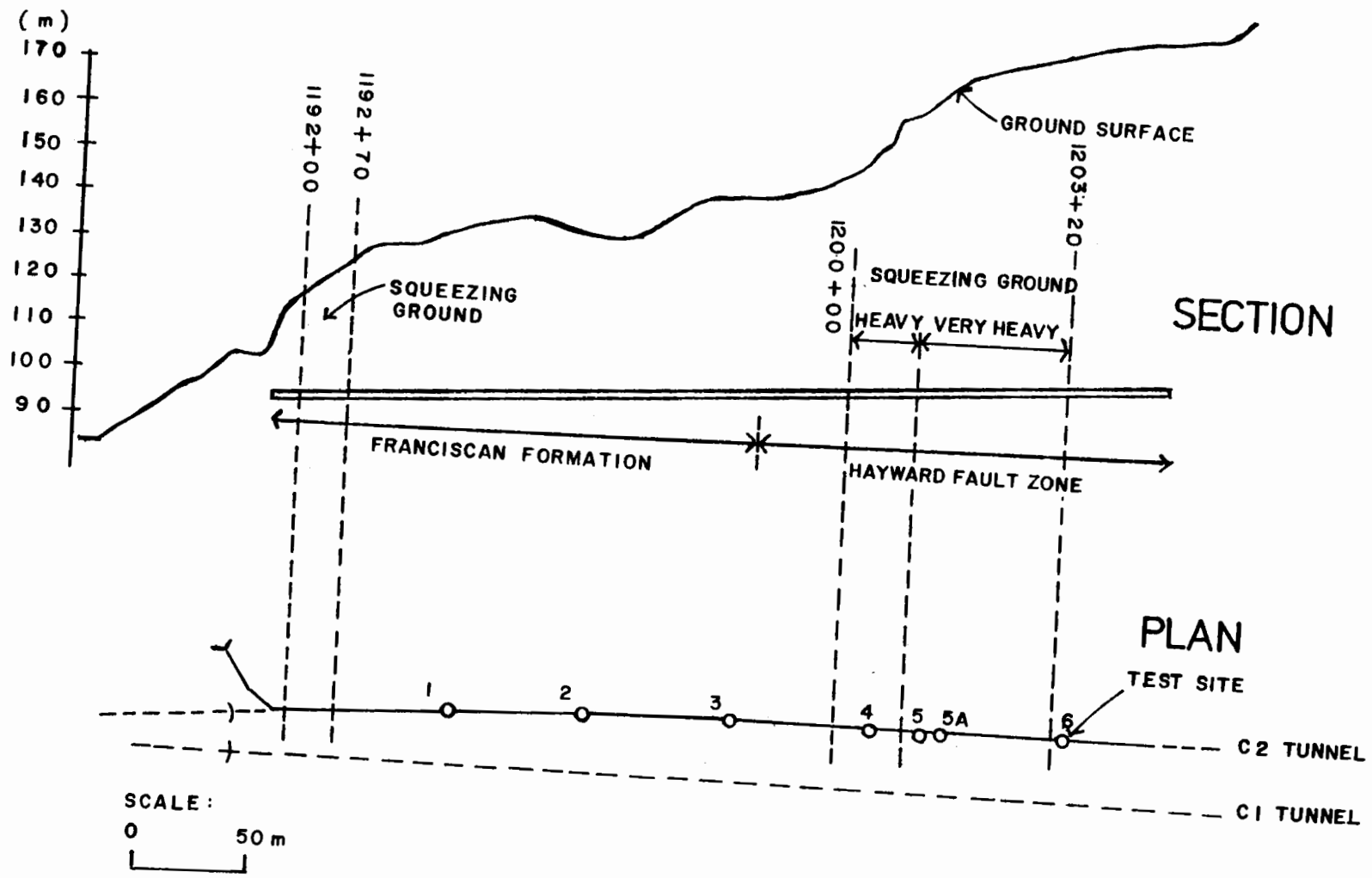


FIGURE 6.1 Plan and section showing ground conditions and instrumentation sites in west portal exploration adit.

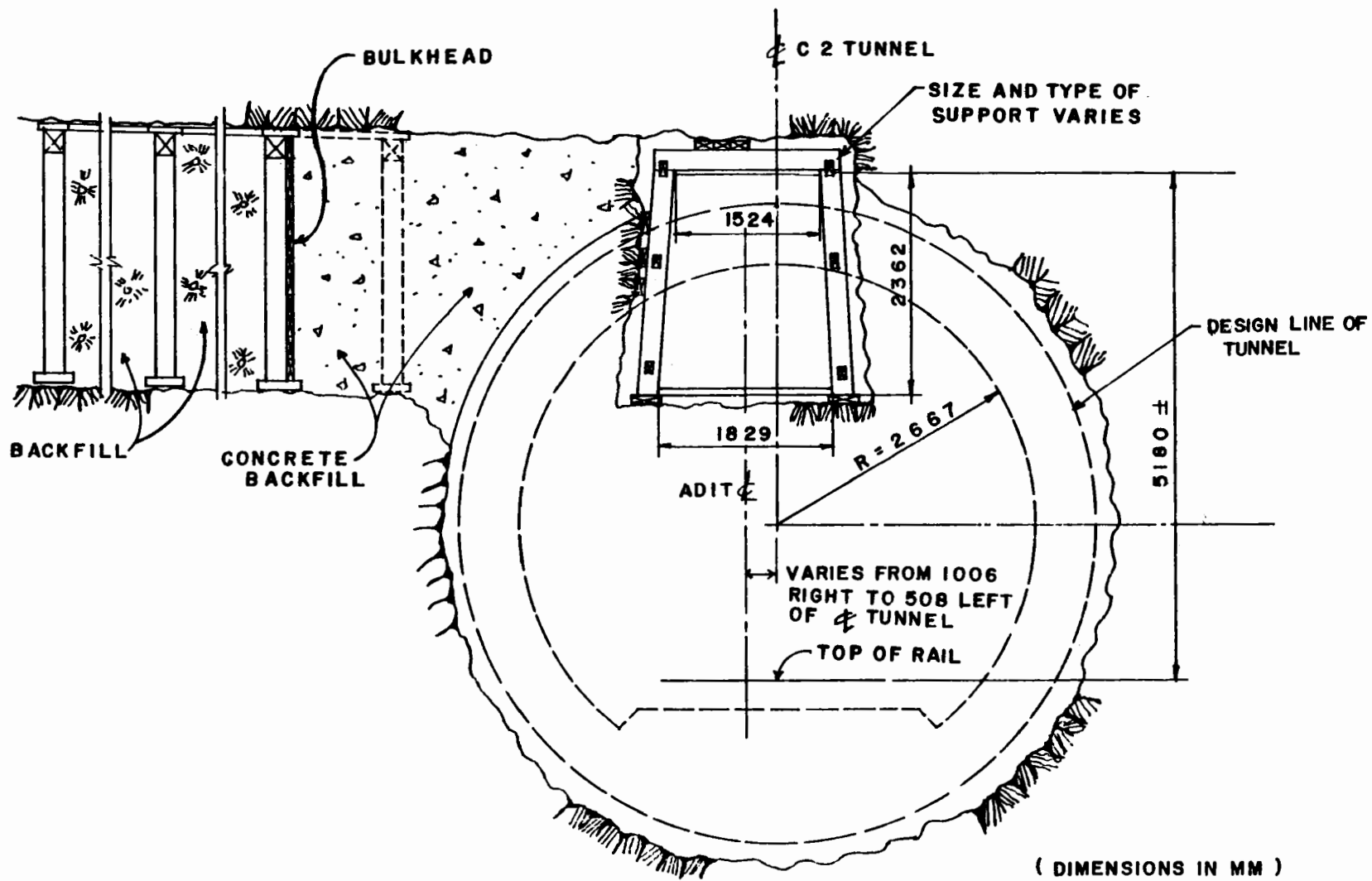


FIGURE 6.2 Position of west portal exploration adit in relation to C2 tunnel.

the excavation. The remaining portion of the movement occurred between 1m and 3m, and perhaps beyond 3m. About one quarter of the total rock movement measured in the Hayward Fault zone occurred within 12 days following excavation, and this was followed by a reduced rate of movement during the monitoring period. These observations are summarised in Table 6.1.

### 6.3. Tunnel Design

From the geological investigations, rock loads were estimated for 19 zones along the tunnel alignment (Bechtel Incorporated, 1964). The Terzaghi load factor (TLF) was used to give the rock load  $H_p$ , where  $H_p = TLF(B+H_t)$ . B is the tunnel width, and  $H_t$  is the tunnel height (Terzaghi, 1946). The values estimated for TLF varied from 0.4 in volcanic rocks to 3.0 in the Wildcat Fault zone. A value of 2.0 was estimated for the Hayward Fault zone. Minutes of the July 29, 1964 meeting of the Board of Consultants indicated that these loads were considered too high, and that lower loads should be used for tunnel design. However the values for the lower loads were not recorded.

The tunnel lining was designed by Bechtel Incorporated who used a method of analysis described by Drucker (1943) (D. Zayakov, pers. comm.). Drucker derived equations from which the lateral passive soil pressure and its effects on the liner thrusts, shears and moments may be calculated for any given set of loading conditions. The analysis was developed for cast iron lined tunnels in soft clays, and considers the lateral resistance to tunnel deformation provided by passive soil pressures. The amount of passive resistance that may develop depends on the horizontal deformation of the tunnel, and the resistance of the soil. Drucker defined a soil constant, K, as the pressure that would cause the soil through which the tunnel was built to compress 25mm. For the BART tunnel design, values were assumed for the rock "compressibility". Rock loads were assumed for the various tunnelling conditions expected, and these were compared with the loads required to

## SUMMARY OF GROUND RESPONSE, WEST PORTAL ADIT

	Hayward Fault Zone	Franciscan Formation
maximum lateral pressure	72 kPa	6 kPa
maximum vertical pressure	45 kPa	10 kPa
time for load to stabilize	> 1 year	few days to 1 month
zone of loosening around adit	25% in first 1 m	50% - 75% in first 1 m
time for deformations to stabilize	25% of total in first 12 days	5 - 20 days

TABLE 6.1 Summary of ground response, west portal adit.

cause failure of the concrete lining. Data from the exploratory adits were not available at the tunnel design stage. Also, it was assumed that there would be no interaction effects between the two tunnels with a separation of 30m. D. Zayakov recalled that the design pressures used were 1.436MPa vertical, and 0.862MPa horizontal.

Because of the possible high rock loads, a circular concrete tunnel liner was constructed although the tunnel was excavated with a horseshoe shaped section. The tunnel inside radius is 76mm larger than used in other parts of the BART system (2.667m compared with 2.591m); this was because of uncertainty of rolling stock clearances at the time of design.

To reduce possible long term hydrostatic loads, an elaborate drainage system was included as an extra precaution. It was also considered desirable to have a flexible lining, so the final lining was kept as thin as practicable (457mm design thickness) and longitudinal reinforcement steel was added (Figure 6.3).

The first design studies for the Berkeley Hills tunnels were concerned with the possibility of rupture along the Hayward Fault (Ziegenfelder and King, 1955). It was recommended that shafts be constructed to allow evacuation if a train should be trapped in the tunnels. These concerns were not raised again until tunnel construction was about to start when a study was made of possible track shifts that could be accommodated within the tunnel cross section. With a tunnel radius of 2.667m and a train clearance envelope radius of 2.591m, an investigation was made of the effect of 610mm horizontal and 305mm vertical fault movement. It was found that if the movement occurred on a single plane, the tunnel radius would need to be increased by 255mm. However, if the fault movement were distributed over about 100m of tunnel in the Hayward Fault zone, 1.341m of horizontal displacement could be accommodated without changing the tunnel radius.

Because of construction difficulties through the Hayward Fault zone, the level of the concrete arch was lowered 50mm. Following construction, the tunnel clearances were

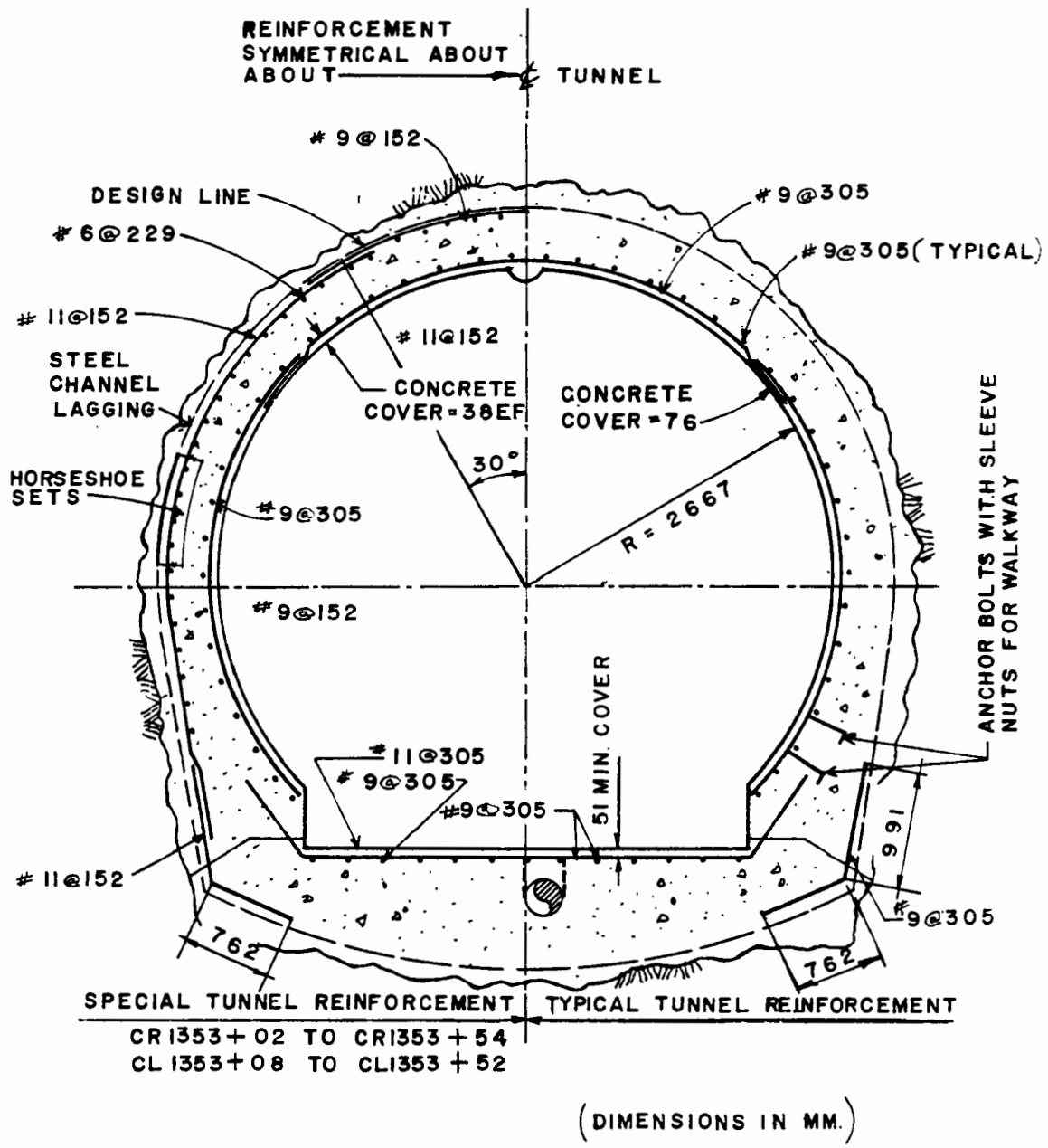


FIGURE 6.3 BART Berkeley Hills Tunnels, concrete liner reinforcement.



further reduced by the addition of conduits, lighting, third rail, and walkway.

To facilitate track realignment following movement along the Hayward Fault, the track was laid on wooden ties rather than a permanent concrete bed through the Hayward Fault zone. This was carried out as a change order to the track construction contract.

Slippage along the Hayward Fault was not discussed in the pre-construction geological reports, and was not considered during the initial design phase (Bugge and Irwin, 1964). A U.S. Geological Survey press release of September 29, 1965, that described the potential for damage to structures that cross the Hayward Fault zone led to modifications in the design of the track system to allow it to be more easily realigned.

#### **6.4. Tunnel Construction**

The construction of the tunnels has been described by Bechtel Incorporated (1968) in a report on the engineering geology of the tunnels, and by Ayres (1969). Additional information was obtained from the Resident Engineer's weekly progress reports.

In March 1965, a 31 million dollars contract for the tunnel was awarded to a joint venture of J.F. Shea Co. Inc. (sponsor), Kaiser Industries Corporation, and Macco Corporation. Excavation of the two tunnels started in May 1965 from four headings, the tunnels holed-through in February 1967, and construction was completed in July 1968.

The tunnels were excavated with a horseshoe cross section. Conventional full face methods of excavation were used, typically with a 1.22m round. Steel sets were 203mm wide flange, continuous rib type, weighing 56.5 and 59.9 kgf per lineal meter (Figure 6.4). The contract specified set spacing to be 1.22m on centres. Steel invert struts were used when required, and were placed from 3m to 5m behind the face. In heavy ground, two sets were placed in each 1.22m advance. Sections of the tunnel that required invert struts and 600mm spacing of sets were in the Hayward Fault zone, the Wildcat Fault zone, and in the

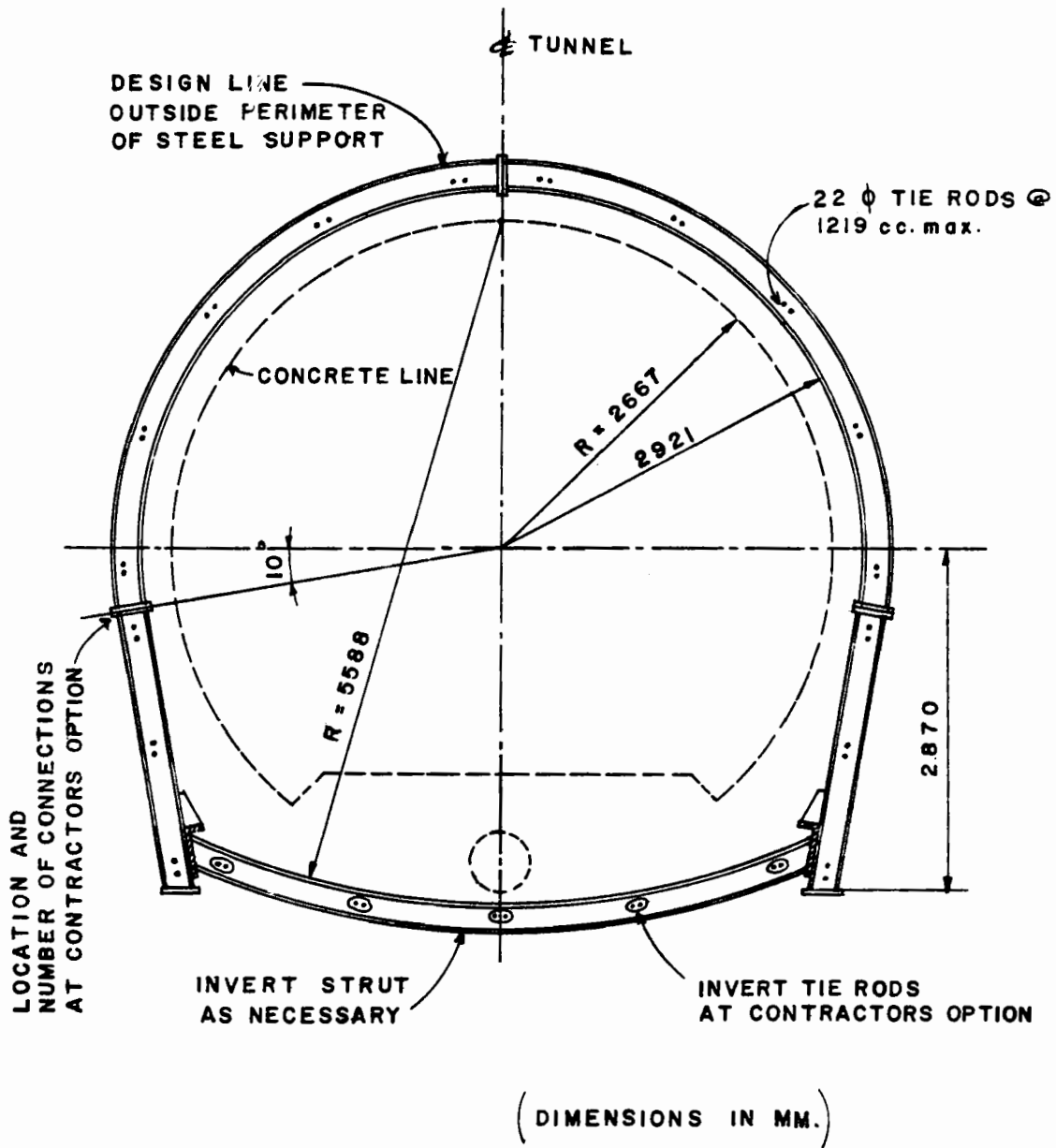


FIGURE 6.4 BART Berkeley Hills Tunnels,  
temporary support.

faulted Siesta Syncline. Heavy ground was also encountered in cross passage 5, in the Wildcat Fault zone. A summary of ground conditions encountered and temporary support used in the C2 tunnel are given in Appendix B.

The greatest tunnelling problems, according to Ayres (1969) arose from squeezing ground encountered in the Hayward and other fault zones. These sections of tunnel were not particularly difficult to excavate, although crown bars, breast boards, and spiling were commonly used. Following excavation, squeezing ground broke timbers and distorted sets. In places the ground squeezed 200 to 250mm from between the sets. On October 8 1965, when the face in the C2 tunnel was at Station 1203+75, measurements across the tunnel indicated that the ground was squeezing the posts together at the rate of about 25mm per day for a distance of 55m back from the face. Horizontal rock bolts 2.44m long were grouted into the ground beside the bottom of each post, and steel channels were attached to the rock bolts and tightened against the posts. Measurements made on October 13 showed that the movement was still continuing at the same rate. Excavation was stopped and 152mm X 200mm timber spreaders were installed on each post over a length of 91m back from the face. This work is shown in progress in Figure 6.5. These measures stopped further movement, and spreaders were replaced with 200mm steel invert struts between Station 1200+35 and the face. Based on experience in the C2 tunnel, invert struts were installed in the C1 tunnel as the heading advanced.

Squeeze generally decreased over a period of one to two months, but was noticed again when retimbering and realigning sets in preparation for placing the final concrete lining. Of 11,101 steel sets that were installed, 1,597 were deformed due to excessive loading to the extent that they required replacement or realignment.

The largest water inflows occurred in basalt, and in chert. Maximum inflow at any one face was estimated to be 41 litres per second. Some minor amounts of methane gas and oil seeps were encountered in the various sedimentary rock units.

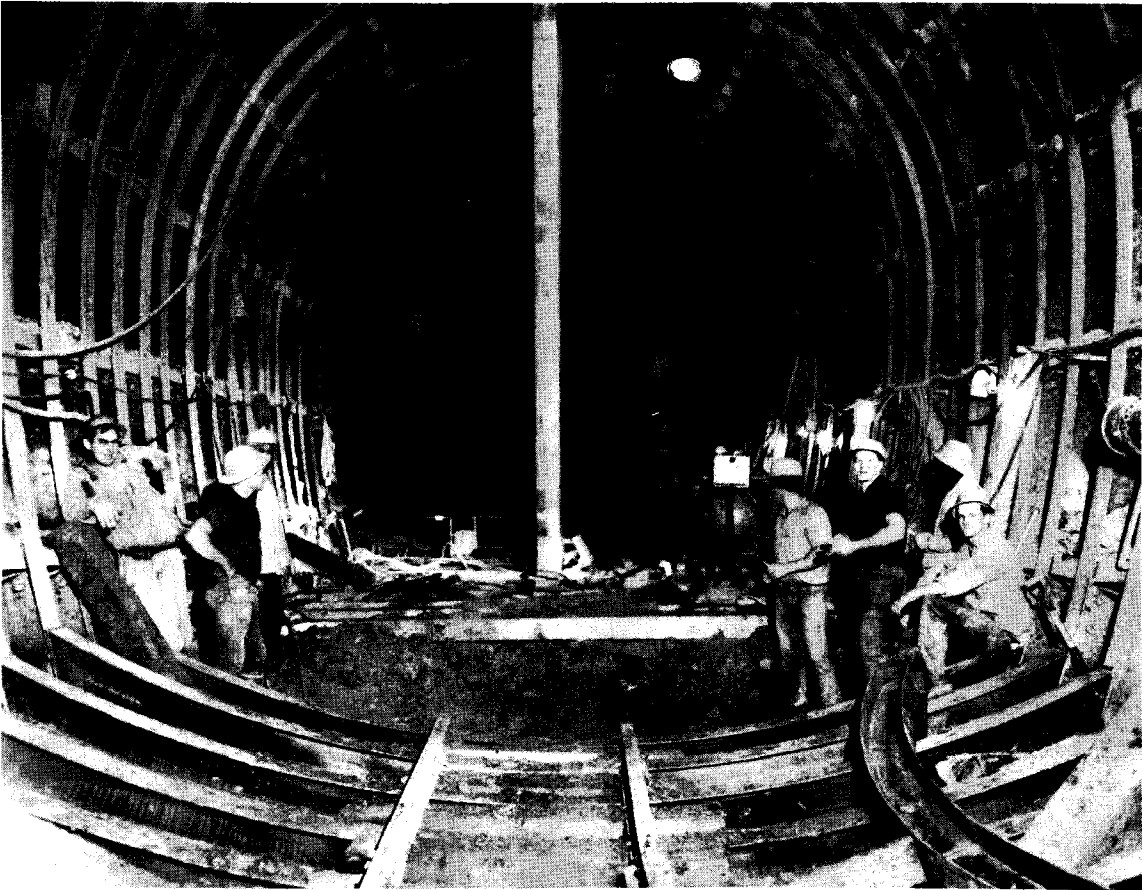


FIGURE 6.5 Excavation of C2 tunnel through Hayward Fault (photograph from BART files).

Invert concrete was placed starting June 1967, and in December 1967 arch concreting was commenced. Arch concrete was placed using telescoping slip forms with a total length of 95m. Concrete was specified to have a strength of 20.69MPa after 28 days. Voids between the concrete lining and rock were grouted. Some 45,000 bags of cement were used in this operation.

### **6.5. Instrumentation During Tunnel Construction**

In February 1965, Bechtel Incorporated engineers proposed a programme of rock instrumentation and geological logging during construction of the Berkeley Hills tunnels. The purpose of this programme was to attempt to determine whether :

- the rock loads assumed for the design of the tunnels were reasonably adequate
- the assumed rock loads were changing due to the construction of the tunnels, and/or due to tectonic forces thus affecting lining requirements and the timing of the placement of lining
- changes, gradual or sporadic, in rock deformation during train operation would endanger high speed trains.

In November 1965, the BART District allocated 100,000 dollars for a rock instrumentation programme and in December 1965, Change Order No. 5 detailed the work that was to be carried out. By July 1966, little progress had been made with rock instrumentation, mainly due to the failure of the contractor to obtain the necessary instruments. As a result of the delay, part of the tunnel, including the section in the Hayward Fault zone, had not been instrumented. In order to have some instrumentation in all parts of the tunnel, particularly in the Hayward Fault zone, a revised instrumentation programme was developed.

In October 1966, Change Order No. 8 was issued to revise Change Order No. 5. By this time considerable funds had been spent with few results, and it was necessary to reduce the scope of the programme. Provision was made in Change Order No. 8 to continuously

monitor the section of tunnel in the Hayward Fault zone, as by now the tunnel designers had become concerned about effects of fault slippage on the tunnel liner.

Between April 1966 and February 1967, 16 instrumentation stations were established in the C2 tunnel between Stations 1218+86 and 1254+25. These stations were some distance away from the Hayward Fault, and have little relevance for this study. Load cells were installed within the steel sets approximately 600mm back from the face during the contractor's normal operation of standing steel sets. They were placed in the crown, on the footblocks, and if there was an invert strut, between the rib and invert strut. There were 4 to 6 load cells at each location, and a total of 75 load cells were installed.

The load cell pressures were recorded at regular intervals until the steel sets were reblocked prior to placing the final lining in March 1967. Different size load cells were used, and these have been documented for test sites 1,2 and 3 only (Bechtel Incorporated, 1966b). Therefore, for the other test sites, it is not possible to convert pressure recorded to load acting in the steel structural system.

From the load cell pressure records, the loads generally increased rapidly during the first two days, or while the tunnel face was less than 12m from the instrumented set. This was followed by a gradual increase in load with time. Normally, the footblock load cells reached a maximum in 15 to 30 days and stabilised. The invert strut and crown load cells generally reached a maximum within 15 to 30 days, then continued increasing very slowly. Unfortunately this work was incompletely documented, and it is not possible to draw any meaningful conclusions from the available data.

## CHAPTER 7

### RESPONSE OF BART TUNNELS TO FAULT SLIPPAGE

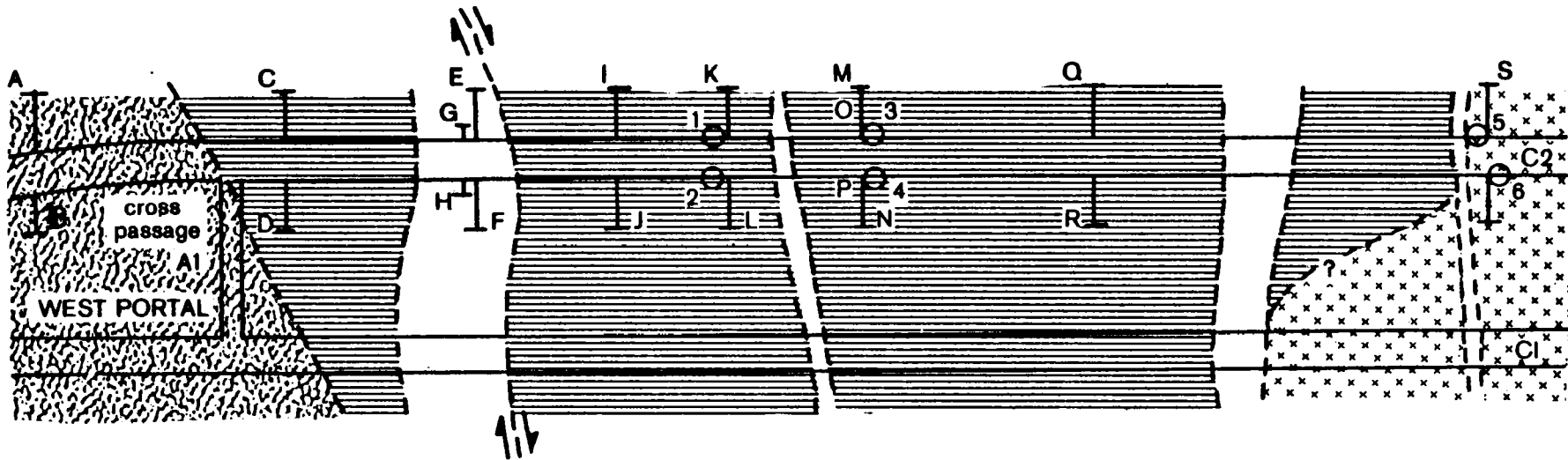
#### **7.1. Instrumentation Since Tunnel Construction**


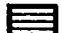

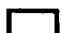

Pressure cells and rock movement indicators (RMIs) were installed in the northern (C2) tunnel shortly before arch concrete was placed. The purpose of this instrumentation was to monitor deformations and changes in loading of the liner in the Hayward Fault zone, should these occur from continued squeezing of the ground or tectonic activity following tunnel construction. These instruments have been monitored on an irregular basis since May 1967.



The location of the pressure cells and RMIs are shown on Figure 7.1. For the purposes of this report, the RMIs have been labelled A through T, and the pressure cells 1 through 6. Contact pressure cells were installed between the rock and concrete liner at three locations, with a cell placed on each side of the tunnel at about spring line. RMIs anchored 9.14m from the tunnel liner were installed at eight locations. At two of these, RMIs were also anchored 3.05m from the tunnel liner (Figure 7.2).

The RMI rods consist of 9.5mm diameter galvanised standard pipe, double wrapped and tarred. Each rod was installed in a 40mm diameter hole that was 600mm longer than the rod. The anchor end of the hole was grouted as was the collar of the hole. Schaevitz linear variable differential transformers (LVDTs) were attached to the end of the RMI rod. The collar of the RMI rod and the LVDT assembly can be inspected through a hole, approximately 400mm in diameter, in the tunnel wall. None of the RMI rods are attached to the tunnel liner.

1198+00      1199+00      1200+00      1201+00      1202+00      1203+00      1204+00      1205+00      1206+00



-  Sandstone
-  Serpentine
-  Rhyolite
-  Gouge
-  Active Shear zone

-  Rock Movement Indicator
-  O<sub>2</sub> Pressure Cell

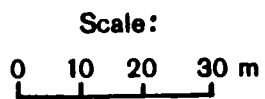


FIGURE 7.1 Section of tunnel in Hayward Fault zone; geology and location of instrumentation.



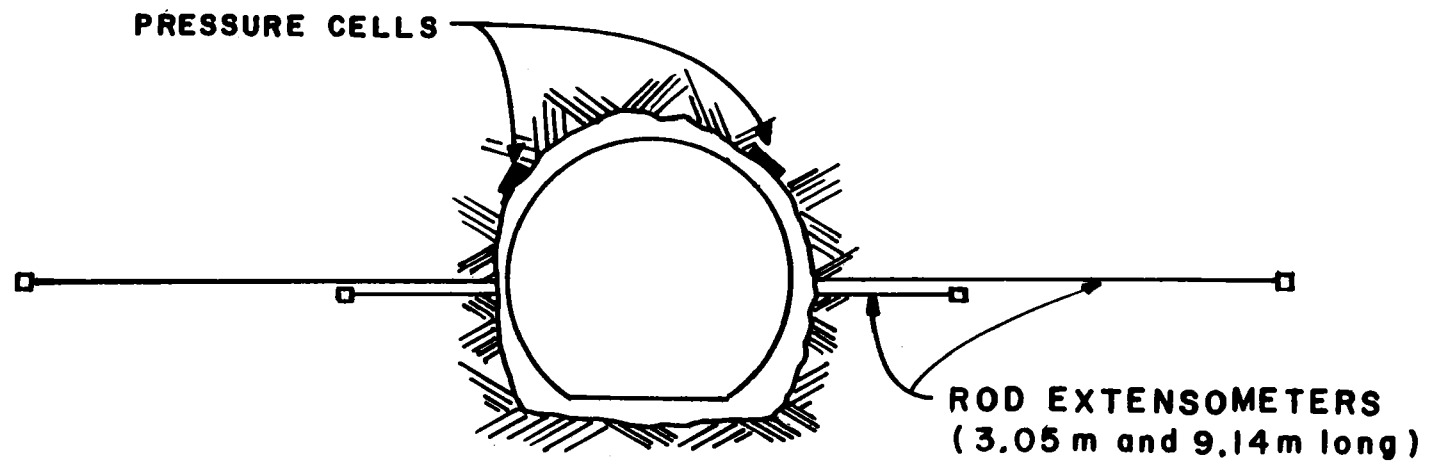


FIGURE 7.2 Instrumentation arrangement at Station 1202+77, C2 tunnel.

Pressure cells were located between the concrete liner and surrounding ground, and were installed immediately ahead of the placement of concrete. Each cell unit is believed to be of the same type as the footblock load cells used during construction instrumentation, however details of cell size and stiffness are not known. Cell pressure is measured by Schaevitz Bourdon type PRBT pressure transducers. Signals from the pressure transducers and LVDTs are lead to Schaevitz electrical junction boxes at each instrumentation station. A Schaevitz TRM-302 portable readout unit is taken into the tunnel to make instrument readings.

The reliability of the instruments was evaluated as part of this study. Each instrument was given a reliability rating on the scale of A,B,C,D, and F (failed), based on the measured isolation resistance of each transducer. Instruments with an A rating had an isolation resistance greater than  $20 M\Omega$  (up to factory specifications), and F was essentially shorted to ground. Ratings B through D indicate decreasing isolation resistance. Table 7.1 gives the reliability ratings for each instrument. With a knowledge of the response of the instruments as they deteriorated, it was possible to inspect the readings from those instruments with low reliability ratings, estimate when failure occurred, and reject all subsequent readings. Readings from RMIs and pressure cells taken over the period from the end of tunnel construction to the present are summarised in Appendix C.

RMI readings show a common trend; a maximum positive value (corresponding to extension of the RMI rod) after a period of 1 to 2 years, followed by a change in direction of movement and a slow rate of contraction. The readings from RMI G do not follow the trend of the other instruments; they show increasing extension since installation. The pressure cells have shown a trend of increasing pressure with time, but with occasional pressure decreases for short periods.

Pins were installed on the walls at Station 1202+72 to enable measurement of convergence with a tape extensometer. According to McCutchen and Snyder (1977), these

## ROCK MOVEMENT INDICATORS

Instrument	Station		Set No.	Rod Length (ft)	Position Above Invert (ft)	Steel Set Spacing (ft)	Junction Box	Channel (DISPL)	Transducer Serial No.	Reliability*
	North Side	South Side								
A	1198+01		187+2'	30	7.8	4	1	1	308	A
B		1198+01	187+2'	30	8.0	4	1	2	307	A
C	1199+44		223+2'	30	7.7	4	2	1	309	F
D		1199+44	223+2'	30	7.9	4	2	2	306	C
E	1200+53		276+1'	30	7.5	2	3	1	315	F
F		1200+53	276+1'	30	7.7	2	3	2	314	A
G	1200+51		275+1'	10	7.3	2	3	3	303	A
H		1200+51	275+1'	10	7.9	2	3	4	302	A
I	1201+35		317+1'	30	7.9	2	3A	1	299	F
J		1201+35	317+1'	30	8.0	2	3A	2	298	C-D
K	1202+01		350+1'	30	7.7	2	4	1	316	D
L		1202+01	350+1'	30	7.8	2	4	2	317	D
M	1202+77		388+1'	30	8.0	2	5	1	313	C
N		1202+77	388+1'	30	7.9	2	5	2	312	F
O	1202+75		387+1'	10	7.9	2	5	3	301	B
P		1202+75	387+1'	10	8.0	2	5	4	300	A
Q	1204+10		453+3'	30	8.2	4	6	1	311	B
R		1204+10	453+3'	30	8.2	4	6	2	310	B
S	1206+38		530+3'	30	7.8	4	7	1	305	A
T		1206+38	530+3'	30	8.2	4	7	2	304	A

## PRESSURE CELLS

Instrument	Station		Set No.	Position Above Invert (ft)	Steel Set Spacing (ft)	Junction Box	Channel (PSI)	Transducer Serial No.	Reliability*
	North Side	South Side							
1	1201+93		346+1'	14.0	2	4A	1	823	D
2		1201+99	349+1'	11.0	2	4A	2	825	D
3	1202+79		389+1'	13.0	2	5	1	824	A
4		1202+77	388+1'	14.0	2	5	2	817	B
5	1206+31		529+0'	13.0	4	7	1	826	B
6		1206+39	531+0'	13.0	4	7	2	827	C

\*Reliability is based on a scale of A, B, C, D, and F (failed)

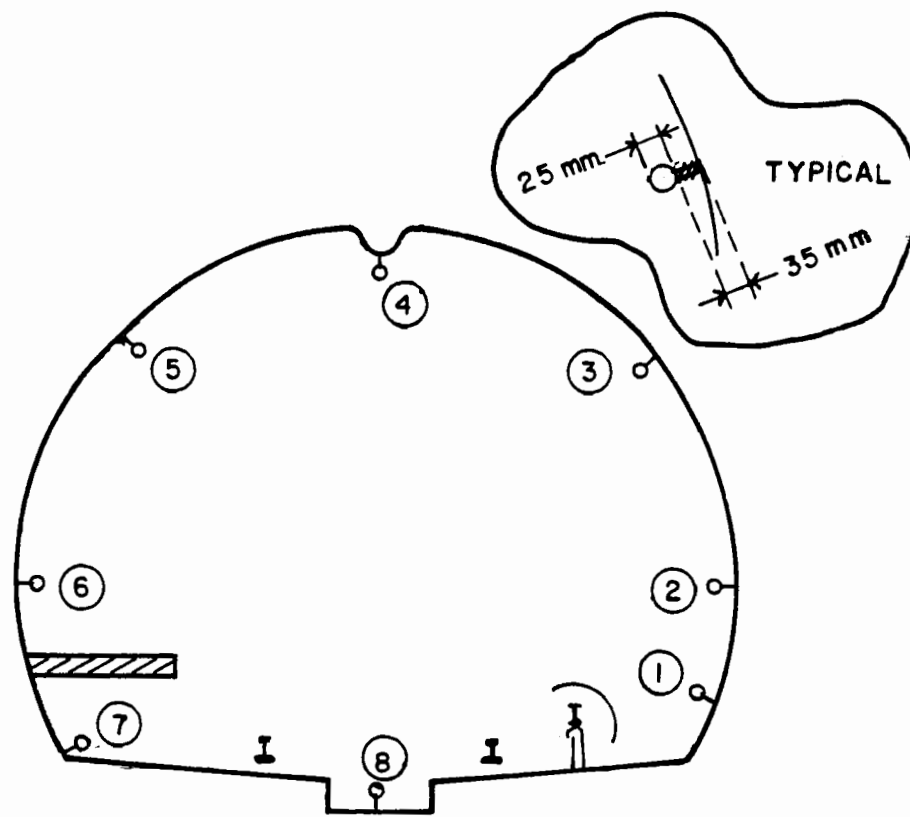
TABLE 7.1 C2 tunnel instrumentation.

measurements can no longer be made. Up until readings were discontinued in 1968, the convergence recorded was 0.25mm (Bechtel Incorporated, 1970). As part of this study, tape extensometer anchor points were installed at ten stations, at 1200+00, 1200+65, 1200+85, 1201+05, and 1201+70 in both C1 and C2 tunnels. Typical location and numbering of extensometer anchor points are shown in Figure 7.3. An attempt was made to place anchor points in the same position at each station. Initial tape extensometer readings were taken in January 1981, and a comparison made of readings between points 2 and 6 for all ten stations. There was a difference of 41mm between the highest and lowest reading, with no apparent pattern. This difference is most likely due to changes in form geometry during placing of the concrete liner, and difficulties in accurately locating the extensometer anchor points, rather than deformation due to fault slippage.

## **7.2. Concrete Liner Cracking Pattern**

The pattern of cracking in the C2 tunnel was logged in July, 1979, from Station 1191+00 near the west portal, to Station 1210+20, a distance of 585m (Appendix D). This included sections of the tunnel on either side of the Hayward Fault zone. A quick inspection was made of the cracking in the remainder of the liner when walking through each tunnel.

Most of the cracks logged during the detailed study were vertical, and normal to the tunnel axis. They were rarely continuous around the tunnel circumference, and usually terminated above invert level. They are interpreted as being due to concrete shrinkage, however some may be due to extension of the tunnel in an axial direction as a consequence of right lateral displacement along the Hayward Fault. The open nature of many of the cracks also suggests this mechanism. Circumferential cracking in a continuously placed concrete liner is usually expected at intervals of 3m to 4m.



### CI TRACK, LOOKING EAST

FIGURE 7.3 Tape extensometer anchor point location.

Another type of cracking found in some parts of the tunnel was longitudinal cracking between the spring line and the crown. Such cracks are interpreted as resulting from high bending stresses caused by the high lateral ground pressures. Photographs from BART files that were taken in October 1969 show these cracks between Stations 1202+60 and 1203+25 in the C2 tunnel.

Between about Station 1200+60 and Station 1201+10 (15.2m) there is a distinctive cracking pattern, with low angle cracks extending from the crown to invert. These cracks are believed to reflect distortion of the tunnel liner due to right lateral slippage along a distinct shear zone within the Hayward Fault zone. A similar cracking pattern was found in the C1 tunnel, at about Station 1200+80. Most of these cracks are open, with an aperture of up to 3mm. They were first observed in 1971 (W. Hazelwood, pers. comm.). On January 31, 1980, a number of glass strips were bonded to the concrete with epoxy, spanning the cracks. Since this time, none of the glass strips have cracked, indicating either that crack aperture has been stable, or that the deformation rate is so slow that it is accommodated by creep of the epoxy rather than fracture of the glass.

Following small earthquakes along the Hayward Fault (April, December 1980) the cracks in the C2 tunnel around Station 1200+80 were most noticeable because they were outlined by a fine white powder, possibly comminuted concrete. This powder was quickly removed by turbulent air from high speed trains. None of the glass strips was broken, suggesting that there was very little, if any, relative movement along the cracks. The same phenomenon was observed in January 1981 (W. Hazelwood, pers. comm.).

More intense cracking of the concrete liner was observed in other sections of tunnel. These cracks appeared to be characteristic of high horizontal ground pressures, although it is possible that they indicate continued tectonic activity in the Berkeley Hills. A close analysis of these areas was outside the scope of this study.

### **7.3. Tunnel Displacement Due To Slippage Along the Hayward Fault**

Various survey networks have been established in and around the BART tunnels, and these can be used to give an indication of ground and tunnel displacement due to slippage along the Hayward Fault.

#### **7.3.1. Construction Surveys**

Theodore V. Tronoff Inc, consulting surveyors, provided horizontal and vertical control for the construction of the BART tunnels (Contract Z-504). Surveying commenced in October 1964; tunnel excavation was from May 1965 to March 1967. Distances were measured with a Model 4 Geodimeter when over 61m, and a Lovar tape when less than 61m. Angles were measured with a Wild T2 theodolite.

The coordinates calculated for pre-existing monuments failed to correspond to published coordinates. In an effort to adjust the control survey to previous surveys, the control survey was repeated on four other occasions up until November 1965. Each survey produced different measurements, and in an effort to reconcile these differences prior to tunnel hole-through, Duff Surveys Inc. were retained to carry out an independent survey (Contract 3C0041).

Duff Surveys Inc. used Wild T2 and T3 theodolites to measure angles, and a Model 4 Geodimeter and a MRA3 Tellurometer to measure distances. This survey produced another set of results which also indicated that the east and west headings were not correctly aligned. A small change in direction of driving was adopted and the tunnels holed-through only slightly misaligned. As far as can be determined, the amount of misalignment was not recorded.

Fault slippage was considered as an explanation for these surveying difficulties, although no attempt was made to allow for this in reconciling the various surveys. Unfortunately, none of these surveys was documented well enough to allow for reevaluation as

part of this study.

### **7.3.2. As Built Survey**

An "as built" survey was carried out by Murray-McCormack (now M and M Consultants), consulting surveyors, starting in November 1968. Survey monuments were established in each tunnel opposite cross passages, and as the permanent track structure would cover these monuments, marks were placed on the tunnel walls to allow their accurate relocation. The marks consist of four nails driven into the tunnel wall; each pair of nails form a diagonal, and the monument lies at the intersection of the diagonals. The alignment survey was referenced to permanent points away from the tunnel portals. Levels were also measured, and bench marks were located in the C2 tunnel by each cross passage.

### **7.3.3. Horizontal Alignment Surveys Since Tunnel Construction**

A horizontal alignment survey for both tunnels across the Hayward Fault zone was devised by Towill Inc., consulting surveyors. This survey has been repeated by BART survey staff on eleven occasions between December 1971 and January 1981.

A Spectra Physics Model 611 HeNe laser is used to produce a straight line using the Fraunhofer effect. This effect occurs whenever a radiated light source is projected through a narrow slit-type aperture, the result being a series of light and dark bands whose widths are dependent upon the frequency of the light source, the width of the aperture, and the intermediate distances. Apart from the laser, which is mounted on a Hewlett Packard alidade, the other equipment consists of an aperture assembly with variable slit attachments, and a screen or target with a series of vertical multi-patterned lines, all of which fit Zeiss TH-2 type tribrachs. The mountings for the equipment are rigid aluminium bars cantilevered from stainless steel plates permanently attached to the south wall of each tunnel. The aluminium bars have been calibrated in decimal feet and are read using a movable



mounting (lateral adjuster) that accepts the Zeiss tribrach.

Field procedure consists of setting the distance from the tunnel wall to the laser and aperture, and moving the screen at each station to intersect the projected light pattern. The distance between the screen and the wall is then measured. When the screen is too far from the laser, both laser and aperture are moved to closer stations, and are set at the same distance from the wall as the screen for that station, thus maintaining the projection of the straight line.

Two laser survey traverses were set up along the south wall in each tunnel. The line in the C1 tunnel is 3114m long with 24 stations, and that in the C2 tunnel is 575m long with 14 stations (Figure 7.4). The C1 traverse is a straight line; the C2 traverse is straight over a length of 338m at the eastern end and curved at the western end.

The results of the surveys were processed by BART on a computer with limited storage capacity, and the program used required that a number of points on each traverse be kept stationary between surveys. This resulted in a distorted displacement pattern. As part of the present study, these survey data were reviewed.

In order to analyse the laser survey data, it was necessary to assume that the bearing between two points along the tunnel did not change between surveys. These two points can then be used to define a straight reference line from which the relative displacement of other points are calculated. To start with, the survey data from the C1 tunnel were analysed. Intuitively, it seemed likely that the two points furthest from the Hayward Fault zone would have moved the least, and would produce the most informative results if they were assumed stationary. A reference line was then generated from the two eastern-most points on the traverse. However when the initial forward and reverse traverses, carried out by Towill Inc. in December 1971, were rotated and translated so that they were coincident at the two "fixed" points, it was found that the offsets calculated at the stations on the reverse traverse did not agree with the offsets measured on the forward traverse. There

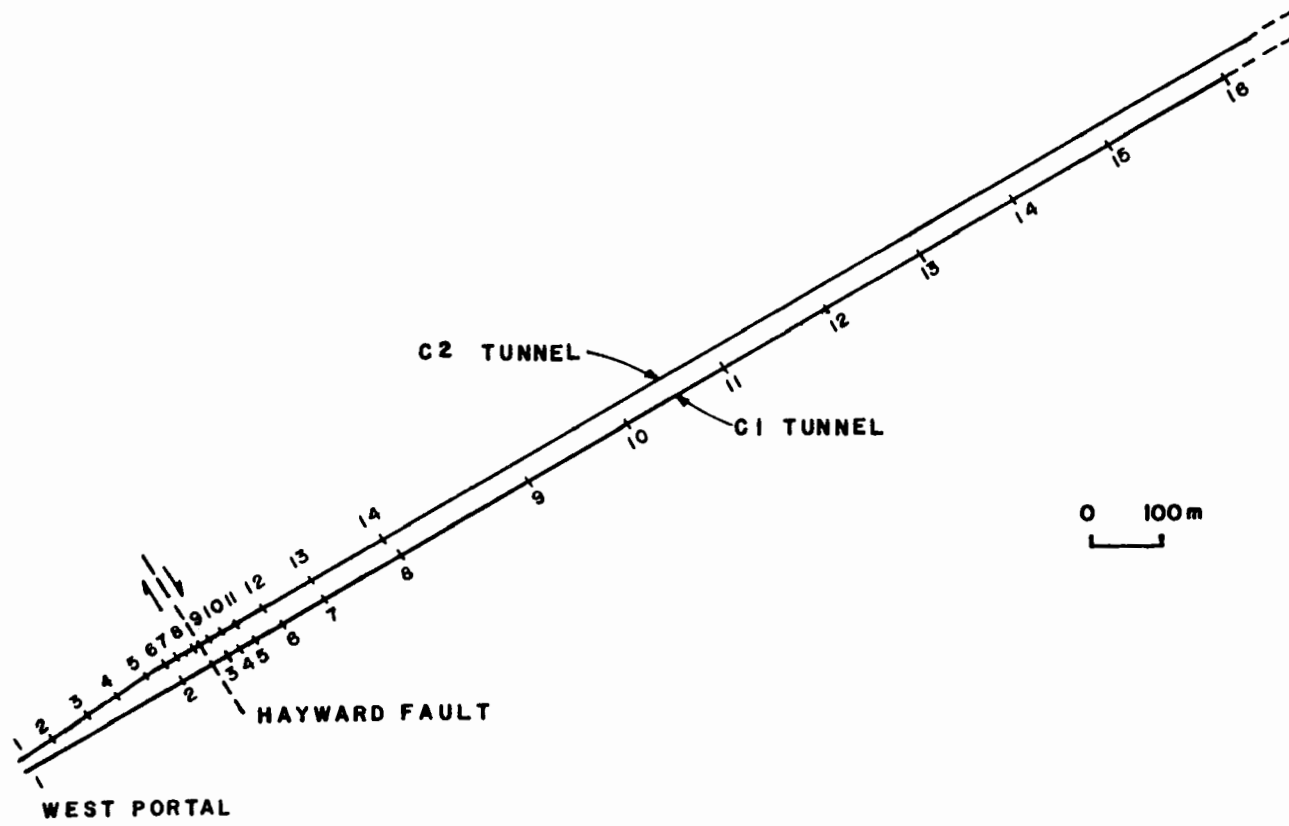


FIGURE 7.4 Laser survey traverses, C1 and C2 tunnels.

was a difference of 1 part in 9026 between the calculated position of the western end of the traverse and the measured position. When Towill Inc. devised the survey, they estimated the accuracy to be 1:1,000,000 (J. Kor, pers. comm.) but for this high accuracy it was assumed that other arbitrary points along the traverse were stationary.

Much of the survey error is probably attributable to the repositioning of the laser at stations along the tunnel. Therefore, if the offsets measured during each laser set-up are analysed independently, there should be a higher accuracy. When the offsets measured in December 1971 at the six stations at the western end of the C1 tunnel were analysed, the difference between forward and reverse traverses showed an agreement (after one had been translated and rotated to coincide with the other), of 1:219,068. This accuracy was not repeated in subsequent surveys undertaken by BART staff, when forward and reverse traverses failed to coincide by about 1:10,000.

The progressive dislocation of the C1 tunnel across the Hayward Fault is shown in Figure 7.5. The displacement curve was calculated assuming that the bearing between laser survey stations 5 and 6, to the east of the Hayward Fault, did not change in the interval between surveys. This figure quite clearly shows right lateral displacement along a narrow zone near Station 1200+80. A similar curve was developed for the C2 tunnel (Figure 7.6). Another way to consider these data is shown in Figures 7.7 and 7.8, where the relative movement between two points on either side of the actively slipping shear zone are plotted against time. The apparent changes from right lateral to left lateral slippage may be a result of survey errors, and perhaps a smooth curve should be drawn within the enclosing error curves. A recent laser survey (January 1981) has not been plotted on Figures 7.7 and 7.8. When the data from this survey were reduced, it was found that the slippage rate has remained more or less constant.

Mr W. Hazelwood, BART surveyor, set up an alignment survey in the C2 tunnel in October 1976 (Survey No. C005-2). Starting from a station located outside the west portal,

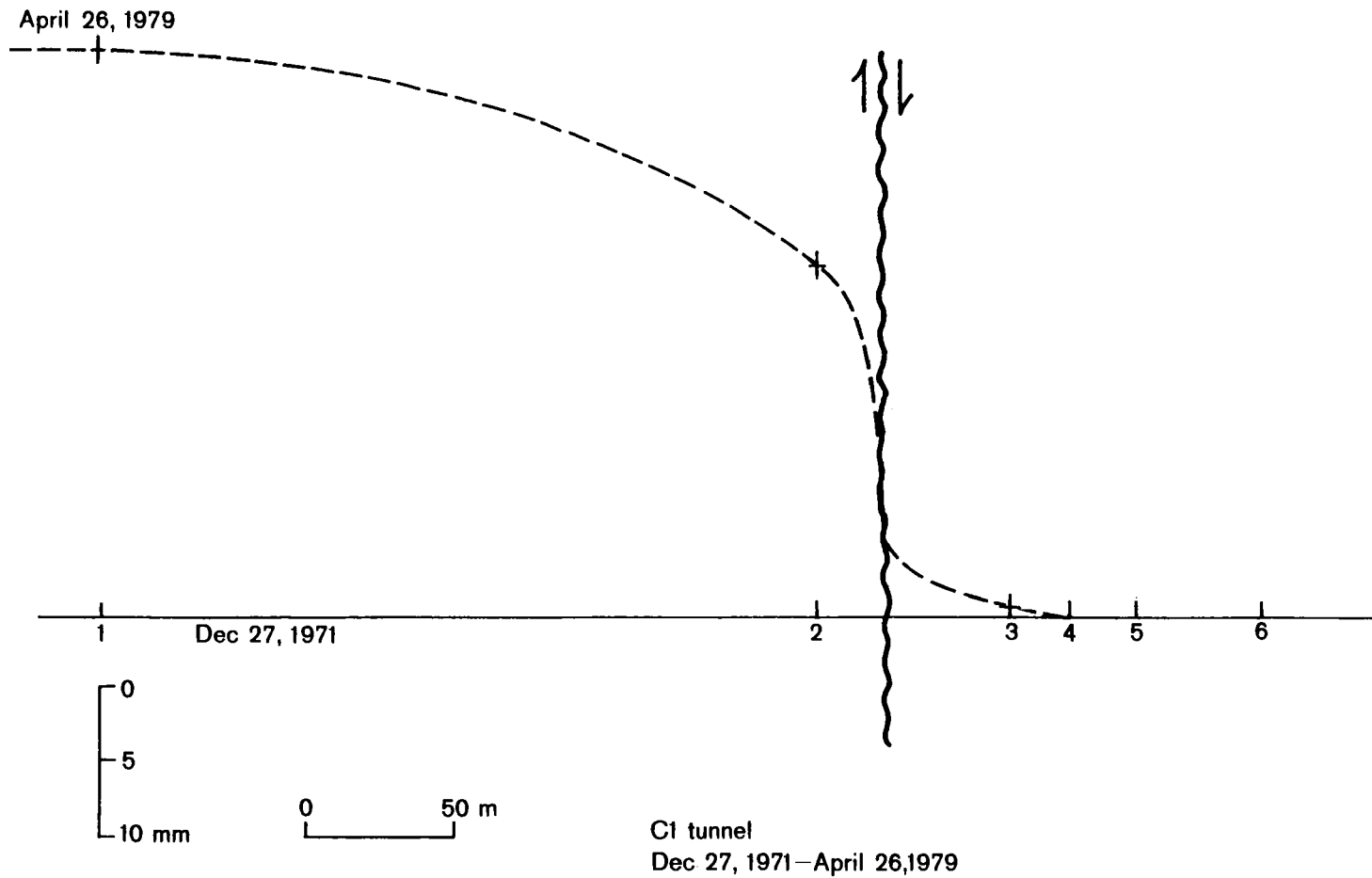
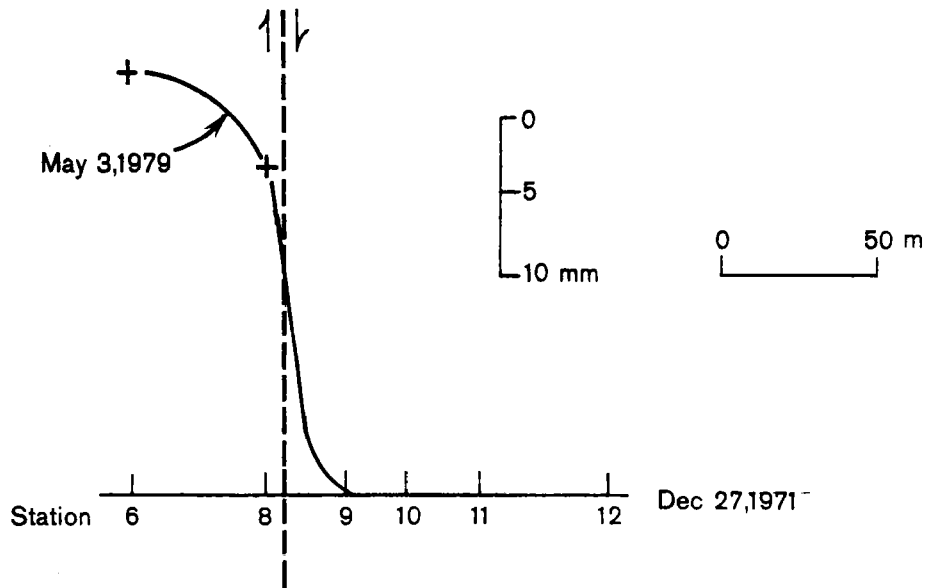


FIGURE 7.5 Laser alignment survey, C1 tunnel.



C2 tunnel  
Dec 27, 1971–May 3, 1979

FIGURE 7.6 Laser alignment survey, C2 tunnel.

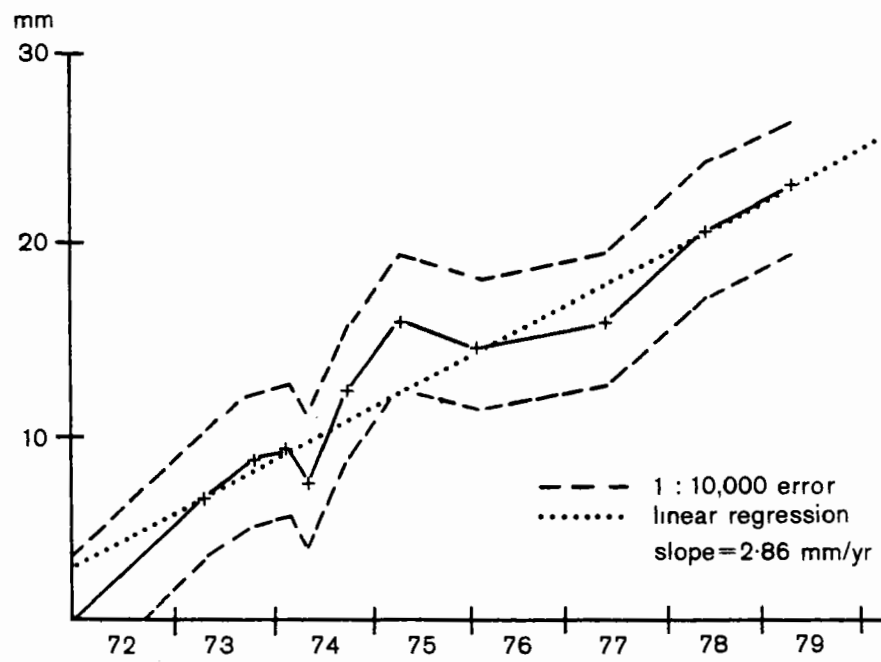


FIGURE 7.7 Displacement of laser alignment survey Station 2 relative to Station 3, C1 tunnel.

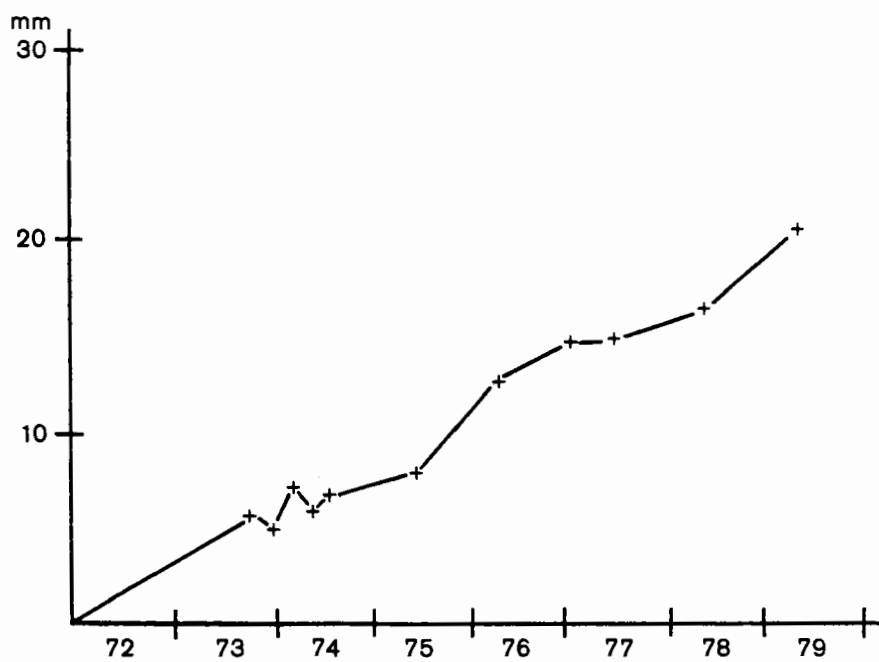


FIGURE 7.8 Displacement of laser alignment Survey Station 8 relative to Station 9, C2 tunnel.

changes in angles between stations over a distance of 2042m inside the tunnel were measured with a Wild T2 theodolite. Distances were assumed constant between surveys. This survey has been repeated on 5 occasions up until June 1979, however these survey data have only recently been reduced as part of this study. Coordinates for the stations were calculated for each survey assuming that there was no change in bearing between the two stations furthest east. This survey quite clearly shows right lateral slippage along the Hayward Fault (Figure 7.9).

The "as built" survey was repeated by BART surveyors, and was completed in January 1981 (BART Survey C003-0). The monuments covered by the permanent track structure were reestablished and an alignment survey run through both tunnels to permanent points away from both portals. After the survey data had been reduced and adjusted, coordinates were calculated for each monument. When compared with coordinates for the 1969 "as built" survey, there had been 180mm right lateral displacement between points at either end of the survey, a distance of 6459m. Points on either side of the Hayward Fault showed right lateral displacement of 32mm over a distance of 729m in the C1 tunnel, and 42.6mm over a distance of 673m in the C2 tunnel.

With this type of survey, any error is cumulative and may be significant. The values calculated for displacement in the C1 and C2 tunnels should be in close agreement, however this was not so, indicating a possible inaccuracy in the survey.

Another way to consider these survey data is to calculate bearing changes between surveys, then each observation is independent of others in the survey and error will not be cumulative. Figure 7.10 shows bearing changes between the 1969 and 1981 surveys in the C1 tunnel, indicating a large change in angle at the Hayward Fault, and shear strain distributed over a distance of about 1.8km to the east of the Hayward Fault.

In February 1981, the "as built" levelling survey was repeated from bench mark CRT18 near the west portal, to bench marks at cross passages on either side of the Hayward



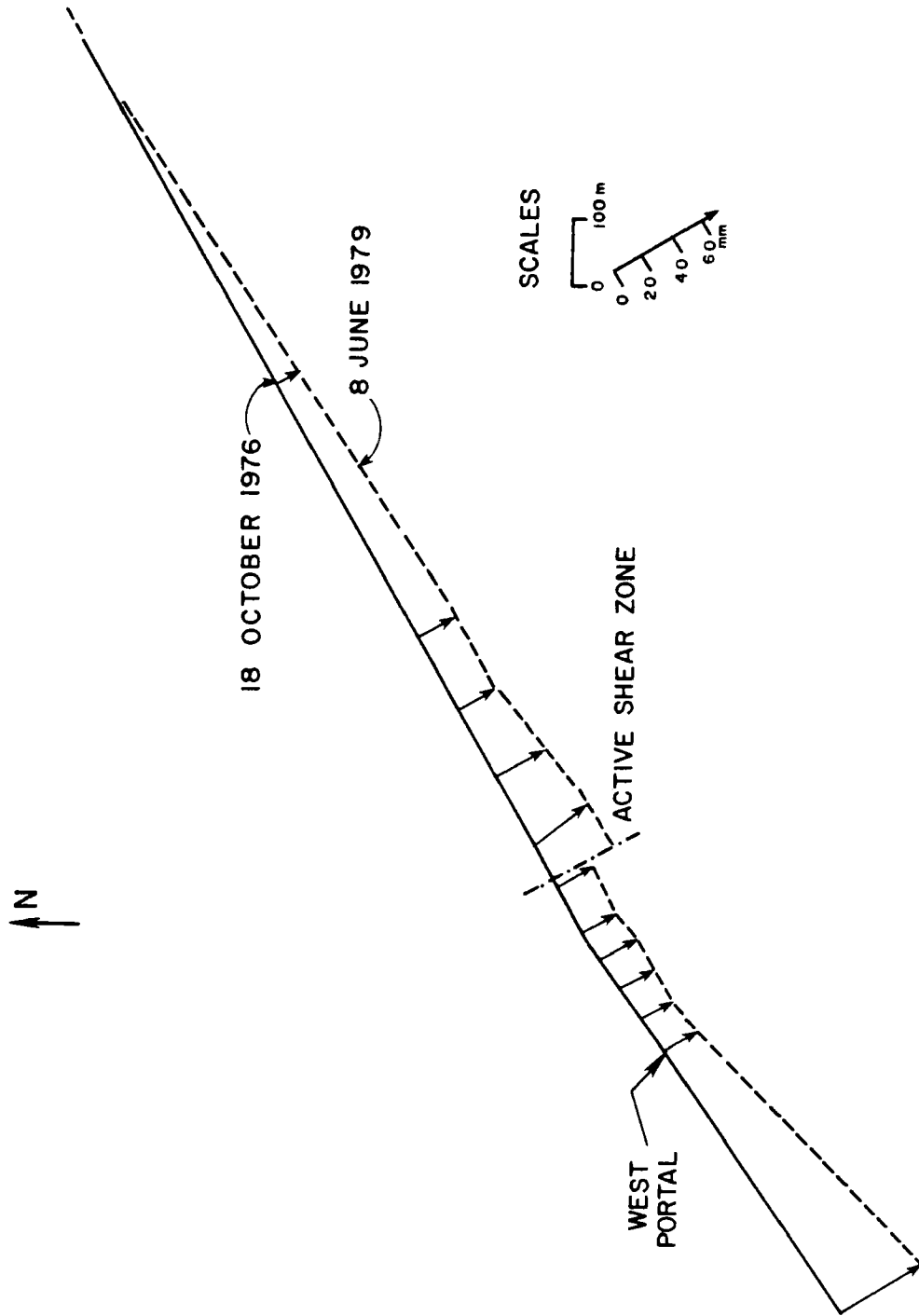


FIGURE 7.9 BART Survey No. C005-2.

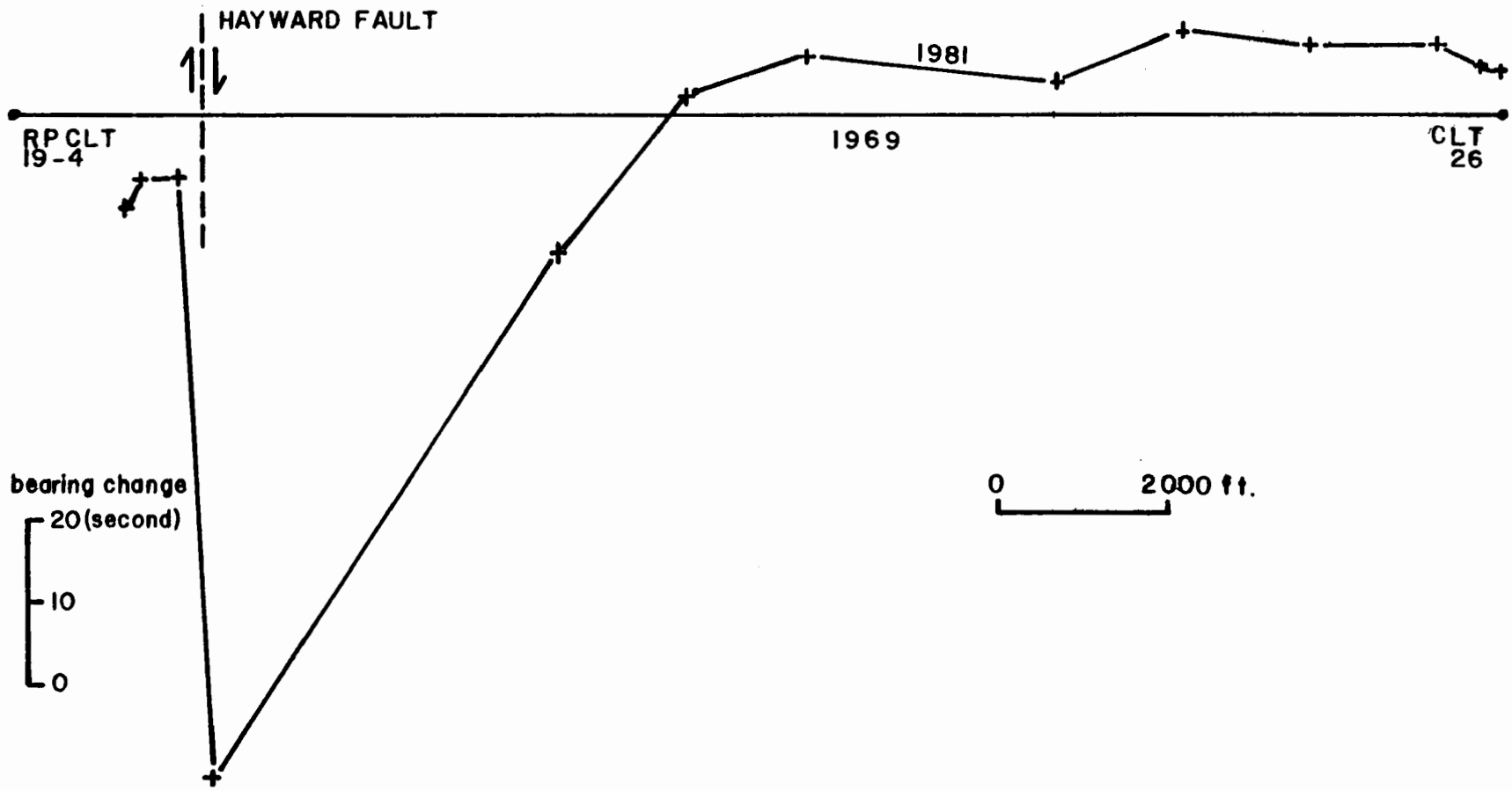


FIGURE 7.10 BART Survey No. C003-0.

Fault. All levels were consistently 27mm to 33mm higher than the 1969 survey, suggesting that bench mark CRT18, founded on a cut and cover section of track, had settled. The relative change in level between the two cross passages on either side of the Hayward Fault was only 5mm (east side uplifted relative to the west), however this is believed to be smaller than the error involved in the survey.

The various surveys that have been carried out across the Hayward Fault indicate that fault slippage can be detected by survey methods. The more recent BART surveys show that right lateral displacement occurs at around Station 1200+80 in the C2 tunnel. This location of fault slippage coincides with a change in the pattern of cracking in the tunnel liner, and a shift in the track (Figure 7.11). The track shift was measured recently (December 1980) and Figure 7.12 shows misalignment of the track from its theoretical location. This figure indicates some 40mm of right lateral displacement over about a 15m length of tunnel. It is not known whether the track has been repositioned by maintenance crews, in which case 40mm may not be the total displacement since the track was constructed in 1971. A similar change in crack pattern and track shift is found in the C1 tunnel at around Station 1200+80.

Previous investigators (Bechtel, 1970) had concluded that fault slippage was occurring in a narrow zone somewhere between Stations 1198+00 and 1204+00, a distance of 183m. McCutchen and Snyder (1977) considered the active fault trace to be located at Station 1202+40 based on their analysis of rock movement indicator and pressure cell data.

The right lateral fault slippage rate calculated from BART Survey No C005-2 is 6.35mm/year between Stations 8 and 11 (a distance of 67.570m). If this rate has been constant since tunnel construction, there should be a total right lateral displacement of the tunnels of some 83mm. These values are higher than calculated from recent survey C003-0, but as mentioned, the errors involved made it difficult to accurately calculate displacements



FIGURE 7.11 C2 tunnel, looking east, showing shift in track at Hayward Fault.

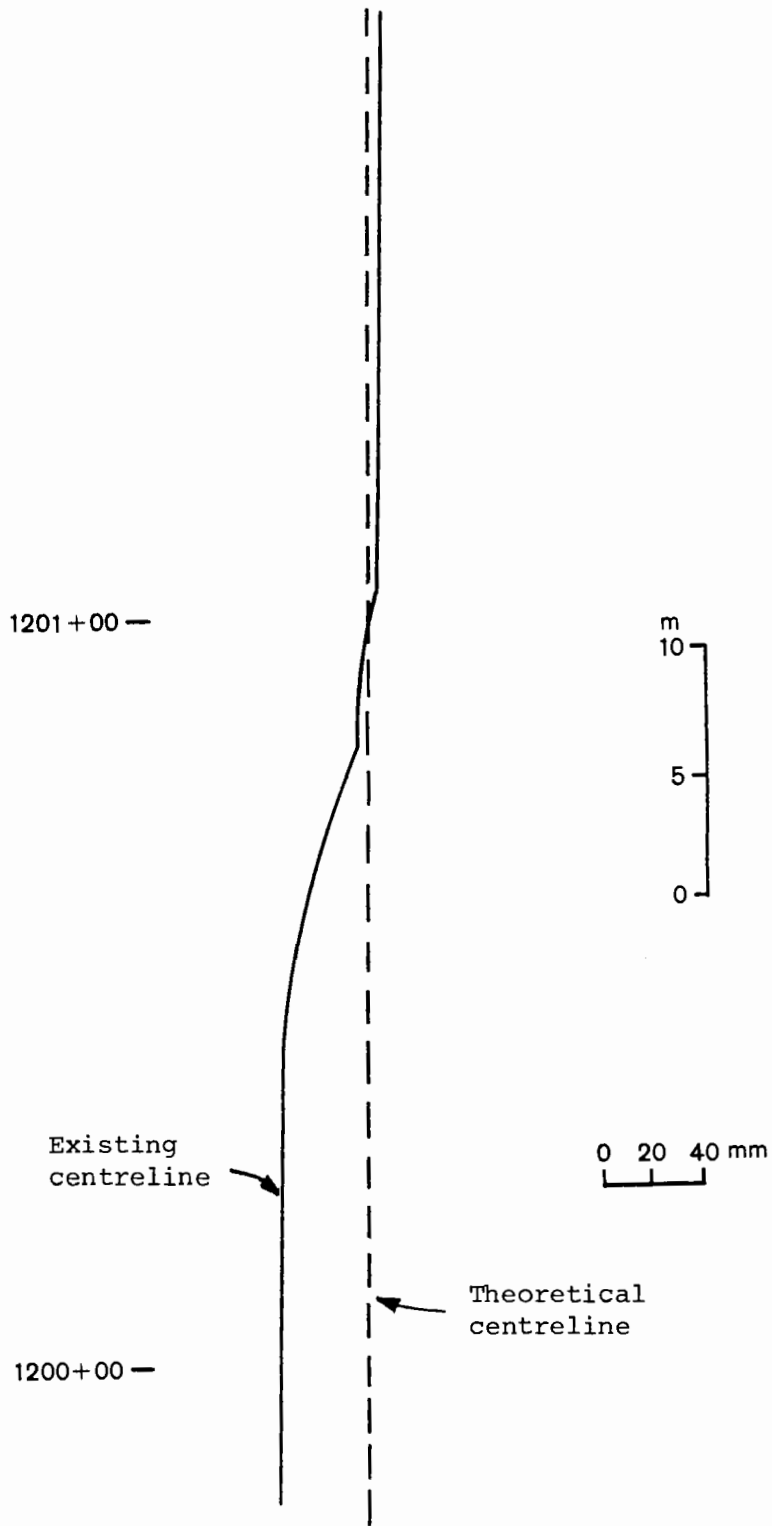


FIGURE 7.12 Track shift in C2 tunnel measured during December 1980 survey.

across the Hayward Fault.

#### **7.4. Squeezing Ground in the Hayward Fault Zone**

Squeezing ground in the Hayward Fault zone was observed in the exploratory adit, where loading on timber sets increased with time and soft material squeezed between the timber supports. When the C2 tunnel was excavated through this zone in September and October 1965, further squeeze occurred requiring extra temporary support. Squeeze generally decreased over a period of one or two months, but was noticed again in November 1967 when sets were realigned before placing the concrete arch.

As mentioned, rock movement indicators (RMIs) were located in the Hayward Fault zone to more closely observe effects of continued squeeze on the tunnel liner. Unfortunately, the RMI instrument heads are not attached to the tunnel liner. Consequently, they are somewhat independent of the liner as it is possible for them to move into the hole in the liner. The RMI readings then do not indicate liner deformations, but give an indication of the ground response close to the tunnel liner.

RMI extension was observed for a period of one to two years after placing the tunnel liner, presumably in response to squeezing ground. Squeeze was therefore initiated in parts of the C2 tunnel in mid-1964 and continued to mid-1968. With the progressive excavation of a small section adit, the full size tunnel, and the retimbering and realigning of sets, it is likely that a large volume of material around the C2 tunnel was disturbed and contributed to squeezing pressures. In the C1 tunnel, the ground was not disturbed by an exploration adit, and experience gained from the C2 tunnel meant that adequate temporary support was installed. Consequently, it can be expected that loading on the tunnel liner due to squeezing ground was lower in the C1 than the C2 tunnel.

Figure 7.13 shows the maximum extension recorded by the 9.14m long RMIs. RMI N and RMI K showed most extension, with 21.8mm and 20.2mm respectively, and were

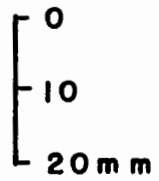
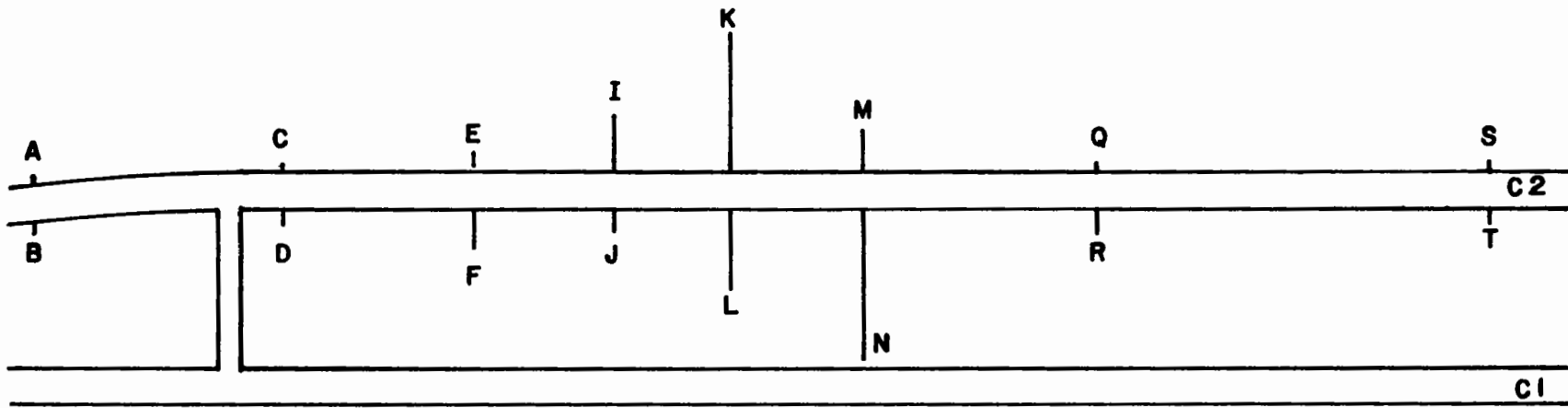


FIGURE 7.13 Maximum rock movement indicator extension.

located in sheared serpentine with clay seams. RMIs located in stiffer materials such as Franciscan sandstone (RMIs A and B) and Leona rhyolite (RMIs S and T) extended less than 0.5mm.

The data from instrumentation stations with different length RMIs can be used to show the change in displacement away from the tunnel liner at the time when maximum RMI extension occurred (Figure 7.14). Two of the curves show that most of the movement was within a 3m zone adjacent to the tunnel liner. The curve with RMI O suggests that most movement occurred at some distance greater than 3m, and the assumption that the 9.14m RMI anchor is fixed may not be valid. Because the RMI heads were not attached to the tunnel liner, these data have limited use.

Pressure cells have generally recorded increasing pressure with time. For the first few years after tunnel construction there was a higher rate of pressure increase; this may have been due to continued squeezing ground.

### **7.5. Ground-Liner Interaction**

The data presented show that the BART Berkeley Hills tunnels are being affected by fault slippage. At about Station 1200+80 in the C1 and C2 tunnels, there is a visible shift in track alignment, a characteristic cracking pattern in the concrete liner, and an alignment change measured by survey methods. The concrete cracking pattern and geology of the section of tunnel around Station 1200+80 in the C2 tunnel are shown at the same scale in Figure 7.15. From a comparison of the geology and concrete liner cracking pattern, it appears that most of the slippage along the Hayward Fault occurs along a narrow shear zone logged during tunnel construction.

The long term rock instrumentation data are also consistent with the observation of fault slippage. Because the rock movement indicators are orientated more or less parallel with the Hayward Fault, they have shown little change in displacement with time, following



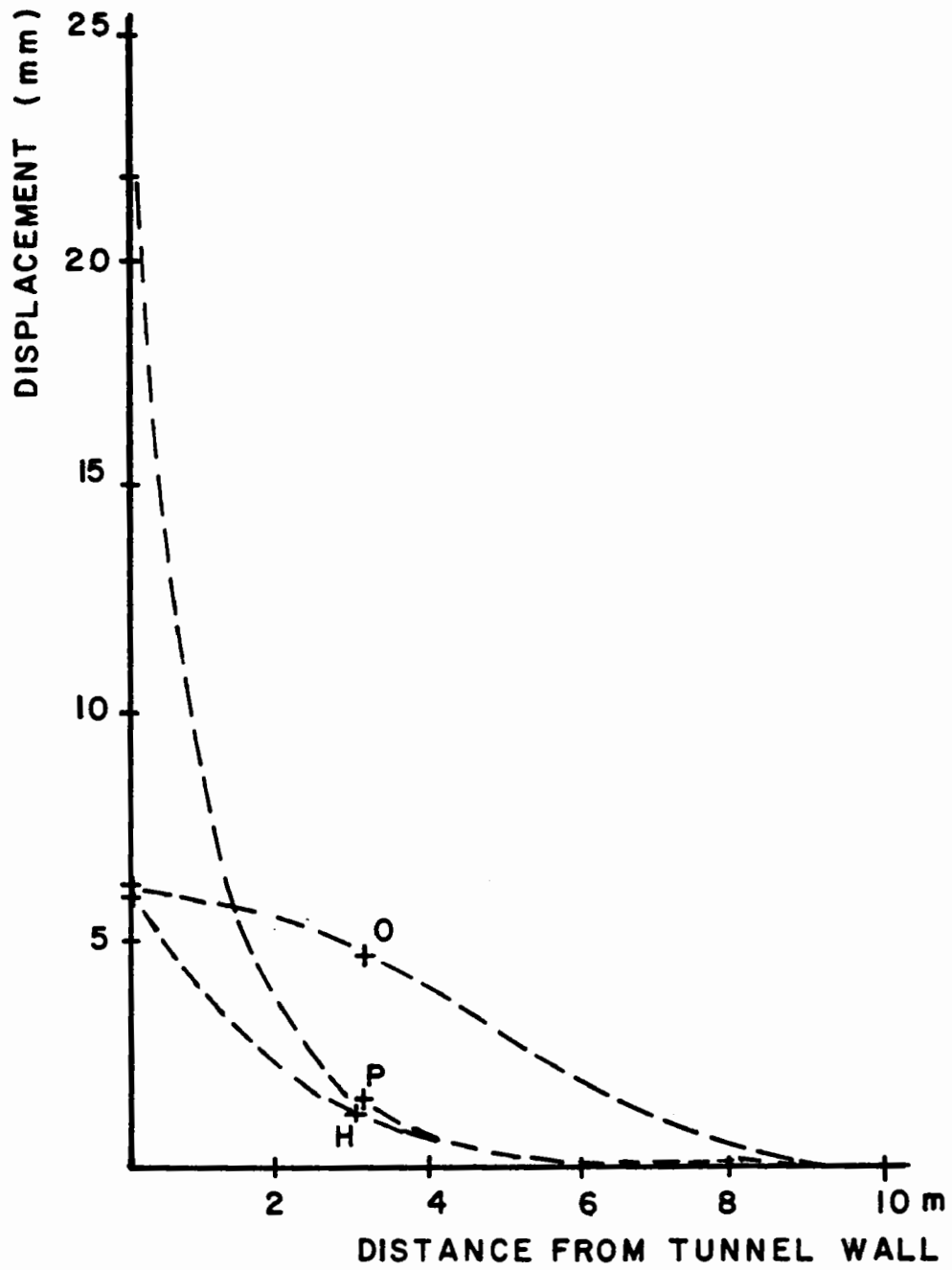
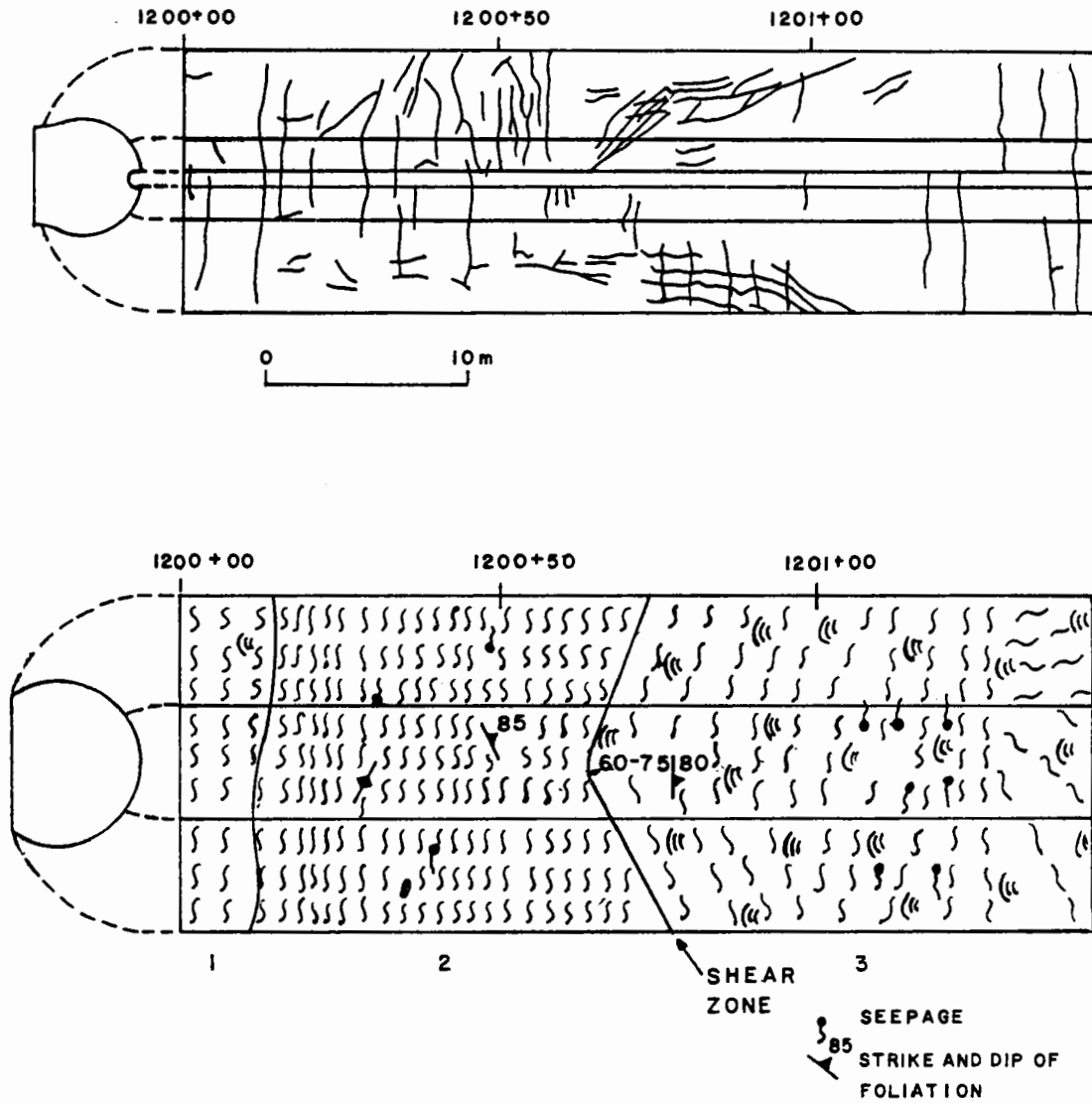


FIGURE 7.14 Ground displacement away from the tunnel liner.



1. Serpentine--sheared, slickensided fragments, clayey and granular gouge.
2. Gouge--rounded, slickensided fragments of serpentine; scattered fragments of black siltstone or shale.
3. Serpentine--sheared, granular gouge and seams of talc, aragonite, chlorite, clay; serpentine slickensided.

FIGURE 7.15 Comparison of geology and liner crack pattern around Station 1200+80, C2 tunnel.

the period when squeeze took place. Pressure cell readings are highest on the northern side of the C2 tunnel east of the active fault (Figure 7.16). When the ground around the tunnel is moving due to right-lateral fault slippage, on the eastern side of the fault passive pressures are built up on the northern wall. Similarly, active pressures develop on the south wall of this section of tunnel. Higher pressures are recorded by cells in contact with stiffer ground (e.g. pressure cell 5 in Leona Rhyolite) than cells in contact with softer serpentine and gouge.

The pressure distribution around the tunnel appears non-uniform, however contact pressure cells such as installed in the BART tunnels can give inaccurate readings if poorly installed. Subsequent development of high point loadings can also give rise to apparent non-uniform loading of the liner.

Little is known about the properties of the pressure cells; they are filled with oil and must therefore have a relatively high stiffness. Also the distribution of stress over the contact areas, and the amount of direct contact between the pressure cell and surrounding rock, and pressure cell and tunnel liner are not known. It is assumed that the pressure cells are affected by the component of *in situ* stress radial to the tunnel liner. Interpretation of gauge readings in terms of changes in *in situ* stress requires an analysis of interaction between rock, pressure cell, and tunnel liner. Boundary conditions for this problem are not well defined, and constitutive equations are required for the three components. Time dependency may be important.

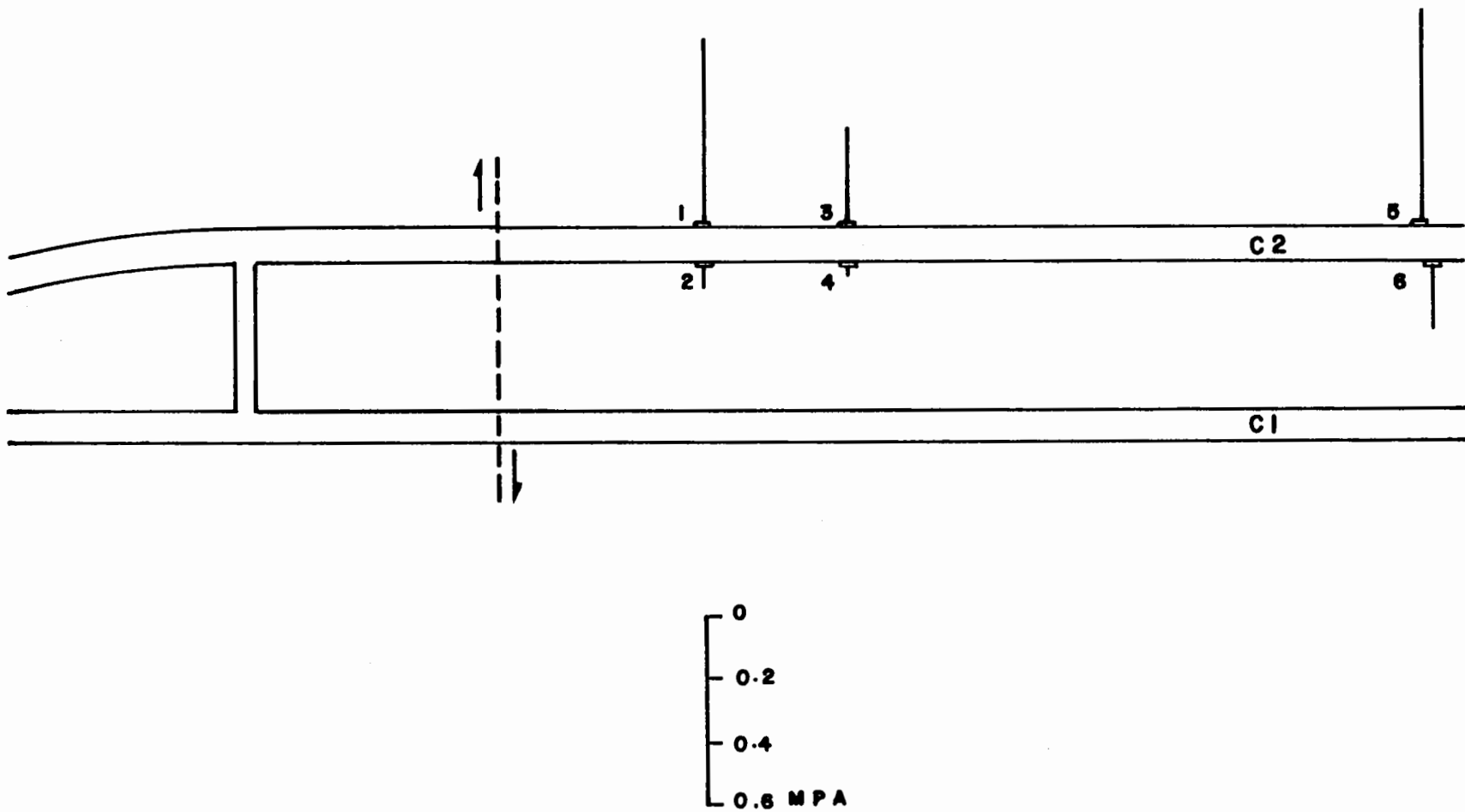


FIGURE 7.16 Pressure distribution along C2 tunnel.

## CHAPTER 8

### MODEL STUDIES OF FAULT - TUNNEL INTERACTION

#### 8.1. Strike Slip Fault Models

If a satisfactory model of fault behaviour can be derived, it should be possible to make some useful predictions of ground deformations and stress changes that can be expected near an active fault. The discussion in this section is restricted to the particular case of strike slip faulting, but could be extended to other kinds of faulting.

In section 8.1.1, the constitutive relations and geometry of a fault zone and surrounding ground subjected to prescribed boundary conditions are modelled. This quasi-static model can then be used to explain deformations and stress changes that occur before, during, and after an earthquake. The interaction of one fault with another is an important part of the problem of deformation in tectonically active areas. In section 8.1.2, fault interactions are modelled by the "Riedel experiment" (after Riedel, 1929). This is an experiment that has been used by geologists in a qualitative way to demonstrate development of shear zones (e.g. Cloos, 1955; Tanner, 1962; Wilcox *et al.*, 1973). In section 8.1.3, a fault model is proposed that explains observed seismic phenomena along the Hayward Fault.

##### 8.1.1. Quasi-Static Fault Models

###### Anderson's Model

The model for faulting proposed by Anderson (1951) can provide insight into primary principal stress magnitude and direction around an active fault. This model combines

empirical results for the failure of rock (the Coulomb failure criterion) with constraints on principal stress directions. For a strike slip fault in isotropic rock, the vertical principal stress is the intermediate principal stress,  $\sigma_2$ . One of the other principal stresses will be higher ( $\sigma_1 > \sigma_2$ );  $\sigma_3$  will be small and may even be tensile (Figure 8.1).

Given the simple case of sliding along a single plane with an angle of friction  $\phi_J$ , it can be shown that the ratio of minimum to maximum principal stresses at limiting equilibrium is :

$$\frac{\sigma_3}{\sigma_1} = \frac{\cot\phi_J - \cot\alpha}{\tan\alpha + \cot\phi_J}$$

where  $\alpha$  is the angle between  $\sigma_1$  and the normal to the fault. Using this relationship, if the relevant angles of friction are known for the shears in a shear zone, the principal stress directions can be calculated for a given geometric arrangement of shears and primary principal stress ratio.

### **Strain-softening Models**

Recent understanding of fault mechanics has developed from the use of strain softening models for fault zones (Stuart, 1979). These models allow the definition of an instability criterion such that the stiffness of the fault becomes less during failure than the stiffness of the elastic surroundings. This is the same instability criterion that is observed during compression testing of rock. Strain softening models can explain fault zone failure either by a stable mode (slippage) or an unstable mode (earthquake).

Clays from fault zones have been recompacted and tested in high pressure triaxial equipment (Wang *et al.*, 1980). Strain softening was observed and is believed to occur in all geological materials, however the stress at which softening takes place is much lower for clays than intact rocks. Geophysical data suggest that clays are present along the San Andreas Fault at depths as great as 10km (Wang *et al.*, 1978).

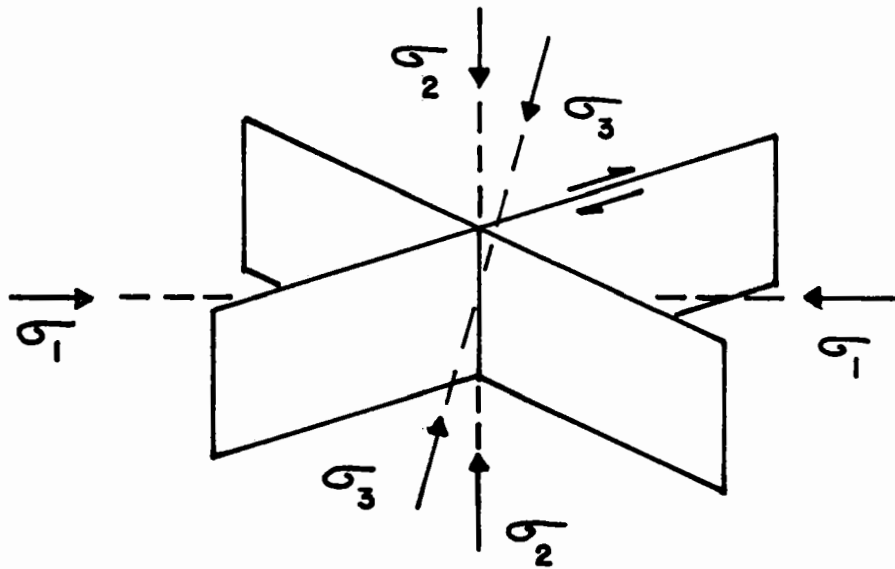


FIGURE 8.1 Principal stress orientations for strike slip faulting.

If a simple fault model is considered (Figure 8.2a) with uniform fault strength, and a surrounding elastic plate with stress-free top and bottom surfaces, then instability conditions can be derived from the stress-strain relationships for the elastic plate and the fault. The elastic plate is strained by increasing displacements  $\pm U$  at a distance  $\pm H$  from the fault. There can be a small displacement along the fault  $2u$ , corresponding to fault slippage.

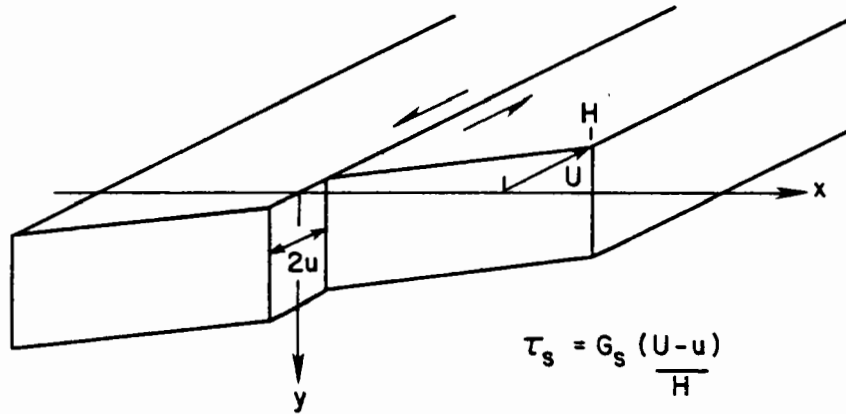
For the elastic plate in simple shear, the shear stress  $\tau_s = G_s \gamma_s$  where  $G_s$  is the shear modulus ( $G_s = \frac{E_s}{2(1+\nu_s)}$ ) and  $\gamma_s$  is the shear strain. Then  $\tau_s = G_s \frac{(U - u)}{H}$ . The fault zone stress-strain law is assumed to be initially strain-hardening (Figure 8.2b), reach a peak stress and then become strain softening. The stiffness of the fault is given by  $K_f = \frac{d\tau_f}{du}$  and the stiffness of the elastic plate is given by  $K_s = \frac{d\tau_s}{du} = \frac{-G_s}{H}$ . The two stiffnesses are independent, and are defined as rates of shear stress change with respect to fault displacement  $u$ , i.e.  $K_f$  and  $K_s$  are slopes of the stress-strain relationships.

As  $U$  increases, the line for the elastic surroundings moves from point 1 to point 2 on Figure 8.2b in a series of parallel lines with slope  $K_s$ . The intersection of this line with the fault stress-strain curve gives  $\tau_f = \tau_s$ ,  $u$ , and thus  $\gamma_s$ . When  $K_f \leq K_s$ , instability occurs because an increase in  $u$  or  $U$  leads to  $\tau_f < \tau_s$ , which does not satisfy static equilibrium.

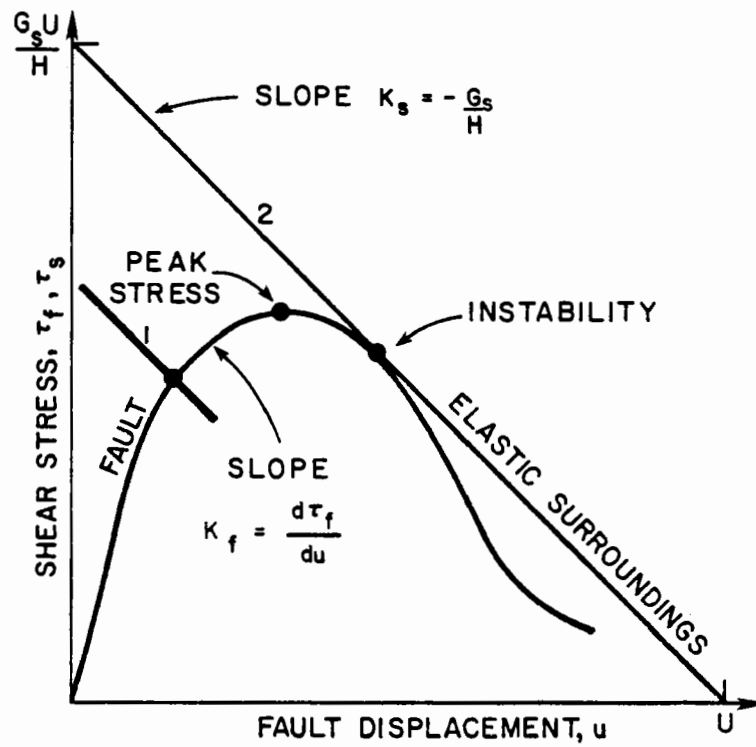
The fault slip rate,  $\frac{du}{dU}$  increases prior to instability because  $\frac{d^2\tau_f}{dU^2} < 0$ . Also, the shear stresses  $\tau_f$  and  $\tau_s$  decrease prior to instability. At the point of instability, energy is released in the form of an earthquake, and there is fault displacement.

In all theories of faulting, the fault slip is driven by release of elastic energy stored in the surrounding rock. This idea was originally proposed in the elastic rebound theory of Reid (1911), based on changes in crustal strain observed after the 1906 earthquake on the San Andreas Fault.





(a)



(b)

FIGURE 8.2 Fault model (after Stuart, 1980).

This simple model of fault behaviour can give some insight into earthquake precursors that might be used for earthquake prediction. From the model,  $\gamma_s$  increases during increasing  $\tau_s$ , reaches a maximum at peak stress, and decreases with decreasing  $\tau_s$ . Thus measuring changes in strain rates can indicate approaching instability. Stuart (1980) defined a dimensionless stiffness ratio  $R = \frac{K_f}{K_s}$  which is readily computed from the rate of change of shear strain with respect to the remote displacement  $U$ . When  $R \geq 1$ , instability is predicted. However, the application of this approach using geodetic survey data is limited by large observation errors, and infrequent surveys. The fault model also shows  $\tau_f$  and  $\tau_s$  to decrease prior to instability, suggesting that if changes in stress can be monitored, it should be possible to predict earthquakes.

A real fault is obviously more complex than suggested by this model. In general, the state of stress in a fault zone will be highly variable, as will the stress-strain relationship for the materials in and around the fault. Time-dependent properties of the materials should also be considered. It is the spatial fluctuations of stress, due to geometric and material irregularities that explain the range of earthquake sizes that occur along a particular section of a fault. Closely spaced barriers, fault segments with higher stiffness, appear to control small magnitude earthquakes. Similarly, larger earthquakes can be expected to occur at barriers with a larger area and spacing.

If a fault is "stuck" at a barrier, it is of interest to know something about the stress changes that occur in adjacent areas as displacement continues. A simple two dimensional finite element model was used to investigate this problem (Figure 8.3). Using the computer program JTROCK (Hittinger and Goodman, 1978) it was possible to model a fault with a line of non-linear joint elements, and the surrounding elastic plate with linear orthotropic quadrilateral isoparametric elements. The vertical boundaries of the upper half of the model were progressively displaced (as in a shear box test) in a right lateral sense to simulate fault motions. The two joint elements in the middle of the model were given a higher

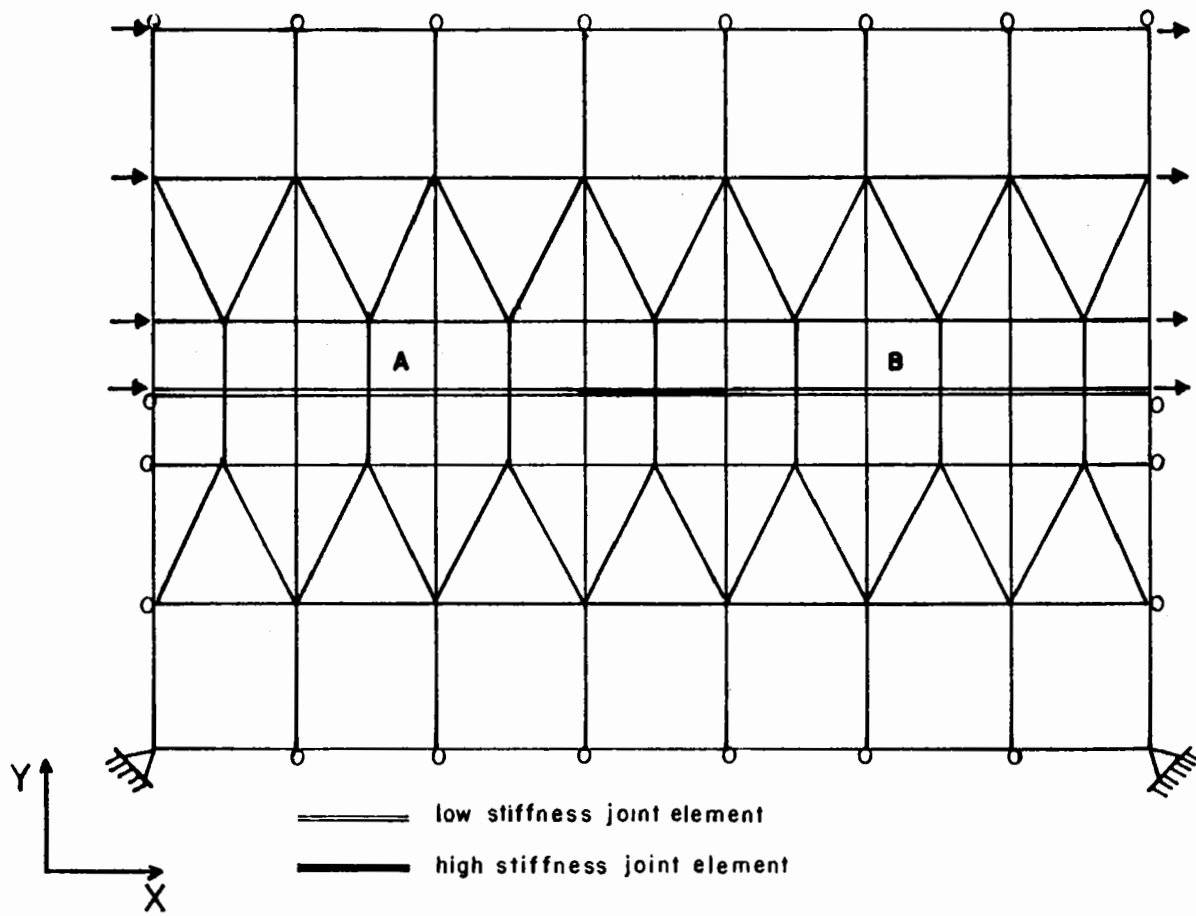


FIGURE 8.3 Finite element model of fault in elastic surroundings.

shear and normal stiffness than the other joint elements to model a fault barrier. Numerical difficulties associated with the model formulation did not allow the solution to converge. It was possible, however, to make a qualitative interpretation of the results.

The change in stress in a quadrilateral element was dependent on its position relative to the high stiffness joint elements. If the principal stresses in element A (Figure 8.3) are considered, as right lateral shear progressed there was an increase in  $\sigma_{xx}$ , and a counter clockwise rotation of principal stress axes. At the same time in element B, there was a decrease in  $\sigma_{xx}$  and a clockwise rotation of principal stresses. If instability could occur in the high stiffness joint elements (i.e. an earthquake) an increase in  $\sigma_{xx}$  would be expected in element B, and a decrease in element A as elastic strain energy was released. This is similar to the observation of Morgenstern and Tchalenko (1967) that following peak strength in a shear box test there is local increase and rotation of principal stresses in the sense opposite to that of the general displacement. Cohen (1980) used a dislocation model to show that near a fault there may be a post-seismic stress rise whose magnitude can be a significant fraction of the stress drop on the fault due to an earthquake.

Within the joint elements, shear stress increased with incremental displacement. For the joint element adjacent to element B, the shear stress increase was an order of magnitude higher than for the joint element adjacent to element A.

### **Dislocation Models**

Dislocation theory, which has developed from studies of crystal physics, can be used to model fault behaviour (e.g. Nason and Weertman, 1973; Eshelby, 1973). The movement along a crystal imperfection at low stress levels leads to deformation; this imperfection is the dislocation, i.e. an internal surface in an elastic solid across which there is a discontinuity of displacement. Dislocations are used to explain the discrepancy of many orders of magnitude between the theoretical and observed shear strengths of crystals. On a

large scale, faults can be considered as dislocations in the earth's crust. Therefore surface strain data obtained by direct measurement can be input into a dislocation model to determine parameters such as stress drop, and slip distribution. In dislocation models the fault slip is imposed as a boundary condition, and the remote stress is held constant. Fault displacement is then not dependent on a fault constitutive law. Dislocation models are often used to obtain fault parameters such as stress drop and seismic moment.

### **Frictional Models**

In frictional models of active faulting (e.g. Dietrich, 1978; Nur, 1978) an earthquake occurs because of the sudden drop in fault shear stress from peak strength to a lower value. An equivalent strain softening model would be either one where instability occurred at a peak shear stress, i.e. the stiffness of the elastic surroundings,  $K_s$ , would be zero (refer Figure 8.3b), or one where no displacement occurred along the fault.

#### **8.1.2. The Mechanics of Shearing along an Interconnected System of Discontinuities**

In the Riedel experiment a slab of "plastic" material (usually clay) is placed over two adjoining boards that are then slowly displaced horizontally (Figure 8.4). A system of *en echelon* discontinuities and their conjugates develop which are referred to as "Riedel shears" and "conjugate Riedel shears" respectively. The clay modelling material adheres to the moving boards to ensure that shear stresses are developed in the clay. Although the sample is unconfined at its upper surface, Tchalenko (1970) considered that the capillary forces that act on the free surface give rise to an "equivalent ambient pressure" throughout the specimen. Tchalenko measured the force required to displace one of the boards relative to the other, and obtained a characteristic force displacement curve (Figure 8.5a). By observing the development of individual shears and the distortion of markers inscribed on the clay

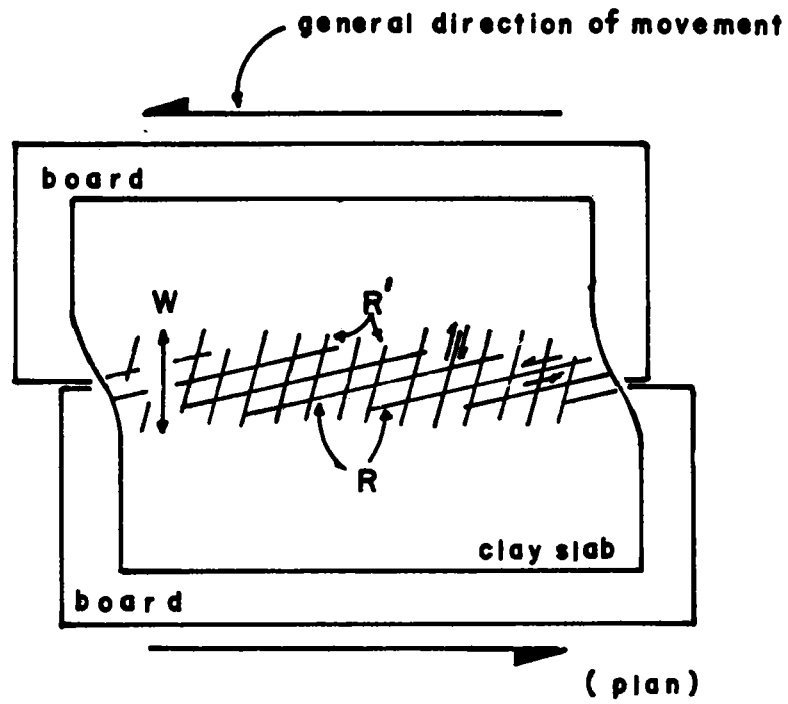


FIGURE 8.4 Riedel experiment.

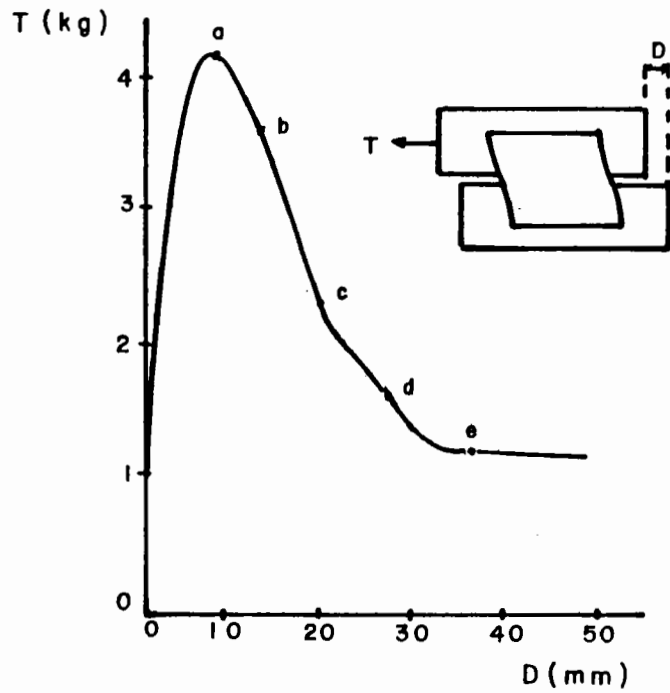


FIGURE 8.5a Force-displacement curve for Riedel experiment.

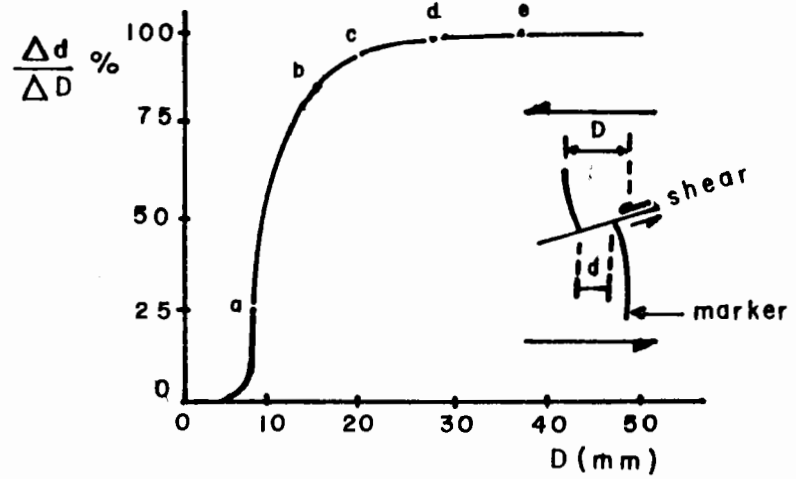


FIGURE 8.5b Proportion of total movement taken up by shears.

surface, the approximate proportion of the board displacement ( $D$ ) taken up by the individual shears ( $d$ ) was measured. Figure 8.5b shows the rapid increase in movement along shears that occurred after the peak strength was reached.

Tchalenko distinguished five stages in the development of a shear zone.

i) Pre-peak strength deformation

The initial displacements cause homogeneous straining in the region of the future shear zone. Circles inscribed on the clay surface are transformed into ellipses, indicating that the deformation is of the simple shear type.

ii) Peak structure

The first shears, Riedel shears ( $R$ ) and conjugate Riedels ( $R'$ ) (Figure 8.6) appear just before peak shear strength is reached, and they are slightly rotated anticlockwise at peak strength.

iii) Post-peak structure

Some Riedel shears are extended into a more horizontal direction, and a few new shears appear at lower angles.  $P$  shears (Figure 8.6) then form approximately symmetrical to the Riedel shears, interconnecting pairs of Riedel shears. Nearly all the total movement is taken up by displacements along shears.

iv) Pre-residual structure

The first continuous horizontal shears, the "principal displacement shears" are formed, isolating elongated lenses of essentially passive material between them.

v) Residual structure

Nearly all displacements take place along a single principal displacement shear superimposed on the interface between the two boards.

In some cases the conjugate Riedel shears appear before the Riedel shears. Because of the large angle that they make with the general direction of movement, the conjugate Riedel shears become passive and distort into an S shape. In simple shear, the Coulomb



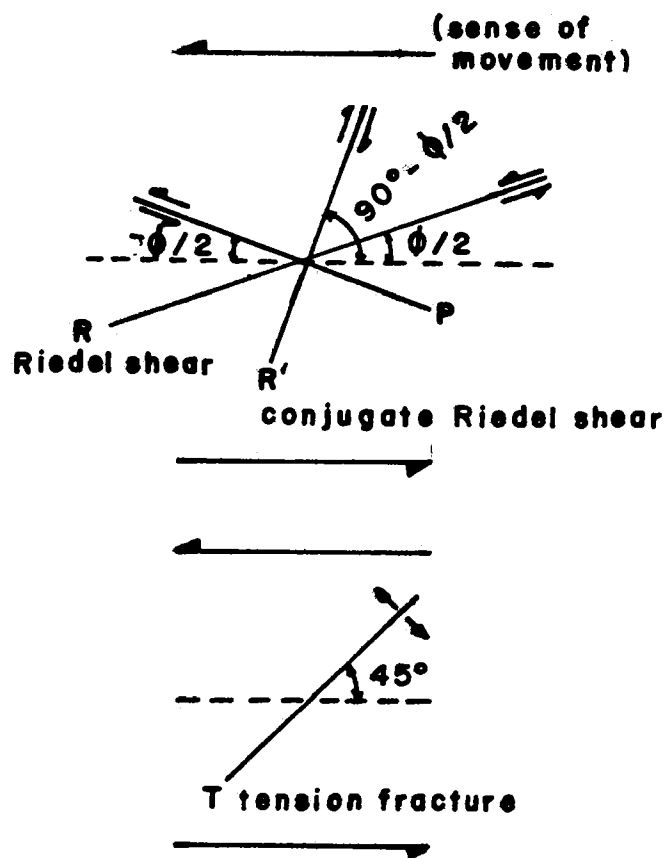


FIGURE 8.6 Mechanistic terminology for simple shear structures.

failure criterion predicts that failure surfaces are inclined at  $\frac{\phi}{2}$  and  $90^\circ - \frac{\phi}{2}$  to the general direction of movement ( $\phi$  is the peak friction angle). The Riedel shears and the conjugate Riedel shears are found to have these orientations in the simple shear experiment. In some cases, tension fractures are formed in place of, or in addition to, the Riedel shears and develop at about  $45^\circ$  to the direction of movement.

In a shear box, the sample can be confined and the level of stresses is much higher than in the Riedel experiment. Tchalenko (1970) carried out a series of tests on a clay that was similar to the clay he used in the Riedel experiment, and observed the structures that formed by stopping the test and preparing thin sections of the sample. The sequence of structures observed in the shear box test were essentially the same as those in the Riedel experiment. This was true for the scale of the entire sample, and on the microscopic scale of a few tens of microns. Near the edges of the shear box specimen where there is kinematic constraint and high stress concentrations, shear structures were found that did not correspond to the Riedel model.

Morgenstern and Tchalenko (1967) reviewed three alternative interpretations of the mechanics of the shear box test and concluded that the stresses in the central portion of the specimen, at or near peak strength ( $\phi_p = 24^\circ$ ) are as shown in Figure 8.7. It was postulated that following the peak strength, the development of a post peak structure (P shears) involved both a reduction of the shearing resistance along the Riedel shears toward the residual strength value, and a local increase and rotation of the principal stresses in the sense opposite to that of the general movement. At the residual stage (if sufficient displacement can be obtained in a shear box), the active portion of the shear zone decreases in width and direct shear conditions are approached. The major principal stress is then predicted to be orientated at  $45^\circ - \frac{\phi}{2}$  to the direction of the shear surface.

Byerlee *et al.* (1978) carried out laboratory shear tests on a saw cut in granite with a sand infilling. The normal stress across the discontinuity was high (200 MPa). Intensely

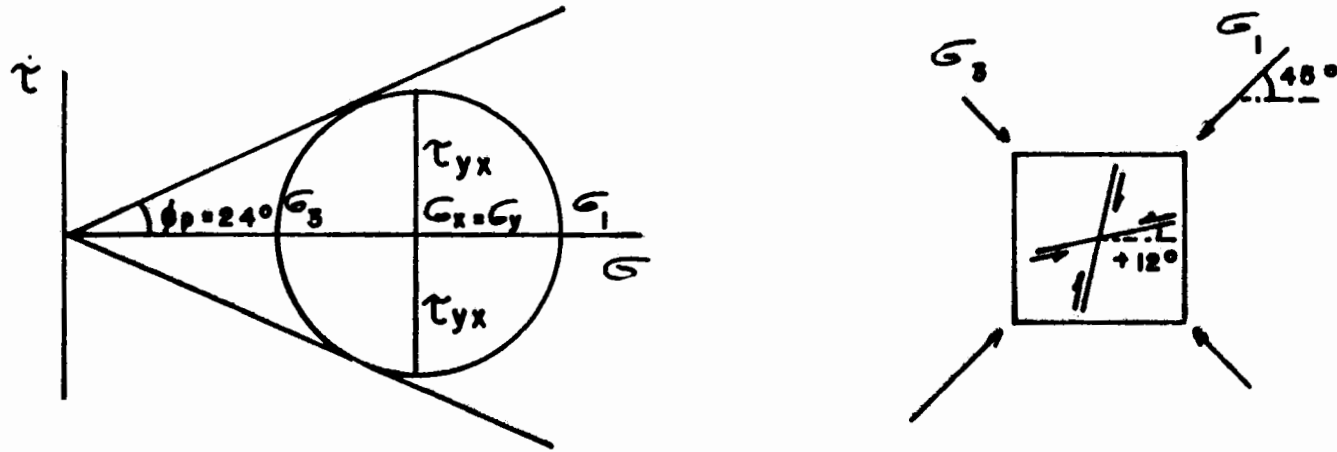


FIGURE 8.7 Stresses at peak strength in a shear box.

sheared material developed parallel to the sliding direction at the boundaries between granite and sand, and an oblique shear was observed at  $20^\circ$  to the plane of the saw cut. In these experiments it was considered that the Riedel shears were controlled by the boundaries of the gouge, rather than the material properties or the direction of the applied stress. The evidence did suggest that stable sliding on the oblique shears preceded sudden slip, which was confined to the margin between the shear zone and the intact rock.

Riedel shears have been observed at various scales, from the microstructure of a clay sheared in a laboratory test, to the ground surface pattern of rupture of an active fault zone. In general, a shear zone at a particular scale is formed by a system of shears on a lower scale; the pattern of these shears is referred to as the shear zone structure. Thus the results from small-scale experiments can be used in the interpretation of displacement patterns in zones where shearing may affect engineering structures. With strike slip faults, it is not possible to follow the development of the shear zone continuously as in a Riedel experiment, or even at intermittent stages as in a shear box test. Usually it is only possible to observe the structures that have resulted following fault displacement, with little indication as to the sequence of development of structures in the shear zone.

Tchalenko and Ambraseys (1970) mapped in detail the surface traces of an active fault in Iran. Surface movements were mainly strike slip, with minor vertical displacements. Ridges and cracks were found to be concentrated in shear zones which were the equivalent of shears described for smaller scales. These zones varied in length from several metres to several hundreds of metres, and in width from about a metre to some tens of metres. In the zone where most of the displacement occurred, Riedel shears and some P structures were recognised, and conjugate Riedel shears were also found.

### **8.1.3. A Model for the Hayward Fault**

A model for the Hayward Fault should be able to explain the following fault phenomena :

- fault slippage at a more or less constant rate
- fault slippage confined to a discrete shear zone
- pressure changes on the BART tunnel liner
- spatial and temporal variations in seismicity
- discrete fault movements with long recurrence intervals.

The strain softening model discussed in section 8.1.1 can be applied to the Hayward Fault. As the fault is approached there is a reduction in rock mass stiffness, due to increased shearing and alteration, reaching a minimum at the low strength clay gouge. Near the ground surface the clay gouge is unable to sustain any appreciable shear stress, therefore fault slippage occurs at a more or less constant rate. Mavko (1980) numerically simulated creep events and earthquakes on a spatially variable model and concluded that slippage along the San Andreas Fault must be confined to the upper 1km to 2km of the fault.

Given several clay gouge zones with similar properties, maximum shear displacement will occur in the widest gouge zone and slippage might be expected to occur at one of the boundaries of the widest zone. This was observed in the BART tunnels (refer Figure 7.1).

At greater depths, where earthquakes occur, strain softening behaviour is expected. At some unknown depth, there is a transition from fault displacement by steady slippage, to fault slippage in discrete steps accompanying earthquakes. Thus steady slippage and earthquakes can be expected along the same fault segment. The seismic record from the Hayward Fault shows spatial and temporal variations in seismicity. This reflects instability occurring at fault barriers that have locally higher stiffness and peak strength. Fault barriers may be due to inhomogeneity of fault zone materials, or local variations in fault geometry.

The difficulties associated with interpretation of the pressure cell records from the BART tunnels were discussed in section 7.5. However it does appear that the pressure readings give some indication of *in situ* stress changes. The pressure cells are orientated with their long axes more or less normal to the strike of the fault, and could be expected to

record changes in stress within the fault zone. The strain softening model predicts a drop in shear stress prior to instability and the time-pressure history for the pressure cells suggested by this fault model is shown in Figure 8.8.

To investigate the relationship between changes in cell pressures and earthquakes, source parameters for earthquakes that occurred along the Hayward Fault were obtained from the U.S. Geological Survey catalogue (see section 5.3). Earthquake magnitude,  $M_L$ ,<sup>1</sup> and focal location data were used to plot cumulative magnitude divided by focal distance against time (Figure 8.9)<sup>2</sup>. The reduced influence of distant earthquakes was taken into account by dividing magnitude of each earthquake by distance of the focus from the BART tunnels.

Earthquake moment,  $M_o$ ,<sup>3</sup> is considered a more fundamental parameter than magnitude, and gives a better estimate of earthquake size. Magnitude measurements are based on a narrow frequency range of the seismic wave spectrum, while moment is based on a wider frequency range. Empirical relationships between magnitude and moment have the form  $M_L = k \log M_o$ , where  $k$  is a constant. Thatcher and Hanks (1973) found that for 138 earthquakes in Southern California,  $\log M_o = 1.5M_L + 16.0$  (in units of dyne-cm), and this relationship is often used for other geographic areas. However order of magnitude variations from this  $M_o - M_L$  relationship are not uncommon. For this study, the antilog of  $M_L$ , which is proportional to moment, was calculated from the U.S. Geological Survey data, and a plot of cumulative  $M_L$  divided by distance was prepared (Figure 8.10). On Figure 8.10, increases in seismic activity are marked by increases in gradient of the curve. This graph shows that changes in seismicity occur at the same time as in Figure 8.9, however there are more abrupt changes reflecting the contribution of a few higher magnitude earthquakes.

<sup>1</sup>  $M_L$  = local magnitude, more or less equivalent to Richter magnitude.

<sup>2</sup> The origin for the time axis on Figures 8.9, 8.10 and 8.11 is January 1, 1967.

<sup>3</sup>  $M_o = \mu DS$ , where  $\mu$  = rigidity,  $D$  = average fault slip,  $S$  = fault area.  $M_o$  is the moment of one of the couples in a double couple representation of a point dislocation.  $M_o$  is also a function of the radiation pattern of the seismic waves and the long period spectral amplitude.

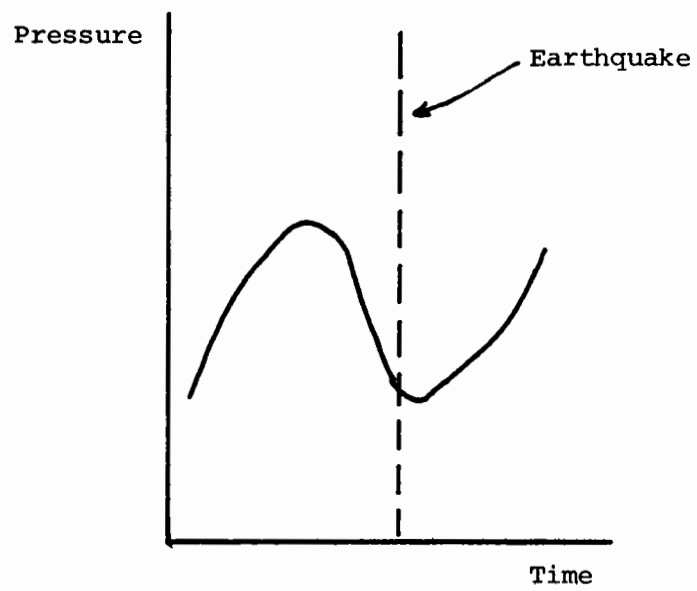


FIGURE 8.8 Pressure cell changes with time as predicted by fault model.

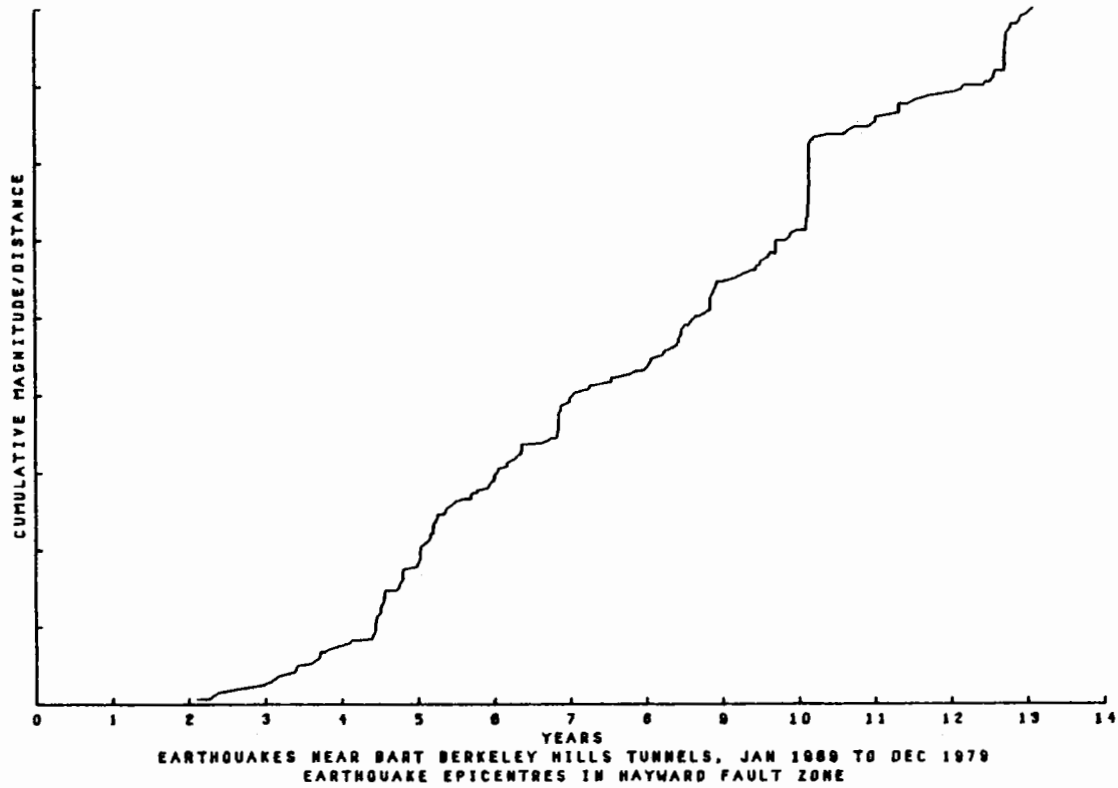


FIGURE 8.9 Earthquakes in Hayward Fault zone near BART tunnels, cumulative magnitude divided by distance.



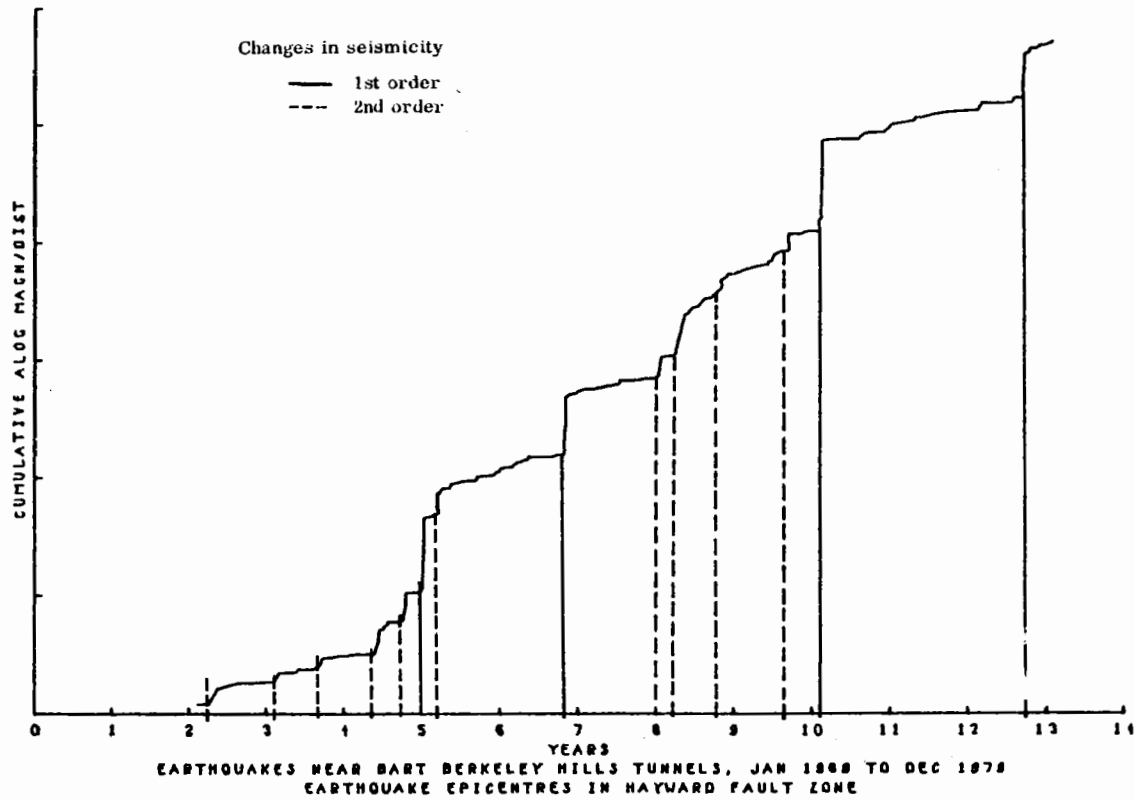


FIGURE 8.10 Earthquakes in Hayward Fault zone near BART tunnels, cumulative antilog magnitude divided by distance.

Pressures recorded from cell 3 were normalised by fitting a straight line through the data. This removed the effect of fault slippage that more or less constantly increases passive pressures on the liner, and the residuals were plotted against time (Figure 8.11). To enable comparisons with the pressure cell data, large increases in seismicity on Figure 8.10 have been marked as first order features, and lesser increases as second order features. The corresponding points in time have been marked on Figure 8.11, where it is found that all first-order increases in seismicity are preceded by a decrease in pressure. Similarly, second order changes in seismicity follow smaller decreases in cell pressure. This was predicted by the strain softening fault model.

Because of the irregular interval between pressure cell readings, parts of the curve in Figure 8.11 are not well defined. It does appear that the pressure decrease prior to seismic activity occurs over a short period, as does the following pressure increase. Therefore, unless pressure cell readings were taken over short intervals, the pressure fluctuations will not be apparent. The sharp increase in cell pressure following seismicity is considered to be due to an increase in passive pressure acting on the tunnel liner, caused by a small amount of slip along the active trace of the Hayward Fault. A statistical correlation between the earthquake data and the pressure cell data was not possible because of the varying time steps between each data point. To use existing computer codes for statistical analysis of a pair of time series data would require interpolation between pressure cell data points. All pressure cell curves have similar shape (refer figures in Appendix C) and the seismicity/pressure change correlation found for pressure cell 3 is also valid for the other pressure cells.

During 1980, the pressure cells were monitored at more frequent intervals than in the past but the seismicity data were not available for comparison. Significant pressure drops were recorded prior to small earthquakes (about magnitude 3) that were reported in the Berkeley area in April and December.

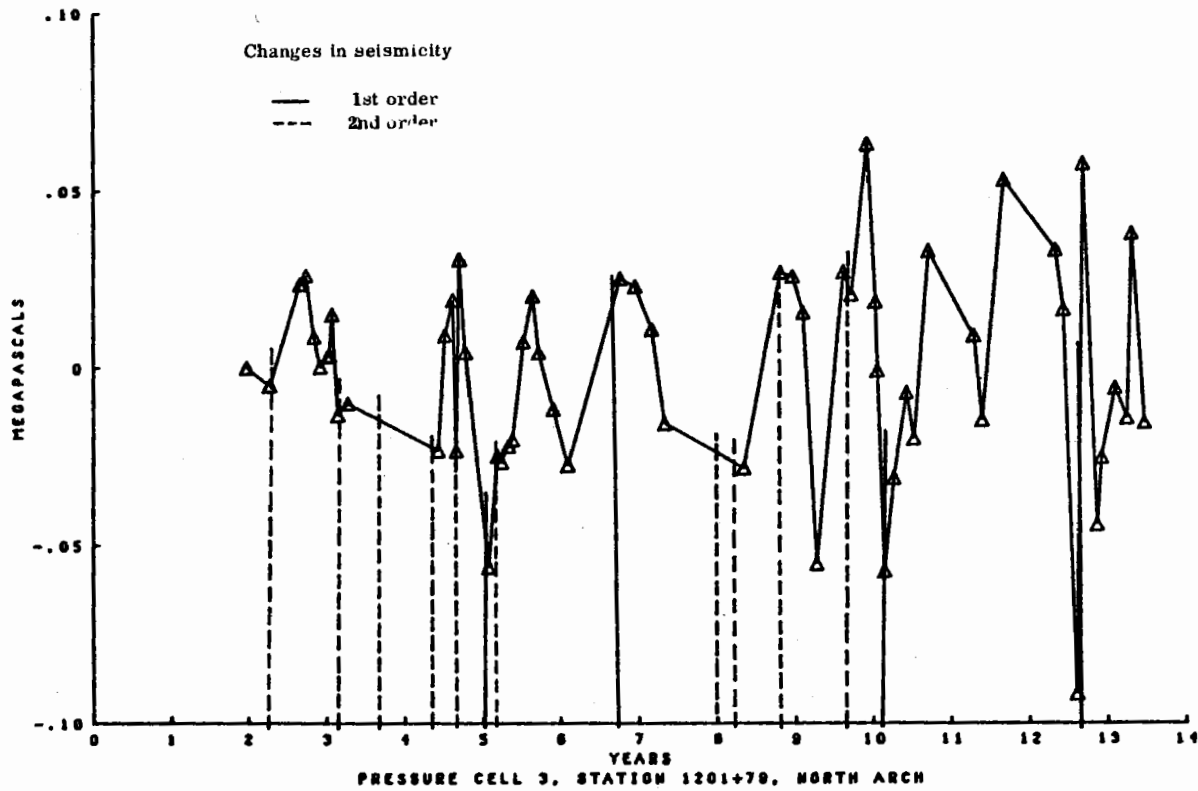


FIGURE 8.11 Pressure cell 3, residuals from linear curve fitting.

Other workers have attempted to monitor *in situ* stress changes near earthquake sources. Swolfs and Brechtel (1977) installed pressure cells close to ground surface in the Wasatch Range near Salt Lake City, Utah. They found an anomalous *in situ* stress change with an amplitude of about 1kPa prior to a rock burst with Richter magnitude less than M 1.0. Hardin and Pratt (1978) described two rosette stress monitor systems that were installed close to the San Andreas Fault zone near Palmdale, California. These instruments were found to be sensitive to local effects of earthtides, rainfall, and temperature changes. It is not known whether these problems were subsequently overcome and true *in situ* stress changes measured.

Most of the large strike slip faults that have undergone considerable displacement have wide fault zones consisting of low strength, strain softening materials. Where such faults are actively slipping, slippage is known to be confined to one distinct surface (Nason 1971). This shear surface can be considered to correspond to the principal displacement shear, part of the residual structure that forms in the Riedel experiment. The Berkeley Hills provide an example of pre-residual structure, that is subparallel displacement shears that isolate a block of essentially passive material. An idealised fault map for this area is shown in Figure 8.12 (compare with Figure 5.3). In a simple interpretation of the Berkeley Hills, the Hayward and Moraga Faults are considered to be principal displacement shears, the Wildcat, Chabot and other subparallel faults are P shears, and the northeast-southwest trending faults are conjugate Riedel shears. While the Hayward Fault is actively slipping, it is functioning as a single displacement shear along which nearly all the displacement takes place.

## **8.2. Two Dimensional Plane Strain Model of a Typical Liner Section**

Conventional tunnel liner design requires the analysis of the load bearing capacity of a section of tunnel liner normal to the tunnel axis. Such analysis can be performed using

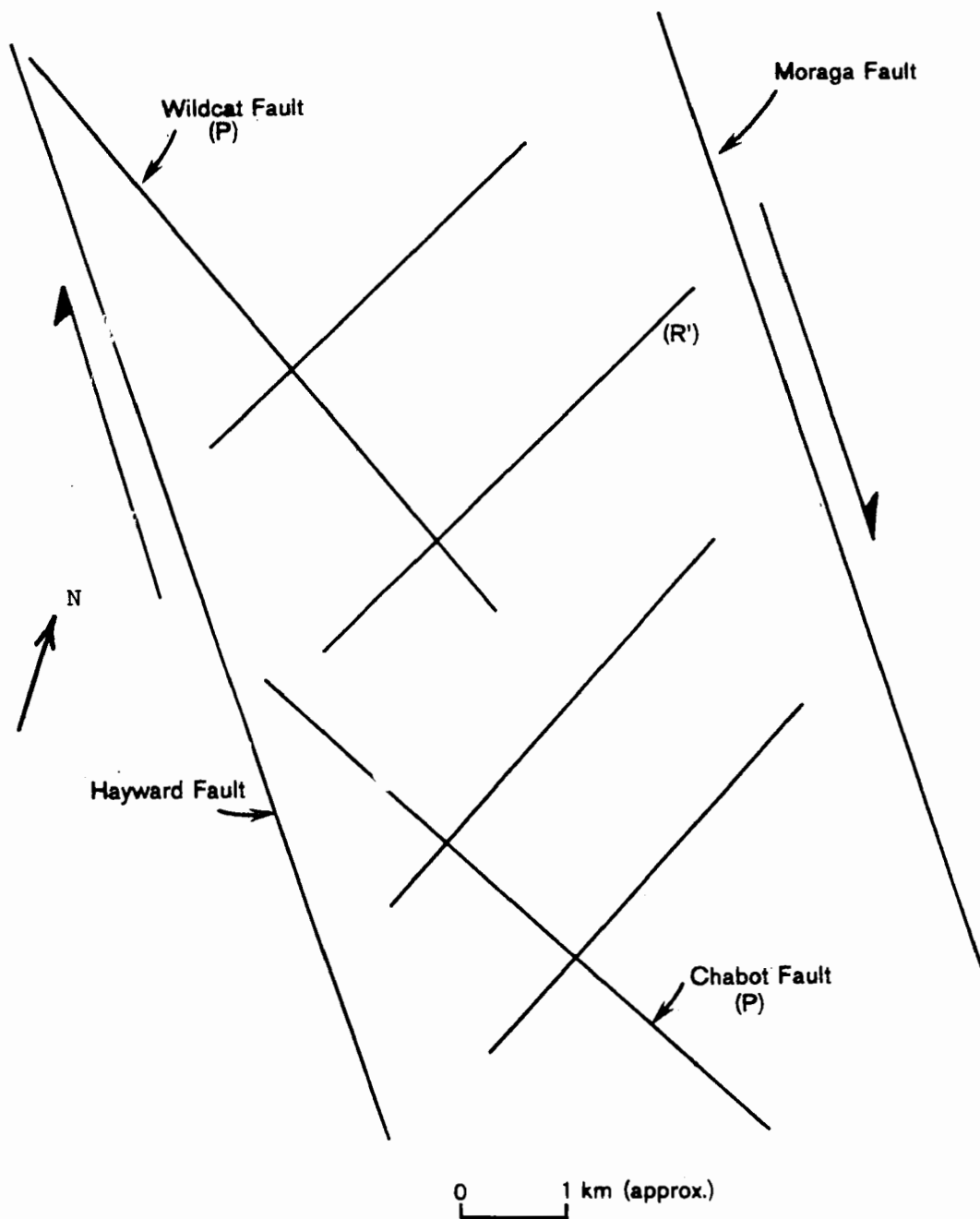


FIGURE 8.12 Idealized fault map, Berkeley Hills.

computer program LINER, a general structural analysis program for tunnel support systems subjected to external loads, or active pressures (Korbin and Krakowski, 1980). The program uses a matrix formulation of the direct stiffness method to determine joint deflections, member end forces, and joint reactions for plane frames subjected to joint loads and displacements. For the purposes of this study, the program was extended to allow consideration of the full tunnel section subjected to asymmetric loading.

The tunnel liner structure is divided into elements with more or less equal length. Each element is defined by two nodal points at the ends of the element midway between liner intrados and extrados. The nodal coordinates are used to establish element position, length, and section properties. Each liner element is represented by a straight beam member joining two adjacent nodal points. The nodal point connection between these elements is a rigid or fixed connection with full transfer of moment.

To model the passive ground reactions that result from liner distortions, a bar element is attached to each liner nodal point directed radially into the surrounding ground. These elements are automatically generated by the program. The connection between the bar element and the liner, and the bar element and the ground is a pinned or zero moment connection. Therefore the bar elements can only accept axial forces, or reactions directed radially from the liner. Passive reactions result from liner displacements or distortions, and are determined from pure bending of the liner structure. The stiffness of the bar element is derived from the modulus of subgrade reaction of the ground, and the tributary area represented by the bar. Bar elements that are in tension are released through an iterative procedure until the calculated axial forces in the remaining elements are zero or compressive.

LINER has three options, to analyse either an uncracked asymmetric, an uncracked symmetric, or a reinforced concrete section. Analysis of a reinforced concrete section requires calculation of the transformed steel areas, and the area of the uncracked or

compressive concrete section. This solution cannot be formed directly and an iterative scheme is used. After each iterative cycle, member forces are calculated from the section properties of the previous iteration.

The BART tunnels were modelled as shown in Figure 8.13, with 26 liner elements and corresponding bar elements. Average reinforcing steel areas were calculated for intrados and extrados, and the reinforced concrete section option was used for all calculations.

### 8.2.1. Bechtel Design Pressures

The response of the tunnel was analysed using Bechtel design pressures of 1.436MPa vertical and 0.862MPa horizontal. Because this loading case is symmetrical about the tunnel centre line, only the right half of the model was analysed (Figure 8.13). There were no modulus of subgrade reaction ( $k_s$ ) data available for the materials encountered in the Berkeley Hills tunnels, therefore a parametric study was undertaken using values for  $k_s$  of 6, 9, 12, 15, and 18 MN/m.

For analyses with  $k_s$  set at 6 and 12 MN/m, the calculated values of moment, stress in extrados and intrados steel, and stress in extrados concrete have been plotted (Figures 8.14, 8.15, 8.16). In these figures, tension is positive and compression is negative.

To investigate the sensitivity of this analysis to modulus of subgrade reaction, Figures 8.17, 8.18, and 8.19 were plotted to show the relationship of  $k_s$  to calculated stresses.

As might be expected, with a low modulus of subgrade reaction, large deformations take place leading to higher stresses. However when  $k_s$  is greater than about 10MN/m, an increase in  $k_s$  has little effect on liner behaviour. For the values of modulus of subgrade reaction used, all steel stresses were lower than yield strength (275 MPa for grade 40 steel). In all cases the intrados concrete was calculated to have cracked in all elements.

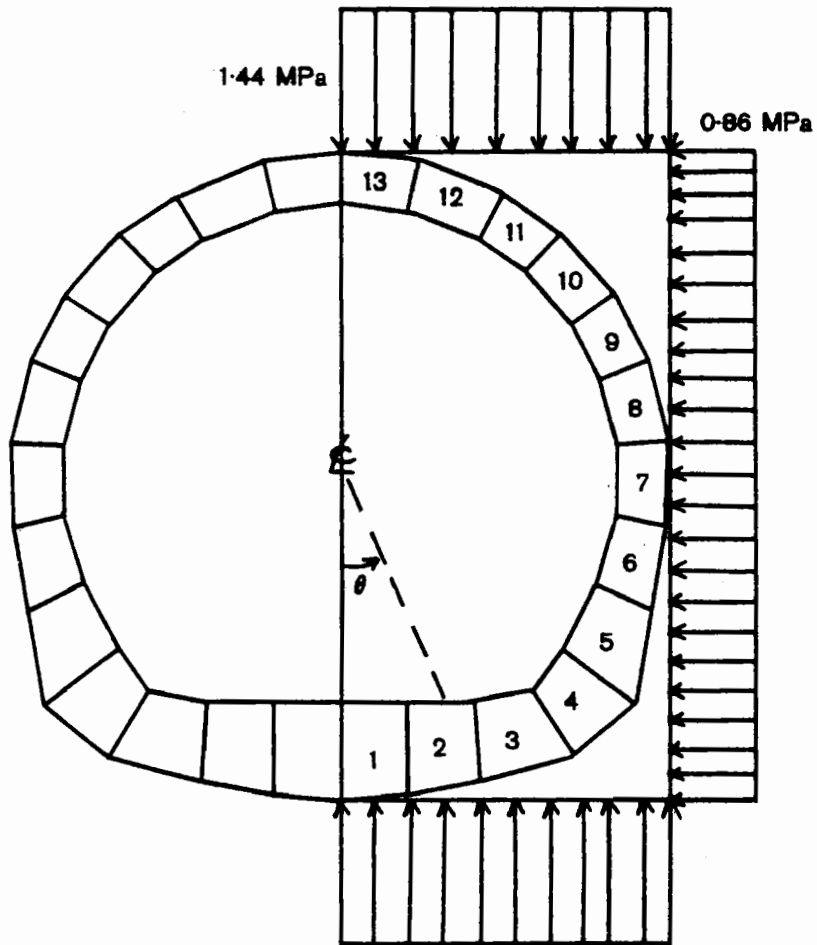


FIGURE 8.13 Model of BART tunnels used for analysis with program LINER.



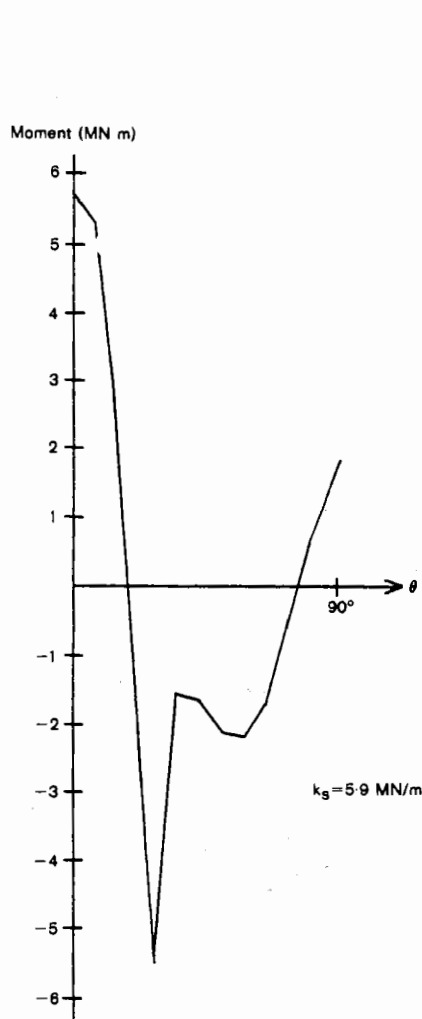


FIGURE 8.14 Moment distribution in tunnel liner, Bechtel design loading.

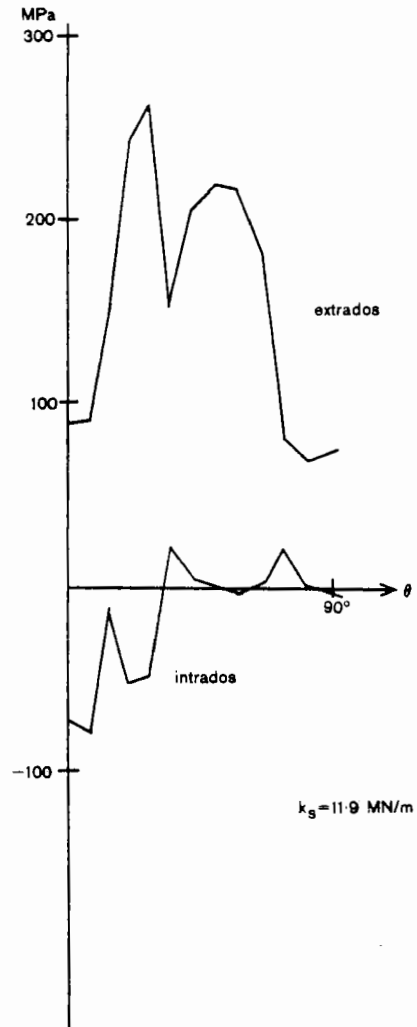


FIGURE 8.15 Steel stress, Bechtel design loading.

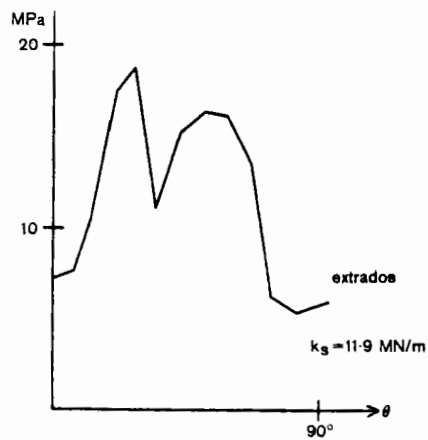


FIGURE 8.16 Extrados concrete stress, Bechtel design loading.

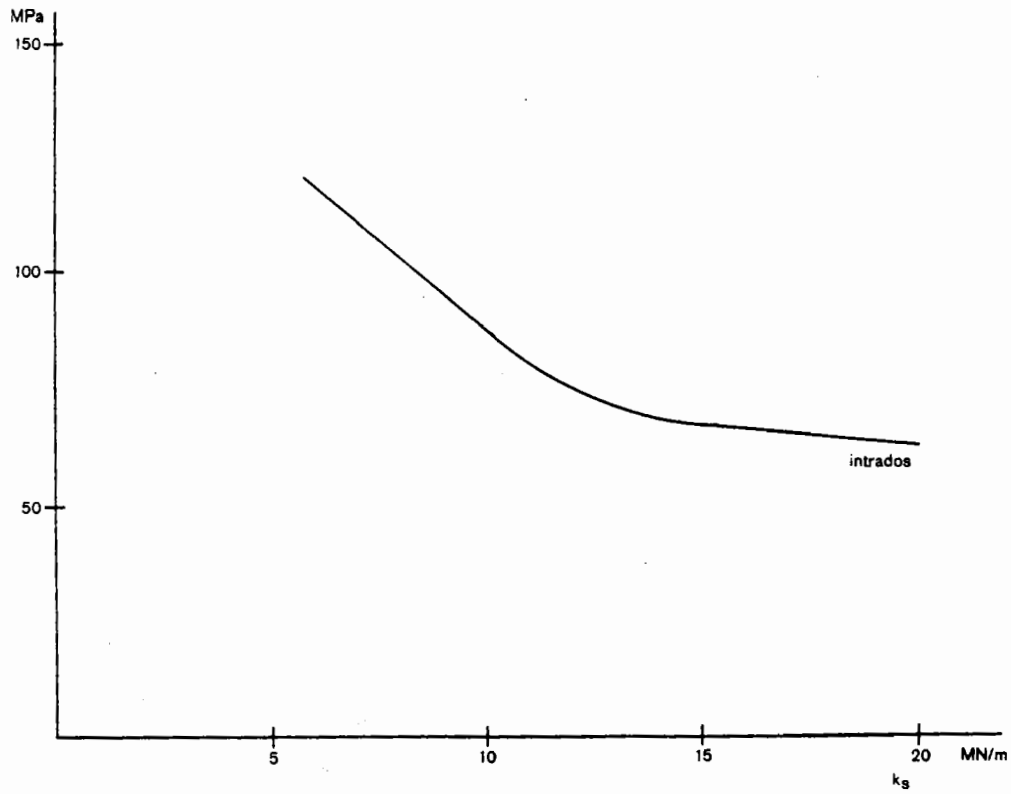


FIGURE 8.17 Intrados steel stress in element 2.

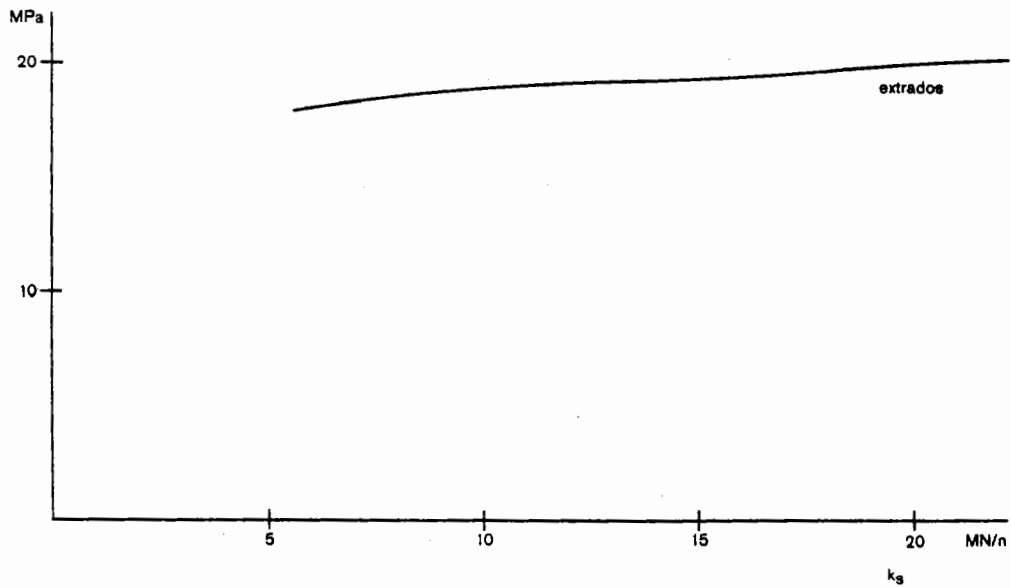


FIGURE 8.18 Extrados concrete stress in element 5 for various values of modulus of subgrade reaction.

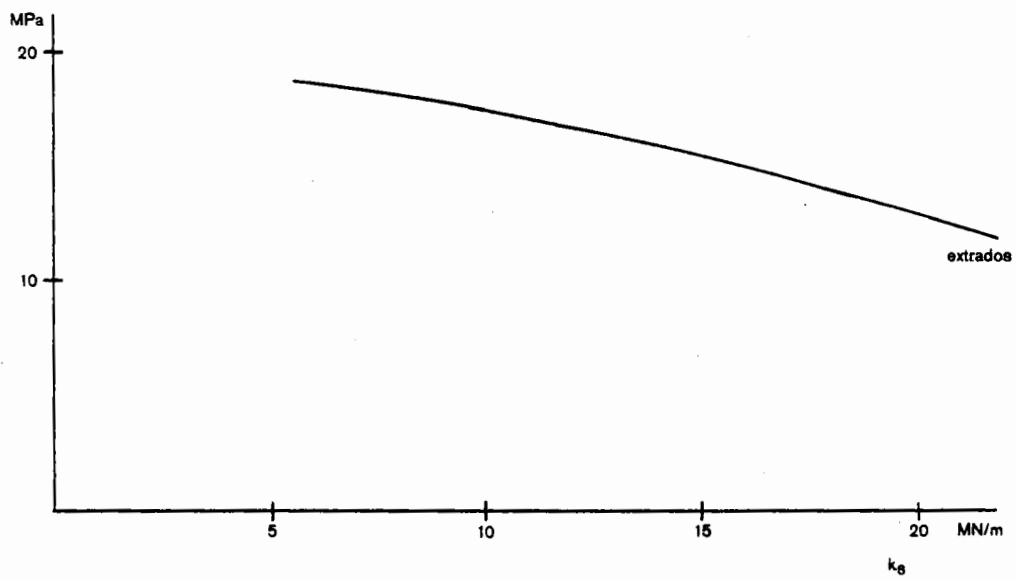


FIGURE 8.19 Extrados concrete stress in element 8 for various values of modulus of subgrade reaction.

### 8.2.2. Pressure Distribution Inferred From Pressure Cell Data

An attempt was made to model the asymmetric pressure distribution that is inferred from the pressure cell data. As discussed in section 7.5, at each of the three instrumented stations, pressure cells on the north side of the tunnel have readings 5 to 6 times higher than on the south side.

The pressures recorded by cells at Station 1206+31 have varied with time, so for the purposes of this analysis a typical pressure of 0.76MPa for cell 5 and 0.14MPa for cell 6 were used. If these pressures are resolved into their horizontal and vertical components, the pressure distribution shown on Figure 8.20 is deduced.

To start with, uniform horizontal pressure distributions of 0.59MPa and 0.11MPa, and a varying vertical pressure were used. The high pressures caused tension in the bar elements on the north side so they released, and pressures increased on the south side due to increasing passive pressures. The pressures on the south side were much higher than has been recorded, indicating that the loading diagram was incorrect.

Maintaining the horizontal and vertical pressures deduced from cell 5, further analyses were undertaken with possible vertical and horizontal pressure distributions. In all these analyses, equilibrium conditions required considerable passive pressures to be developed in the region of cell 6. Even though some of the loading conditions were strongly asymmetric, the stresses calculated were always less than those calculated with the Bechtel design loads.

### 8.3. Axi-symmetric Model

When a tunnel and surrounding ground are symmetric about the tunnel axis, a two-dimensional axi-symmetric model can be used to show three-dimensional behaviour. Axi-symmetric solids are defined using a cylindrical coordinate system  $(r, \theta, z)$ ; the solid body

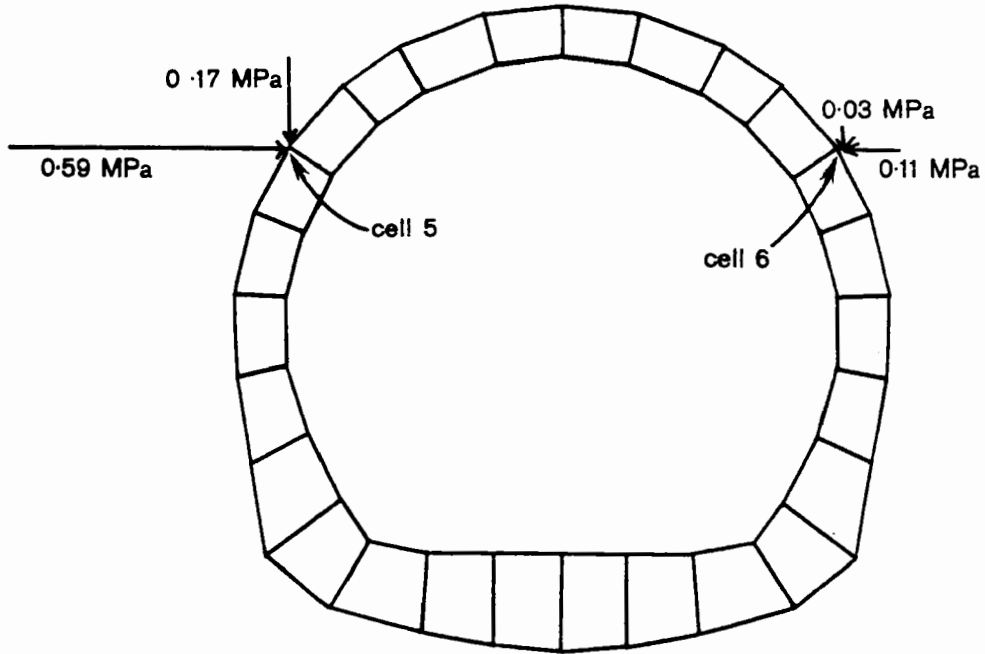


FIGURE 8.20 Pressure distribution on C2 tunnel liner at Station 1206+31.

is developed by revolving a plane  $\theta = \text{constant}$  about the  $z$  axis (Figure 8.21). Thus the shape of the body is completely defined by any plane of  $\theta = \text{constant}$ .

Axi-symmetric solids can be subdivided into discrete volumes and methods of finite element analysis used to calculate stresses and strains. For the purposes of this study, computer code FEAP was used (Taylor, 1977). FEAP uses a macro programming language in order to solve different types of finite element problems, including those with axisymmetric, orthotropic 9 node elements. In the formulation of the axisymmetric finite element mesh, each node has coordinates  $(r, z)$  for all values of  $\theta$  between 0 and  $2\pi$ . This defines a nodal circle. Elements are then formed by the two dimensional connection of nodes in the  $r$ - $z$  plane, which when revolved around the  $z$  axis form a solid torus. As the model is not discretised in the  $\theta$  direction, an analytic function is used to calculate element stresses and strains for  $\theta$  between 0 and  $2\pi$ .

A finite element model was prepared for the section of C2 tunnel through the Hayward Fault zone. It was assumed that there is no interaction between C1 and C2 tunnels, therefore the C2 tunnel was not included in the model. The finite element model consisted of 43 elements with 207 nodal points, and had dimensions of 724m by 290m (Figure 8.22). Four different materials were modelled; sandstone, serpentine, rhyolite, and gouge. It was necessary to model the boundaries between these materials normal to the tunnel axis. However the strike of the strata in this section of the Berkeley Hills is close to normal to the tunnel axis and the strata is steeply dipping, therefore the assumption of axisymmetry is reasonable.

The tunnel liner was modelled as an 800mm thick shell with material properties  $E = 31,000\text{MPa}$  and  $\nu = 0.2$ . Because of the requirement for axial symmetry, it was not possible to model the invert concrete which is considerably thicker than the arch. There were no data available for the elastic properties of the surrounding ground and initial values chosen for  $E$  and  $\nu$  were obtained from the literature. A limited parametric study was made

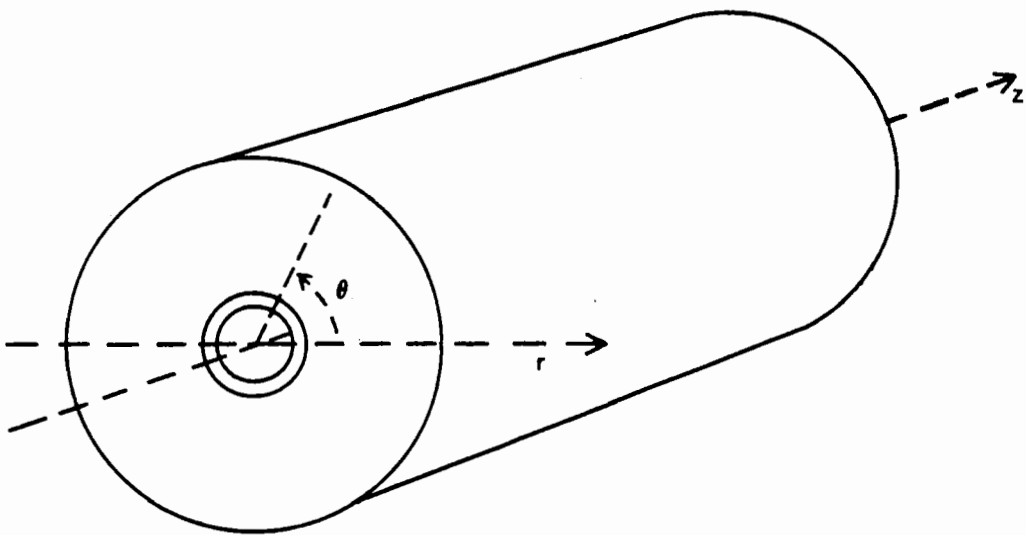


FIGURE 8.21 Definition of axisymmetric solid.

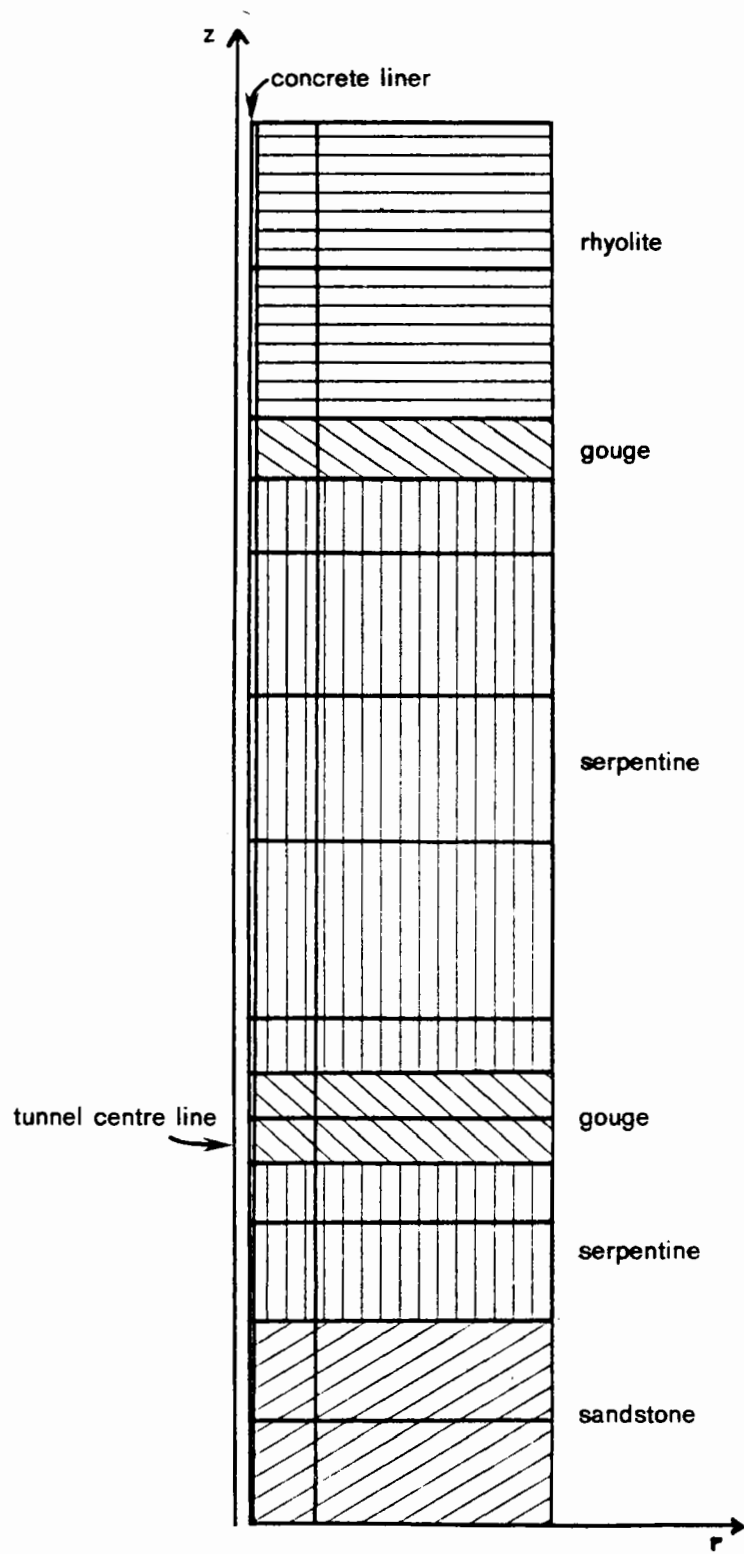


FIGURE 8.22 Axi-symmetric finite element model of C1 tunnel and surrounding ground.



of the effect of varying elastic constants. When the following material properties were used, the calculated deflected shape of the tunnel best modelled the surveyed shape.

	E (MPa)	$\nu$
sandstone	9000	0.25
serpentine	3400	0.3
rhyolite	10400	0.2
gouge	1000	0.4

Right lateral slippage along the Hayward Fault was simulated by displacing nodal points along the western side of the finite element mesh in the -r direction. This asymmetric loading of an axisymmetric body can be modelled by computer code FEAP; a Fourier series expansion is used.

The deformed mesh that resulted from 500mm displacement of the western boundary of the model relative to the fixed eastern boundary is shown in Figure 8.23. Much of the displacement takes place in the widest gouge zone near the contact between gouge and serpentine. This coincides with the active shear zone discussed in Chapter 7. The 500mm displacement of the model was required to produce 80mm displacement near the active trace of the Hayward Fault. It should be emphasised that this result is derived from a purely elastic model. Displacements associated with discrete slip along the fault were not considered. If a discontinuity was included in the gouge zone, or if the gouge was modelled as a plastic material, the calculated displacements within the fault zone would most likely have been larger than 80mm for 500mm of lateral slippage.

The interpretation of the results of this model is limited by the lack of survey data that would allow exact modelling of fault motions. If there has been any vertical movement along the Hayward Fault then interaction between ground and liner will be different from the case of right lateral slippage only. Also, it is not possible to model a realistic *in situ* stress state with an axisymmetric model. This large model with a coarse mesh cannot be used to calculate stresses in the tunnel liner accurately. It is apparent from the deformed mesh, however, that most of the interaction between liner and ground takes place

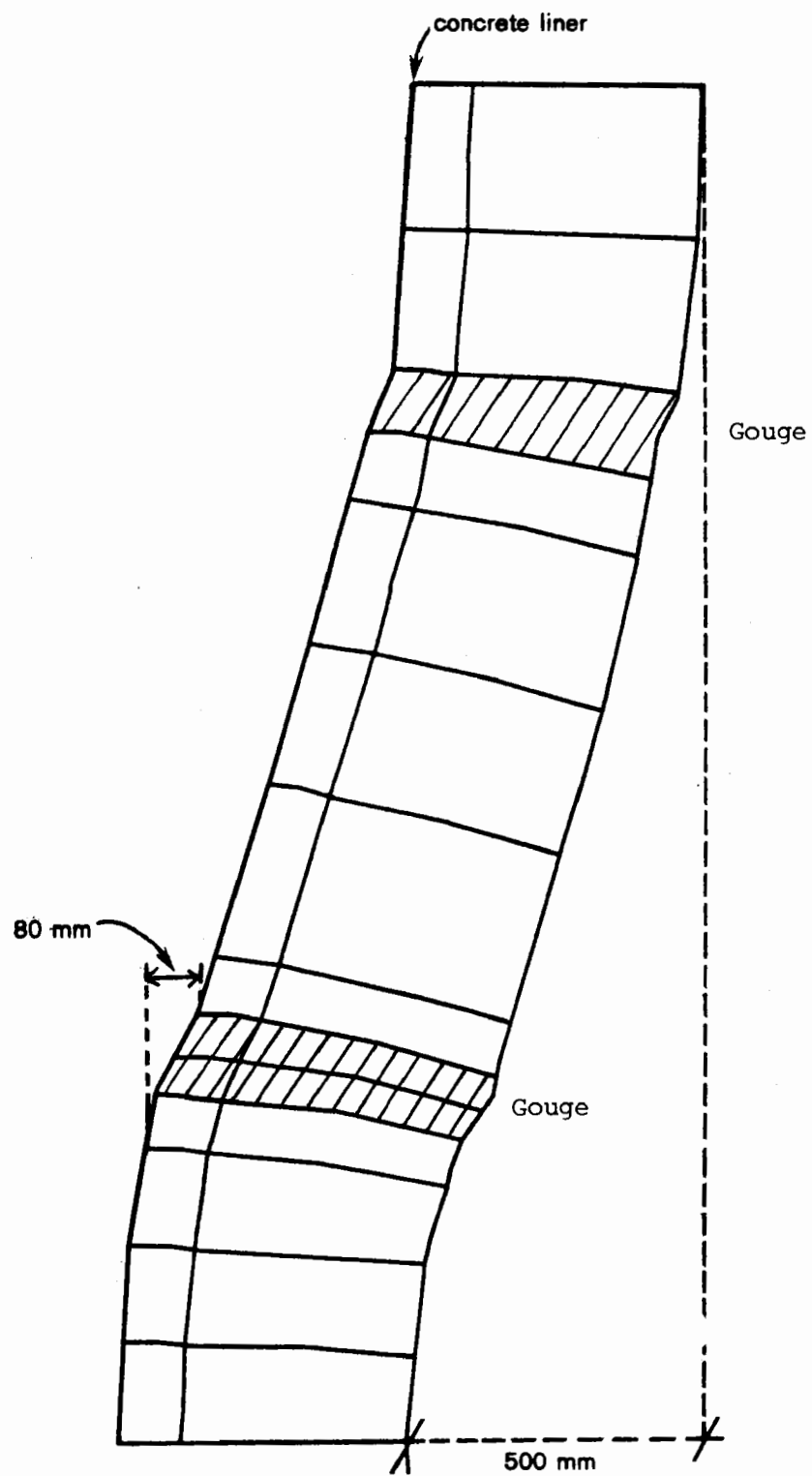


FIGURE 8.23 Deformed mesh.

in the wide gouge zone, as might have been expected.

## CHAPTER 9

### CONCLUSIONS

Seismic phenomena that can cause tunnel damage are fault displacement and ground vibration. Where tunnel liners are well constructed, damage resulting from strong ground shaking is minor as accelerations at depth are normally less than those recorded at the ground surface. Fault displacement inevitably causes damage to tunnels through active faults, as demonstrated in the review of case histories. Fault activity was not taken into account during the location, design, and construction of these tunnels.

Squeezing ground in an active fault zone is normally only a problem during tunnel construction. By the time the final liner is installed, time dependent deformation of the surrounding ground and subsequent loading of the support system should have been largely reduced.

The BART tunnels through the Berkeley Hills have been displaced about 80mm right laterally by the Hayward Fault since the concrete liner was constructed in 1968. This has occurred over a short section of both tunnels near Station 1200+80, resulting in distortion of the tracks and cracking of the liner. This location was found to correspond with a shear zone logged during tunnel construction. The slippage has been at a more or less constant rate of between 6 and 8mm per year, and appears to be a simple right lateral shearing motion. This has also caused extension of the section of tunnel liner in the fault zone, as indicated by open cracks in the liner. Records from water supply tunnels through the Berkeley Hills also indicate liner damage by slippage along the Hayward Fault.

Various surveys have been undertaken in connection with the BART tunnels, which when repeated, have detected slippage along the Hayward Fault. Careful surveying appears

to be necessary for monitoring future tunnel behaviour. The tape extensometer data can not be used to deduce changes in liner shape since construction, however, when readings are taken over a period of time, it should be possible to monitor changes in liner geometry due to continued slippage.

In the early design stage, slippage on the Hayward Fault was not considered. However, the tunnel diameter is 76mm greater than the standard BART clearance envelope as at the time the final rolling stock dimensions had not been established. When slippage was considered at a later stage, it was found that the extra clearance could accommodate 610mm horizontal and 305mm vertical displacement, provided that this movement was distributed over about 100m of tunnel. Train-tunnel clearances have since been reduced by fault slippage, lowering of the arch during construction, and the addition of conduits, lighting, third rail, and walkway.

In a review of the instrumentation data collected since tunnel construction, the performance of the instruments was investigated, and each instrument was given a reliability rating; some had failed. Rock movement indicators which are orientated parallel with the strike of the Hayward Fault, have not detected any movement after the immediate post construction period. The rock movement indicator heads do not appear to have been attached to the concrete liner, and this has limited their value in deformation analyses. Pressure cells on the north wall of the tunnel show increasing passive pressures with time, while active pressures have developed on the south side. This observation is consistent with right lateral fault displacement. It was assumed that there is no interaction between the two tunnels, but it is possible that the low pressures on the south side of the C2 tunnel have been enhanced by unloading of the pillar between the tunnels.

The assumed rock loads used by Bechtel Inc. to design the tunnel liner were conservative. Although an extensive instrumentation programme was conducted in small adits at each portal, the data obtained were not used for tunnel design. The maximum pressures

recorded in the west portal test adit, 45kPa vertical and 72kPa horizontal, are much less than the pressures that are recorded on the liner at present. This is because of the small size of the test adit compared with the tunnel, the low stiffness of support relative to that of the ground, and the short time over which the pressures were recorded.

The pressure distribution around the tunnel liner in the Hayward Fault zone may be indeterminate. An attempt was made, however, to model pressure cell readings by using the computer program LINER to examine the response of the tunnel liner to various pressure distributions. It proved impossible to reproduce the low pressures recorded on the south side of the C2 tunnel. This could be explained by the response of the relatively stiff tunnel liner to shear displacement. Given the shear strain gradient to the east of the active shear zone, the south side of the tunnel would be expected to develop passive action between the liner and adjacent rock. The south side of the tunnel would necessarily display an active loading condition, with the associated lower contact pressure between the liner and rock. This effect cannot be modelled with a two dimensional analysis.

One of the assumptions made when using the axi-symmetric finite element program to model the C1 tunnel and surrounding ground was that there was no interaction between C1 and C2 tunnels. As discussed, this may not be valid. Another assumption was that the liner properties were the same around the tunnel cross section. From the two dimensional plane strain analyses, the thick invert attracted higher moments, and higher steel stresses. Using the axi-symmetric model it was possible to reproduce more or less the deformed shape of the C1 tunnel, at least in the horizontal plane. As was expected, most of the right lateral displacement took place in the softer gouge zone.

A strain softening model was developed for the Hayward Fault that explained observed fault behaviour. It is significant that the pressure cells in the C2 tunnel appear to reflect changes in *in situ* stress that are associated with seismic activity. Pressure cell readings were taken at more frequent intervals during 1980, and pressure drops in April and

December made it feasible to predict earthquake events, although not their location or size. The measurement of *in situ* stress change at several locations along an active fault could be used to predict earthquake location and give some indication of size.

The structure of the Berkeley Hills was discussed in terms of a Riedel shear model. By understanding the mechanism that has given rise to the geological structures in this area, it should be possible to predict along which faults there will be further displacement as shearing continues along the Hayward Fault. The implication for the BART tunnels is that if major displacement occurs along the Hayward Fault, smaller displacements might be expected along other faults in the Berkeley Hills. Hence, damage to the tunnels would not necessarily be confined to the Hayward Fault zone.

It is not possible to make accurate predictions of the behaviour of the BART tunnels. Fault slippage can nevertheless be expected to continue to displace the tunnels, and track realignment must be regularly maintained. When detailed geometric data are available for the section of the tunnels in the Hayward Fault zone, it should be possible to calculate how much future track realignment can be accommodated. Cracking of the concrete liner in this section of tunnel has occurred, and monitoring of the cracks should continue, as an increase in crack aperture would indicate yielding of steel reinforcement.

## CHAPTER 10

## RECOMMENDATIONS FOR FUTURE MONITORING

**10.1. Existing Instrumentation**

As previously discussed, readings from a number of the rock movement indicators are no longer reliable. Also, the RMIs do not provide data that are relevant to liner response. It is recommended that future reading of these instruments be given low priority.

Similar problems were found with the pressure cell reliability, however these data are more relevant. It is recommended that pressure cells 3 and 4 on either side of the C2 tunnel at about Station 1202+77 be monitored, preferably remotely. This will enable continual observation of loading of the tunnel liner due to right lateral shear along the Hayward Fault. As discussed in Chapter 8, these cells appear to be responding to *in situ* stress changes precursory to earthquakes, and can provide valuable geophysical data. Of the remaining pressure cells, only cell 5 is reliable and should be read on a regular basis.

Careful surveying is in this case the most important monitoring tool, although it is not a continuous monitoring system. A short alignment survey should be set up through the fault zone in both tunnels to measure offsets from a theoretical centreline, of closely spaced survey points. This survey will produce curves similar to Figure 7.12. The track should not be used as a reference because it is likely to be realigned. This survey can be quickly carried out, and should be repeated every six months. At the same time, the laser survey should be repeated using only the first set-up points near the west portal of each tunnel.

The "as built" survey requires much longer field time. This should be repeated once every ten years, or when unusual movements have been indicated by other observations.



Tape extensometer anchor points have been established to determine liner distortion in a plane normal to the tunnel axis. To date, only initial readings have been made. It is recommended that observations are made every two months between the following anchor points; 4 and 8, 2 and 6, 3 and 7, and 1 and 5 (Figure 7.3). If large changes in cross-sectional geometry are detected, other chords should be measured to accurately determine liner distortion.

## **10.2. Proposed Future Instrumentation**

### **10.2.1. Vertical alignment across fault zone**

Changes in level across the active fault zone can be continuously monitored with a water-filled conduit connected to a suitable device that measures changes in water level. The conduit should span 30m of the C2 tunnel between Stations 1200+25 and 1201+23. Such a device should be able to measure changes in level with a sensitivity of at least  $10^{-3}$ mm.

### **10.2.2. Axial changes in tunnel length**

Extension of the tunnel liner across the active fault zone can be measured by a creepmeter, i.e. a tensioned wire anchored to points on either side of the fault. Changes in wire length are measured by either an LVDT or a resistance potentiometer. A 30m long creepmeter with anchor points at Stations 1200+25 and 1201+23, and one 20m long with anchor points at Stations 1200+41 and 1200+00 are recommended for the C2 tunnel.

The device for measuring length changes should have a sensitivity of less than  $10^{-3}$ mm, less than 0.15mm hysteresis, and a recording range of at least 25mm.

These instruments will also monitor a small component of shear displacement that takes place normal to the tunnel axis. Careful monitoring of axial changes and alignment

changes can more precisely give shear offset along the tunnel.

### **10.2.3. Horizontal alignment across fault zone**

As discussed in section 10.1, a short alignment survey is the most appropriate method by which to monitor the right lateral displacement of the tunnel liner. It is appreciated that this may be difficult to carry out on a regular basis because of train operating requirements. Consequently, a permanently installed laser with an automatic position monitoring system should be given further consideration. There may be problems in employing such a system; it would be unique, and costs could be high.

### **10.2.4. Ground-lining interaction**

Deterioration of the concrete liners in the Hayward Fault zone will be preceded by yielding of longitudinal reinforcing steel. To detect the onset of yield it is recommended that at two test sections in the C2 tunnel (Stations 1200+70 and 1200+85), intrados steel reinforcement should be located and exposed at 6 to 8 places. Weldable type strain gauges with adequate environmental protection can be placed on the steel reinforcing bars, and changes in strain monitored with time.

It is recommended that glass strips placed over cracks in the C2 tunnel be observed whenever surveying is undertaken. Any cracking of glass strips should be noted, as well as the formation of new cracks.

As it is difficult to monitor the condition of the slickline, it is recommended that it be completely removed in the Hayward Fault zone, i.e. between Stations 1198+00 and 1207+00 in both tunnels.

### 10.3. Recording System

Various options for recording data from pressure cells, creepmeters, the water level meter, and strain gauges are available. They include :

- manual readings at the instrument station
- signal conditioning and wiring to a remote reading station
- chart recording at a remote reading station
- digital recording and playback system utilising a micro-computer device
- signal conditioning and monitoring at BART Central Train Control.

This list is in increasing order of complexity and hardware cost.

If a remote readout capability is not provided, the interval between readings should not exceed two months. All data should be plotted on a common time base, either as displacements, strains, or pressures as appropriate. Survey information should be reduced in a similar way to that presented in this report, and regular reviews of data undertaken.

## REFERENCES

- ANDERSON, E.M. 1951 : *The Dynamics of Faulting*. Oliver and Boyd, Edinburgh ; 206p
- AYRES, M.O. 1969 : Case history - Berkeley Hills twin transit tunnels. *Proceedings of the Second Symposium on Rapid Excavation, Sacramento CA* ; 10-26 - 10-37.
- BECHTEL INCORPORATED 1964 : Engineering geology of the proposed rapid transit Berkeley Tunnel. Unpublished Report.
- BECHTEL INCORPORATED 1965 : Berkeley Hills tunnel, results of laboratory rock testing. Unpublished Report.
- BECHTEL INCORPORATED 1966a : Results of field rock testing. Unpublished Report.
- BECHTEL INCORPORATED 1966b : Preliminary report on Berkeley Hills tunnel instrumentation. Unpublished Report.
- BECHTEL INCORPORATED 1968 : Completion report of the construction engineering geology of the Berkeley Hills tunnel, Central Contra Costa Line. Unpublished Report.
- BECHTEL INCORPORATED 1970 : BARTD Berkeley Hills tunnels, Hayward Fault zone instrumentation. Unpublished Report.
- BLANCHARD, F.B.; LAVERTY, G.L. 1966 : Displacements in the Claremont water tunnel at the intersection with the Hayward Fault. *Bulletin of the Seismological Society of America* 56 ; 291-293.

- BOLT, B.A.; MARION, W.C. 1966 : Instrumental measurement of slippage on the Hayward Fault. *Bulletin of the Seismological Society of America* 56 ; 305-316.
- BOLT, B.A.; STIFLER, J.; UHRHAMMER, R. 1977 : The Briones Hills earthquake swarm of January 8, 1977, Contra Costa County, California. *Bulletin of the Seismological Society of America* 67 ; 1555-1564.
- BONILLA, M.G. 1966 : Deformation of railroad tracks by slippage on the Hayward Fault in the Niles district of Fremont, California. *Bulletin of the Seismological Society of America* 56 ; 281-289.
- BONILLA, M.G. 1979 : Historic surface faulting - map patterns, relation to subsurface faulting, and relation to preexisting faults. *U.S. Geological Survey Open File Report 79-1239* ; 36-65.
- BUGGE, W.A.; IRVIN, L.A. 1964 : Designing the San Francisco Bay Area rapid transit system. *Civil Engineering, American Society of Civil Engineers* 34 (10) ; 58-63.
- BURFORD, R.O.; NASON, R.D.; HARSH, P.W. 1978 : Studies of fault creep in Central California. *U.S. Geological Survey Earthquake Information Bulletin* 10 ; 174-181.
- BYERLEE, J.D.; MJACHKIN, V.; SUMMERS, R.; VOEVODA, O. 1978 : Structures developed in fault gouge during stable sliding and stick-slip. *Tectonophysics* 44 ; 161-171.
- CALIFORNIA DEPARTMENT OF WATER RESOURCES 1974 : California State Water Project. *California Department of Water Resources Bulletin No. 200, Sacramento, CA.*

- CASE, J.E. 1963 : Geology of a portion of the Berkeley and San Leandro Hills, California. University of California, Berkeley, PhD dissertation.
- CASE, J.E. 1969 : Upper Cretaceous and Lower Tertiary rocks, Berkeley and San Leandro Hills, California. *U.S. Geological Survey Bulletin 1251-J*.
- CLOOS, E. 1955 : Experimental analysis of fracture patterns. *Bulletin of the Geological Society of America* 66 ; 241-256.
- CLUFF, L.S. 1978 : Geologic considerations for seismic microzonation. *Proceedings of Second International Conference on Microzonation, San Francisco, CA.* ; 135-152
- CLUFF, L.S.; STEINBRUGGE, K.V. 1966 : Hayward fault slippage in the Irvington-Niles districts of Fremont, California. *Bulletin of the Seismological Society of America* 56 ; 257-279.
- COHEN, S.C. 1980 : Postseismic viscoelastic deformation and stress. 2. Stress theory and computation; dependence of displacement, strain and stress on fault parameters. *Journal of Geophysical Research* 85 ; 3151-3158.
- DIETRICH, J.H. 1978 : Time-dependent friction and the mechanics of stick-slip. *Pure and Applied Geophysics* 116 ; 790-806.
- DOWD, M.W. 1974 : Earthquakes and underground structures. *Proceedings of the Conference on Earthquake Engineering for Water Projects, Sacramento, CA* ; 99-107.
- DOWDING, C.H.; ROZEN, A. 1978 : Damage to rock tunnels from earthquake shaking. *Proceedings of the Geotechnical Division, American Society of Civil Engineers*

104 ; 175-191.

DRUCKER, M.A. 1943 : Determination of lateral passive soil pressure and its effect on tunnel stresses. *Journal of the Franklin Institute* 235 (5) ; 499-512.

DUKE, C.M.; LEEDS, D.J. 1959 : Effects of earthquakes on tunnels. *Proceedings of RAND Second Protective Construction Symposium, Santa Monica, CA.*

ESHELBY, J.D. 1973 : Dislocation theory for geophysical applications. *Transactions of the Royal Society, London, A* 274 ; 331-338.

EMERY, J.J.; JOSHI, V.H. 1980 : Seismic response of underground openings. *Proceedings of 13th Canadian Rock Mechanics Symposium, Toronto* ; 177-180.

GUTENBERG, B.; RICHTER, C.F. 1954 : *Seismicity of the earth and associated phenomena.* Princeton University Press ; 310p.

HARDIN, E.H.; PRATT, H.R. 1978 : Final report summary, the Terra Tek stress monitoring system, theory, calibration, and data from the Palmdale area, California, and Salt Lake City, Utah. Terra Tek Report TR78-76.

HART, E.W. 1980 : Fault-rupture hazard zones in California. *California Division of Mines and Geology Special Publication* 42.

HART, E.W. 1978 : Zoning for the hazard of surface fault rupture in California. *Proceedings of the Second International Conference on Microzonation, San Francisco, CA* ; 635-645.

HERD, D.G. 1978 : Map of Quaternary faulting along the northern Hayward Fault zone; Mare Island, Richmond, Briones Valley, Oakland West, San Leandro, Hay-

ward, and Neward 7.5' Quadrangles, California. *U.S. Geological Survey Open File Report 78-308*.

HITTINGER, M.; GOODMAN, R.E. 1978 : A computer program for stress analysis of two-dimensional, discontinuous rock masses. *University of California, Berkeley, Geotechnical Engineering Report UCB/GT/78-04*.

HOWARD, T.R. 1972 : Characteristics of gouge material in relation to underground stability problems. University of California, Berkeley, PhD dissertation.

KING, C.Y.; NASON, R.D.; TOCHER, D. 1973 : Kinematics of fault creep. *Transactions of the Royal Society, London, A 274* ; 355-360.

KOCH, T.W. 1933 : Analysis and effects of current movements on an active fault in Buena Vista oil field, Kern County, California. *Bulletin of the American Association of Petroleum Geologists 17* ; 694-712.

KORBIN, G.E.; KRAKOWSKI, T.E. 1980 : LINER, a computer program for the structural analysis of tunnel support systems. Unpublished report, Lachel-Hansen and Associates, and Berkowitz Associates.

KUESEL, T.R. 1968 : Structural design of the Bay Area Rapid Transit system. *Civil Engineering, American Society of Civil Engineers 38 (4)* ; 46-50.

KUESEL, T.R. 1969 : Earthquake design criteria for subways. *Proceedings of the American Society of Civil Engineers, Journal of the Structural Division 95* ; 1213-1231.

KUPFER, D.H.; MUESSIG, S.; SMITH, G.I.; WHITE, G.N. 1955 : Arvin-Tehachapi earthquake damage along the Southern Pacific Railroad near Bealville, California. *California Division of Mines Bulletin 171* ; 67-74.



- LAWSON, A.C. 1908 : The California earthquake of April 18, 1906. *Carnegie Institute of Washington Publication 87.*
- LEE, V.W.; TRIFUNAC, M.D. 1979 : Response of tunnels to incident SH-waves. *Proceedings of American Society of Civil Engineers, Journal of the Engineering Mechanics Division 105* ; 643-659.
- LENSEN, G.J. 1976 : Tectonic hazards and their effect on town planning. *Bulletin of the International Association of Engineering Geologists 14.*
- LOUDERBACK, G.D. 1942 : Faults and earthquakes. *Bulletin of the Seismological Society of America 32* ; 305-330.
- MAVKO, G.M. 1980 : Simulation of creep events and earthquakes on a spatially variable model (Abstract). *EOS, Transactions of the American Geophysical Union 61* ; 1120.
- MCCUTCHEN, W.R.; SNYDER, W.G. 1977 : BART Berkeley Hills tunnel instrumentation results and interpretations, Hayward Fault zone. BART Design Staff Report.
- MCHUGH, C.A.; LESTER, F.W. 1979 : Catalog of earthquakes along the San Andreas Fault system in Central California for the year 1975. *U.S. Geological Survey Open-File Report 79-1138.*
- MEADE, B.K.; SMALL, J.B. 1966 : Current and recent movement on the San Andreas Fault. *California Division of Mines and Geology Bulletin 190* ; 385-391.
- MILLER, R.W. 1968 : Results of triangulation for earth movement study, vicinity of Berkeley, El Cerrito, and Fremont, California. *U.S. Department of*

*Commerce, National Ocean Survey Report.*

MILLER, R.W. 1970 : Results of triangulation for earth movement study, vicinity of Berkeley, El Cerrito, and Fremont, California. *U.S. Department of Commerce, National Ocean Survey Report Supplement No 1.*

MOODY, J.G.; HILL, M.J. 1956 : Wrench fault tectonics. *Bulletin of the Geological Society of America* 67 ; 1207-46.

MORGENSTERN, N.R.; TCHALENKO, J.S. 1967 : Microscopic structures in kaolin subjected to direct shear. *Geotechnique* 17 ; 309-328.

NASON, R.D. 1971 : Investigations of fault creep slippage in northern and central California. University of California, San Diego, PhD dissertation.

NASON, R.D.; WEERTMAN, J. 1973 : A dislocation theory analysis of fault creep events. *Journal of Geophysical Research* 78 ; 7745-7751.

NASU, N. 1931 : Comparative studies of earthquake motions above-ground and in a tunnel. *Bulletin of the Earthquake Engineering Research Institute, Tokyo Imperial University* 9 ; 454-472.

NUR, A. 1978 : Nonuniform friction as a physical basis for earthquake mechanics. *Pure and Applied Geophysics* 116 ; 964-991.

OWEN, G.N.; SCHOLL, R.E. 1980 : Earthquake engineering of large underground structures. URS/John A. Blume and Associates, San Francisco, Final Report Contract NSF PFR-7706505.

OWEN, G.N.; SCHOLL, R.E.; BREKKE, T.L. 1979 : Earthquake engineering of tunnels.

*Proceedings of Rapid Excavation and Tunneling Conference, Atlanta, GA. ;*  
709-721.

OWEN,G.N.; YANEV, P.I.; SCHOLL, R.E. 1980 : Considerations for developing seismic design criteria for nuclear waste storage repositories. URS/John A. Blume and Associates, San Francisco, Report for U.S. Department of Energy Nevada Operations Office.

PECK, R.B. 1969 : Deep excavation and tunneling in soft ground. *State of the Art Volume, Seventh International Conference on Soil Mechanics and Foundation Engineering, Mexico City ;* 225-290.

PRESCOTT, W.H.; LISOWSKI, M.; SAVAGE, J.C. 1980 : Geodetic measurement of crustal deformation on the San Andreas, Hayward and Calaveras Faults near San Francisco, California (Abstract). *EOS, Transactions of the American Geophysical Union 61 ;* 1126.

RADBRUCH, D.H. 1967a : Approximate location of fault traces and historic surface ruptures within the Hayward Fault zone between San Pablo and Warm Springs, California. *U.S. Geological Survey Miscellaneous Geologic Investigations Map I-522.*

RADBRUCH, D.H. 1967b : History of earth movement in Alameda and Contra Costa Counties. *Proceedings of Panel Discussion on Crustal Movement and the Surveyor, East Bay Council on Surveying and Mapping.*

RADBRUCH, D.H. 1969 : Areal and engineering geology of the Oakland East Quadrangle, California. *U.S. Geological Survey Map GQ-769.*

- RADBRUCH, D.H.; CASE, J.E. 1967 : Preliminary geologic map and engineering geologic information, Oakland and vicinity, California. *U.S. Geological Survey Open File Report*.
- RADBRUCH, D.H.; LENNERT, B.J. 1966 : Damage to culvert under Memorial Stadium, University of California, Berkeley, caused by slippage in the Hayward Fault zone. *Bulletin of the Seismological Society of America* 56 ;295-304.
- RADBRUCH-HALL, D.H. 1974 : Map showing recently active breaks along the Hayward Fault zone and the southern part of the Calaveras Fault zone, California. *U.S. Geological Survey Miscellaneous Investigations Map I-813*.
- REID, H.F. 1911 : The elastic rebound theory of earthquakes. *University of California Bulletin of Department of Geology* 6 ; 413-444.
- RICHTER, C.F. 1935 : An instrumental earthquake magnitude scale. *Bulletin of the Seismological Society of America* 25 ; 1-32.
- RIEDEL, W. 1929 : Zur Mechanik geologischer Brucherscheinungen. *Centralblatt für Mineralogie, Geologie, und Palaontologie Abt. B (8)* ; 354-368.
- ROSENBLUETH, E. 1977 : Soil and rock mechanics in earthquake engineering. *Proceedings of International Conference on Dynamic Methods in Soil and Rock Mechanics* 3 ; 3-62.
- RUTTER, E.H. 1979 : The mechanical properties of kaolinite fault "gouge" at moderate confining pressure, 20° C. *International Journal of Rock Mechanics Mining Sciences and Geomechanics Abstracts* 16 ; 407-410.
- SAUL, R.B. 1975 : Geology of the southeast slope of the Santa Susana Mountains and

geologic effects of the San Fernando earthquake. *California Division of Mines and Geology Bulletin* 196 ; 53-70.

SCHULTZ, S.S.; BURFORD, R.O.; NASON, R.D. 1976 : Catalog of creepmeter measurements in central California from 1973 through 1975. *U.S. Geological Survey Open-File Report* 77-31.

SHIMAZAKI, K.; SOMERVILLE, P. 1978 : Summary of the static and dynamic parameters of the Izu-Oshima-Kinkai earthquake of January 14, 1978. *Bulletin of the Earthquake Research Institute, University of Tokyo*, 53 ; 613-628.

SHUKLA, D.K.; RIZZO, P.C.; STEPHENSON, D.E. 1980 : Earthquake load analysis of tunnels and shafts (preprint). *Proceedings of 21st U.S. Rock Mechanics Symposium*.

SIEH, K.E. 1977 : Pre-historic large earthquakes produced by slip on the San Andreas Fault at Pallet Creek, California. *Journal of Geophysical Research* 82 ; 3907-3939.

STEINBRUGGE, K.V.; MORAN, D.F. 1954 : An engineering study of the Southern California earthquake of July 21, 1952, and its aftershocks. *Bulletin of the Seismological Society of America* 44 ; 201-350.

STEINBRUGGE, K.V.; ZACHER, E.G. 1960 : Creep on the San Andreas Fault; fault creep and property damage. *Bulletin of the Seismological Society Society of America* 50 ; 389-396.

STUART, W.D. 1979 : Quasi-static earthquake mechanics. *Reviews of Geophysics and Space Physics* 17 ; 1115-1120.

STUART, W.D. 1980 : Stiffness method for anticipating earthquakes. *Bulletin of the*

*Seismological Society of America (in press).*

SWOLFS, H.S.; BRECHTEL, C.E. 1977 : The direct measurement of long-term stress variations in rock. *Proceedings of the 18th U.S. Symposium on Rock Mechanics, Keystone, CO.* ; 4C51-4C53.

TAKAHASI, R. 1931 : Results of the precise levellings executed in the Tanna railway tunnel and the movement along the slickenside that appeared in the tunnel. *Bulletin of the Earthquake Engineering Research Institute, Tokyo Imperial University* 9 ; 435-453.

TANNER, W.F. 1962 : Surface structural patterns obtained from strike-slip models. *Journal of Geology* 70 ; 101-107.

TAYLOR, C.L.; CLUFF, L.S. 1977 : Fault displacement and ground deformation associated with surface faulting. *Proceedings of American Society of Civil Engineers Conference on the Current State of Knowledge of Lifeline Earthquake Engineering* ; 338-353.

TAYLOR, R.L. 1977 : Computer procedures for finite element analysis. Chapter 24 in *The Finite Element Method* by O.C. Zienkiewicz, McGraw-Hill Book Co. (U.K.) Ltd.

TCHALENKO, J.S. 1970 : Similarities between shear zones of different magnitude. *Bulletin of the Geological Society of America* 81 ; 1625-1640.

TCHALENKO, J.S.; AMBRASEYS, N.N. 1970 : Structural analysis of the Dasht-e Bayaz (Iran) earthquake fractures. *Bulletin of the Geological Society of America* 81 ; 41-60.

- TERZAGHI, K. 1946 : Rock defects and loads on tunnel supports. In *Tunneling with Steel Supports* (Proctor, R.V.; White, T.L. eds) Commercial Shearing Inc., Youngstown, OH.
- THATCHER, W.; HANKS, T. 1973 : Source parameters of Southern California earthquakes. *Journal of Geophysical Research* 78 ; 8547-8576.
- TSUNEISHI, Y.; ITO, T.; KANO, K. 1978 : Surface faulting associated with the 1978 Izu-Oshima-Kinkai earthquake. *Bulletin of the Earthquake Research Institute, University of Tokyo*, 53 ; 649-674.
- UNIVERSITY OF CALIFORNIA 1978 : Dwight-Derby site reuse study. *University of California, Berkeley, Draft Environmental Impact Report*.
- WANG, C.Y.; LIN, W.; WU, F.T. 1978 : Constitution of the San Andreas fault zone at depth. *Geophysical Research Letters* 6 ; 476.
- WANG, C.Y.; MAO, N.H.; WU, F.T. 1980 : Mechanical properties of clays at high pressures. *Journal of Geophysical Research* 85 ; 1462-1468.
- WEIDLINGER, P.; NELSON, I. 1980 : On seismic analysis and design of underground lifelines. *Proceedings of the American Society of Civil Engineers, Journal of the Technical Councils of ASCE* 106 ; 185-200.
- WILCOX, R.E.; HARDING, T.P.; SEELY, D.R. 1973 : Basic wrench tectonics. *Bulletin of the American Association of Petroleum Geologists* 57 ; 74-96.
- WILT, J.W. 1958 : Measured movement along the surface trace of an active thrust fault in the Buena Vista Hills, Kern County, California. *Bulletin of the Seismological Society of America* 48 ; 169-176.

YAMASHITA, P.A.; BURFORD, R.O. 1973 : Catalog of preliminary results from an 18-station creepmeter network along the San Andreas Fault system in central California for the time interval June 1969 to June 1973. *U.S. Geological Survey Open File Report.*

YOUNG, G.J. 1929 : Driving the Claremont tunnel. *Engineering and Mining Journal* 127 ; 832-834.

ZIEGENFELDER, R.F.; KING, E.H. 1955 : Technical report on the Berkeley Hills tunnel. Parsons, Brinckerhoff, Hall and MacDonald unpublished report.



## APPENDIX A

RESULTS OF INSTRUMENTATION FROM WEST  
PORTAL EXPLORATION ADIT

Rock instrumentation was located at six stations in the west portal adit (see Figure 6.1). Three of the sites, 1,2, and 3, were in Franciscan Formation, and sites 4,5, and 6 were in the Hayward Fault zone. Load cells were also installed in the area where additional support consisting of jump sets and diamond-shaped bracing were required; this was designated test site 5A. The arrangement of instruments in a typical test section is shown in Figure A.1. The instruments were monitored for about one year, up until the time they were disturbed by excavation of the C2 tunnel.

Load cells were usually placed near the face as soon as possible after excavation. Where jump sets were installed in squeezing ground, the instruments were not installed until some time after that part of the adit was excavated. Evaluation of load cell readings was based on the assumption that rock loads were transmitted evenly to the supports, and that the load cells were installed in a uniform manner. In many places where load cells were located between rock and support, contact of the rock or lagging may have resulted in lower load values being calculated. Lower values were also calculated when load cells were placed within a jump set support, as the lagging was uneven and higher loads may have been carried by the original sets. Rock pressures were determined by summing either roof or wall loads obtained from the load cells on one set and dividing them by the surface area of the rock supported by the set. Maximum lateral and vertical rock pressures were 72kPa and 48kPa in the Hayward Fault zone, and 6kPa and 10kPa in the Franciscan Formation. Load cells in the Hayward Fault zone showed a steady increase in pressure which did not

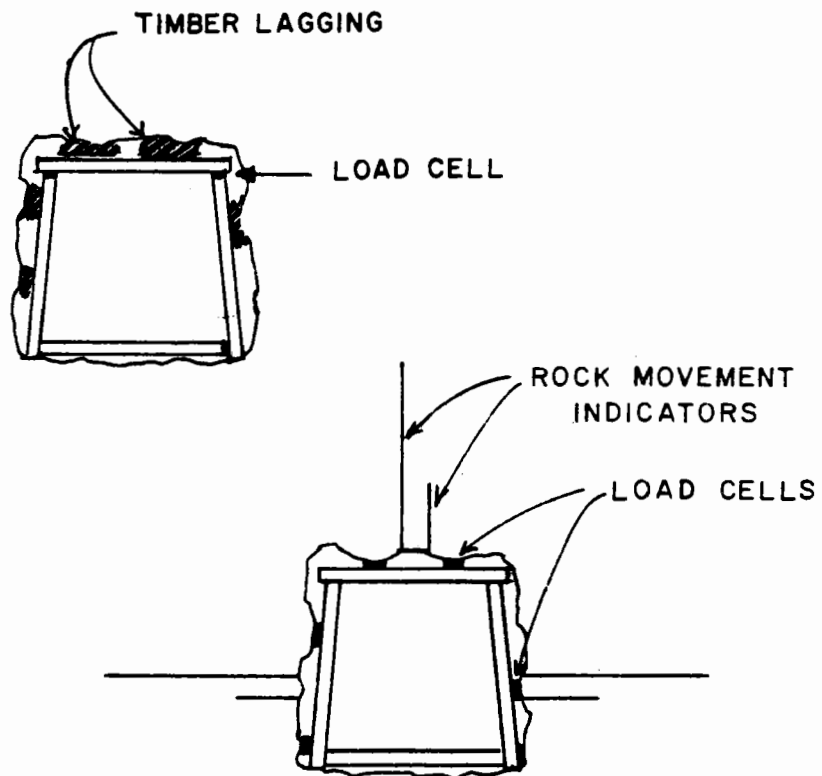


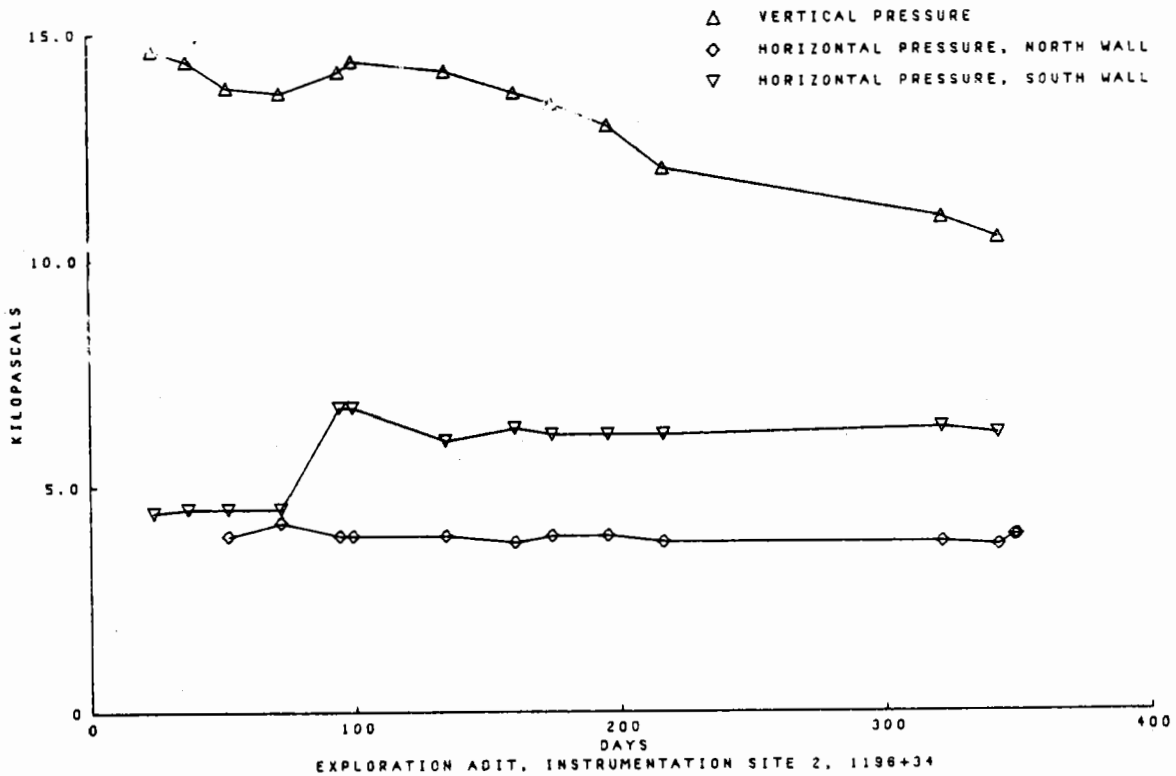
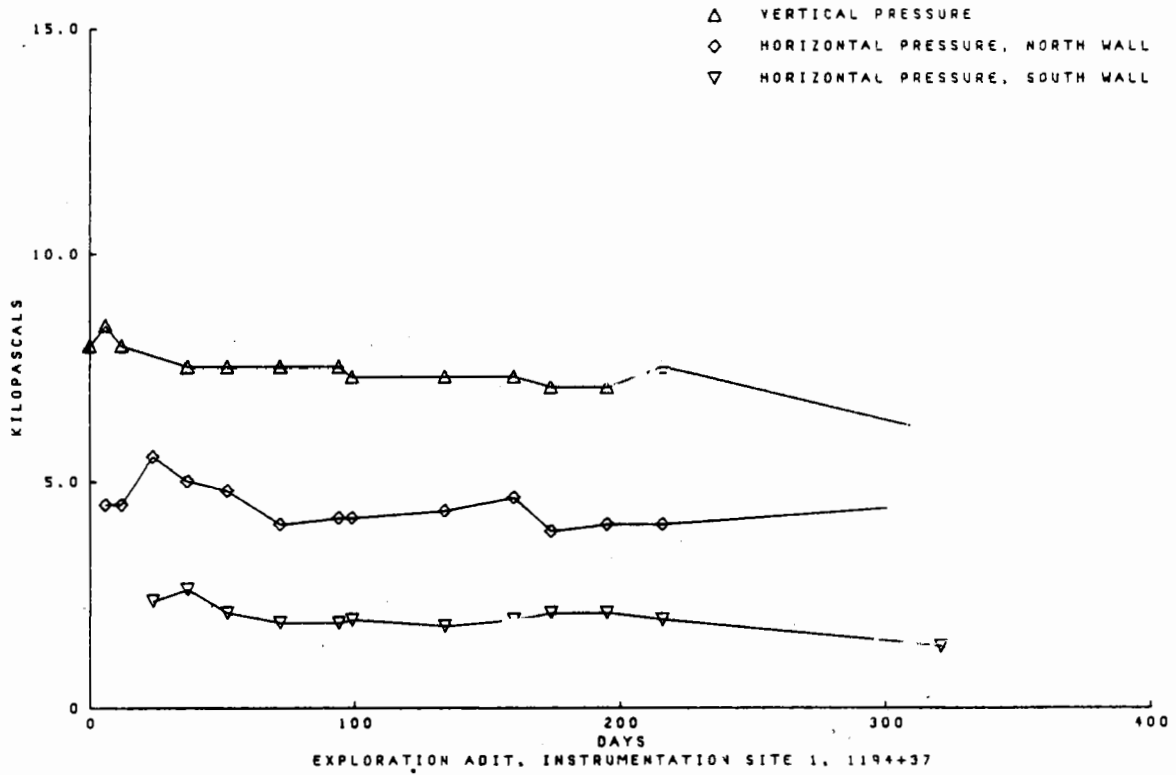
FIGURE A.1 Instrumentation arrangement in west portal exploration adit.

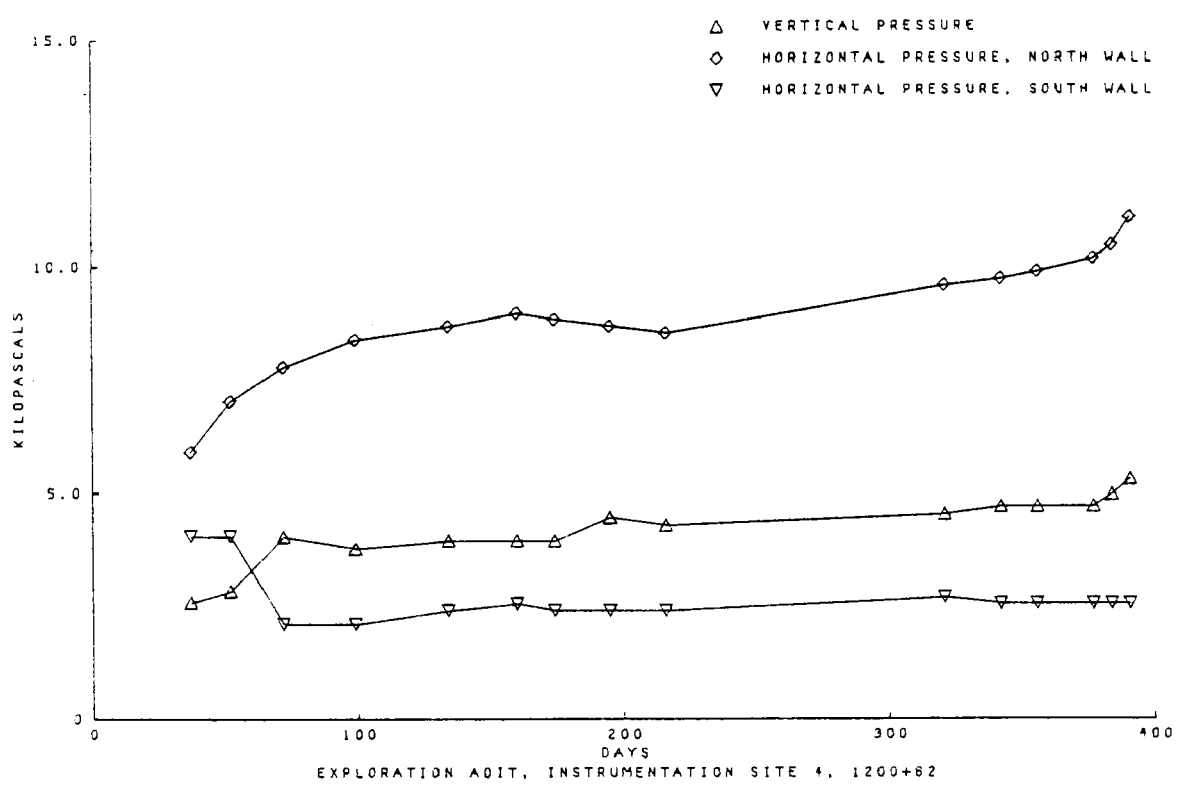
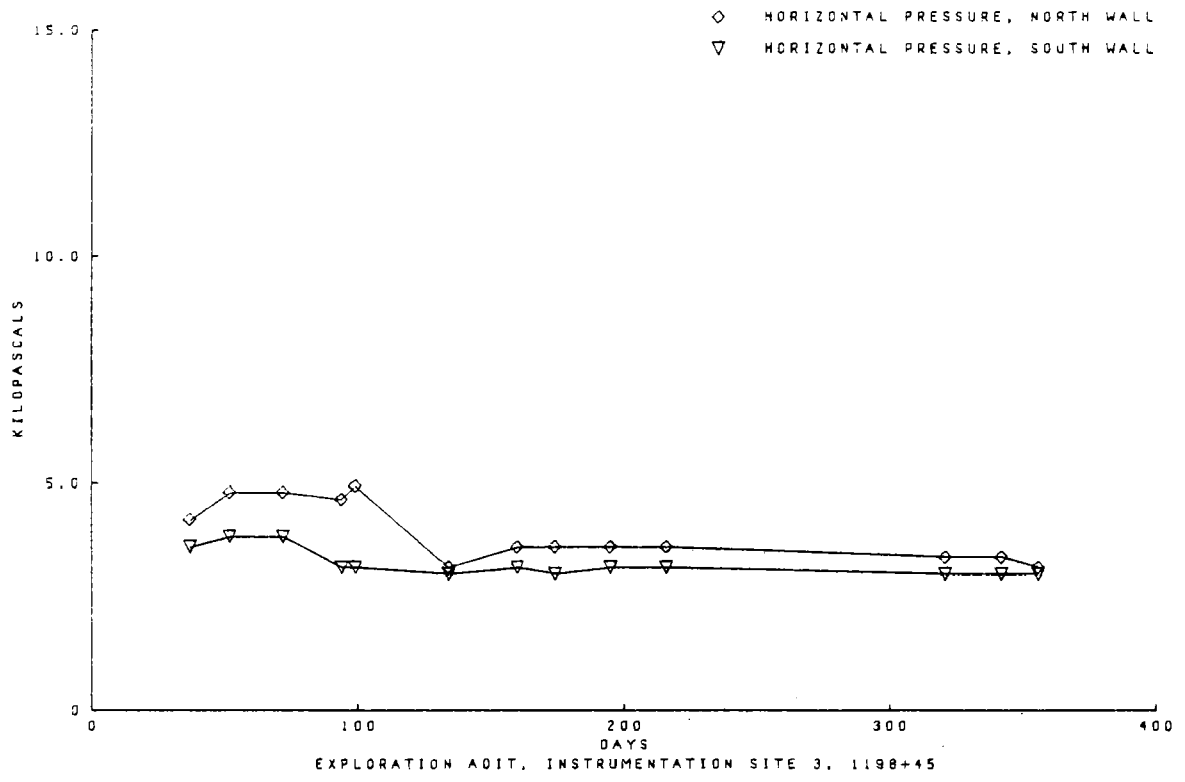
stabilise during a monitoring period of about one year. In Franciscan Formation, rock pressures stabilised within a period of a few days to one month following the time of installation. Pressures increased again as the face of the C2 tunnel was advanced towards the instrumented set.

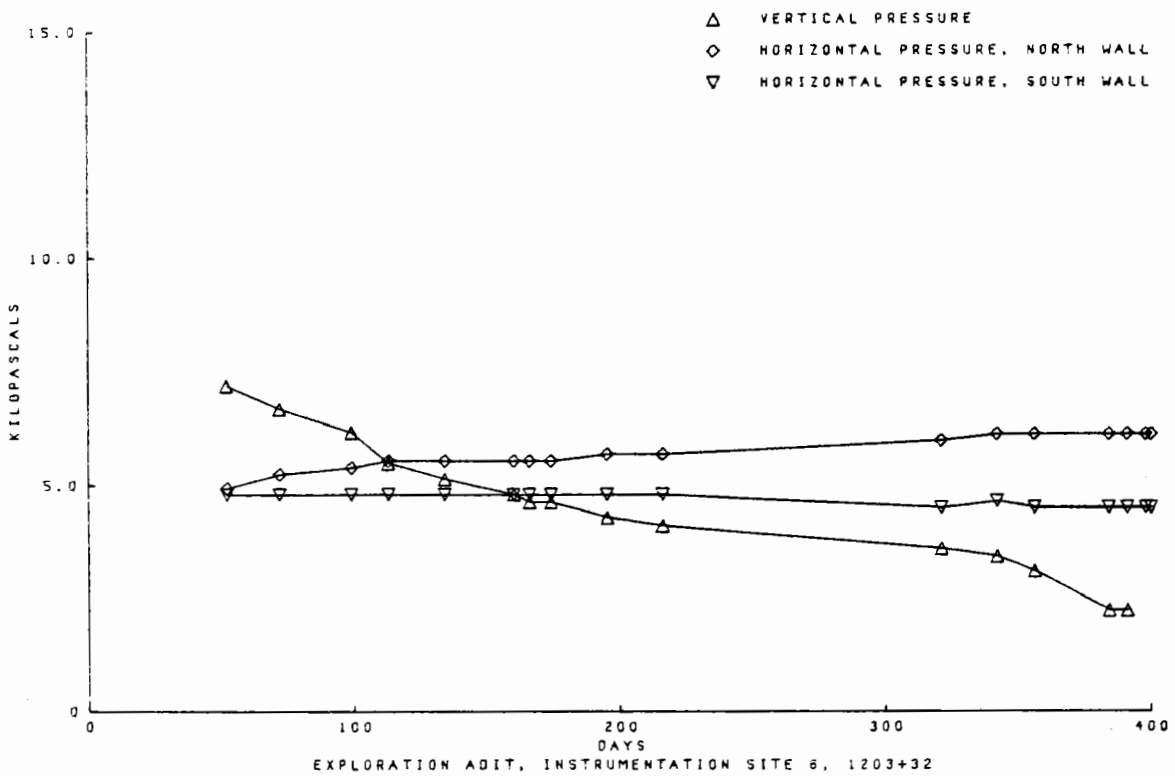
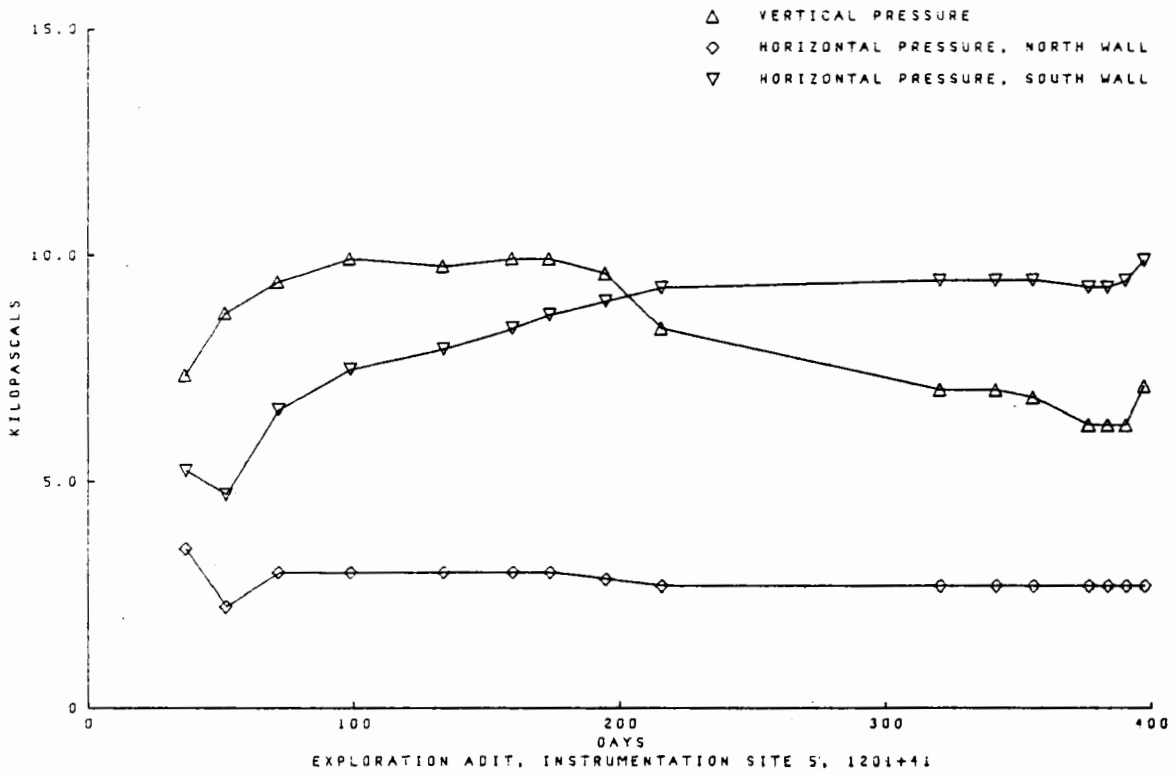
Rock movement indicators (RMIs) were installed as close as possible to the face to record initial relaxation of the rock. They consisted of a 6mm diameter steel rod grouted to the bottom of a drill hole, and passing through a sleeve to the tunnel wall. Displacement of the rod relative to the collar of the hole was measured using a dial gauge.

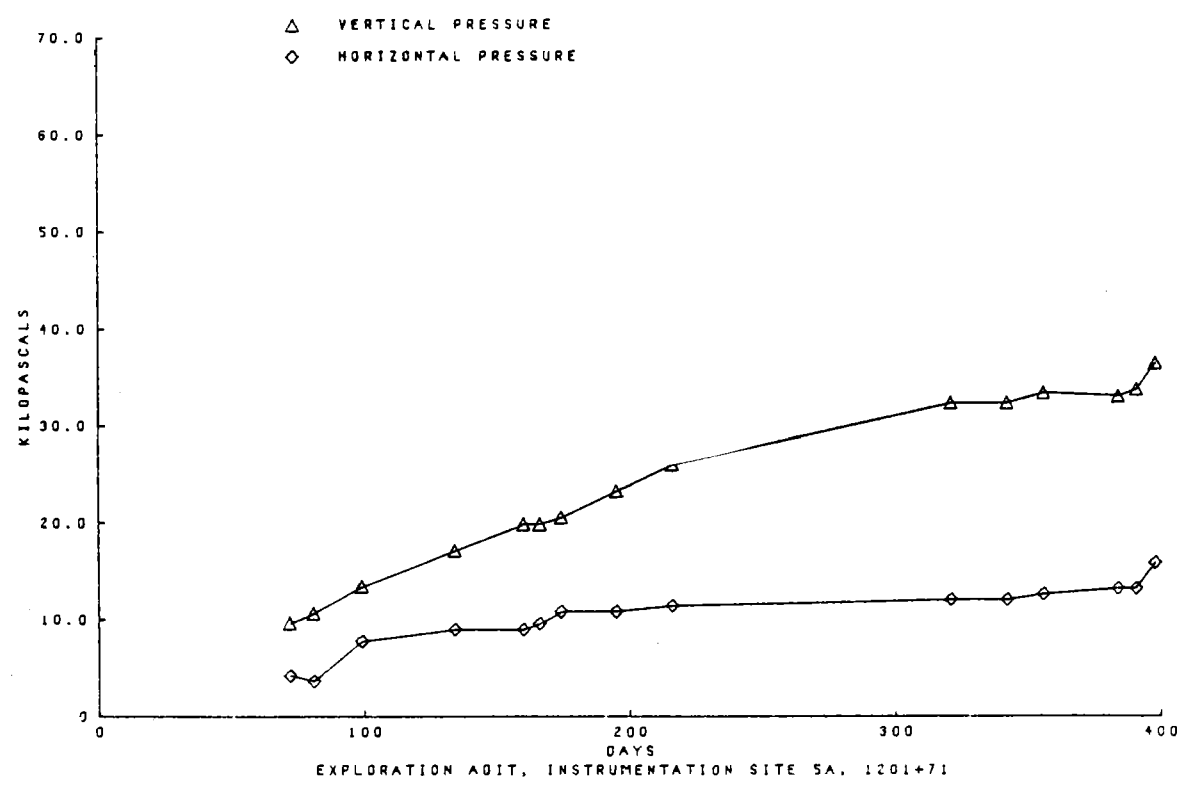
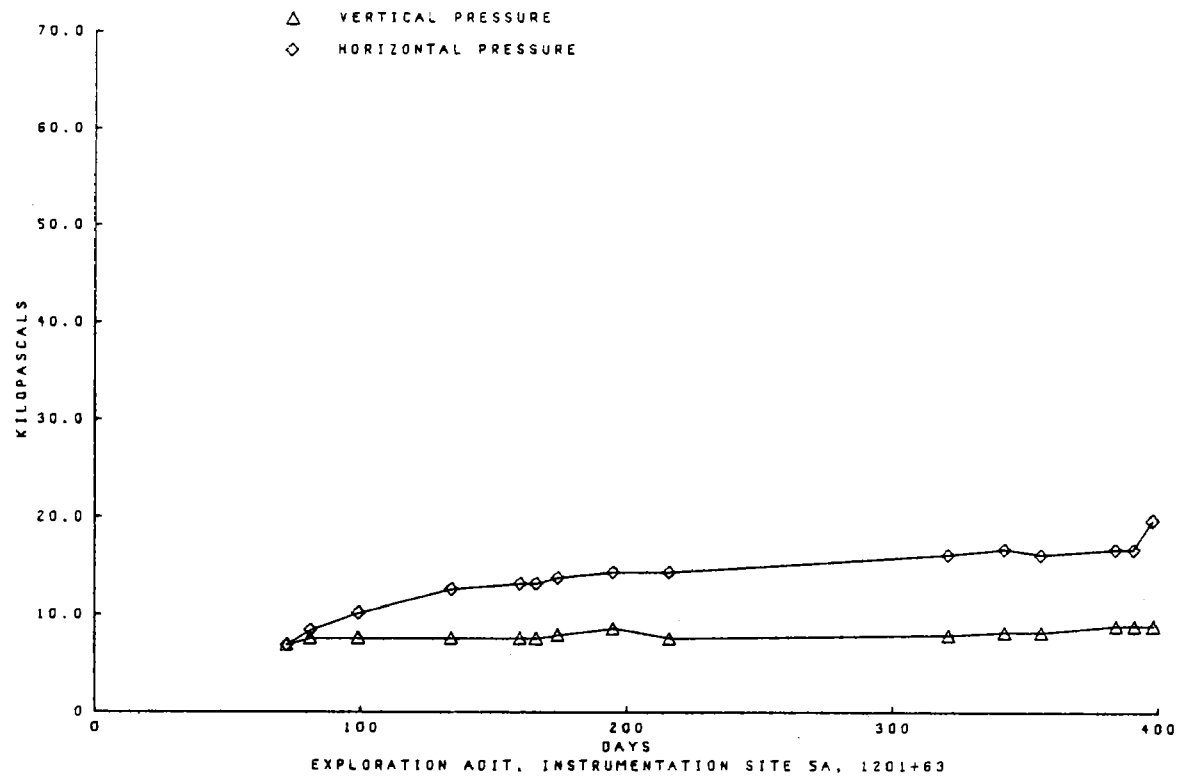
A tape extensometer was used to measure movement between pairs of extensometer pins anchored horizontally to the wall rock and steel support, and vertically to the rock in the roof and invert. Tape extensometer readings were compared with the 3.05m RMI readings to determine whether or not movement was occurring in the rock at a distance greater than 3.05m from the tunnel wall.

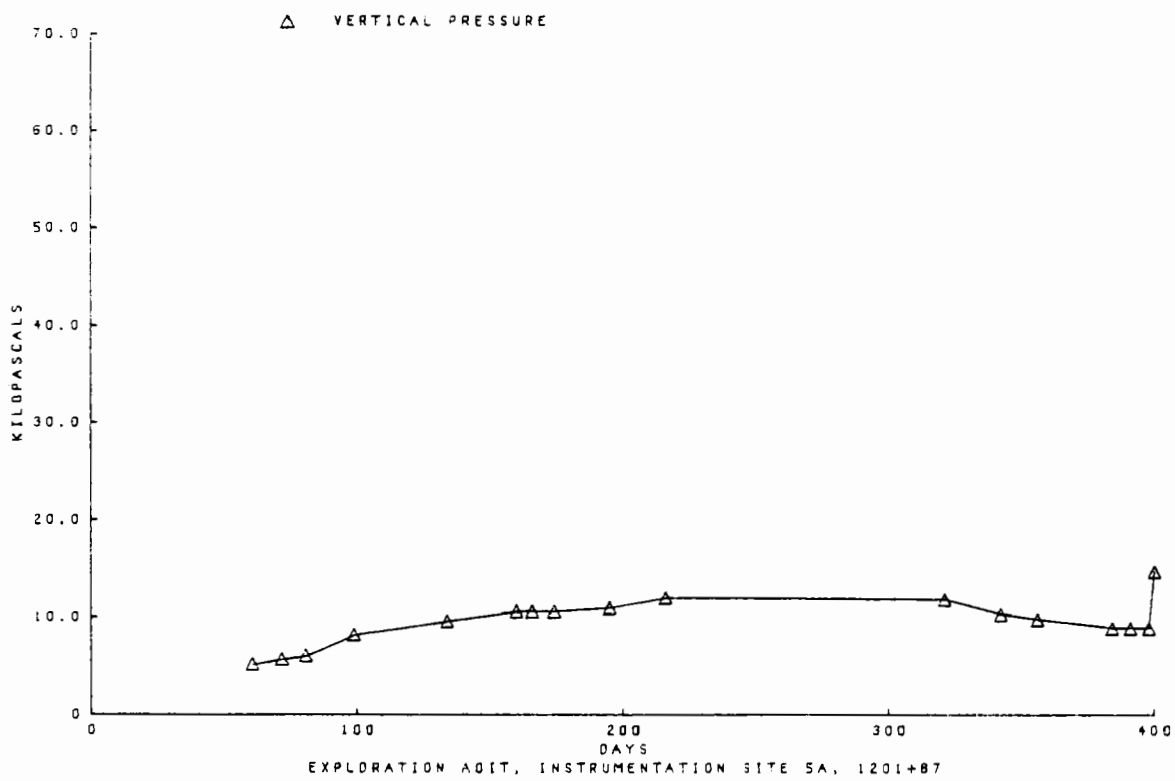
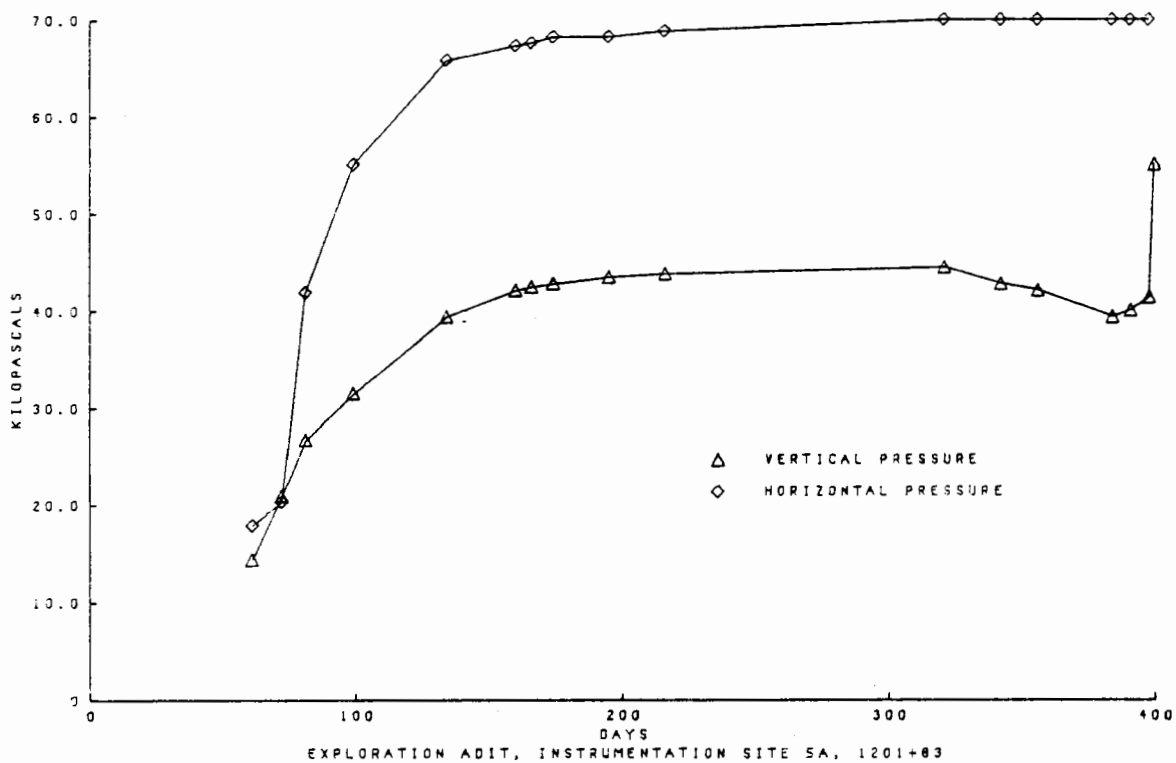
Data from rock movement indicator readings, and horizontal and vertical pressure curves for each instrumentation station are given in Figure A.2 (i - xxix).



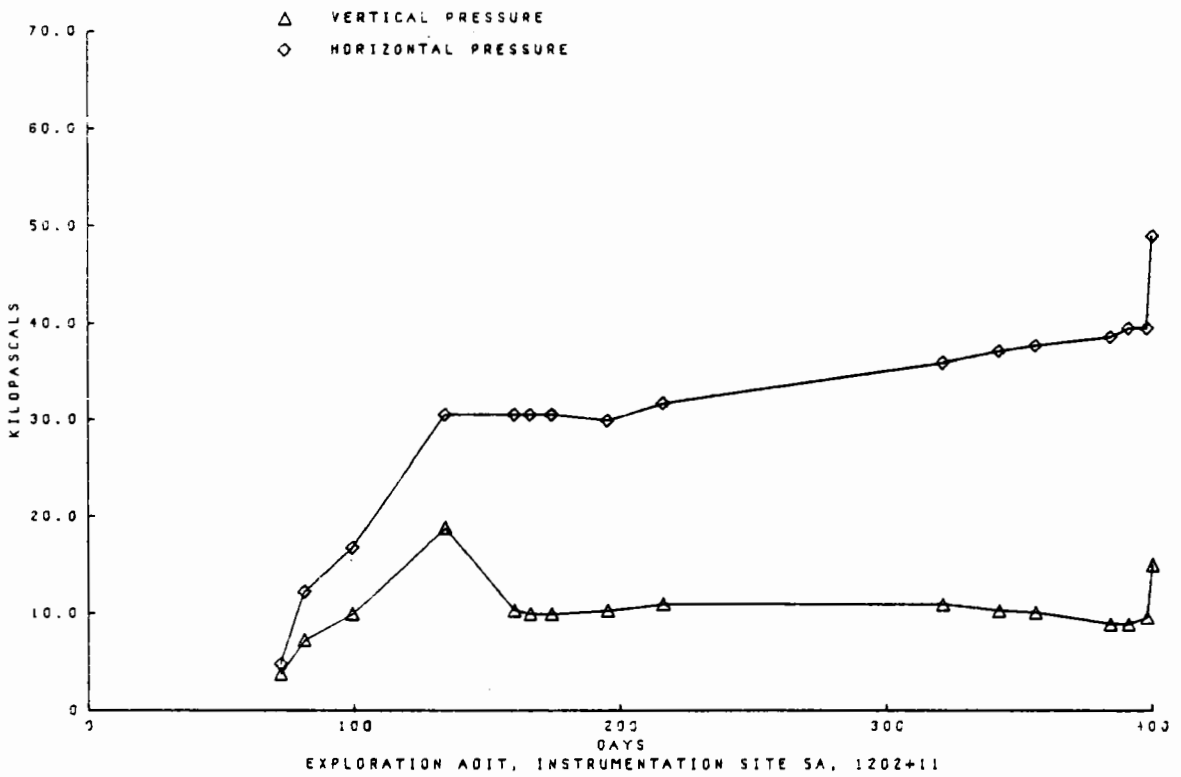
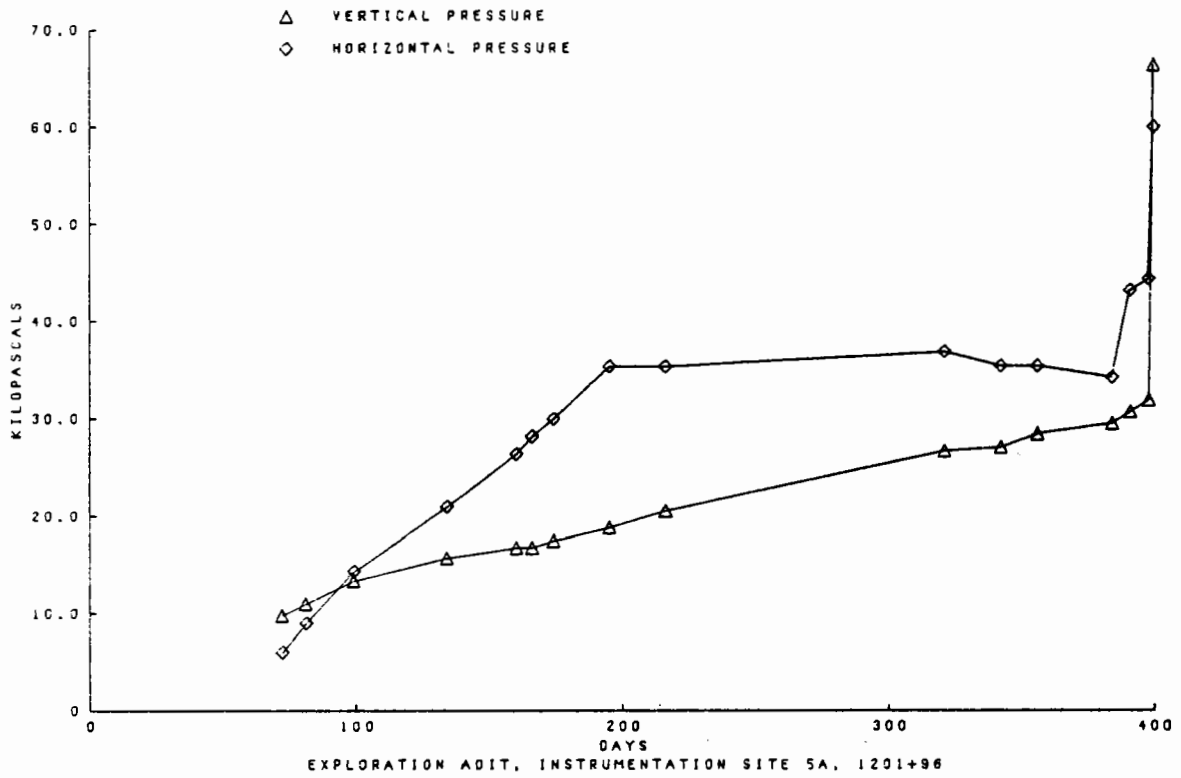


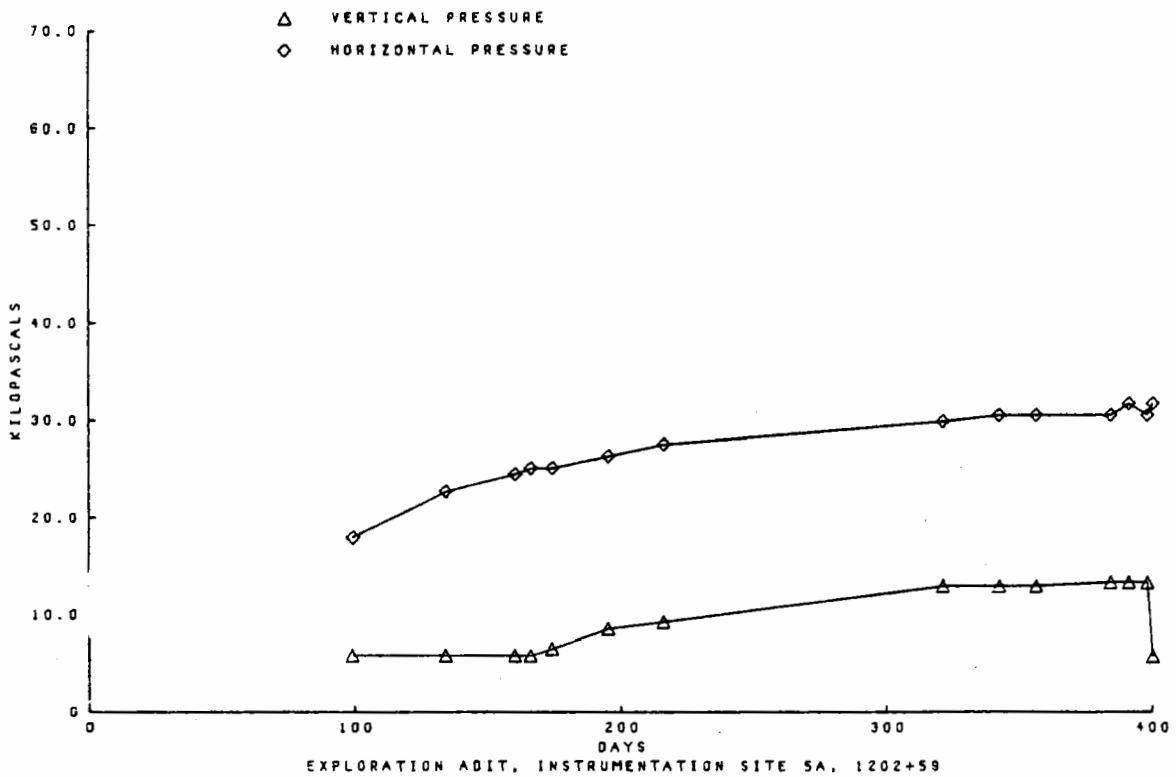
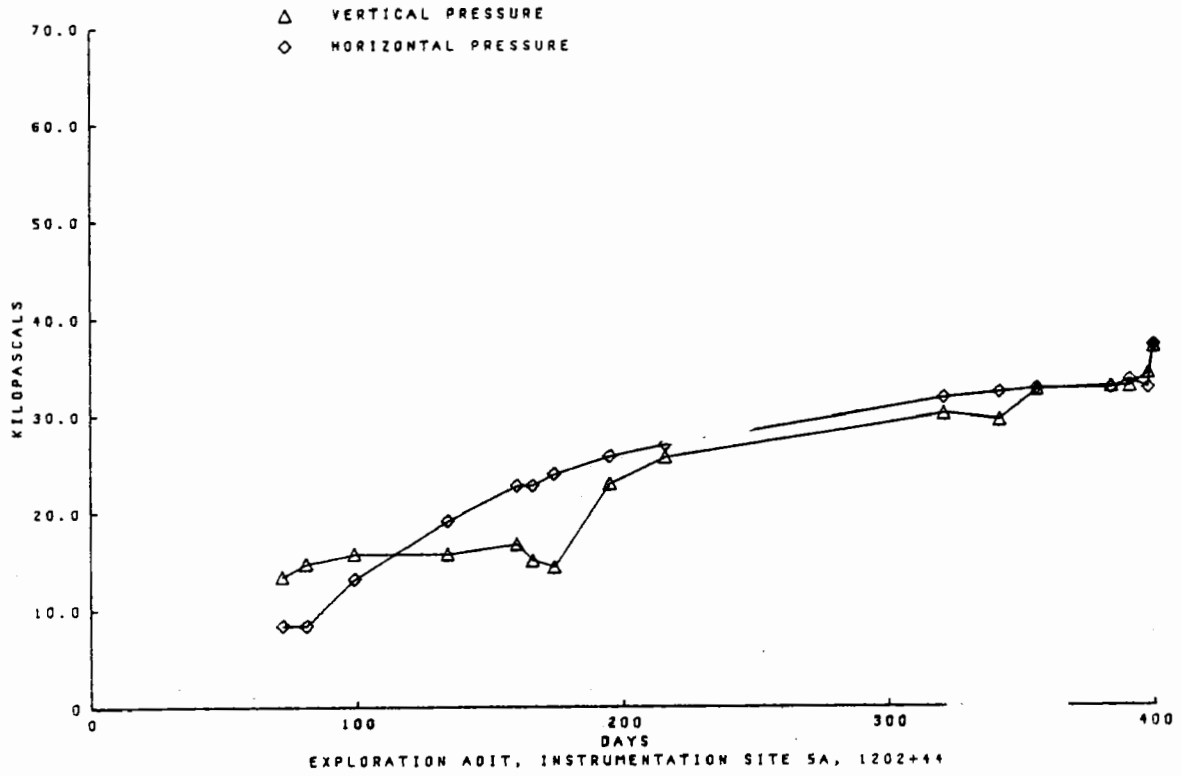


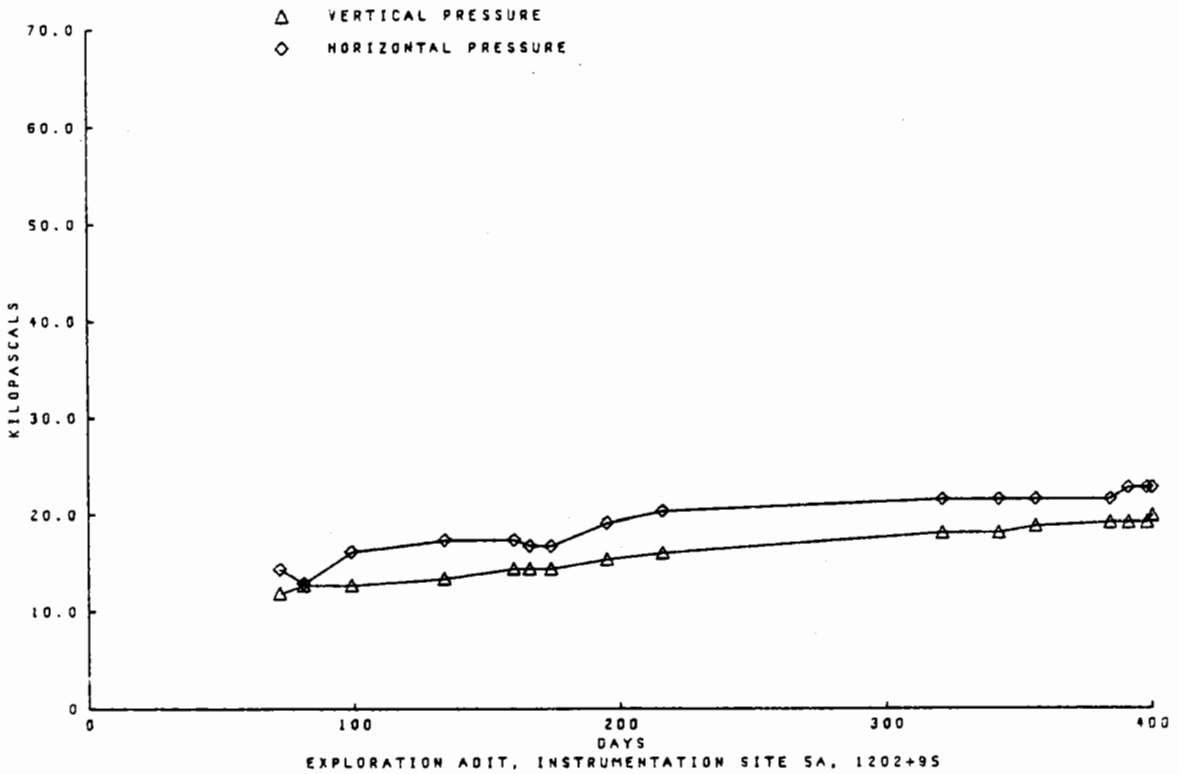
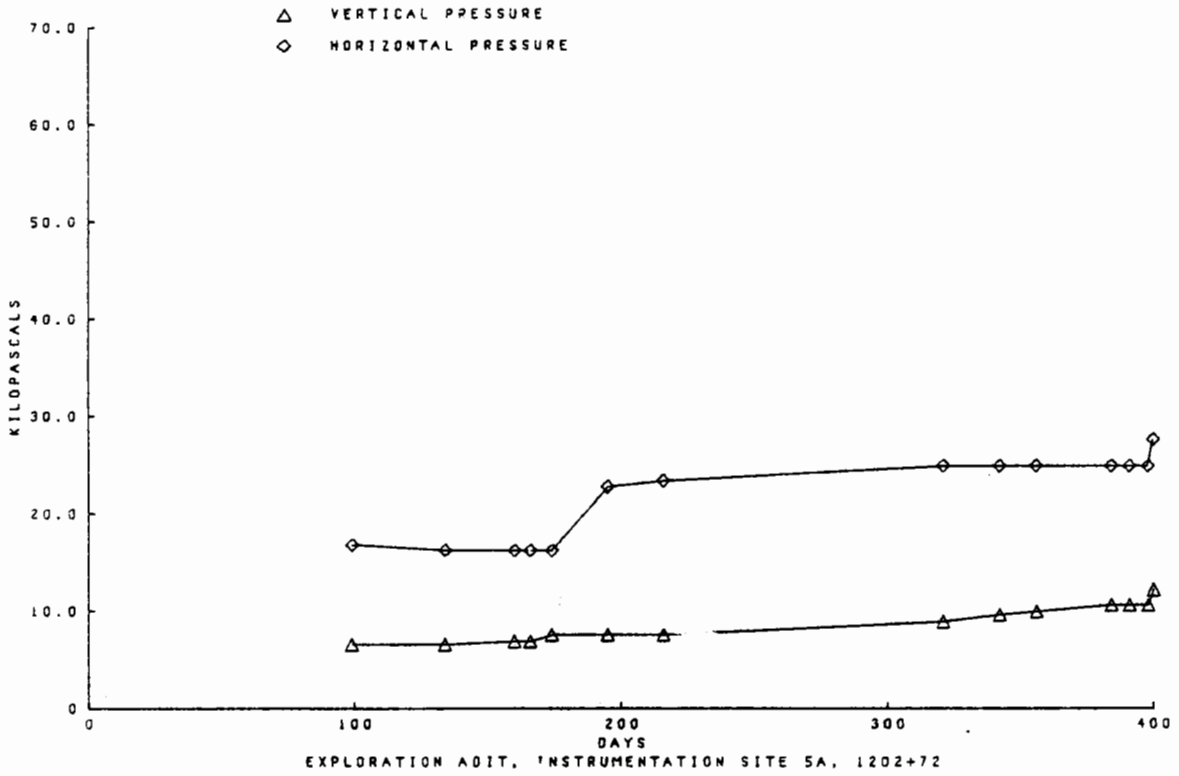


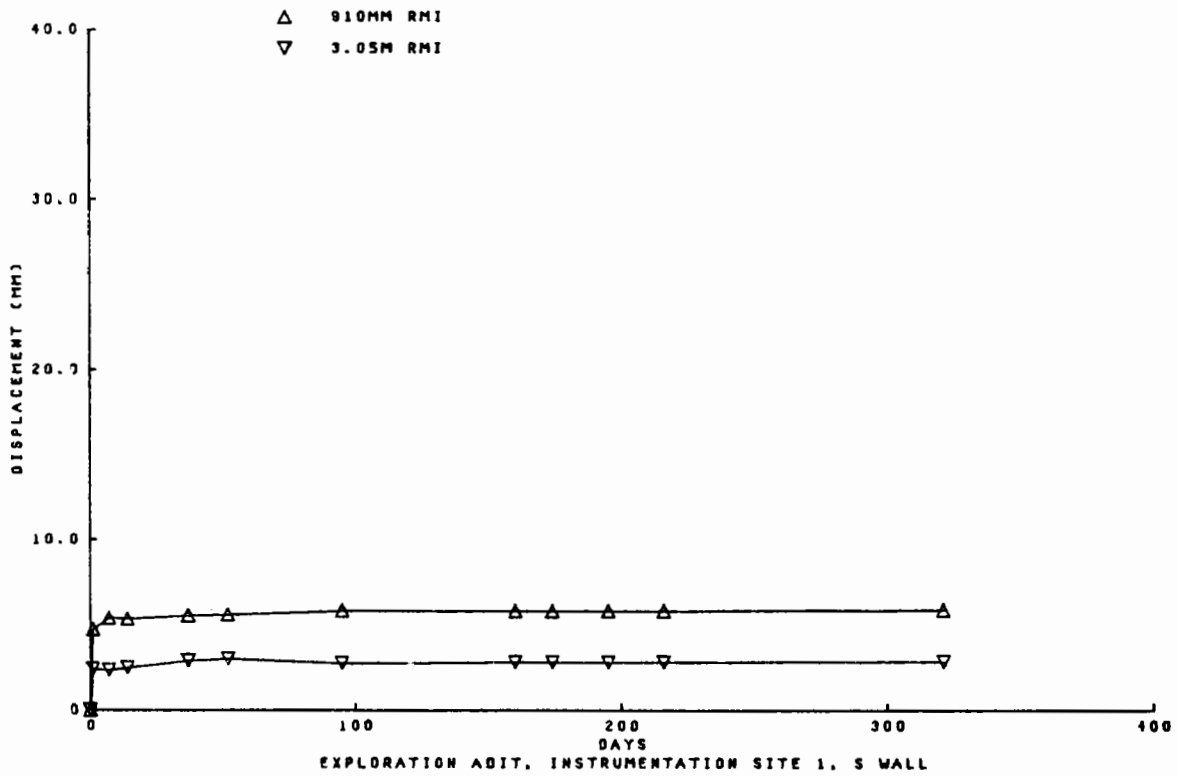
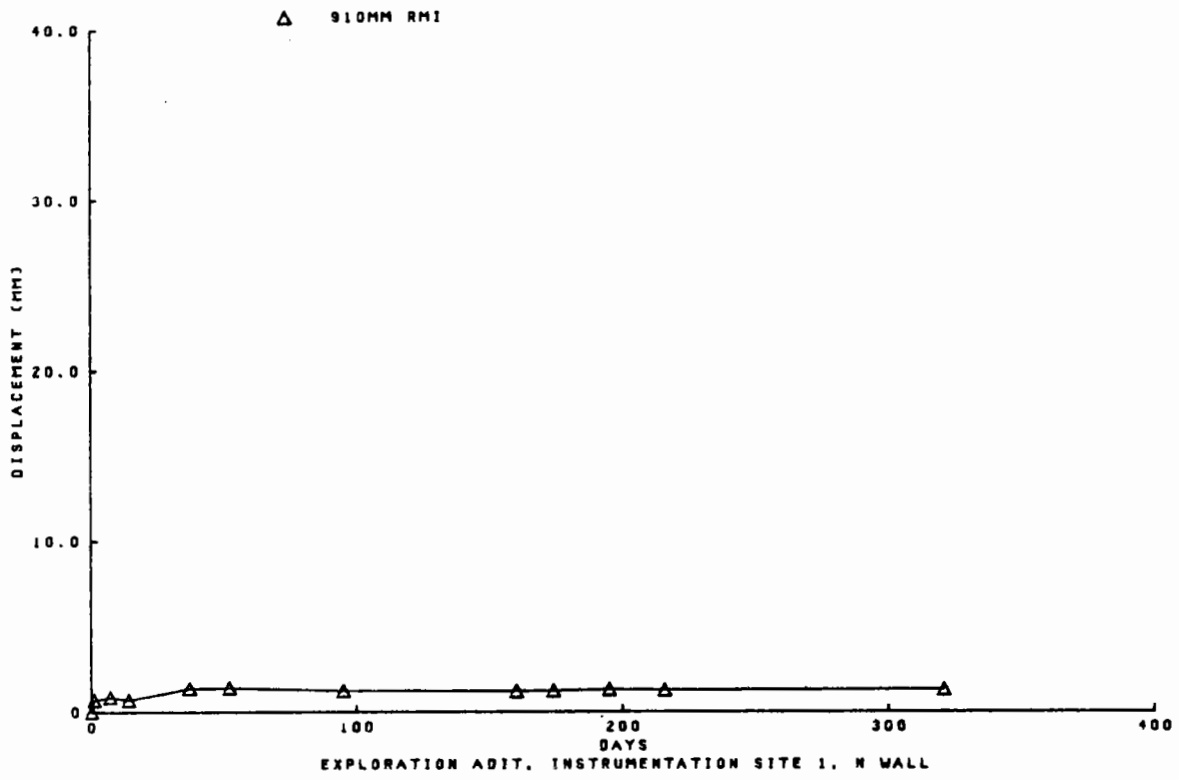


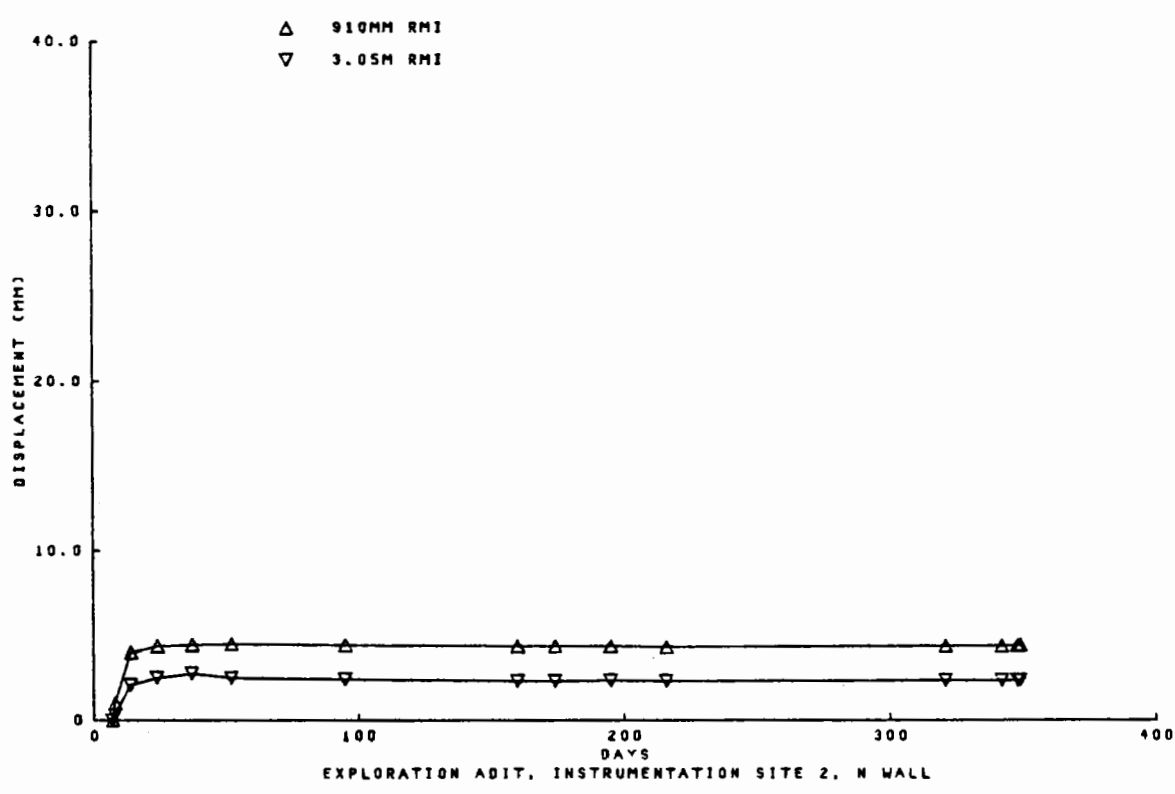
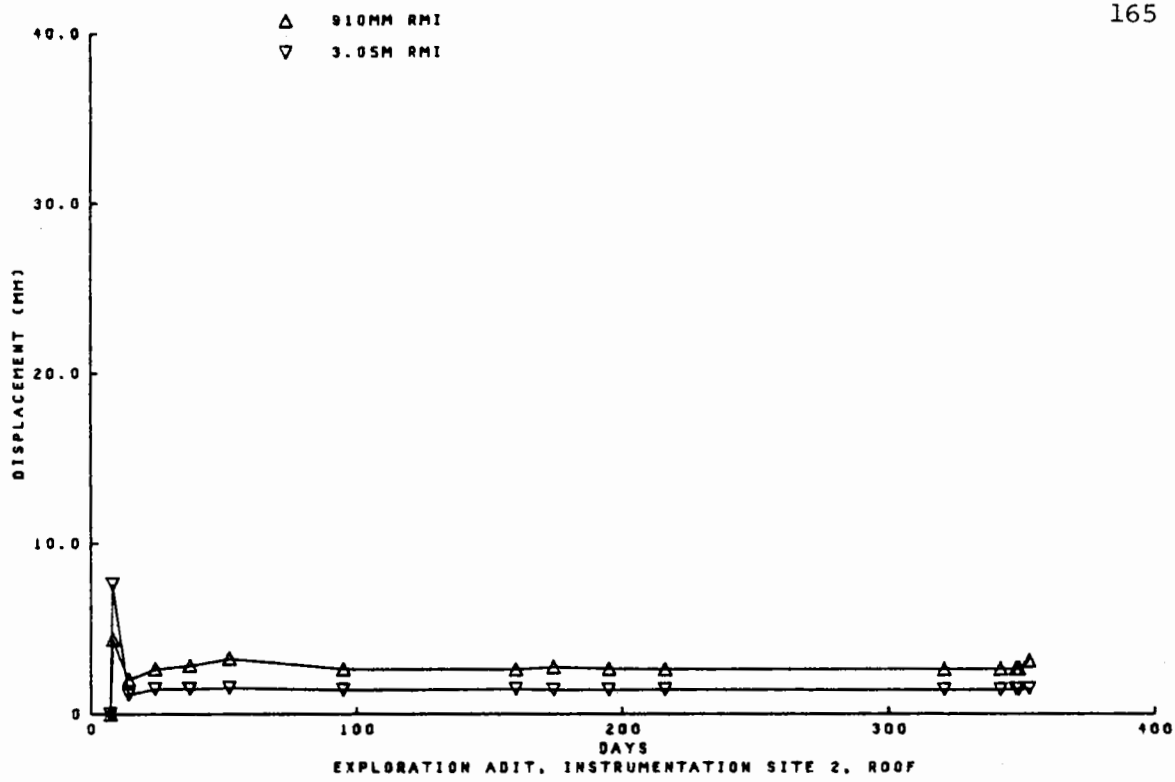


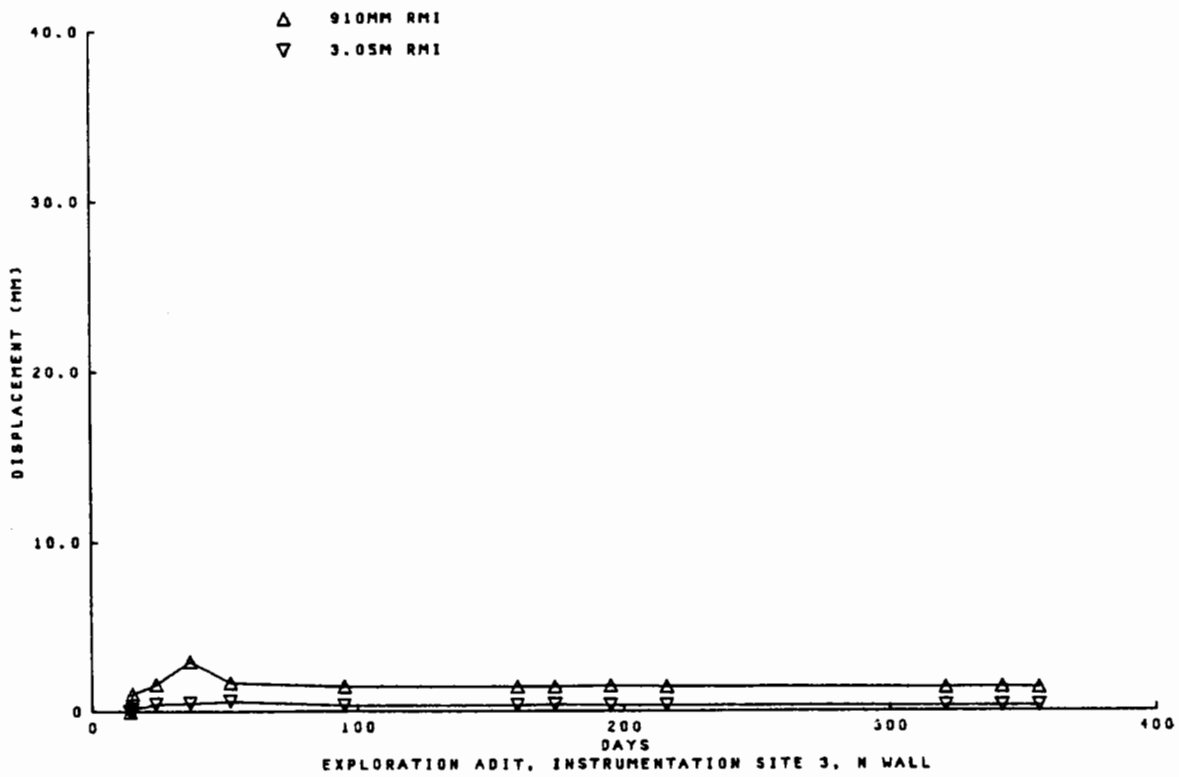
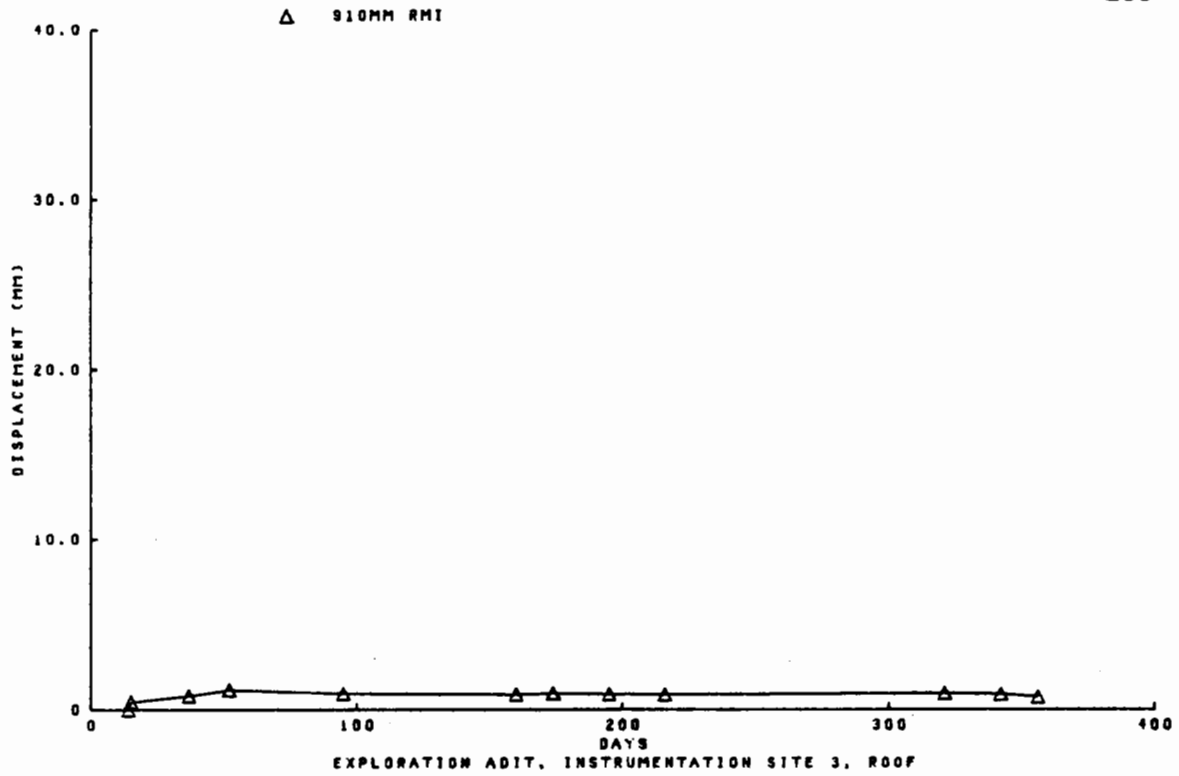


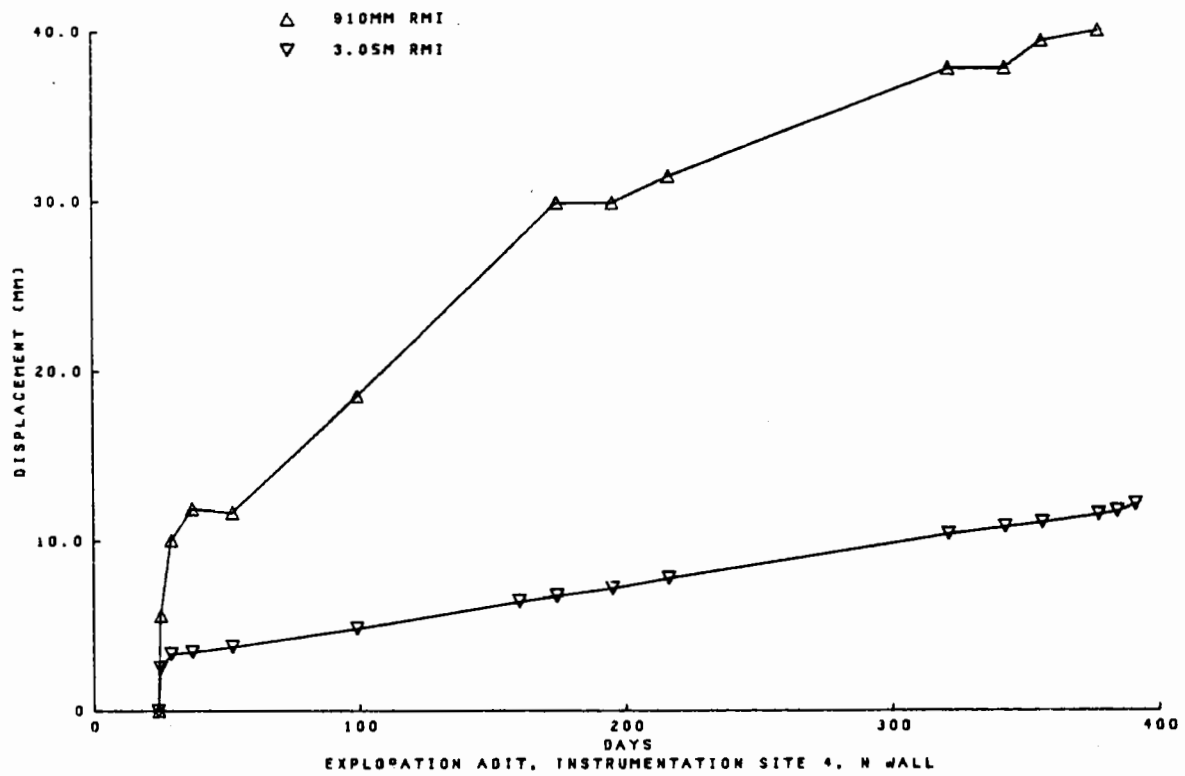
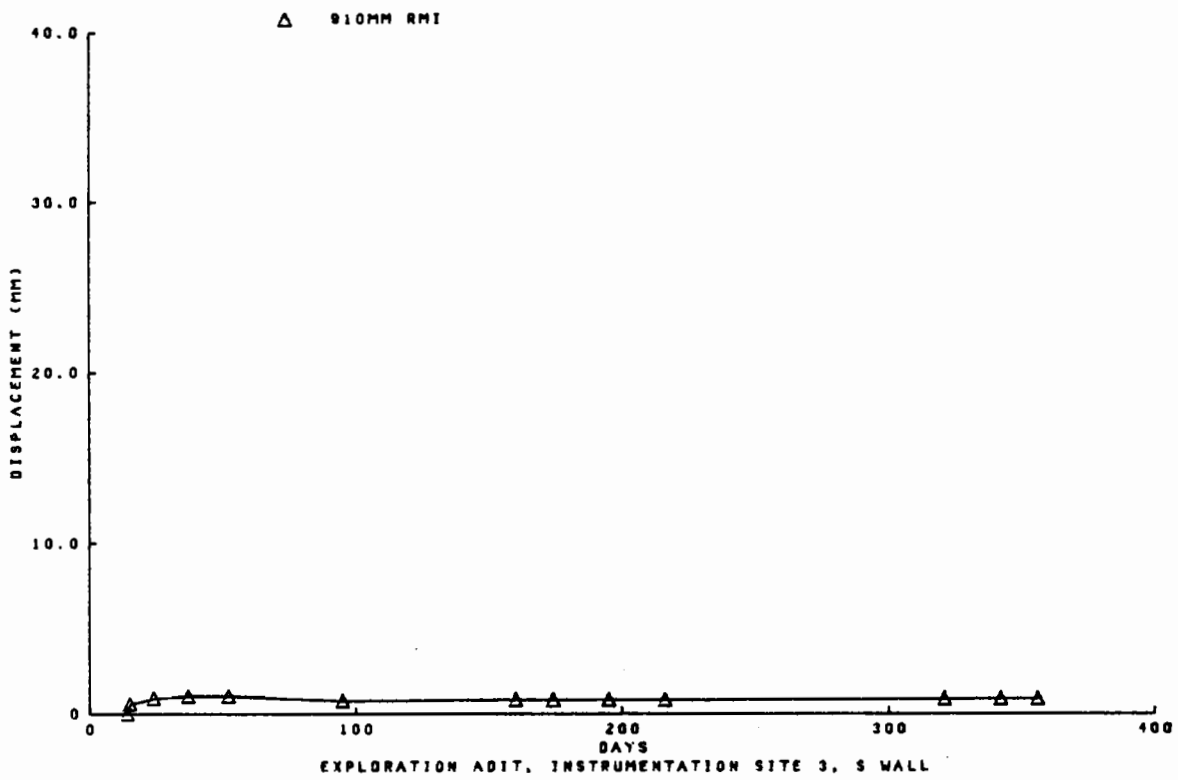


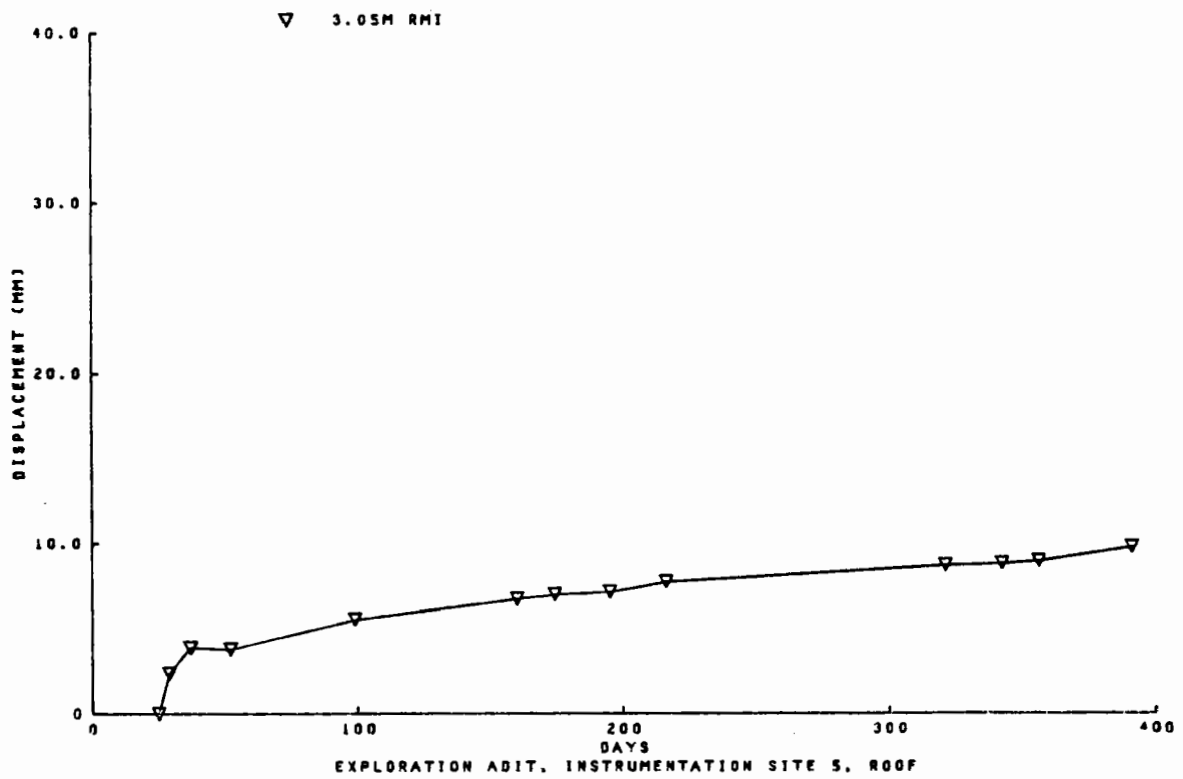
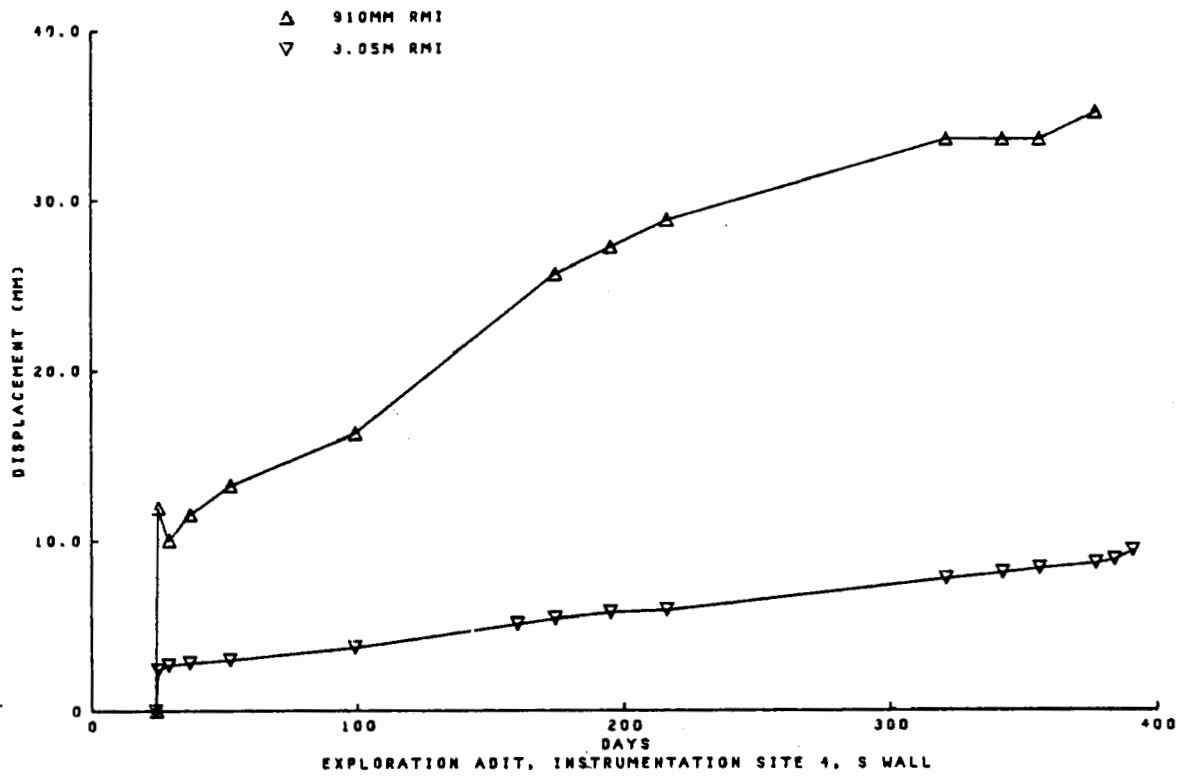




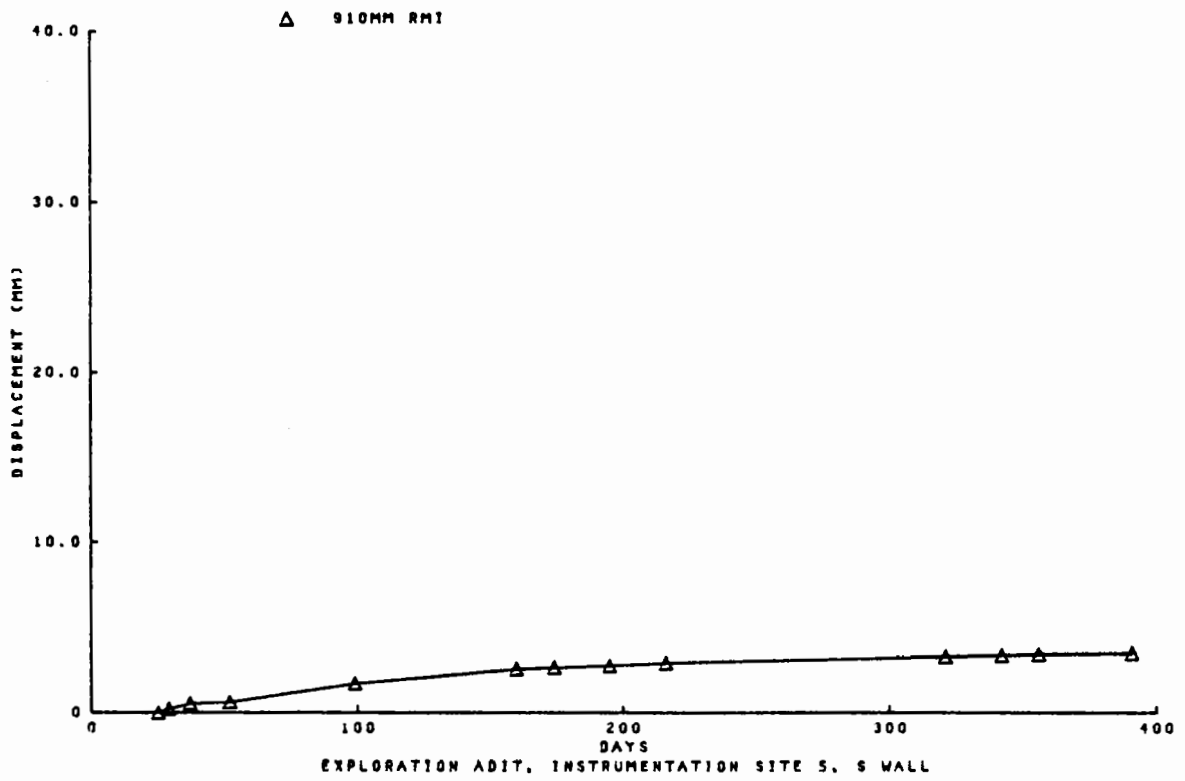
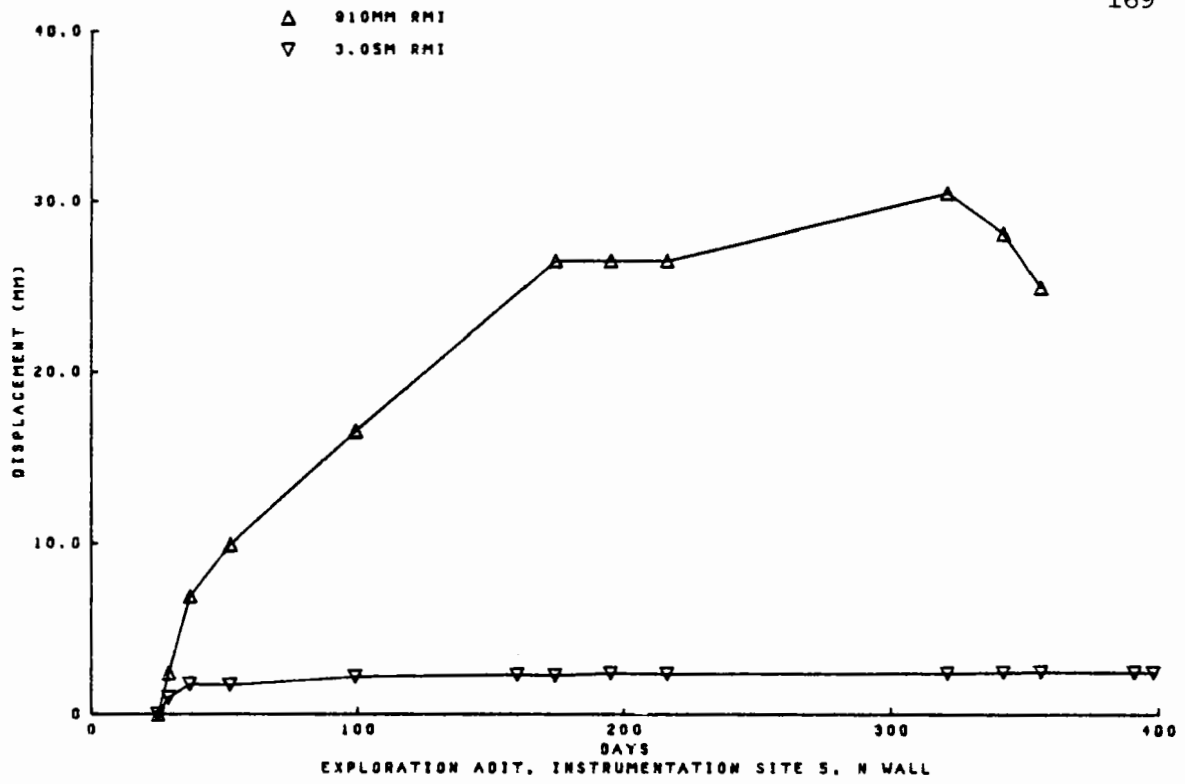


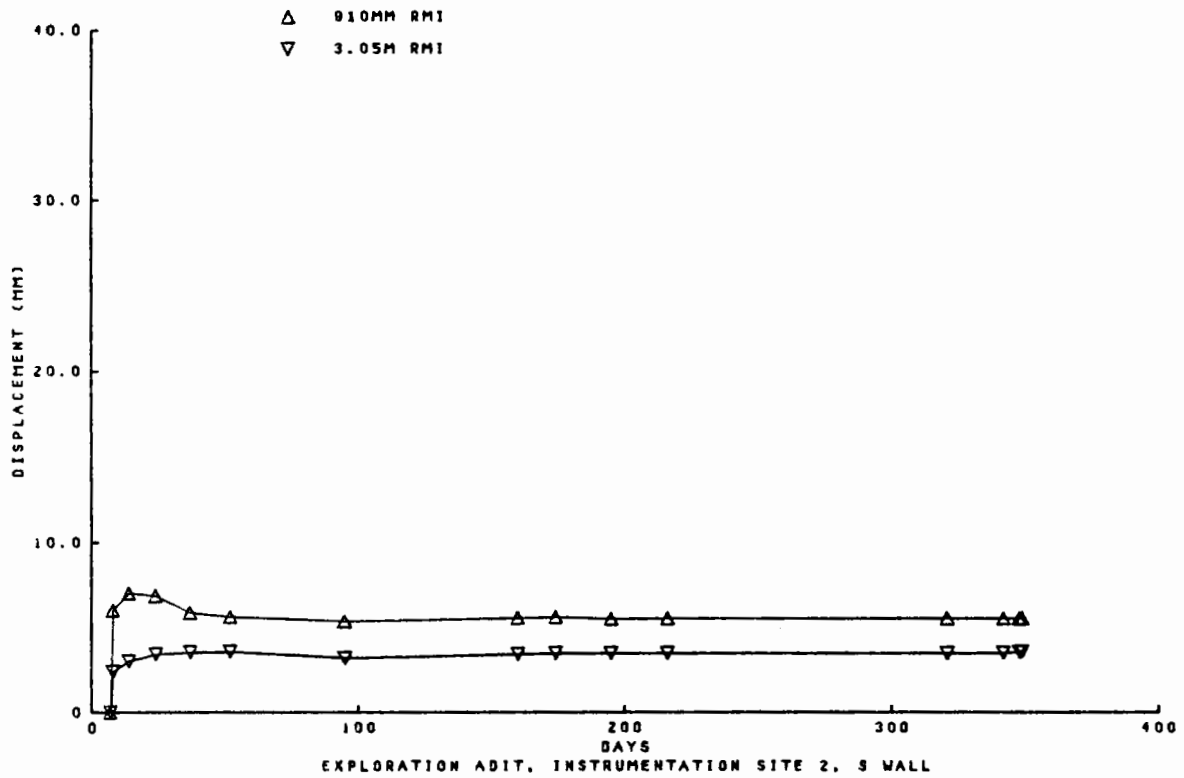












## APPENDIX B

GROUND CONDITIONS ENCOUNTERED AND TEMPORARY  
SUPPORT USED IN THE C2 TUNNEL

Ayres (1969) discussed the methods used to excavate and support the tunnel during construction. The following tabulated summary from his paper shows the different methods used over sections of the C2 tunnel.

*Station 1191+00 to 1198+80*

Formation: Franciscan Formation, sandstone with shale  
and gouge seams.

Length	238m	
Full face, no crown bars	103m	43%
Crown bars only required	18m	8%
Crown bars and breast boards required	106m	45%
Crown bars, breast boards and spiling	11m	4%
Average driving rate	3.4m per 16 hour day	

Steel spiling used at portal and in one gouge seam.

*Station 1198+80 to 1206+30*

Formation: Hayward Fault zone. Serpentine and gouge.

Heavy and squeezing ground in strutted section.

Length	229m	
Crown bars and breast boards required	229m	100%
Invert struts	157m	79%
Average driving rate	3.8m per 24 hour day	

*Station 1206+30 to 1207+10*

Formation: Rhyolite with clay seams

Length	24m	
Full face, no crown bars	24m	100%
Invert struts	2.4m	10%
Average driving rate	4.9m per 24 hour day	

Struts required at easterly contact zone.

*Station 1207+10 to 1250+50*

Formation: Sheared and broken sandstone and shale. The heaviest ground encountered occurred in the sheared shales of this section.

Length	1323m	
Full face, no crown bars	121m	9%
Crown bars only required	187m	14%
Crown bars and breast boards	1010m	77%
Crown bars, breast boards and spiling	- 5m	
Invert struts	721m	55%
Average driving rate	5.2m per 24 hour day	

Spiling was required in two short runs in wet sheared shale.

*Station 1250+50 to 1263+50*

Formation: Laminated chert and sandstone.

Length	396m	
Full face, no crown bars	173m	44%
Crown bars only required	49m	12%
Crown bars and breast boards	161m	41%

Crown bars, breast boards and spiling	13m	3%
Invert struts	38m	10%
Average driving rate	5.5m per 24 hour day	

Invert struts required in westerly contact zone. Chert thinly laminated and carried considerable water. Spiling was required in three wet running sections of chert. Full face driving was mostly in sandstones on the easterly end. The tunnel was holed through at Station 1254+75.

*Station 1263+50 to 1313+50*

Formation: Siltstone, sandstone, conglomerate and volcanics.

Length	1524m	
Full face, no crown bars	1426m	93%
Crown bars only required	21m	1%
Crown bars and breast boards	76m	5%
Crown bars, breast boards and spiling	1.2m	
Invert struts	105m	7%
Average driving rate	8.9m per 24 hour day	

Invert struts required in three shear zones 64m, 32m and 30m wide. Crown bars and breast boards were required in the shorter two of these zones and in seven other areas of shearing. The rest of the driving was in good rock.

*Station 1313+50 to 1315+70*

Formation: Siltstone and sandstone, badly sheared and faulted. Siesta Syncline and fault.

Length	67m	
Crown bars, breast boards and invert struts	67m	100%
Average driving rate	2.4m per 24 hour day	

*Station 1315+70 to 1353+40*

Formation: Siltstone, sandstone, conglomerate and volcanics.

Length	1149m	
Full face, no crown bars	1009m	88%
Crown bars only required	68m	6%
Crown bars and breast boards	25m	2%
Crown bars, breast boards and spiling	48m	4%
Invert struts	15m	1%

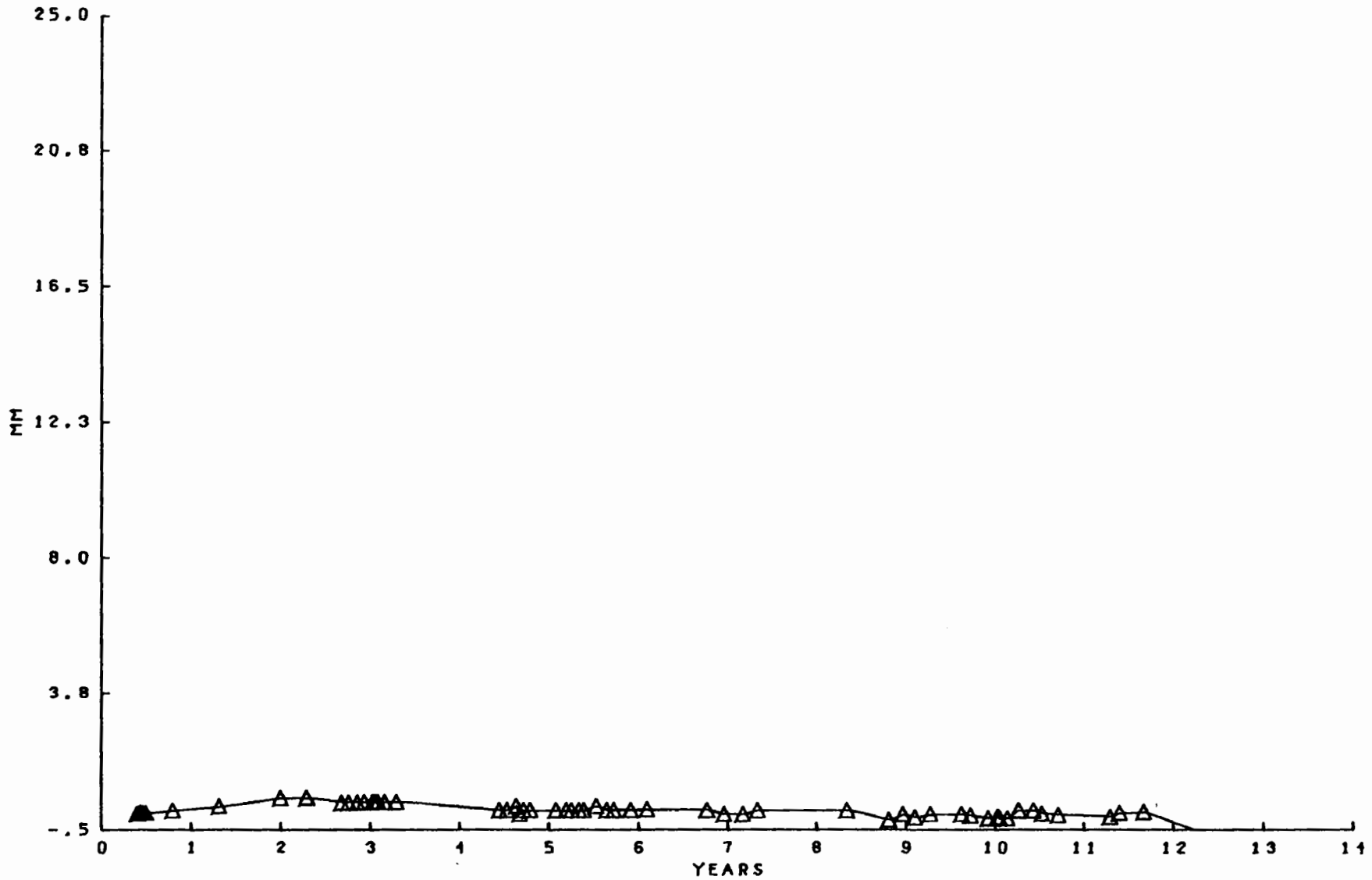
Average driving rate 6.6m per 24 hour day

Generally, the ground was good. Spiling was required in three wet, faulted, and fractured volcanic zones totalling 62m in length where the driving rate averaged about 2.6m per day. Crown bars and breast boards were required in eight sheared zones. Driving rate in these zones was about 3.8m per day.

## APPENDIX C

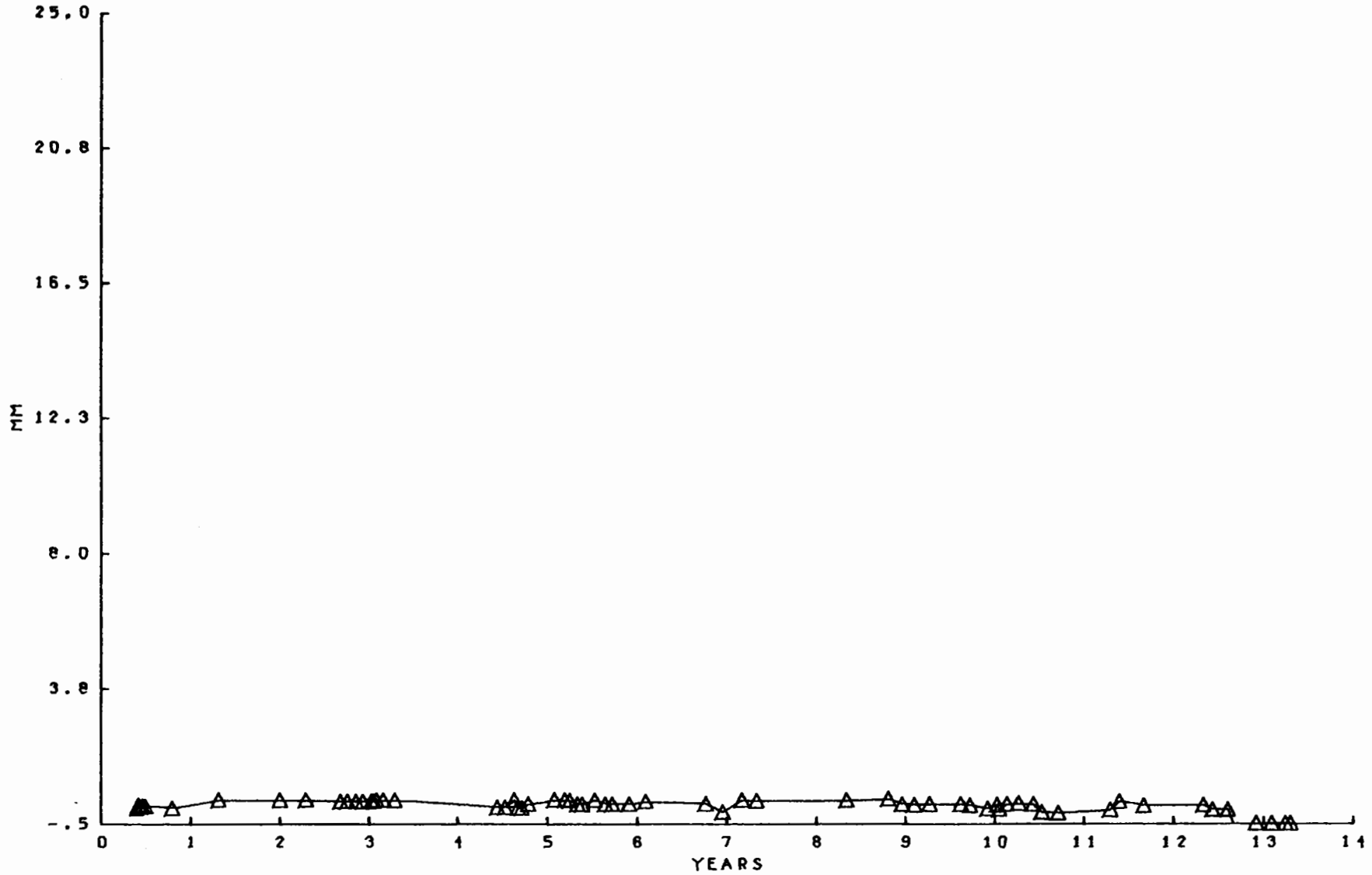
INSTRUMENTATION DATA FROM SECTION  
OF C2 TUNNEL IN HAYWARD FAULT ZONE

Plots of rock movement indicator (Figure C.1 i - xx) and pressure cell data (Figure C.2 i - vi) from the C2 tunnel in the Hayward Fault zone. Zero time ordinate for these figures corresponds to January 1, 1967.

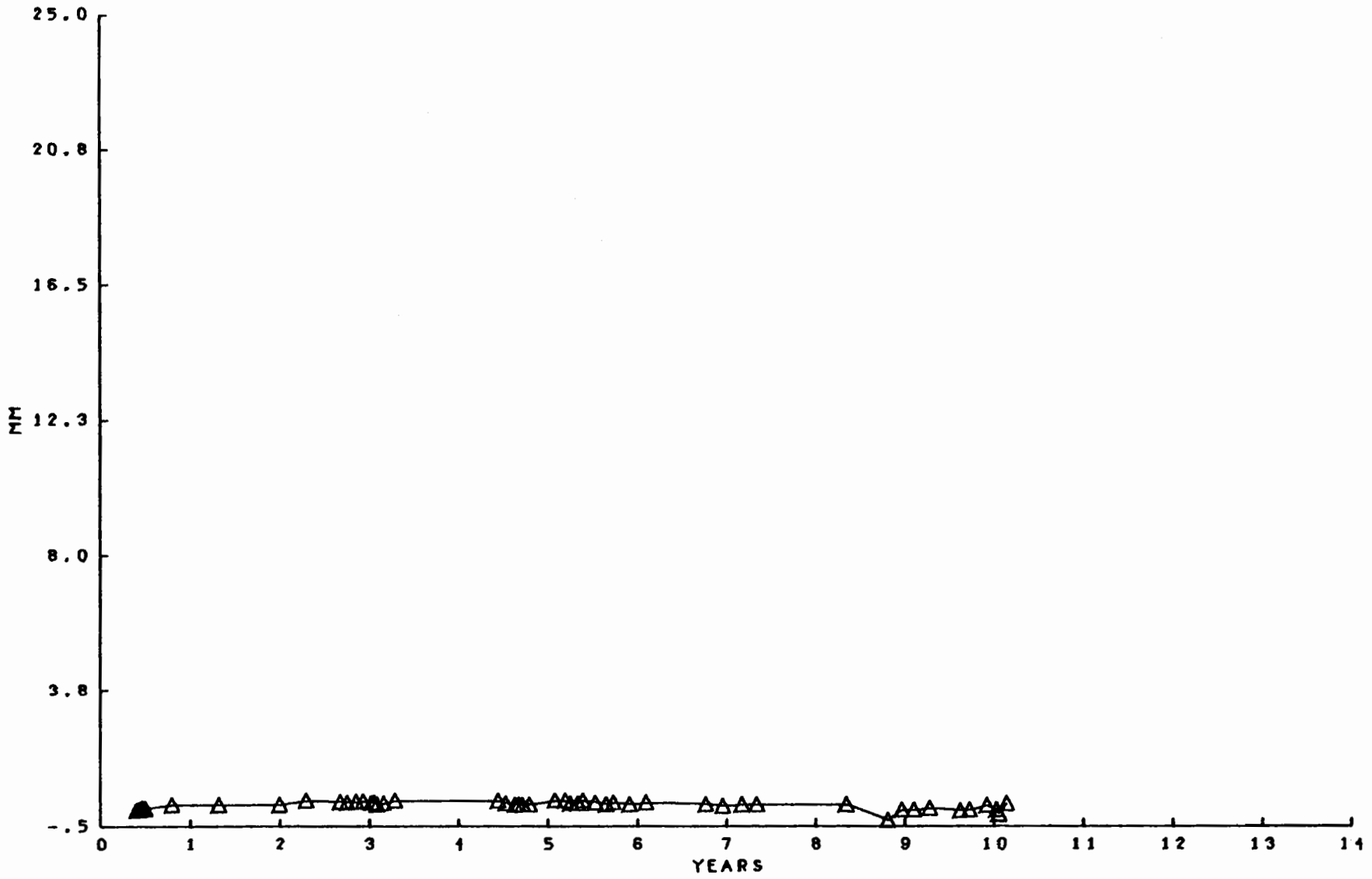


EXTENSOMETER A, STATION 1198+01, NORTH WALL, 30 FT  
 BART TUNNELS HAYWARD FAULT ZONE INSTRUMENTATION

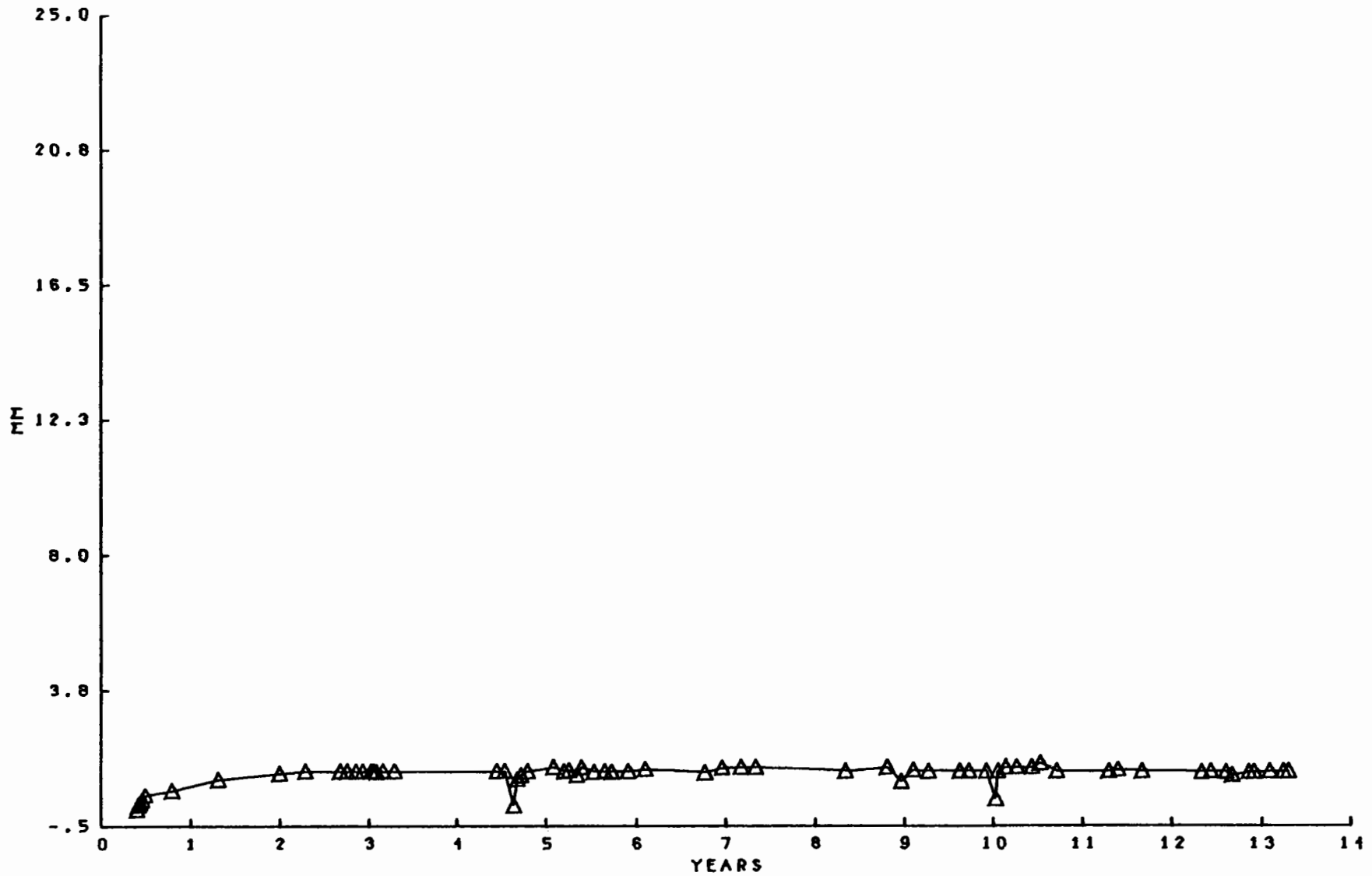




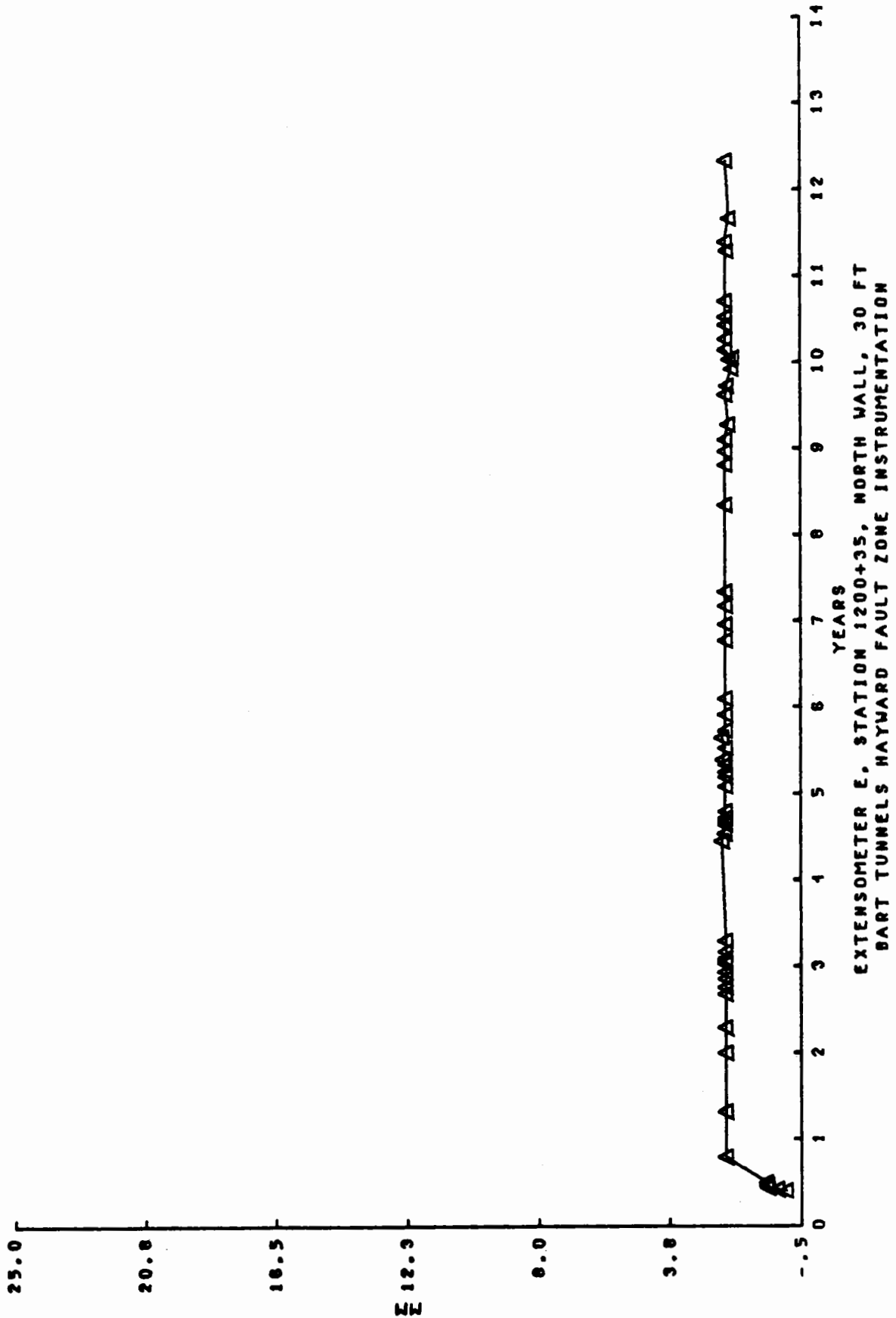
EXTENSOMETER B, STATION 1198+01, SOUTH WALL, 30 FT  
 BART TUNNELS HAYWARD FAULT ZONE INSTRUMENTATION

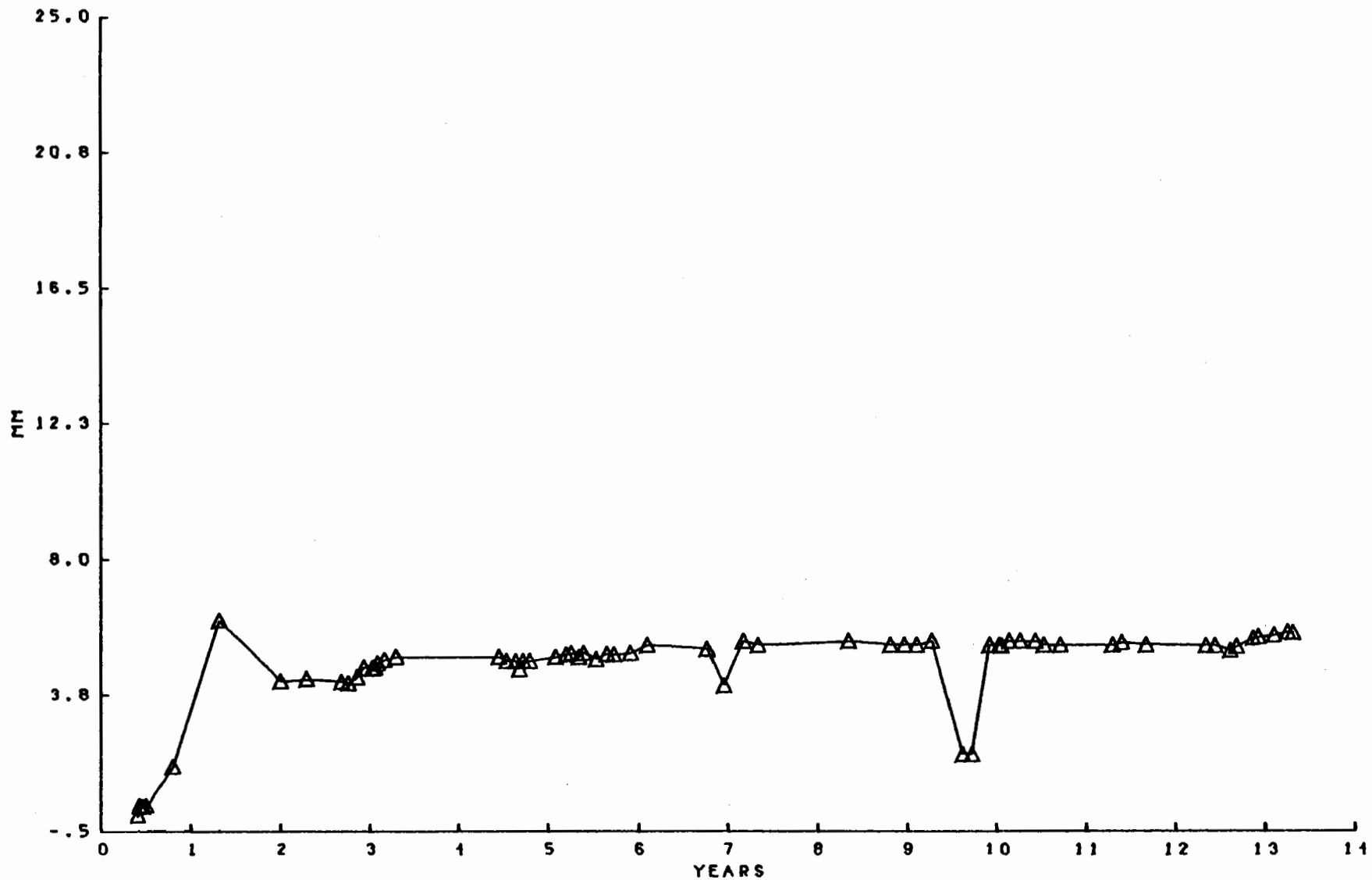


EXTENSOMETER C, STATION 1199+11, NORTH WALL, 30 FT  
 BART TUNNELS HAYWARD FAULT ZONE INSTRUMENTATION

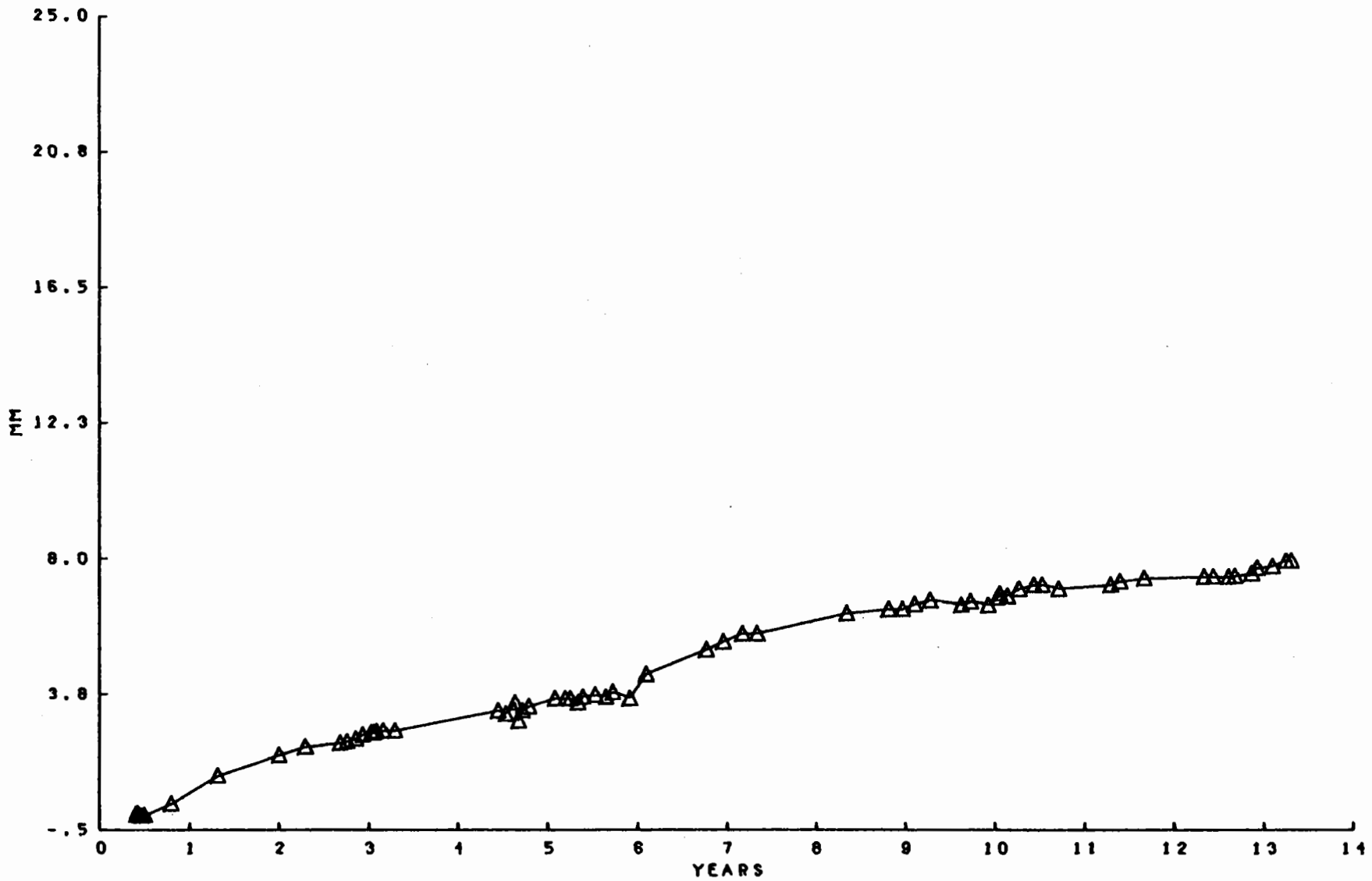


EXTENSOMETER D, STATION 1199+44, SOUTH WALL, 30 FT  
 BART TUNNELS HAYWARD FAULT ZONE INSTRUMENTATION

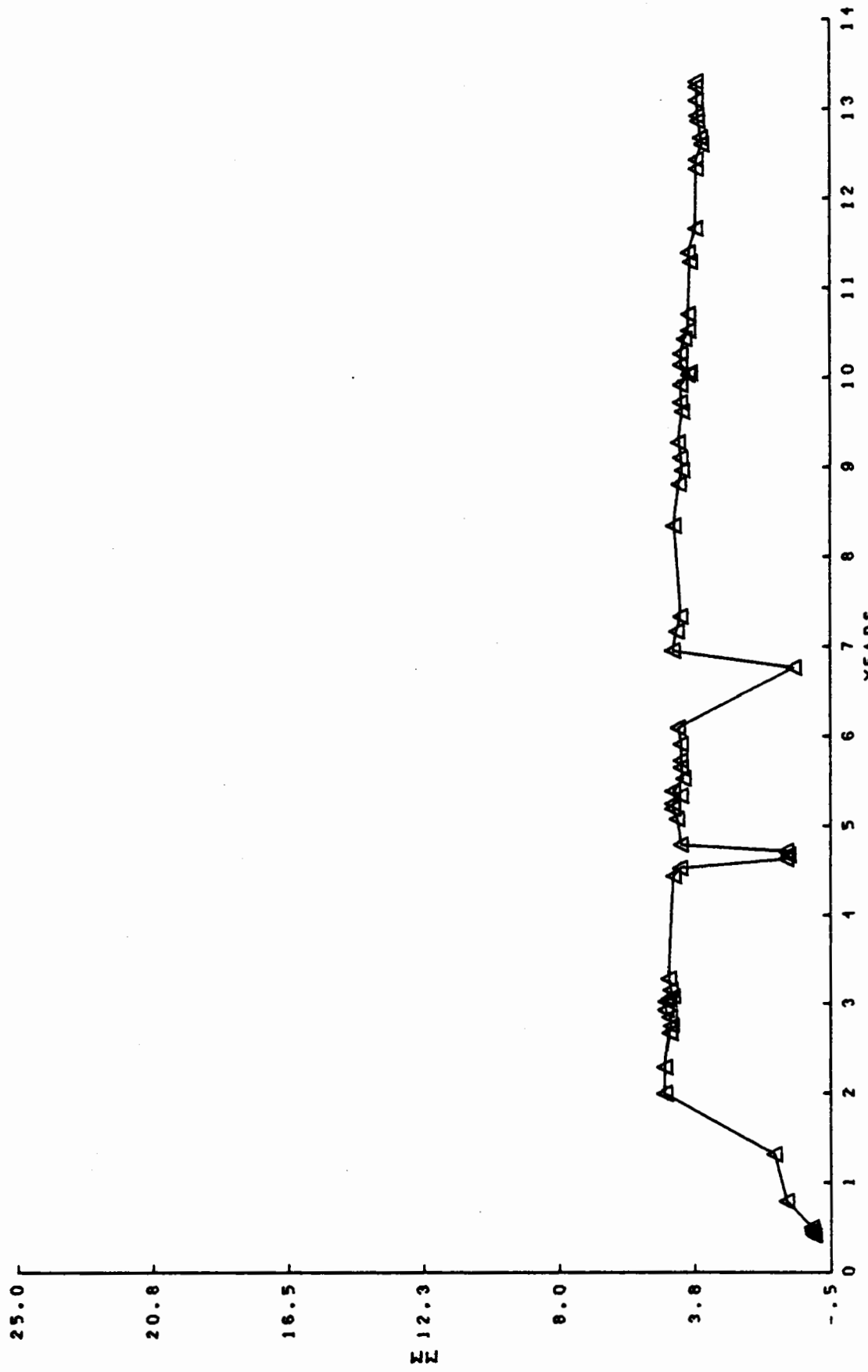




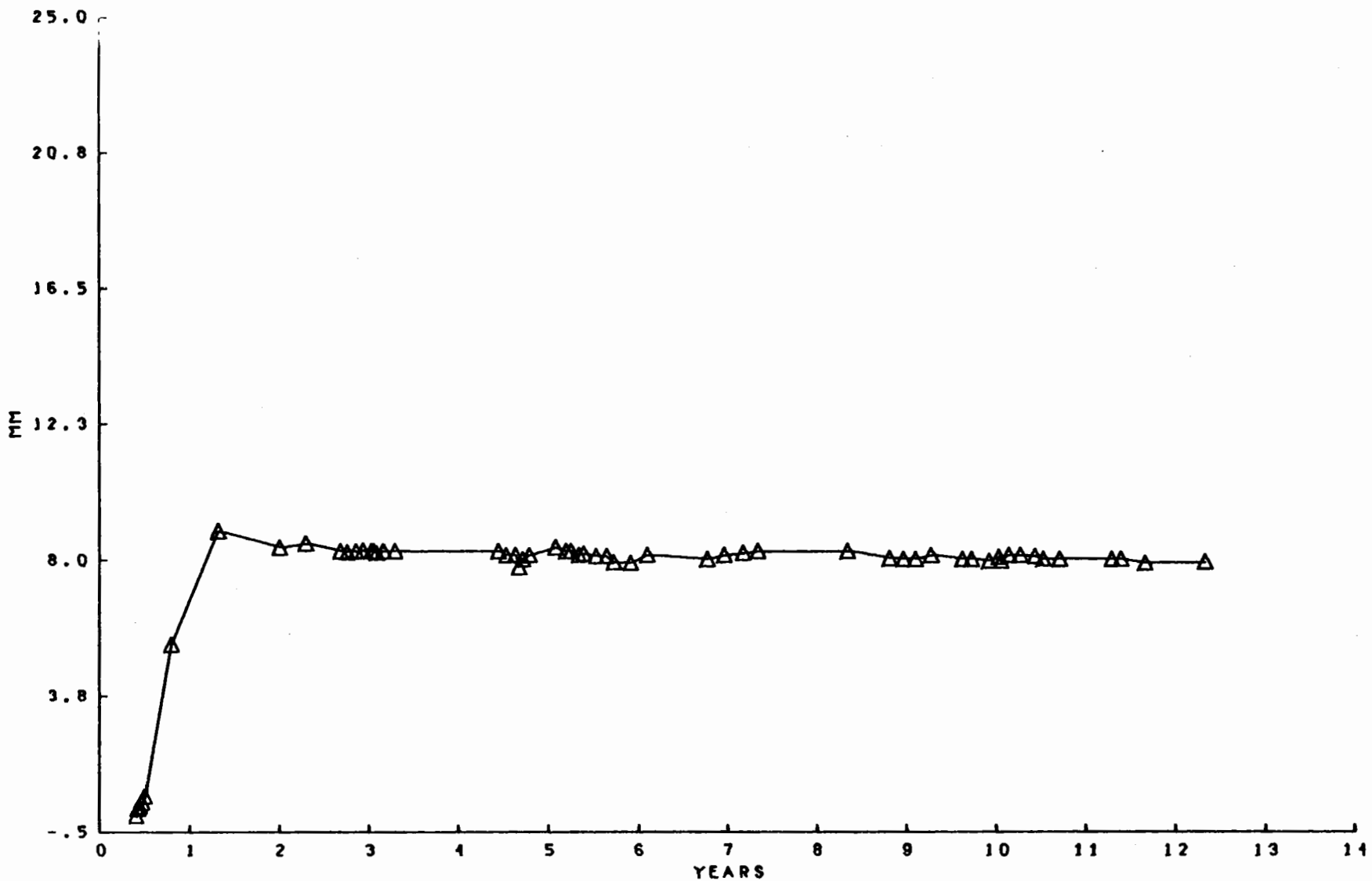
EXTENSOMETER F, STATION 1200+53, SOUTH WALL, 30 FT  
 BART TUNNELS HAYWARD FAULT ZONE INSTRUMENTATION



EXTENSOMETER G, STATION 1200+51, NORTH WALL, 10 FT  
 BART TUNNELS HAYWARD FAULT ZONE INSTRUMENTATION

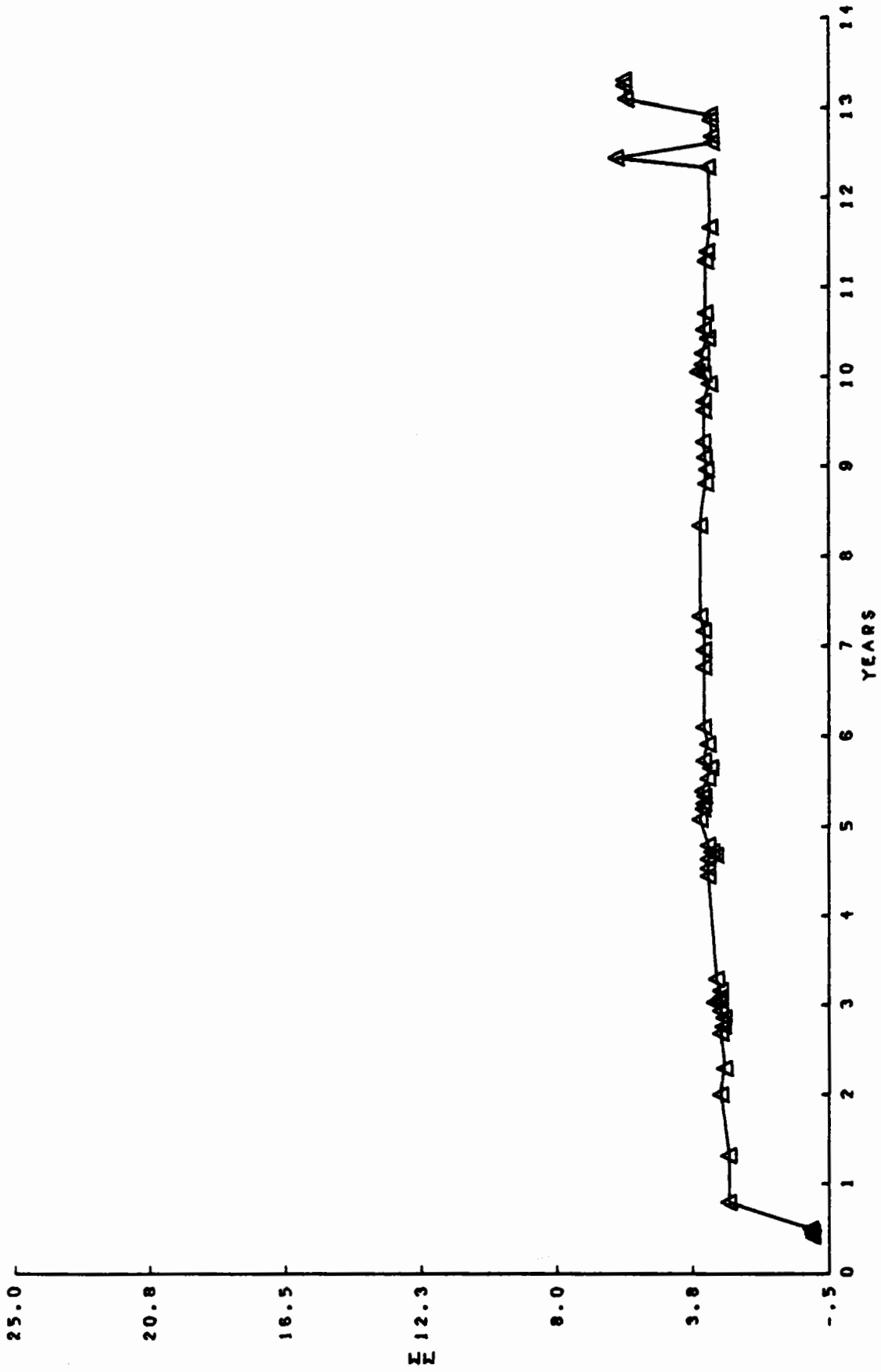


EXTENSOMETER H, STATION 1200+51, SOUTH WALL, 10 FT  
BART TUNNELS HAYWARD FAULT ZONE INSTRUMENTATION

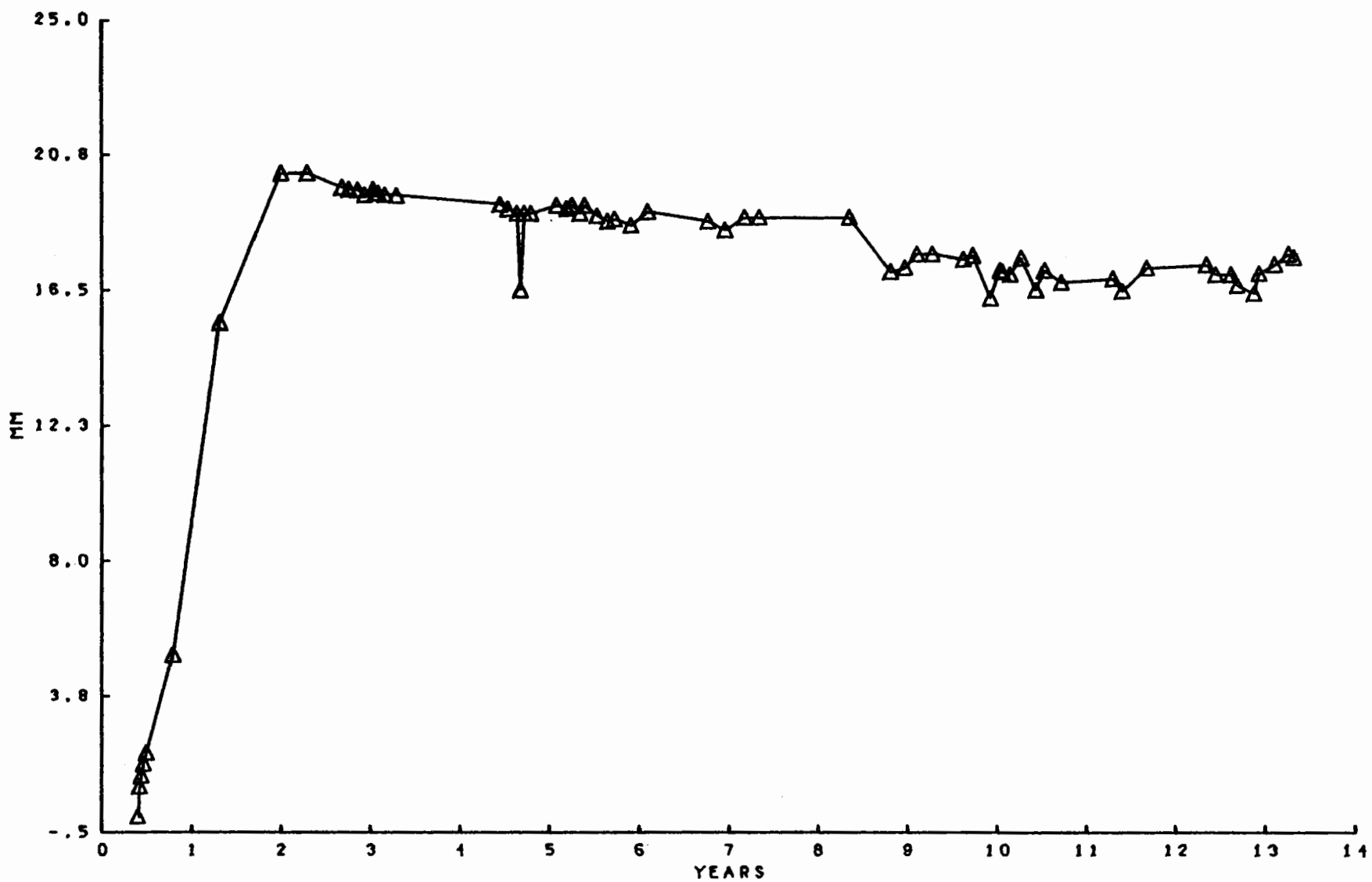


EXTENSOMETER I, STATION 1201+35, NORTH WALL, 30 FT  
 BART TUNNELS HAYWARD FAULT ZONE INSTRUMENTATION

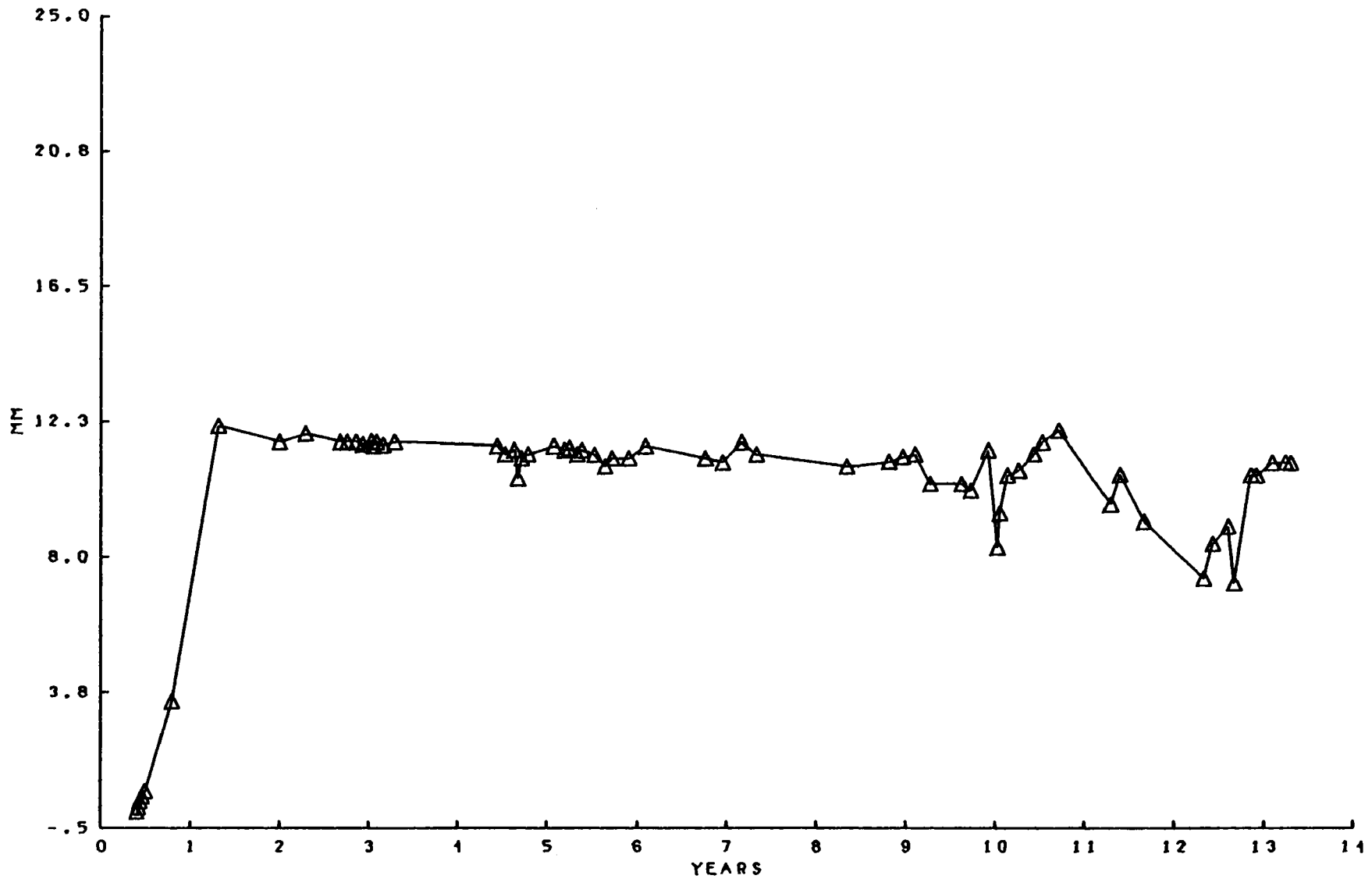




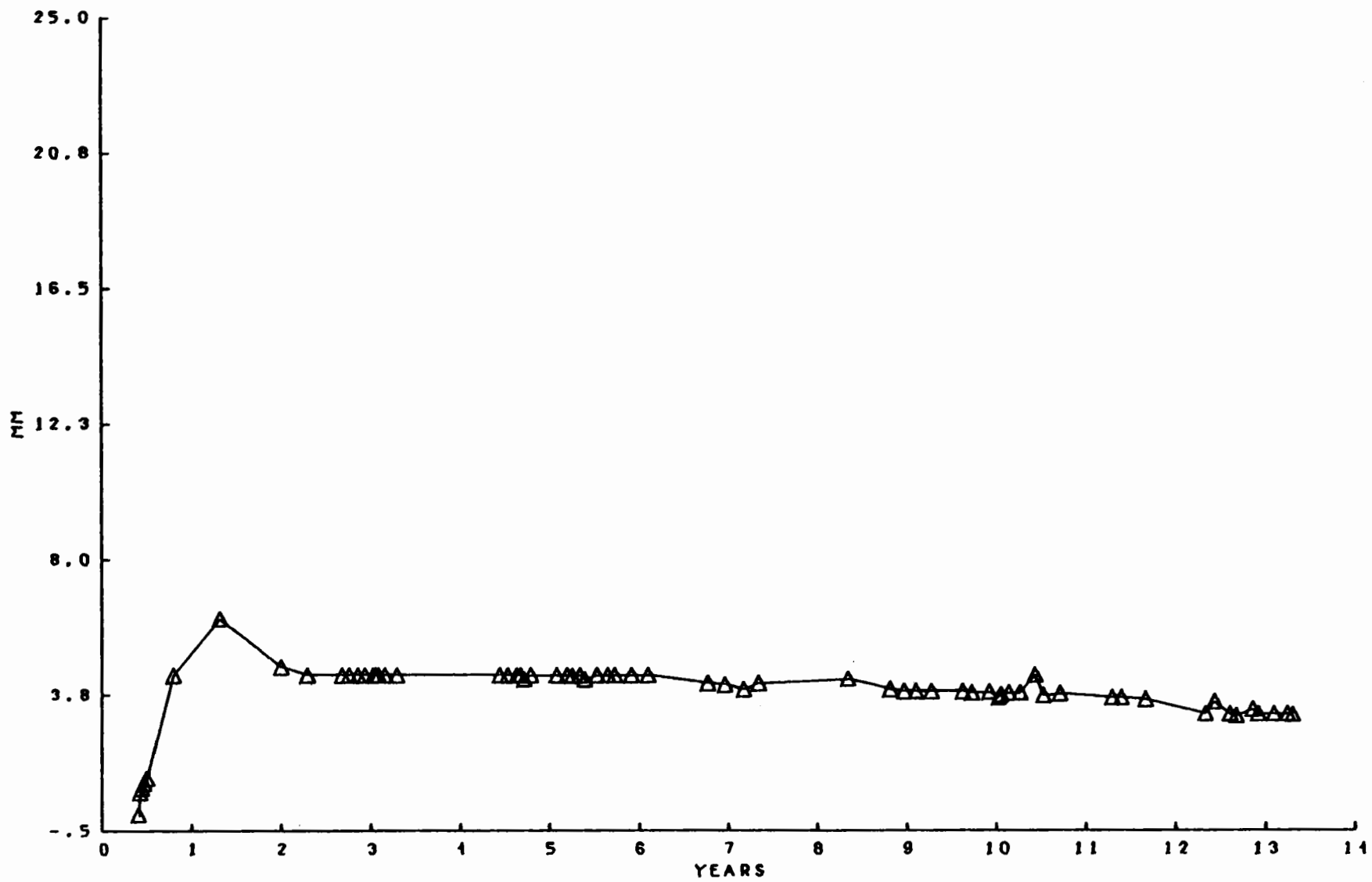
EXTENSOMETER J. STATION 1201+35, SOUTH WALL, 30 FT  
BART TUNNELS HAYWARD FAULT ZONE INSTRUMENTATION



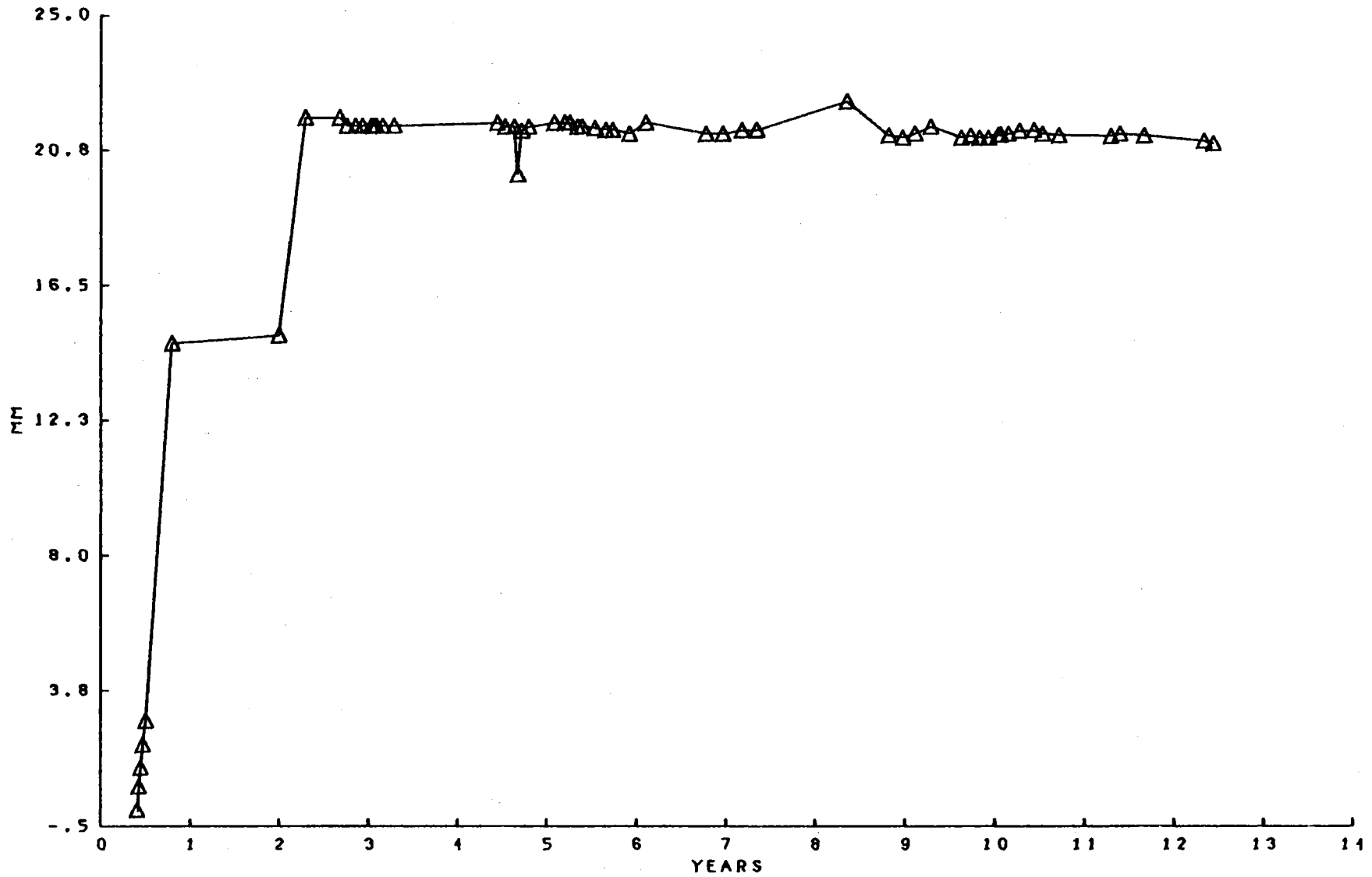
EXTENSOMETER K, STATION 1202+01, NORTH WALL, 30 FT  
 BART TUNNELS HAYWARD FAULT ZONE INSTRUMENTATION



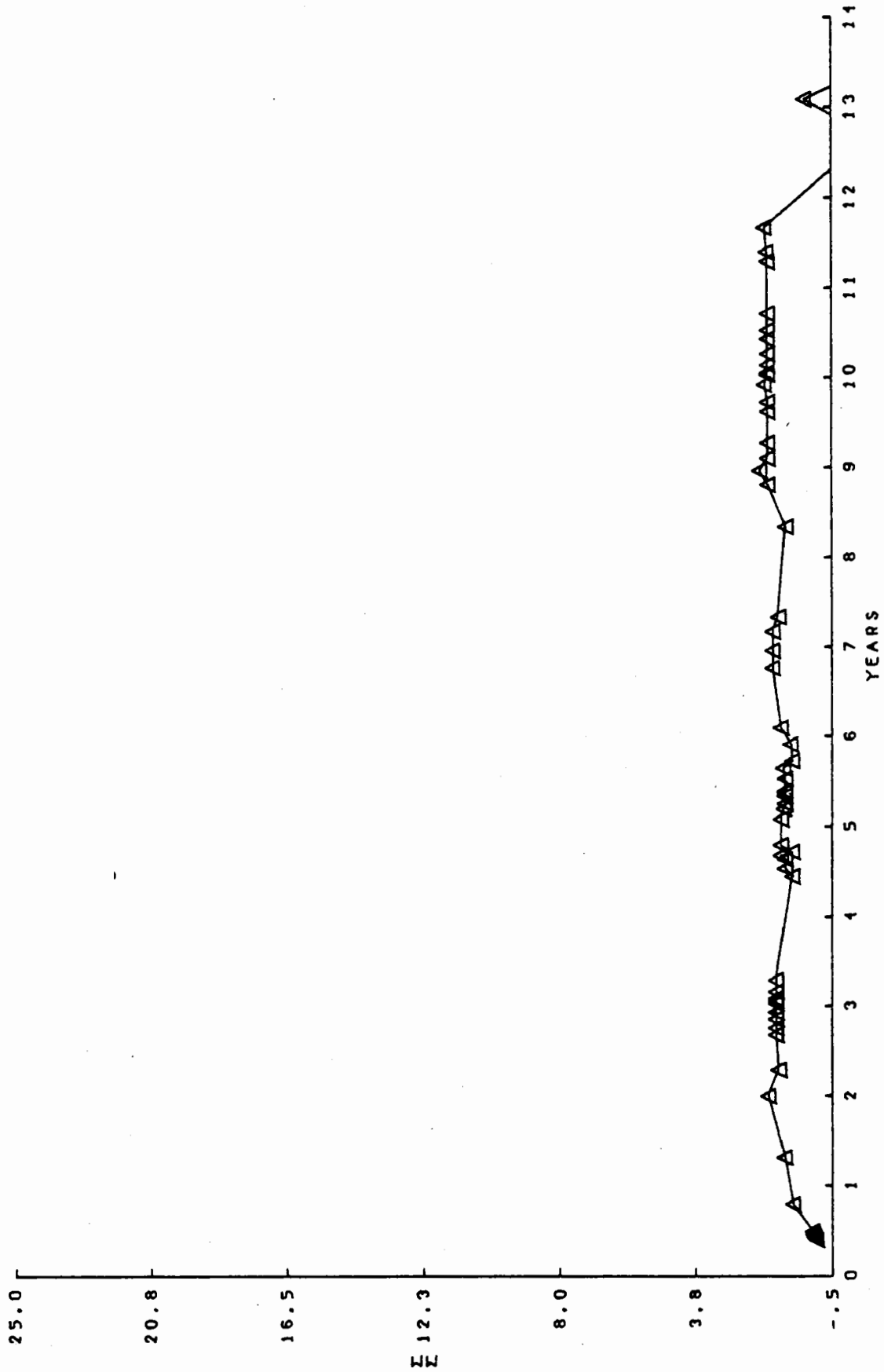
EXTENSOMETER L, STATION 1202+01, SOUTH WALL, 30 FT  
 BART TUNNELS HAYWARD FAULT ZONE INSTRUMENTATION



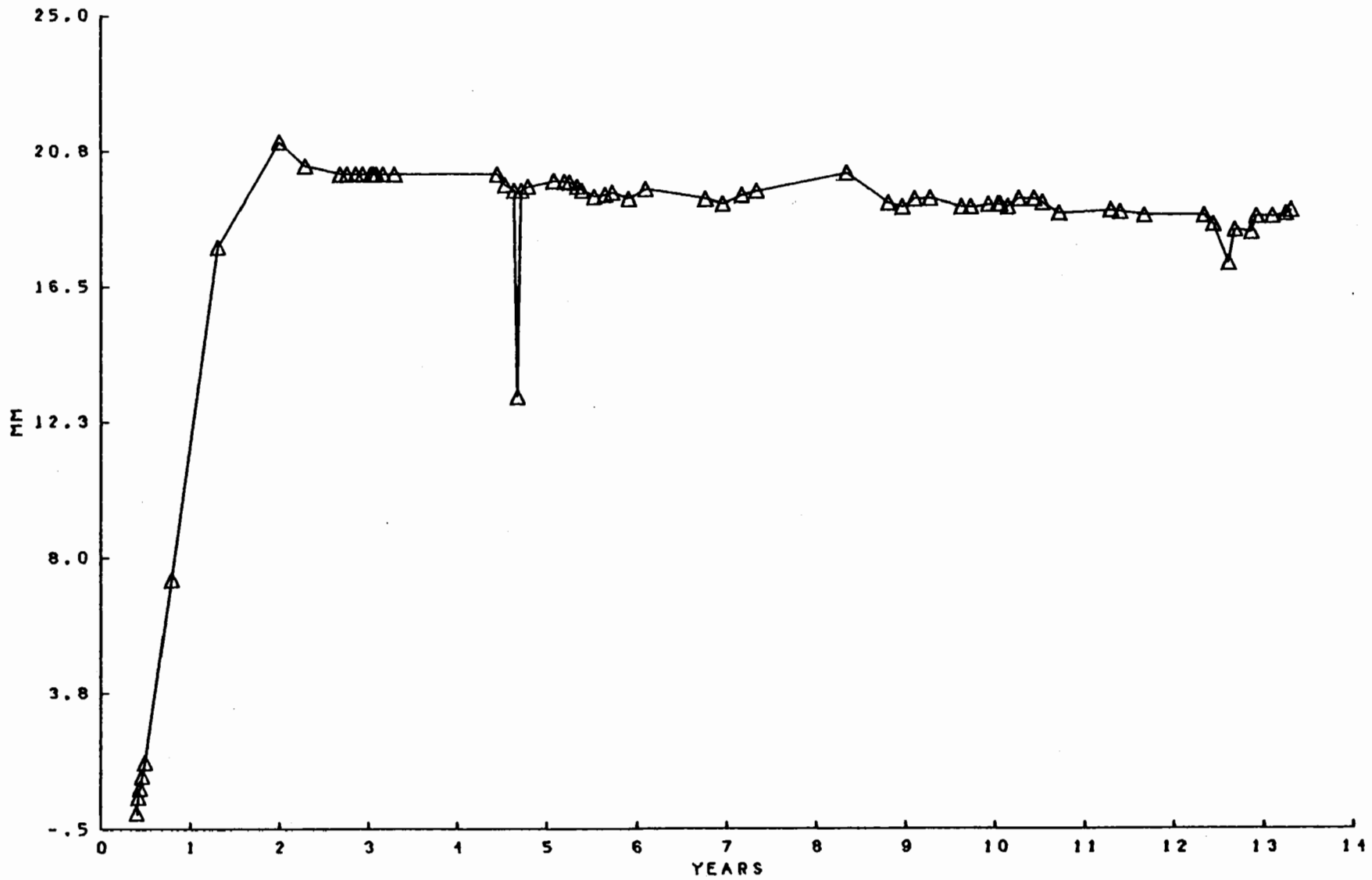
EXTENSOMETER M, STATION 1202+77, NORTH WALL, 30 FT  
 BART TUNNELS HAYWARD FAULT ZONE INSTRUMENTATION



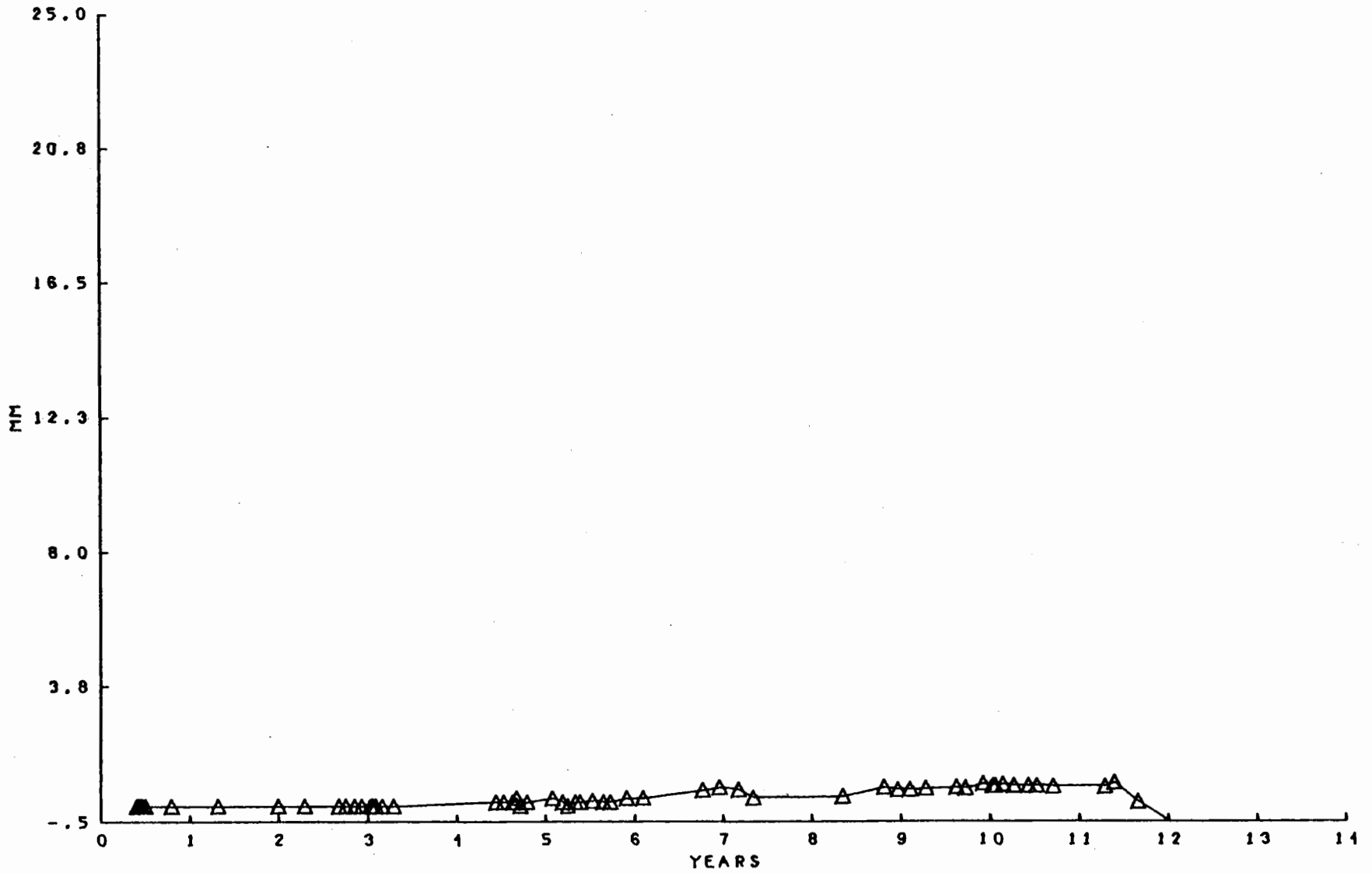
EXTENSOMETER N. STATION 1202+77, SOUTH WALL, 30 FT  
 BART TUNNELS HAYWARD FAULT ZONE INSTRUMENTATION



EXTENSOMETER 0, STATION 1202+75, NORTH WALL, 10 FT  
BART TUNNELS HAYWARD FAULT ZONE INSTRUMENTATION

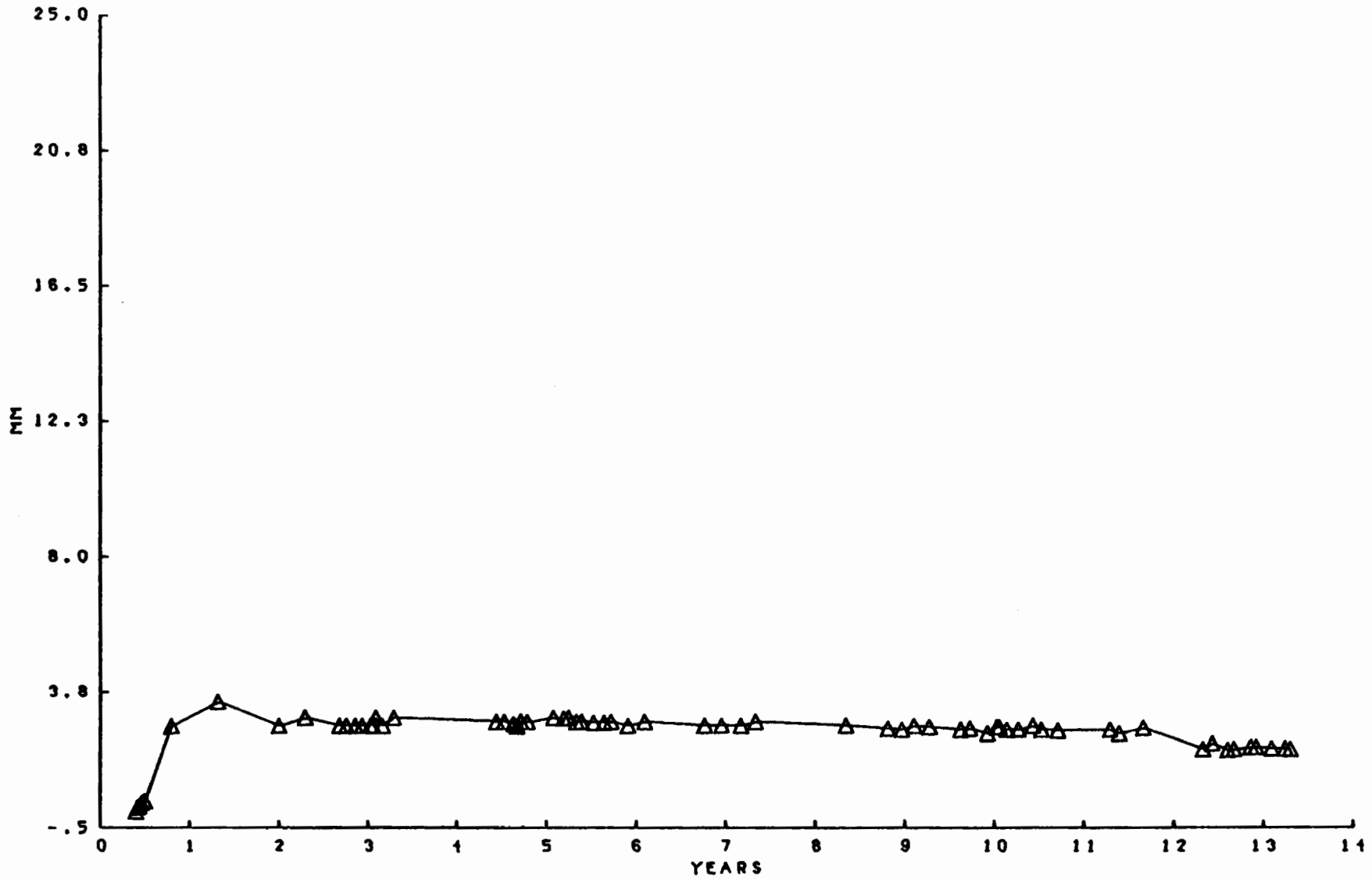


EXTENSOMETER P, STATION 1202+75, SOUTH WALL, 10 FT  
 BART TUNNELS HAYWARD FAULT ZONE INSTRUMENTATION

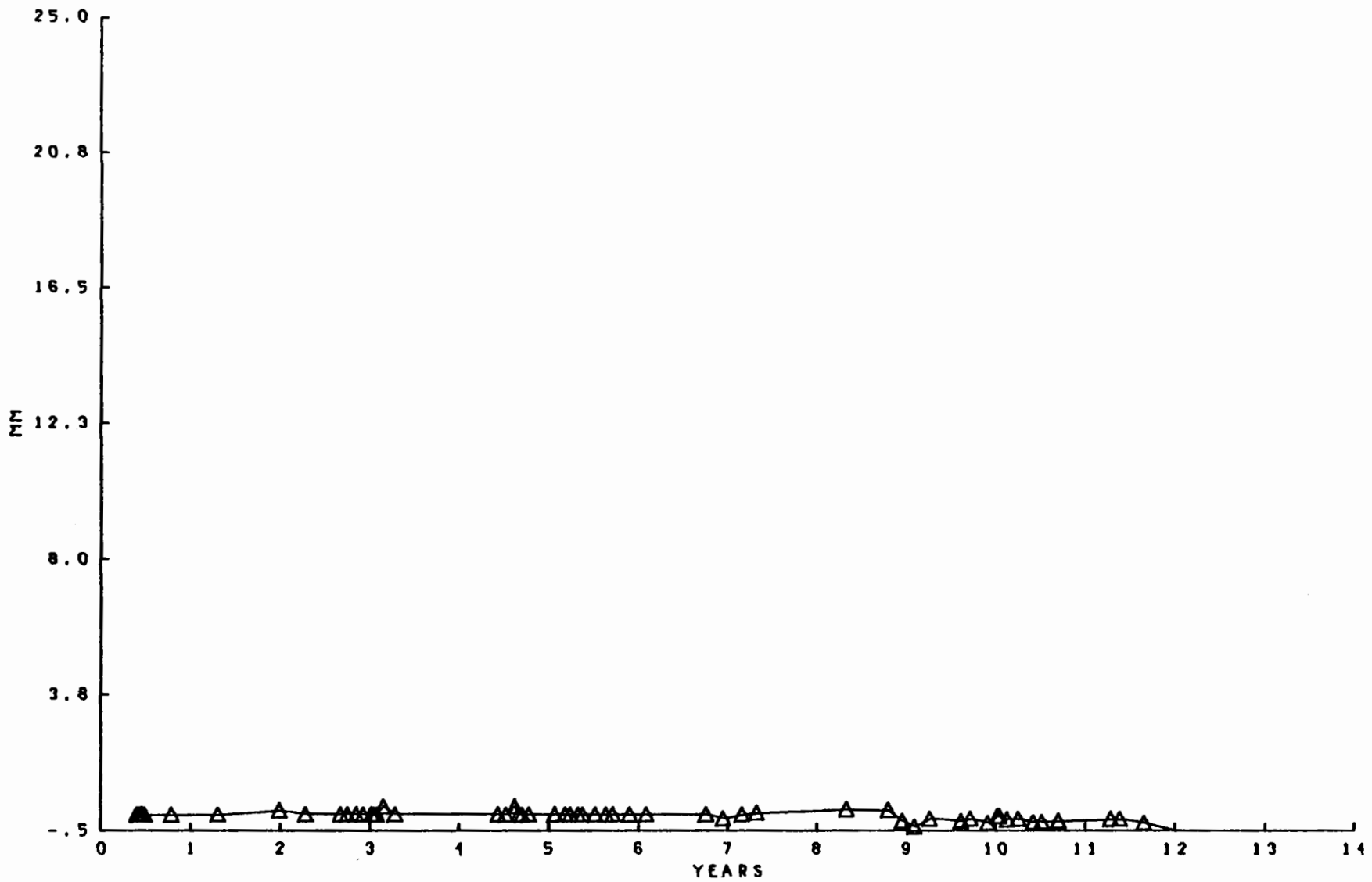


EXTENSOMETER 0, STATION 1204+10, SOUTH WALL, 30 FT  
 BART TUNNELS HAYWARD FAULT ZONE INSTRUMENTATION

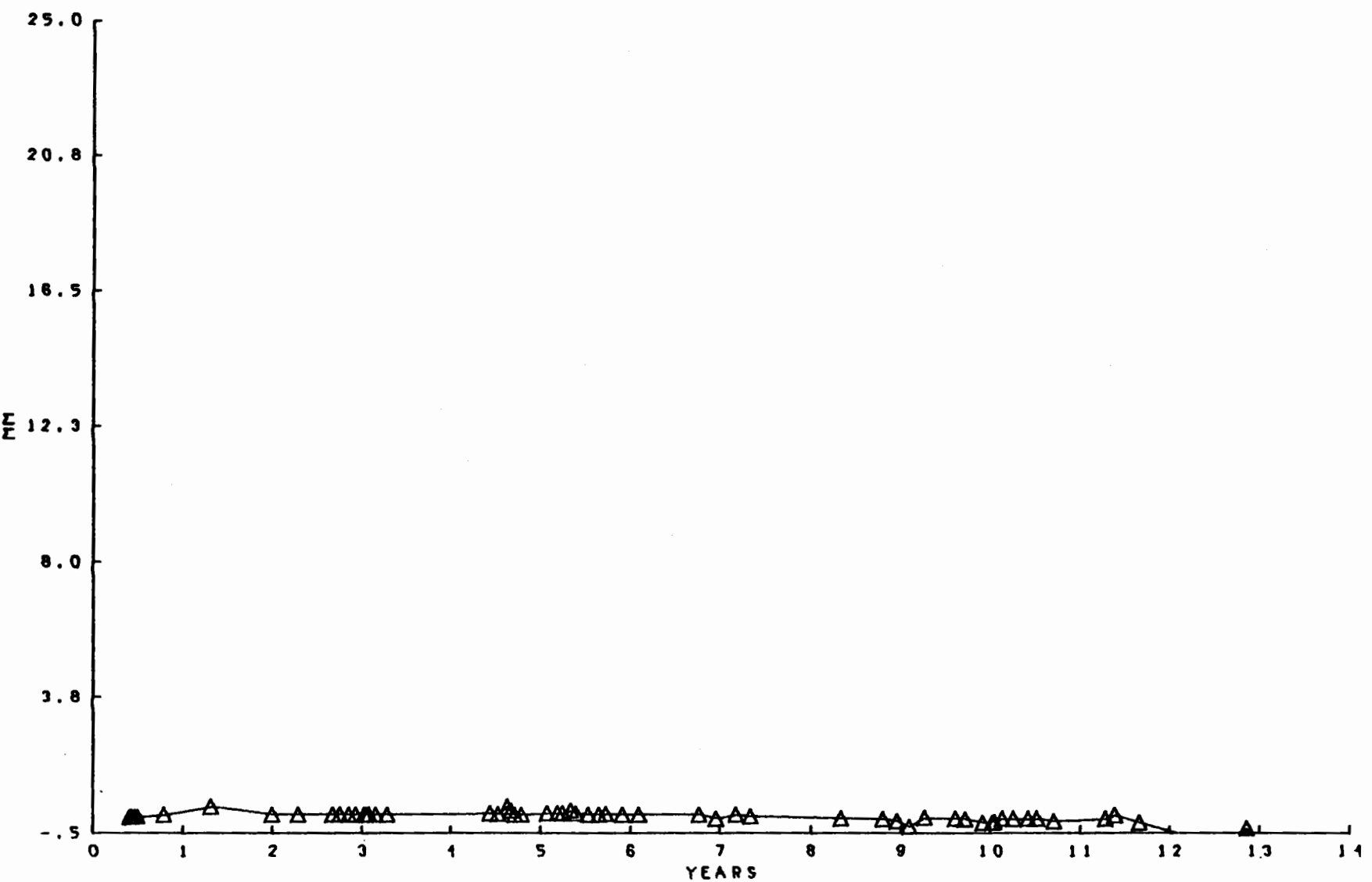




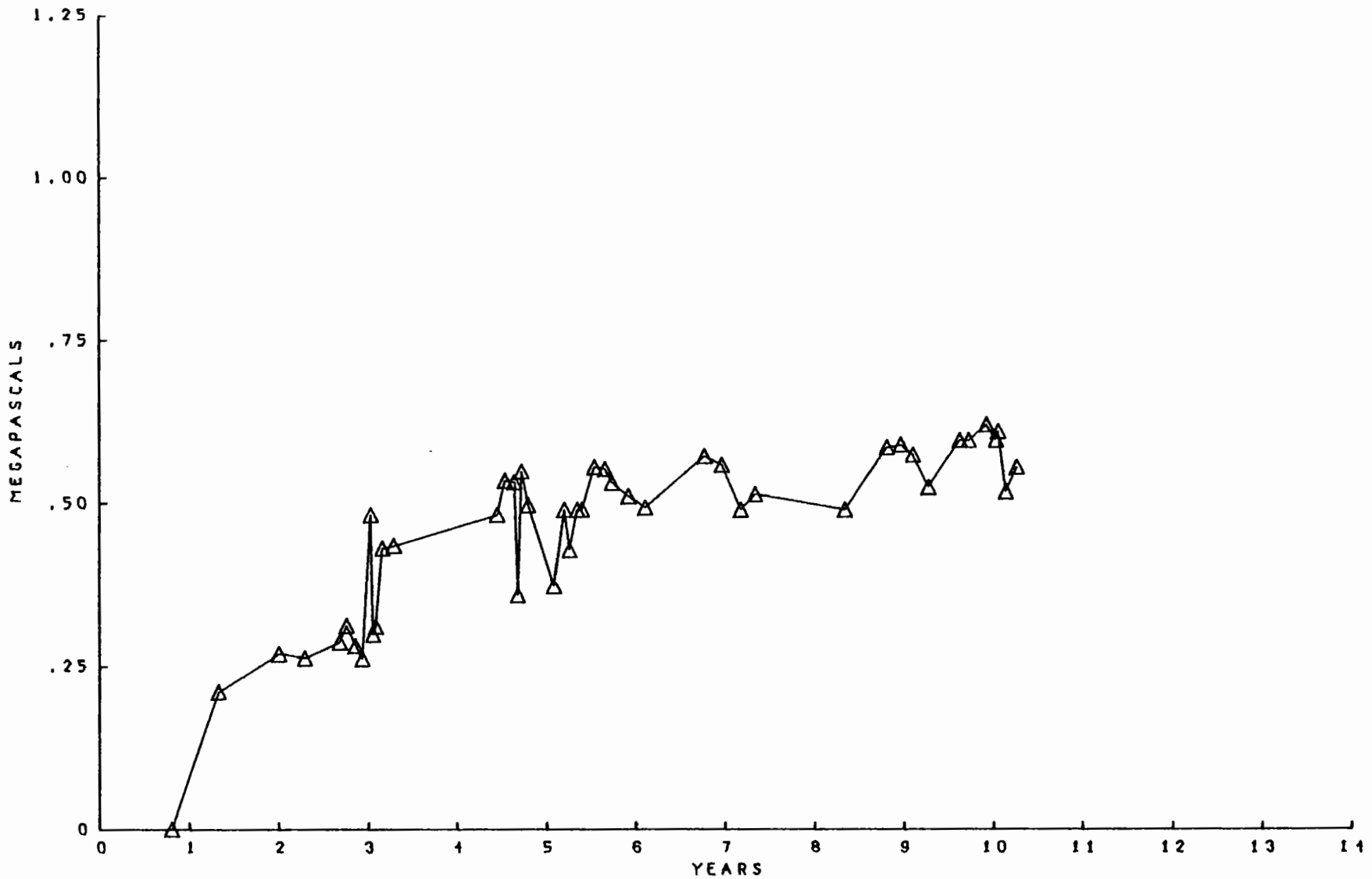
EXTENSOMETER R, STATION 1201+10, SOUTH WALL, 30 FT  
 BART TUNNELS HAYWARD FAULT ZONE INSTRUMENTATION



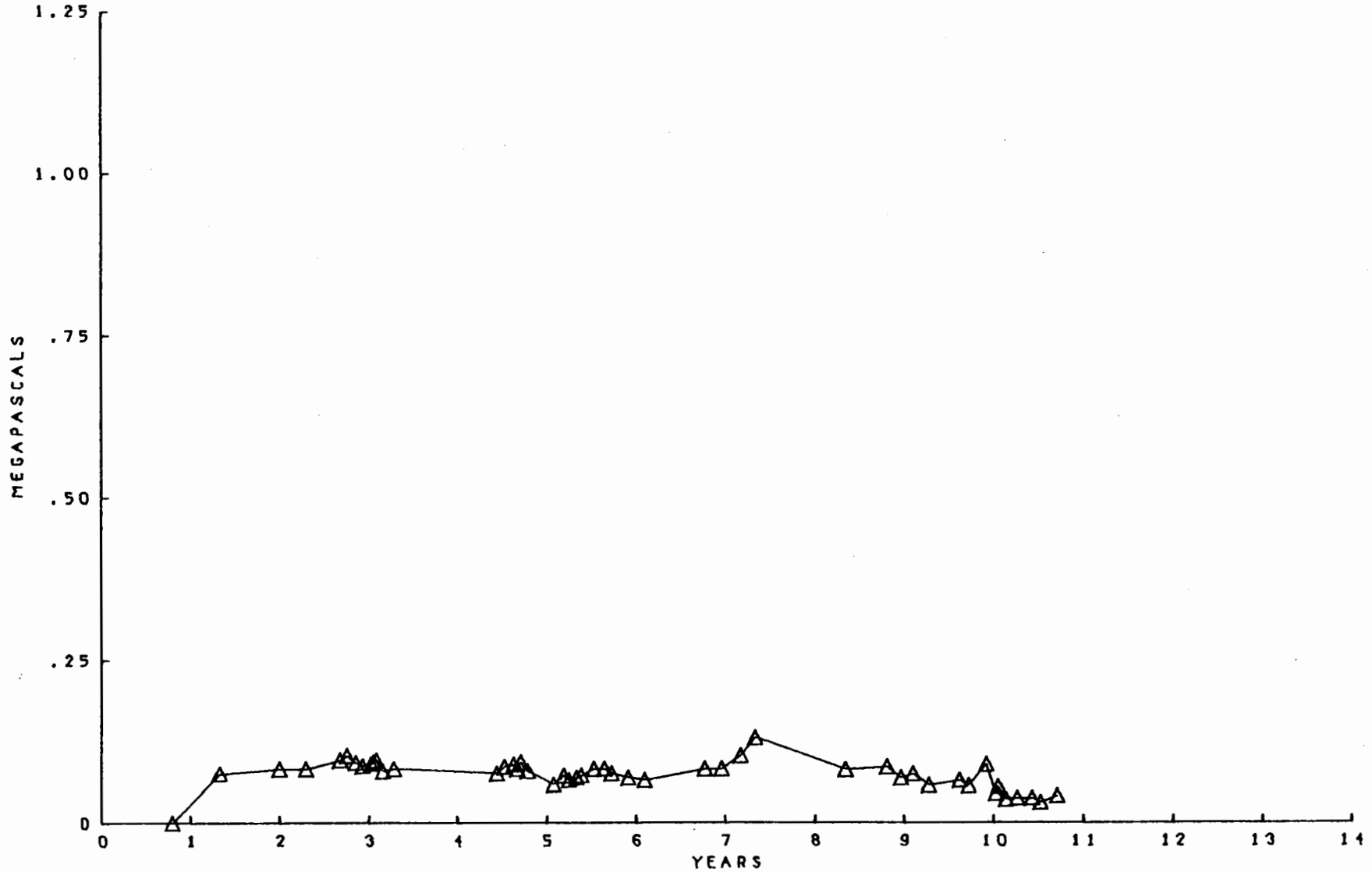
EXTENSOMETER S, STATION 1208+38, NORTH WALL, 30 FT  
 BART TUNNELS HAYWARD FAULT ZONE INSTRUMENTATION



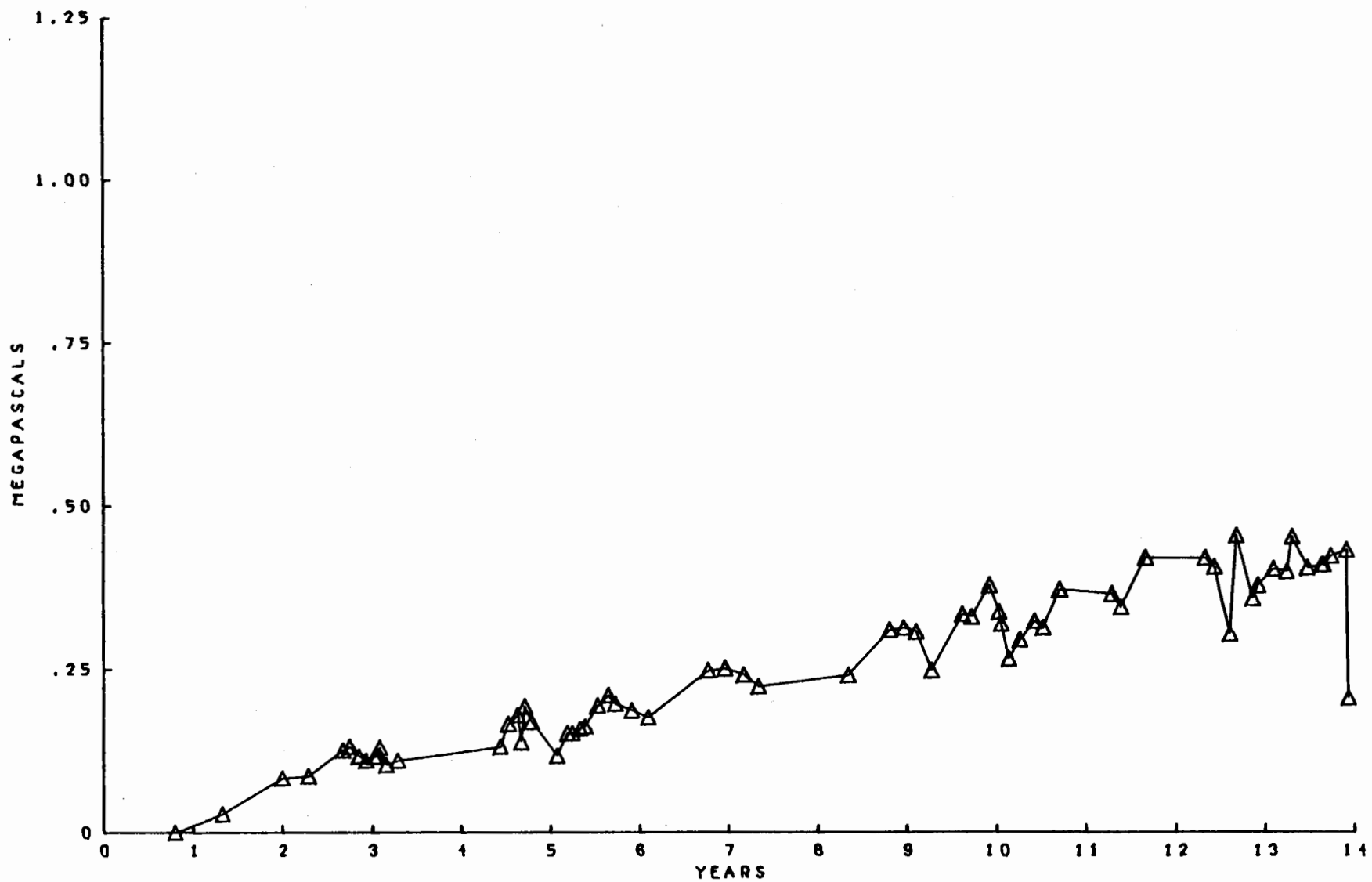
EXTENSOMETER T, STATION 1206+38, SOUTH WALL, 30 FT  
 BART TUNNELS HAYWARD FAULT ZONE INSTRUMENTATION



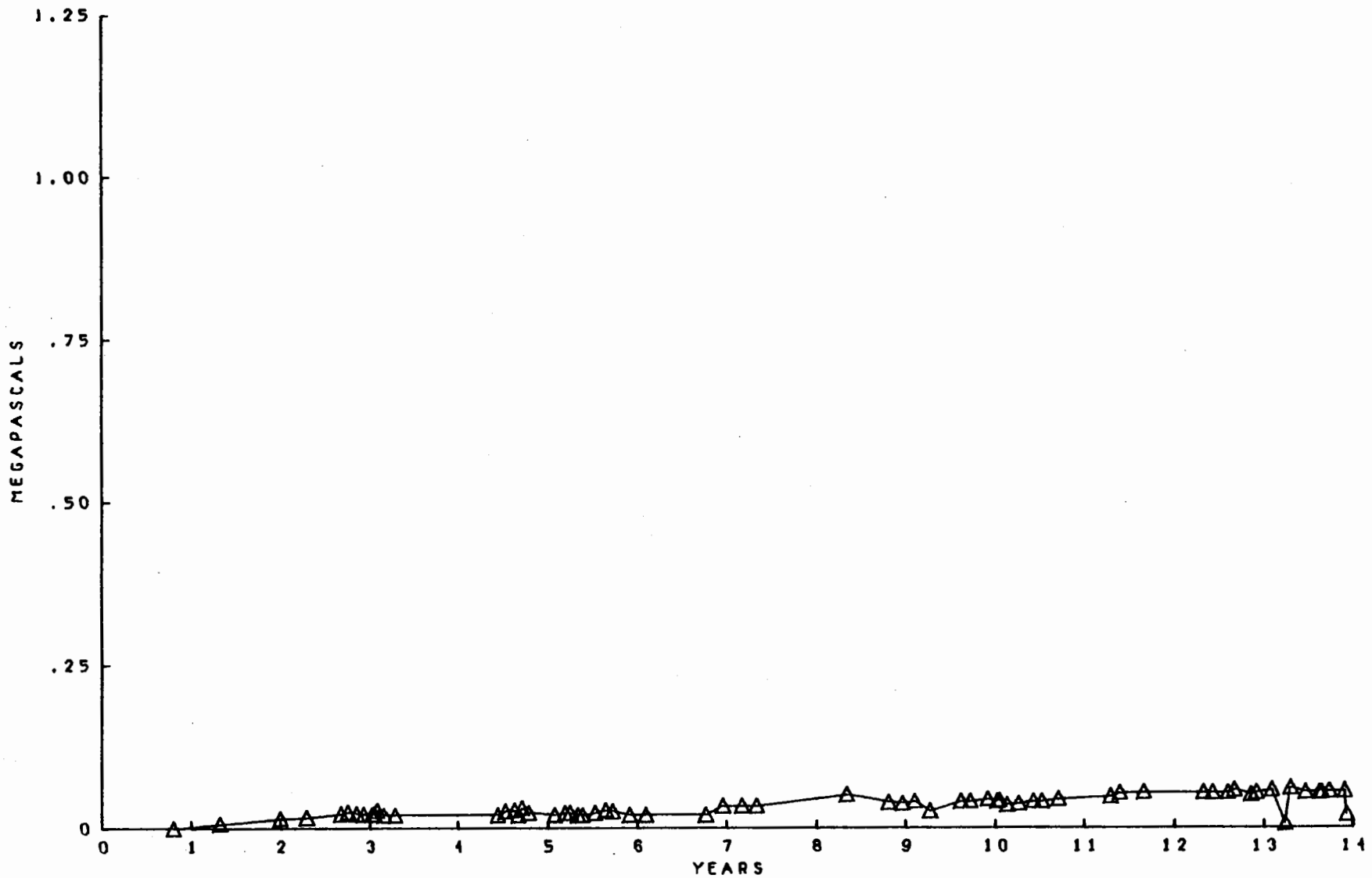
PRESSURE CELL 1, STATION 1201+93, NORTH ARCH  
 BART TUNNELS HAYWARD FAULT ZONE INSTRUMENTATION



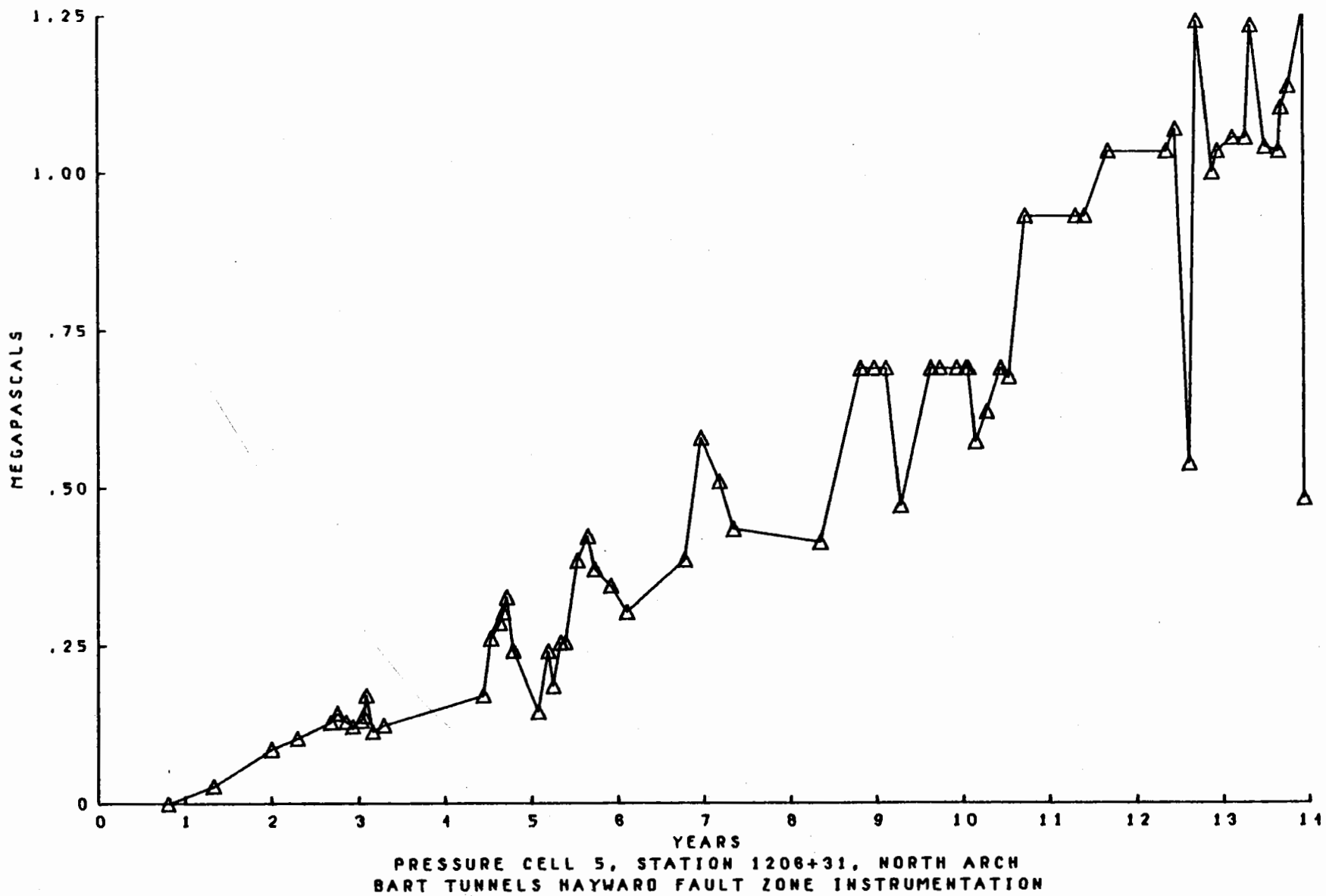
PRESSURE CELL 2, STATION 1201+99, SOUTH ARCH  
 BART TUNNELS HAYWARD FAULT ZONE INSTRUMENTATION



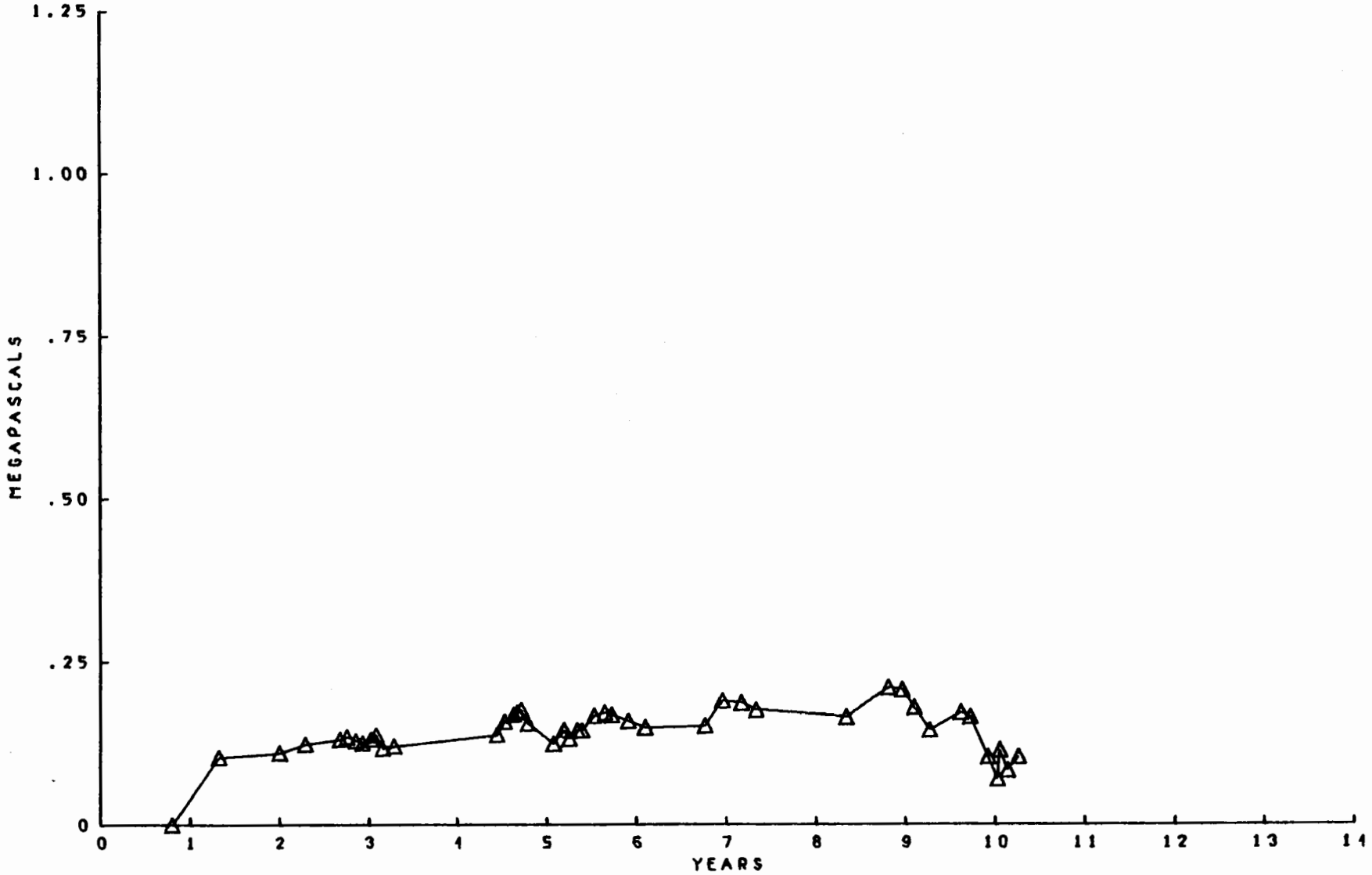
PRESSURE CELL 3, STATION 1201+79, NORTH ARCH  
 BART TUNNELS HAYWARD FAULT ZONE INSTRUMENTATION



PRESSURE CELL 4, STATION 1202+77, SOUTH ARCH  
 BART TUNNELS HAYWARD FAULT ZONE INSTRUMENTATION



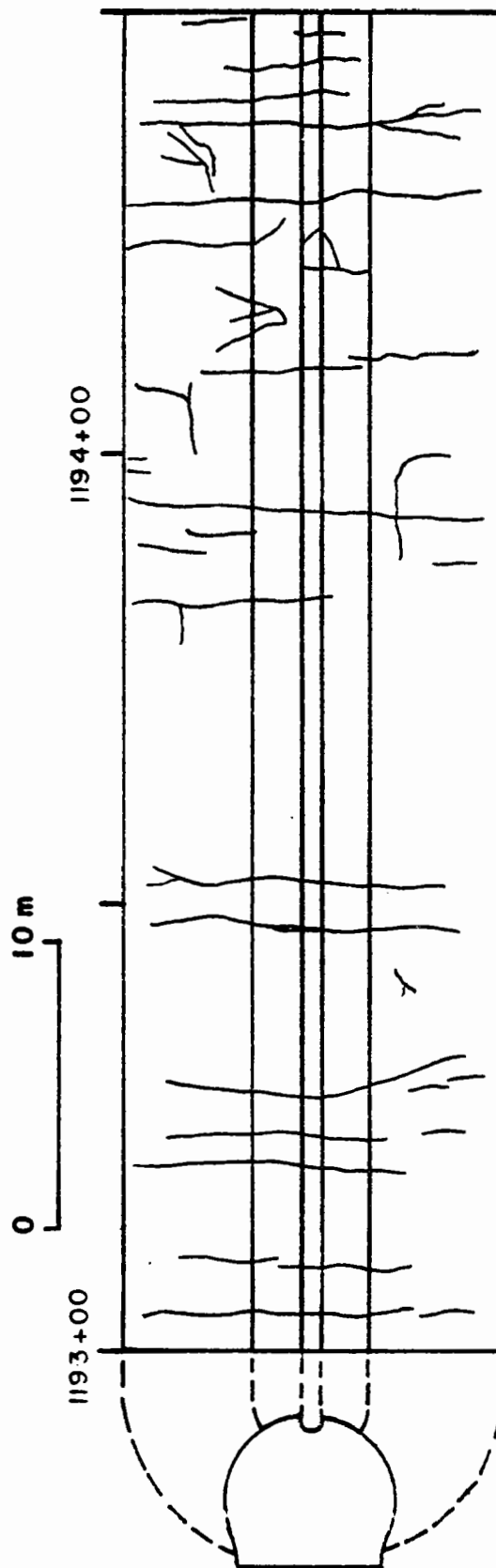
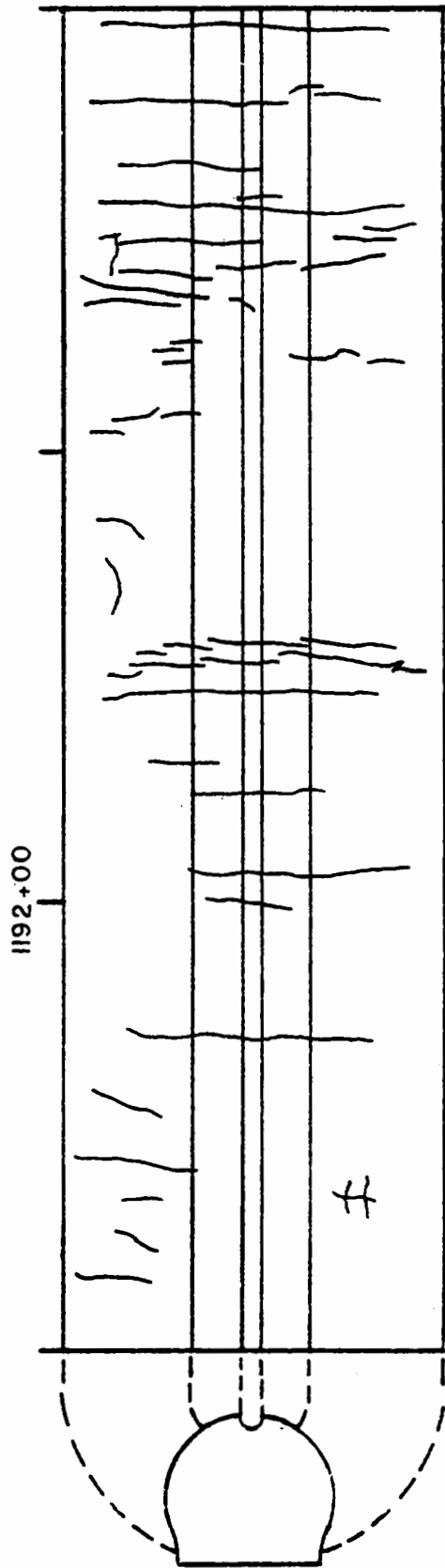


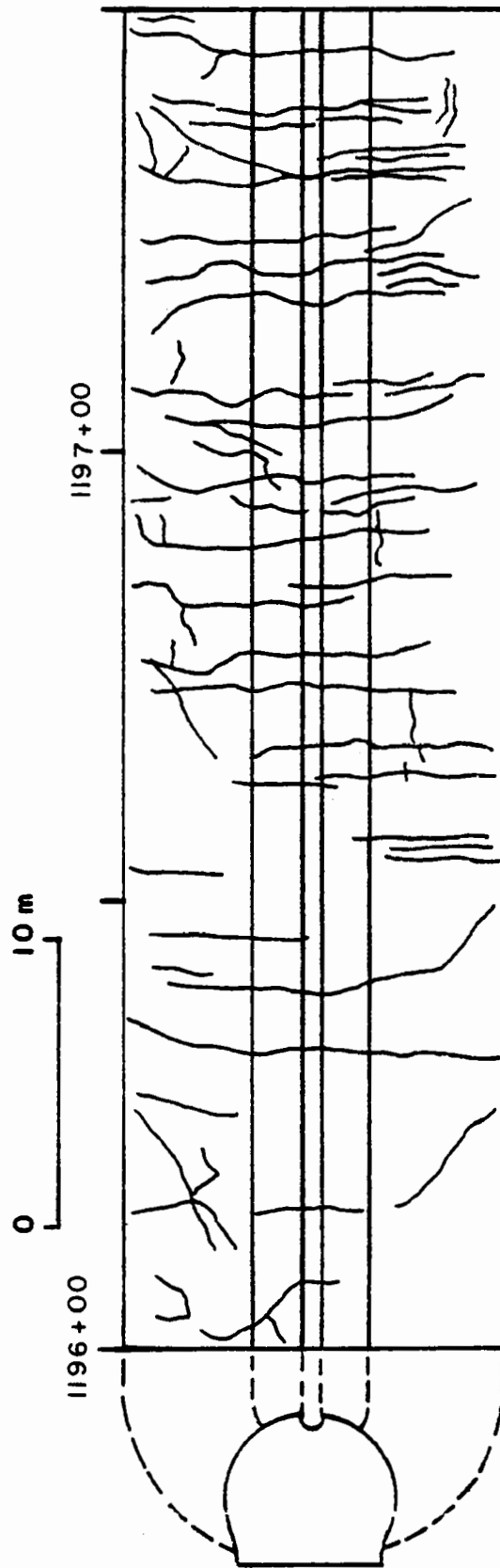
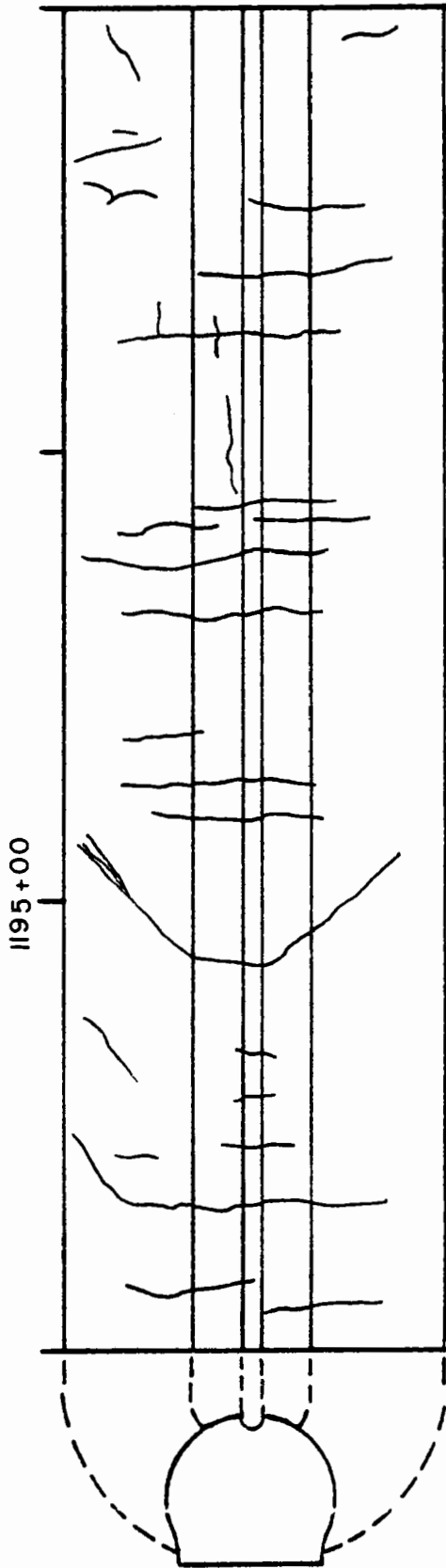


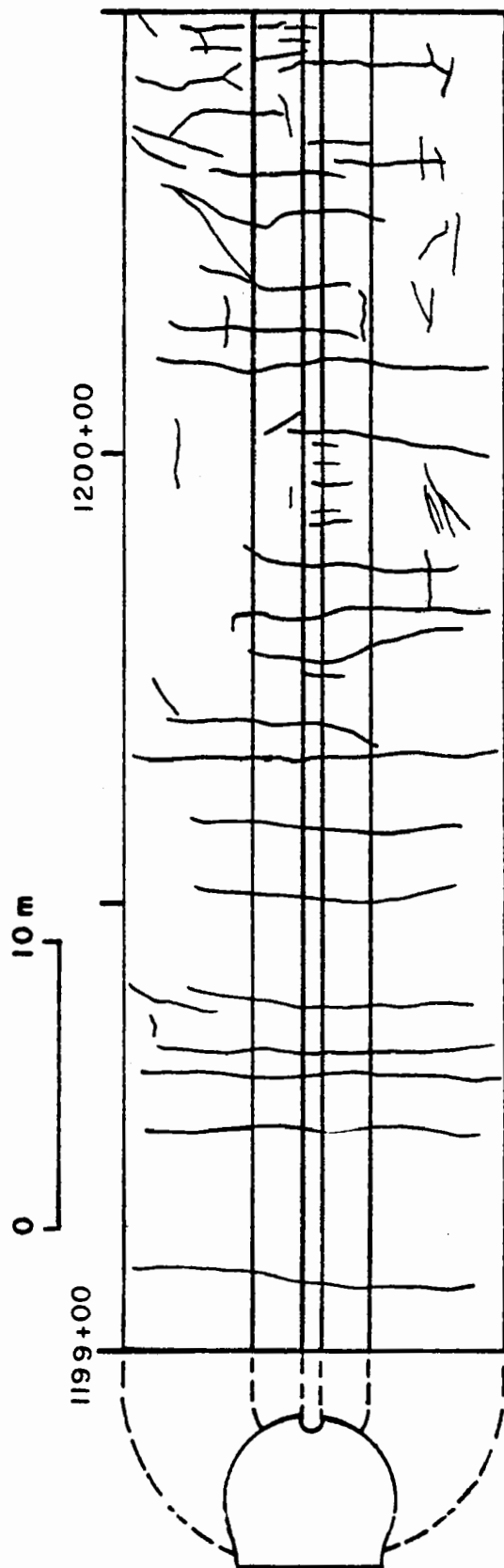
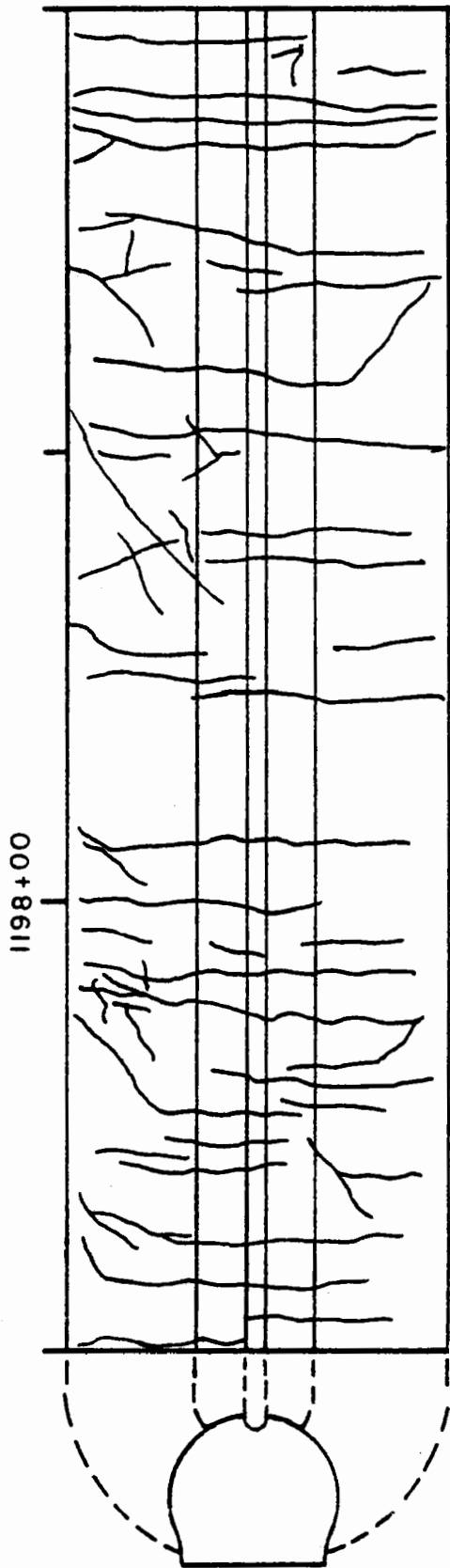
PRESSURE CELL 8, STATION 1206+39, SOUTH ARCH  
BART TUNNELS HAYWARD FAULT ZONE INSTRUMENTATION

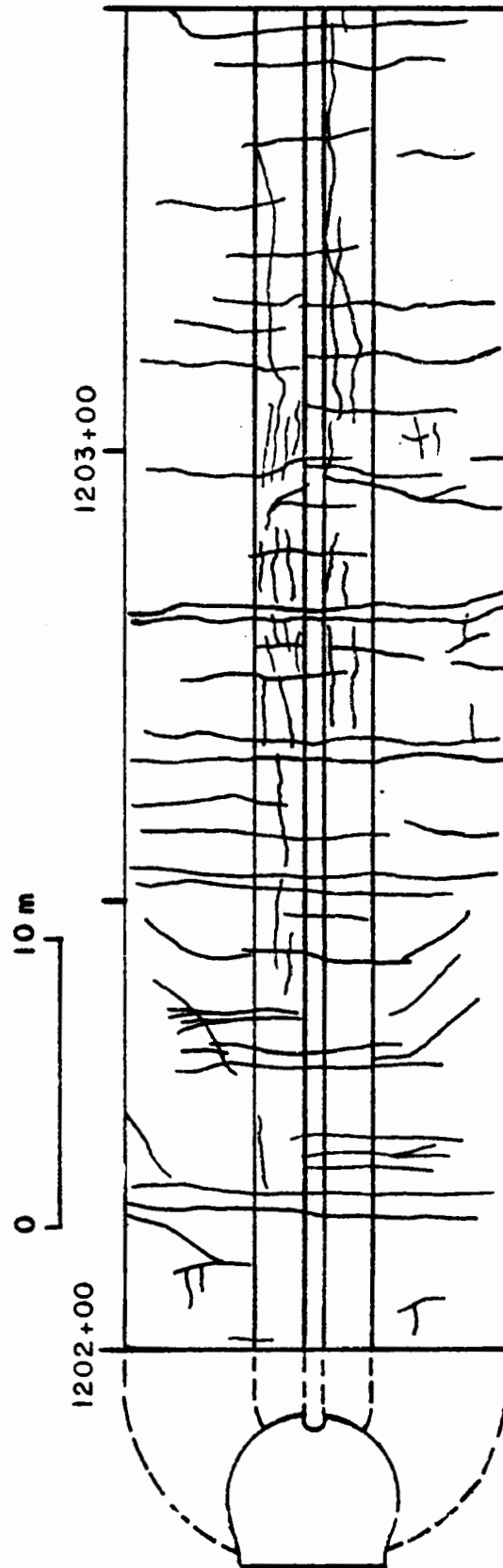
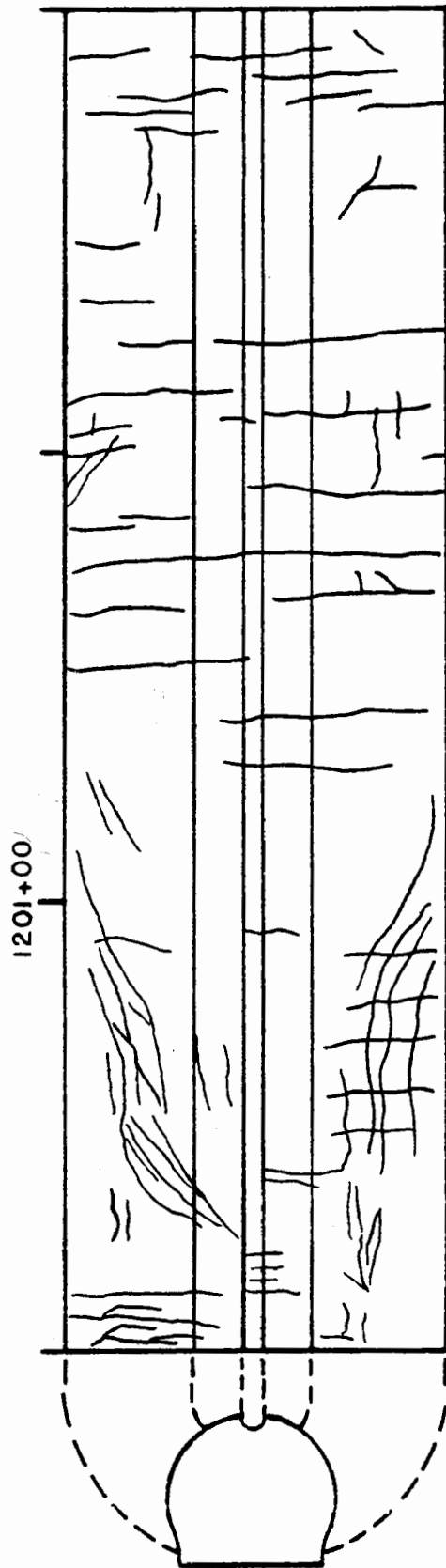
**APPENDIX D****LOG OF CONCRETE LINER CRACKS  
IN PART OF C2 TUNNEL**

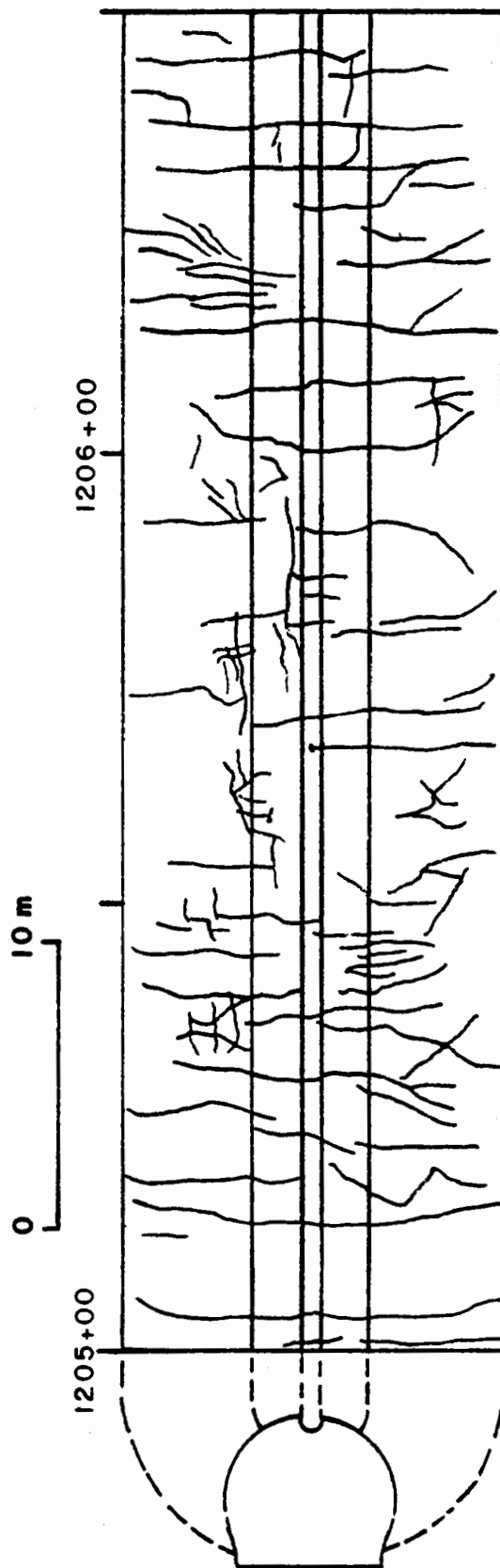
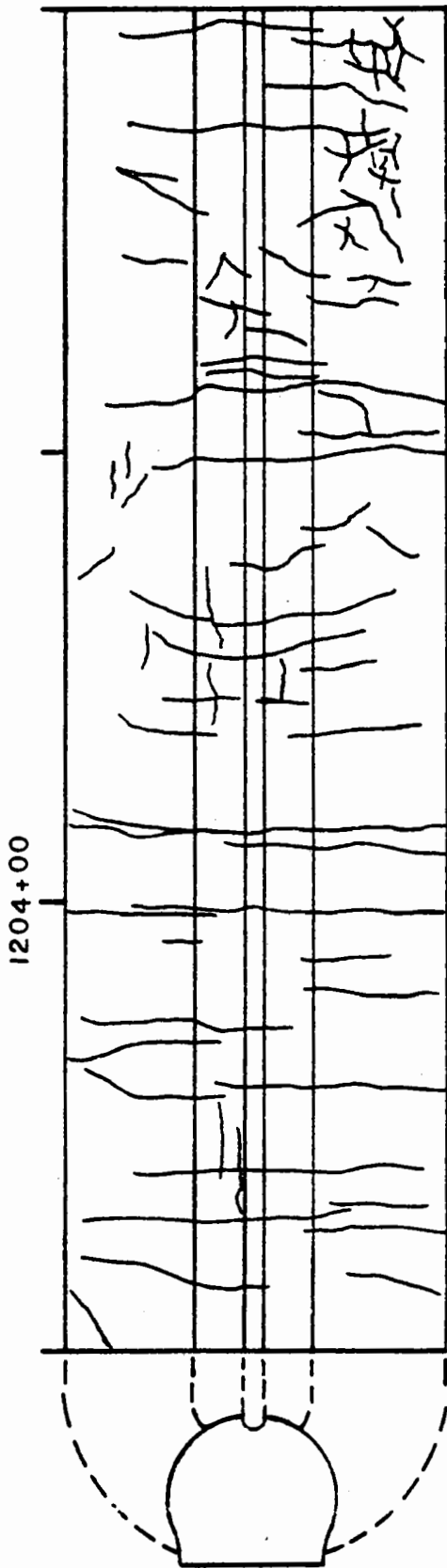
The log of concrete liner cracking, C2 tunnel, from Stations 1191+00 to 1210+20 is given in Figure D.1 (i - vi). The logs were compiled in September, 1979.

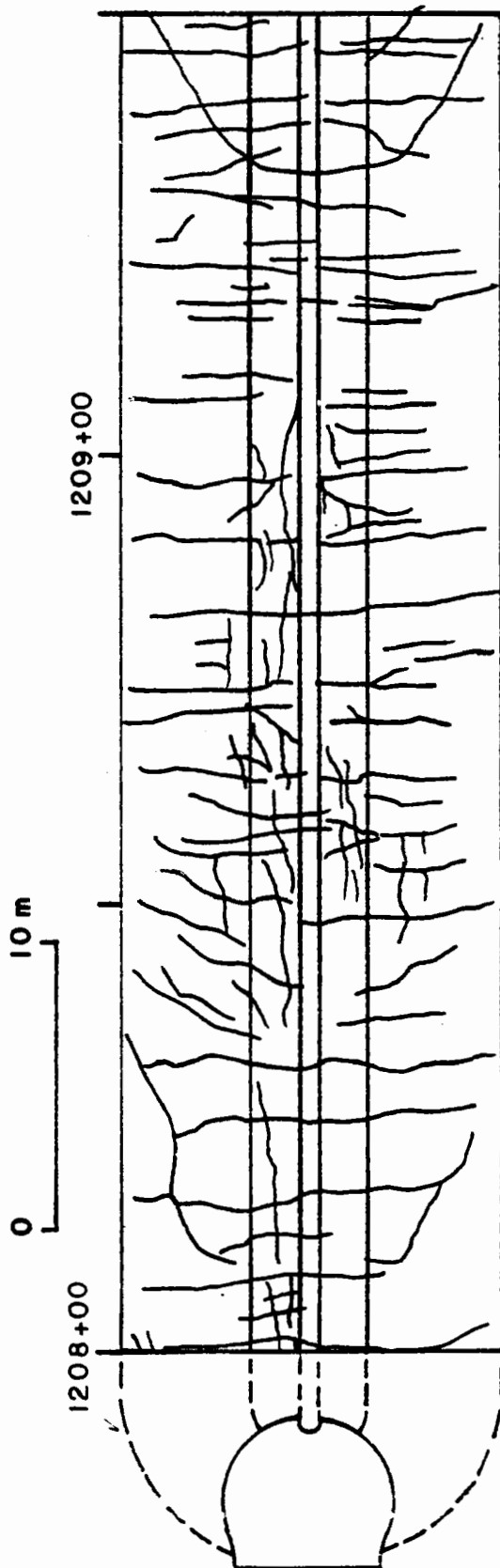
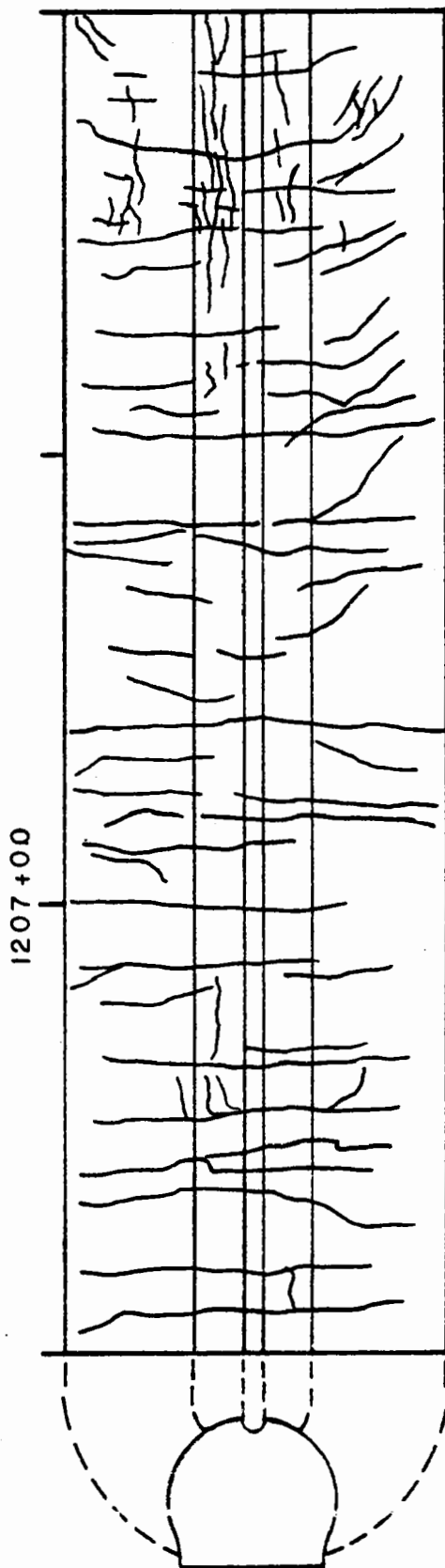


















NOTICE

This document is disseminated under the sponsorship of the Department of Transportation, Urban Mass Transportation Administration in the interest of information exchange. The United States Government assumes no liability for the contents or use thereof.

